

ASSESSING, MONITORING AND MAPPING FOREST
RESOURCES IN THE BLUE NILE REGION OF SUDAN USING
AN OBJECT-BASED IMAGE ANALYSIS APPROACH

Dissertation for awarding the academic degree

Doctor of Natural Science (Dr. rer. Nat.)

Submitted by

MSc. Mustafa Mahmoud El-Abbas Mustafa

born on 06.04.1977 in Khartoum

Supervisors:

Prof. Dr. habil Elmar Csaplovics, Technical University of Dresden,
Institute of Photogrammetry and Remote Sensing

Prof. Dr. Elnour Abdalla Elsiddig, University of Khartoum, Faculty
of Forestry, Department of Forest Management

Dr. habil. Hannelore Kusserow, Free University of Berlin, Institute of
Geographical Sciences

Dresden, 28.01.2015

Explanation of the doctoral candidate

This is to certify that this copy is fully congruent with the original copy of the thesis with the topic:

"Assessing, Monitoring and Mapping Forest Resources in the Blue Nile Region of Sudan Using an Object-based Image Analysis Approach"

Dresden, 27.02.2015

Mustafa Mahmoud El-Abbas Mustafa

TABLE OF CONTENTS

Chapter 1 INTRODUCTION	1
1.1. Background and motivation.....	1
1.1.1. Overview	1
1.1.2. Deforestation and land degradation.....	2
1.1.3. Remote sensing and forest resource assessment.....	4
1.2. Research hypotheses	7
1.3. Objectives	8
Chapter 2 STUDY AREA	11
2.1. Overview.....	11
2.2. Introduction to the study area	11
2.2.1. General description.....	11
2.2.2. Vegetation.....	12
2.2.3. Climate.....	14
2.2.4. Topography and soil	16
2.3. Test sites.....	16
2.3.1. LU/LC level.....	16
2.3.2. Forest stand level	19
Chapter 3 THEORETICAL BACKGROUND OF OBIA APPROACHES AND FOREST RESOURCE ASSESSMENT.....	21
3.1. Overview.....	21
3.2. Introduction.....	21
3.3. Object based image analysis	23
3.3.1. Image segmentation.....	24
3.3.2. Image objects hierarchy.....	27
3.3.3. Image object information extraction and feature measures.....	29
3.3.4. Nearest neighbour classification.....	34
3.3.5. Rule based classification	36
3.3.6. An application of object-based approach for mapping earth surface features	38
3.3.7. Quality assessment	47
Chapter 4 DATA AND RESEARCH APPROACHES.....	49
4.1. Overview.....	49
4.2. Data.....	49
4.2.1. Earth observation data	49

4.2.2.	Field survey data.....	53
4.3.	Methodology	57
4.3.1.	Atmospheric correction	57
4.3.2.	Geometric correction	58
4.3.3.	Image classification	59
4.3.4.	Change detection	72
4.3.5.	Classification accuracy assessment	73
4.3.6.	Forest parameters estimation and model validation	74
Chapter 5	LAND USE/ LAND COVER ANALYSES	81
5.1.	General overview	81
5.2.	Pixel-based classification of Aster imagery by maximum likelihood (ML) classifier.....	82
5.3.	OBIA approaches.....	85
5.3.1.	Segmentation result	85
5.3.2.	Hierarchical classification	86
5.3.3.	Object-based classification of Aster imagery by Nearest Neighbor (NN) classifier.....	88
5.3.4.	Object-based classification of Aster imagery by rule-based (RB) method	91
5.4.	OBIA vs. per pixel classification.....	93
5.4.1.	Classification of agricultural land.....	96
5.4.2.	Classification of residential areas	98
5.4.3.	Discrimination of vegetation classes	101
5.5.	Scale issue and hierarchical OBIA for mapping LU/LC	104
5.5.1.	Overview	104
5.5.2.	Pixel-based classification of higher resolution RapidEye scene	105
5.5.3.	Object-based classification of higher resolution RapidEye scene.....	108
5.5.4.	Overall assessment of the approaches based on the two selected scales.....	110
5.6.	Summary	112
Chapter 6	SPATIOTEMPORAL OBJECT-BASED IMAGE ANALYSES AND DRIVING FORCES	117
6.1.	General overview	117
6.2.	Land use/ land cover classification and accuracy assessment	119
6.2.1.	Land use/ land cover classification.....	119
6.2.2.	Accuracy assessment based on error matrix.....	122
6.2.3.	Accuracy assessment based on best classification result.....	124

6.3.	Distribution of LU/LC during the periods 1990, 1999 and 2009	126
6.3.1.	Trend, rate and magnitude of land use/ land cover changes.....	128
6.4.	Spatiotemporal object-based post-classification analysis	132
6.4.1.	Forest cover change dynamics 1990- 1999	134
6.4.2.	Forests cover change dynamics 1999- 2009.....	138
6.4.3.	Overall evaluation of the adopted approach in mapping forest cover change dynamics.....	143
6.5.	Major driving forces of forest cover loss and restoration problems	147
6.5.1.	Deterioration of forest cover in the area.....	147
6.5.2.	Driving forces of forest cover loss	148
6.5.3.	Restoration of destroyed forests	149
6.6.	Summary	152
Chapter 7 OBJECT-BASED TEXTURE MEASURES AND FOREST INVENTORY ...		155
7.1.	General overview	155
7.2.	Segmentation.....	157
7.3.	Descriptive analysis of field data.....	157
7.4.	Image metrics and forest inventory.....	160
7.4.1.	Volume	160
7.4.2.	Height	161
7.4.3.	Density.....	162
7.4.4.	Basal area.....	163
7.5.	Development of the regression model to estimate <i>Acacia nilotica</i> stand volume	164
7.5.1.	Model validation.....	167
7.6.	Mapping forest stand volume in Alambwa <i>Acacia nilotica</i> pure stand.....	170
7.7.	Summary	172
Chapter 8 CONCLUSIONS, RECOMMENDATIONS AND FUTURE WORK		175
8.1.	Conclusions.....	175
8.1.1.	Overview	175
8.1.2.	Land Use/ Land cover categorical level	175
8.1.3.	Integrated framework of change analysis.....	177
8.1.4.	Continuous forest structural attributes level.....	178
8.2.	Recommendations.....	179
8.3.	Limitations	181
8.4.	Future work.....	181

REFERENCES	183
APPENDIXES	203

LIST OF TABLES

Table 1-1: Old united Sudan forest cover, source FRA 2010	3
Table 4-1: Specifications of TERRA ASTER image used for the study.....	50
Table 4-2: Specifications of LANDSAT TM images used for the study	52
Table 4-3: Specifications of RapidEye data used for the study.....	52
Table 4-4: Land Use/ Land Cover (LU/LC) patterns of the study area.....	54
Table 4-5: Levels of segmentation parameters for LU/LC analysis.....	63
Table 4-6: Segmentation parameters applied for forest stand level	75
Table 5-1: Error matrix of maximum likelihood classification	84
Table 5-2: Error matrix of nearest neighbour classification.....	90
Table 5-3: Error matrix of rule-based classification.....	93
Table 5-4: Quantitative results of the LU/LC classes.....	96
Table 5-5: Error matrix of maximum likelihood classification	107
Table 5-6: Error matrix of rule-based classification.....	110
Table 6-1: Overall accuracy and kappa index of the best classification results	124
Table 6-2: Accuracy assessment of the classified LANDSAT image (1990)	125
Table 6-3: Accuracy assessment of the classified LANDSAT TM image (1999)	125
Table 6-4: Accuracy assessment of the classified TERRA ASTER image (2009)	126
Table 6-5: Land use/ land cover distribution during the period 1990- 2009	128
Table 6-6: LU/LC change; trend, rate and magnitude (1990- 2009).....	131
Table 6-7: LU/LC change matrix of fused images1990-1999 (ha)	136
Table 6-8: LU/LC change matrix of fused images1999-2009 (ha)	139
Table 6-9: Accuracy assessment based on the best classification result for the change map of 1990-1999.....	144
Table 6-10: Accuracy assessment based on the best classification result for the change map of 1999-2009.....	145
Table 6-11: Non-site specific accuracy assessment for the change maps (1990-1999 and 1999-2009).....	146
Table 6-12: Goods and services attained from the forests.....	147
Table 6-13: Local community’s perception about the causes of forest cover loss.....	149
Table 6-14: Local community’s perception about the mission that it may stimulate the recovery process	152
Table 7-1: Statistical summary of stand parameters for each volume class and its total ...	158

Table 7-2: Pearson’s correlation coefficient matrix for <i>Acacia nilotica</i> plantation average stand variables	160
Table 7-3: Pearson’s correlation coefficient between image metrics and stand volume....	160
Table 7-4: Pearson’s correlation coefficient between image metrics and stand height.....	161
Table 7-5: Pearson’s correlation coefficient between image metrics and stand density	162
Table 7-6: Pearson’s correlation coefficient between image metrics and stand basal area	163
Table 7-7: Summary table of generated models and statistics for the forest stand volume and the derived metrics	166
Table 7-8: The coefficients of the best fitted models equation with stand volume.....	168

LIST OF FIGURES

Figure 2-1: Location of the selected test sites	12
Figure 2-2: The average temperature during the year in the study area	15
Figure 2-3: Rainfall pattern in the study area	15
Figure 2-4: The average precipitation rate during the year in the study area	16
Figure 2-5: Some of the main features observed in the study area.....	18
Figure 4-1: spatial distribution of the ground truth data.....	51
Figure 4-2: Collection procedure of plot level forest inventory data	56
Figure 4-3: FLAASH atmospheric correction model input parameters window	58
Figure 4-4: Comparison of different experimental segmentation results	62
Figure 4-5: The nearest neighbour classification principle	65
Figure 4-6: Part of the training and test area mask in eCognition	66
Figure 4-7: Sample editor window shown the histogram of the selected TTA Mask	67
Figure 4-8: Feature space optimization	69
Figure 4-9: Equiprobability contours defined by a maximum likelihood classifier.....	72
Figure 5-1: Structure of the results achieved from LU/LC image analysis.....	82
Figure 5-2: Thematic map from 2009 TERRA ASTER scene using maximum likelihood classifier.....	83
Figure 5-3: Final segmentation result of TERRA ASTER imagery.....	86
Figure 5-4: Hierarchical classification system	87
Figure 5-5: Thematic map from 2009 TERRA ASTER scene using NN classifier	89
Figure 5-6: Thematic map from 2009 TERRA ASTER scene using rule-based classifier ..	92
Figure 5-7: Summary statistics of producer's accuracy	94
Figure 5-8: Summary statistics of user's accuracy.....	95
Figure 5-9: A typical form of semi-mechanized rainfed agriculture.....	97
Figure 5-10: Misclassified areas in agricultural field.....	98
Figure 5-11: Partial view of housing pattern.....	99
Figure 5-12: Misclassified areas of Merau village in the study area.....	100
Figure 5-13: Misclassified areas of vegetation classes.....	103








Figure 5-14: Reestablishment of <i>Acacia nilotica</i> plantation	104
Figure 5-15: Thematic map from 2010 RapidEye using maximum likelihood classifier ..	106
Figure 5-16: Thematic map from 2010 RapidEye using rule-based classifier	109
Figure 5-17: Overall accuracy comparison	111
Figure 6-1: Structure of the results for spatiotemporal OBIA analysis	118
Figure 6-2: Thematic maps of study area used for spatiotemporal analyses	121
Figure 6-3: Producer’s accuracy obtained from rule-based method.....	123
Figure 6-4: User’s accuracy obtained from rule-based method	123
Figure 6-5: Illustration of the post-spatiotemporal analysis	133
Figure 6-6: Change map “from-to” parent classes (1990-1999)	137
Figure 6-7: Change area “from-to” parent classes (1990-1999).....	137
Figure 6-8: Change map “from-to” child classes (1990- 1999)	138
Figure 6-9: Change map “from-to” parent classes (1999- 2009)	141
Figure 6-10: Change area “from-to” parent classes (1999-2009).....	141
Figure 6-11: Change map “from-to” child classes (1999- 2009)	142
Figure 6-12: Land clearance for mechanized farming.....	143
Figure 6-13: Total annual precipitation in the study area.....	149
Figure 6-14: Total production of cereal crops in Sinnar state	150
Figure 6-15: A typical pattern in dry season of abandoned agriculture	151
Figure 7-1: Modeling steps to estimate <i>Acacia nilotica</i> attributes	156
Figure 7-2: Average tree parameters based on sampled areas.....	159
Figure 7-3: observed vs. predicted forest stand volume based on RapidEye	168
Figure 7-4: observed vs. predicted forest stand volume based on Aster	169
Figure 7-5: Map of estimated volume in Alambwa forest.....	171

ACRONYMS AND ABBREVIATIONS


AI	Artificial Intelligence
ASTER	Advanced Space borne Thermal Emission and Reflection Radiometer
DBH	Diameter at Breast Height
DN	Digital number
EO	Earth Observing
ERSDAC	Japan's Earth Remote Sensing Data Analysis Center
FAO	Food and Agriculture Organization
FNC	Sudan's Forest National Corporation
FRA	Forest Resource Assessment
FSO	Feature Space Optimization
GCP	Ground Control Point
GEOBIA	Geographic Object-Based Image Analysis
GIS	Geographic Information System
GLCM	Gray-level Co-occurrence Matrix
GPS	Global Positioning System
ha	Hectare
LU/LC	land use/land cover
METI	Japan's Ministry of Economy, Trade and Industry
ML	Maximum Likelihood
NASA	National Aeronautics and Space Administration
NCDC	National Climatic Data Center
NDVI	Normalized Difference Vegetation Index
NN	Nearest Neighbour
OBIA	Object Based Image Analysis
OLV	Object Layer Value
PCA	Principal Component Analysis
PPS	Population Proportional to Size
R	Coefficient of determination
RB	Rule Based
RMSE	Residual Mean Square Error
SPSS	Statistical Package for the Social Sciences
SWIR	Short Wave Infrared
TIR	Thermal Infrared
TM	Thematic Mapper
TTA	Training and Test Area Mask


UNCD	United Nations Capital Development Fund
USGS	United States Geological Survey
UTM	Universal Transverse Mercator projection
VNIR	Visible and Near-Infrared


AUTHOR'S PUBLICATIONS


-  El-Abbas, M. M.; Csaplovics, E., and Deafalla, T. H. H. 2013. Remote sensing and spatial analysis based study for detecting deforestation and the associated drivers. In Proc. of SPIE International Conference, 23-26 September, Dresden, Germany. Earth Resources and Environmental Remote Sensing/GIS Applications IV, 88931U. Ulrich Michel, Daniel L. Civco, and Karsten Schulz (Eds.), Vol. 8893, DOI: 10.1117/12.2029252, 8.
-  El Abbas, M. M.; Csaplovics, E. and Deafalla, T. H. H. 2013. Forest structure estimates with GEOBIA and multiscale optical sensors. In Proc. of SPIE International Conference, 23-26 September, Dresden, Germany. Earth Resources and Environmental Remote Sensing/GIS Applications IV, 88931U. Ulrich Michel, Daniel L. Civco, and Karsten Schulz (Eds.), Vol. 8893, DOI: 10.1117/12.2029243, 12.
-  El-Abbas, M. M. and Csaplovics, E. 2013. Multiscale GEOBIA for the Quantification of Forest Cover Loss in Blue Nile Region.. In proc. of living Planet Symposium, 9–13 September, Edinburgh, UK. Edited by L. Ouwehand, ESA SP-722, ISBN 978-92-9221-286-5, 8.
-  El-Abbas, M. M.; Csaplovics, E. and Deafalla, T. H. H. 2013. Integrated Assessment of Agroforestry System for Sustainable Land Management in Dry African Savanna. In Proc. of Tropentag 2013 International Conference. Agricultural development within the rural-urban continuum, 17- 19 September, Stuttgart, Germany. Eric Tielkes (Eds.), ISBN: 978-3-95404-498-6, ID. 745, 160.
-  El-Abbas, M. M.; Csaplovics, E.; Deafalla, T. H. H. 2013. Knowledge-Based approach of Multi-Source Spatiotemporal Data for Sustainable Forest Management. COST Action FP0804 Decision support systems for Sustainable Forest Management: In Proc. of FORSYS 2013 Conference, 24-26 April, Umea, Sweden. Program and book of abstract.
-  El-Abbas, M. M. and Csaplovics E. 2012. Advancing the Quantification of Forest Cover Loss Using Multi-Spectro-Temporal Imagery in Blue Nile Region. In International Scientific Conference, Forestry Science and Practice For The Purpose of Sustainable Development of Forestry, Banja Luka, Republic of Srpska/ B&H. Zoran Govedar, Vojislav Dukić (Eds.), Session: II, Proceedings: 40, 49.
-  El-Abbas, M. M. and Csaplovics, E. 2012. Spatiotemporal object-based image analyses in the Blue Nile area using optical multispectral imagery. In SPIE 8538, Earth Resources

and Environmental Remote Sensing/GIS Applications III, Edinburgh, Scotland. Shahid Habib; Ulrich Michel; Daniel L. Civco; David Messinger; Antonino Maltese (Eds.), Proceedings of SPIE Vol. 8538 (SPIE, Bellingham, WA 2012), 85380X.

 El-Abbas, M. M.; Csaplovics, E. and Deafalla, T. H. H. 2012. Spatio-temporal Integration of Socio-economic Factors Related to the Land-cover Changes in the Blue-Nile Region, Sudan. In Tropentag 2012, International Research on Food Security, Natural Resource Management and Rural Development, Resilience of agricultural systems against crisis, jointly organized by the Universities of Göttingen and Kassel/Witzenhausen, September, Göttingen, Germany. Eric Tielkes (Eds.), Session: VI, Modeling, Systems modeling, ISBN: 978-3-9801686-7-0, 460.

 El Abbas, M. M. and Csaplovics E. 2011. Object-based Land Cover Mapping of Multi-spectral Imagery in Semi-arid Areas. In Tropentag 2011, Development on the margin, October 2011, Bonn, Germany. Mathias Becker, Christine Kreye, Christina Ripken, Eric Tielkes (Eds.), Session: Systems under stress, Land use and management, ISBN: 978-3-9801686-7-0, 447.

 El Abbas, M. M. and Csaplovics E. 2011. Object-based vs. per-pixel classification of aster imagery for land cover mapping in semi-arid areas. In SPIE, Earth Resources and Environmental Remote Sensing/GIS Applications II, Editors: Ulrich Michel; Daniel L. Civco, Proceedings of SPIE Vol. 8181 (SPIE, Bellingham, WA 2011), 818100.

 El-Abbas, M. M.; Csaplovics E. and Röhle, H. 2011. Developing forest parameters estimation model using object-based Texture Measure of ASTER Imagery Data in the Blue Nile forest, Sudan. In IUFRO International Conference Research Priorities in Tropical Silviculture: Towards New paradigms? 15-18 November, Montpellier, France. Plinio Sist (Eds.), Parallel Session: 2, Proceedings: 39, 73.

ACKNOWLEDGMENT

To almighty GOD: for manifold blessings and guidance up to now and in future.

First of all. I would like to express my gratitude to my supervisor, Prof. Dr. habil. Elmar Csaplovics for guiding me through the PhD research. His insight has always enlightened me. From him I learned how to think critically, how to select problems, how to solve them, and how to present their solutions. He gave me energy to tackle new problems. The opportunity to work with new high resolution dataset that became available at the finalization stages of my study and with automated interpretation methods with valuable softwares for mapping and analyses which made this thesis possible. I appreciate very much his open mind and patience towards an unknown and uncertain world.

I would also like to extend my deepest appreciation to the members of my graduate committee, Prof. Dr. habil. Dominik Faust (head of the exam commission) for his generous support especially during the first period of my stay in TU Dresden and Professor Dr. habil. Heinz Röhle (a member of the committee and examiner) for his kind support. My extend thanks for Dr. habil. Hannelore Kusserow (Free university of Berlin) and Prof. Dr. Elnour Abdalla Elsidig (University of Khartoum) for spending their valuable time on the evaluation of this study.

Data for the study described in the thesis have been obtained from several organizations, including DLR (Deutschland für Luft- und Raumfahrt) under the RESA (RapidEye Science Archive) project, NASA's Earth Observing System (EOS) and USGS (United States Geological Survey). Financial support for the study has been obtained from the Ministry of Higher Education and Scientific Research (Sudan) and University of Khartoum. Special appreciation also for the German Academic Exchange Service (DAAD) for their financial support during the finalization stage of my work. Thanks extended to the GFF (Gesellschaft von Freunden und Förderern der TU Dresden) for their valuable financial support for the field work and their support to attend some local and international scientific events. I extend my thanks to all these organizations for their generous support.

I am thankful to the Forest National Cooperation (FNC) offices in Khartoum, Sinner and Singa for their unlimited logistic support during the field work. Sincere gratitude goes to Dr. Abdelazim Mirghani, the general manager of the Forestry National Corporation (FNC), Mr. Mamoun Gasim, Mr. Ahmed Ibrahim and Mr. Alsadig Alamin, without their assistance it would not have been possible for me to carry out the field work.

My appreciation is also due to my colleagues at the University of Khartoum. Very special thanks to Dr. Mohsin Hassan Abdalla principal of the University of Khartoum, Mrs. Islah Shaban, Dr. Abdalla Mirghani El Tayeb Dean of Faculty of Forestry and Dr. Dafa-Alla Mohamed Dafa-Alla Head of the Forest Management Department, Faculty of Forestry.

I would like to thank my colleagues and staff members at the Institute of Remote Sensing, TU Dresden for their continuous cooperation and helpfulness. The support I receive from you is sincerely acknowledged and appreciated. Very special thanks extended to Dipl. Ing. Stephan Schoeps, Dr. Ing. Christine Wessollek, Dr. Ing. Jana Schmidt for their support when it was most needed. Also I would like to extend my gratitude to Dr. Mohamed Hamid for his kind support for the analysis of part of my field data. My thanks also will go to all Sudanese colleagues and friends for their warmly accompanying during our stay in Germany.

Thank you to my family in Khartoum and Karkoj Al-Sharif Mohammad Elameen for their unlimited spiritual and moral support, and who missed us for the years we were in Germany. I cannot thank my parents, enough for everything they meant to me throughout my life. Last, but certainly not least, then there is my wife Taisser, what I can say... you are always my source of energy, I really thank for the constant support and encouragement. To you I dedicate this work.

ABSTRACT

Following the hierarchical nature of forest resource management, the present work focuses on the natural forest cover at various abstraction levels of details, i.e. categorical land use/land cover (LU/LC) level and a continuous empirical estimation of local operational level. As no single sensor presently covers absolutely all the requirements of the entire levels of forest resource assessment, multisource imagery (i.e. RapidEye, TERRA ASTER and LANDSAT TM), in addition to other data and knowledge have been examined. To deal with this structure, an object-based image analysis (OBIA) approach has been assessed in the destabilized Blue Nile region of Sudan as a potential solution to gather the required information for future forest planning and decision making. Moreover, the spatial heterogeneity as well as the rapid changes observed in the region motivates the inspection for more efficient, flexible and accurate methods to update the desired information.

An OBIA approach has been proposed as an alternative analysis framework that can mitigate the deficiency associated with the pixel-based approach. In this sense, the study examines the most popular pixel-based maximum likelihood classifier, as an example of the behavior of spectral classifier toward respective data and regional specifics. In contrast, the OBIA approach analyzes remotely sensed data by incorporating expert analyst knowledge and complimentary ancillary data in a way that somehow simulates human intelligence for image interpretation based on the real-world representation of the features. As the segment is the basic processing unit, various combinations of segmentation criteria were tested to separate similar spectral values into groups of relatively homogeneous pixels. At the categorical subtraction level, rules were developed and optimum features were extracted for each particular class. Two methods were allocated (i.e. Rule Based (RB) and Nearest Neighbour (NN) Classifier) to assign segmented objects to their corresponding classes.

Moreover, the study attempts to answer the questions whether OBIA is inherently more precise at fine spatial resolution than at coarser resolution, and how both pixel-based and OBIA approaches can be compared regarding relative accuracy in function of spatial resolution. As anticipated, this work emphasizes that the OBIA approach is can be proposed as an advanced solution particularly for high resolution imagery, since the accuracies were improved at the different scales applied compare with those of pixel-based approach. Meanwhile, the results achieved by the two approaches are consistently high at a finer RapidEye spatial resolution, and much significantly enhanced with OBIA.

Since the change in LU/LC is rapid and the region is heterogeneous as well as the data vary regarding the date of acquisition and data source, this motivated the implementation of post-

classification change detection rather than radiometric transformation methods. Based on thematic LU/LC maps, series of optimized algorithms have been developed to depict the dynamics in LU/LC entities. Therefore, detailed change “from-to” information classes as well as changes statistics were produced. Furthermore, the produced change maps were assessed, which reveals that the accuracy of the change maps is consistently high.

Aggregated to the community-level, social survey of household data provides a comprehensive perspective additionally to EO data. The predetermined hot spots of degraded and successfully recovered areas were investigated. Thus, the study utilized a well-designed questionnaire to address the factors affecting land-cover dynamics and the possible solutions based on local community's perception.

At the operational structural forest stand level, the rationale for incorporating these analyses are to offer a semi-automatic OBIA metrics estimates from which forest attribute is acquired through automated segmentation algorithms at the level of delineated tree crowns or clusters of crowns. Correlation and regression analyses were applied to identify the relations between a wide range of spectral and textural metrics and the field derived forest attributes. The acquired results from the OBIA framework reveal strong relationships and precise estimates. Furthermore, the best fitted models were cross-validated with an independent set of field samples, which revealed a high degree of precision. An important question is how the spatial resolution and spectral range used affect the quality of the developed model this was also discussed based on the different sensors examined.

To conclude, the study reveals that the OBIA has proven capability as an efficient and accurate approach for gaining knowledge about the land features, whether at the operational forest structural attributes or categorical LU/LC level. Moreover, the methodological framework exhibits a potential solution to attain precise facts and figures about the change dynamics and its driving forces.

KURZFASSUNG

Da das Waldressourcenmanagement hierarchisch strukturiert ist, beschäftigt sich die vorliegende Arbeit mit der natürlichen Waldbedeckung auf verschiedenen Abstraktionsebenen, das heißt insbesondere mit der Ebene der kategorischen Landnutzung / Landbedeckung (LU/LC) sowie mit der kontinuierlichen empirischen Abschätzung auf lokaler operativer Ebene. Da zurzeit kein Sensor die Anforderungen aller Ebenen der Bewertung von Waldressourcen und von Multisource-Bildmaterialien (d.h. RapidEye, TERRA ASTER und LANDSAT TM) erfüllen kann, wurden zusätzlich andere Formen von Daten und Wissen untersucht und in die Arbeit mit eingebracht. Es wurde eine objekt-basierte Bildanalyse (OBIA) in einer destabilisierten Region des Blauen Nils im Sudan eingesetzt, um nach möglichen Lösungen zu suchen, erforderliche Informationen für die zukünftigen Waldplanung und die Entscheidungsfindung zu sammeln. Außerdem wurden die räumliche Heterogenität, sowie die sehr schnellen Änderungen in der Region untersucht. Dies motiviert nach effizienteren, flexibleren und genaueren Methoden zu suchen, um die gewünschten aktuellen Informationen zu erhalten.

Das Konzept von OBIA wurde als Substitution-Analyse-Rahmen vorgeschlagen, um die Mängel vom früheren pixel-basierten Konzept abzumildern. In diesem Sinne untersucht die Studie die beliebtesten Maximum-Likelihood-Klassifikatoren des pixel-basierten Konzeptes als Beispiel für das Verhalten der spektralen Klassifikatoren in dem jeweiligen Datenbereich und der Region. Im Gegensatz dazu analysiert OBIA Fernerkundungsdaten durch den Einbau von Wissen des Analytikers sowie kostenlose Zusatzdaten in einer Art und Weise, die menschliche Intelligenz für die Bildinterpretation als eine reale Darstellung der Funktion simuliert. Als ein Segment einer Basisverarbeitungseinheit wurden verschiedene Kombinationen von Segmentierungskriterien getestet um ähnliche spektrale Werte in Gruppen von relativ homogenen Pixeln zu trennen. An der kategorische Subtraktionsebene wurden Regeln entwickelt und optimale Eigenschaften für jede besondere Klasse extrahiert. Zwei Verfahren (Rule Based (RB) und Nearest Neighbour (NN) Classifier) wurden zugeteilt um die segmentierten Objekte der entsprechenden Klasse zuzuweisen.

Außerdem versucht die Studie die Fragen zu beantworten, ob OBIA in feiner räumlicher Auflösung grundsätzlich genauer ist als eine gröbere Auflösung, und wie beide, das pixel-basierte und das OBIA Konzept sich in einer relativen Genauigkeit als eine Funktion der räumlichen Auflösung vergleichen lassen. Diese Arbeit zeigt insbesondere, dass das OBIA Konzept eine fortschrittliche Lösung für die Bildanalyse ist, da die Genauigkeiten - an den verschiedenen Skalen angewandt - im Vergleich mit denen der Pixel-basierten Konzept verbessert wurden.

Unterdessen waren die berichteten Ergebnisse der feineren räumlichen Auflösung nicht nur für die beiden Ansätze konsequent hoch, sondern durch das OBIA Konzept deutlich verbessert.

Die schnellen Veränderungen und die Heterogenität der Region sowie die unterschiedliche Datenherkunft haben dazu geführt, dass die Umsetzung von Post-Klassifizierungs-Änderungserkennung besser geeignet ist als radiometrische Transformationsmethoden. Basierend auf thematische LU/LC Karten wurden Serien von optimierten Algorithmen entwickelt, um die Dynamik in LU/LC Einheiten darzustellen. Deshalb wurden für Detailänderung "von-bis"-Informationsklassen sowie Veränderungsstatistiken erstellt. Ferner wurden die erzeugten Änderungskarten bewertet, was zeigte, dass die Genauigkeit der Änderungskarten konstant hoch ist.

Aggregiert auf die Gemeinde-Ebene bieten Sozialerhebungen der Haushaltsdaten eine umfassende zusätzliche Sichtweise auf die Fernerkundungsdaten. Die vorher festgelegten degradierten und erfolgreich wiederhergestellten Hot Spots wurden untersucht. Die Studie verwendet einen gut gestalteten Fragebogen um Faktoren die die Dynamik der Änderung der Landbedeckung und mögliche Lösungen, die auf der Wahrnehmung der Gemeinden basieren, anzusprechen.

Auf der Ebene des operativen strukturellen Waldbestandes wird die Begründung für die Einbeziehung dieser Analysen angegeben um semi-automatische OBIA Metriken zu schätzen, die aus dem Wald-Attribut durch automatisierte Segmentierungsalgorithmen in den Baumkronen abgegrenzt oder Cluster von Kronen Ebenen erworben wird. Korrelations- und Regressionsanalysen wurden angewandt, um die Beziehungen zwischen einer Vielzahl von spektralen und strukturellen Metriken und den aus den Untersuchungsgebieten abgeleiteten Waldattributen zu identifizieren. Die Ergebnisse des OBIA Rahmens zeigen starke Beziehungen und präzise Schätzungen. Die besten Modelle waren mit einem unabhängigen Satz von kreuz-validierten Feldproben ausgestattet, welche hohe Genauigkeiten ergaben. Eine wichtige Frage ist, wie die räumliche Auflösung und die verwendete Bandbreite die Qualität der entwickelten Modelle auch auf der Grundlage der verschiedenen untersuchten Sensoren beeinflussen.

Schließlich zeigt die Studie, dass OBIA in der Lage ist, als ein effizienter und genauer Ansatz Kenntnisse über die Landfunktionen zu erlangen, sei es bei operativen Attributen der Waldstruktur oder auch auf der kategorischen LU/LC Ebene. Außerdem zeigt der methodischen Rahmen eine mögliche Lösung um präzise Fakten und Zahlen über die Veränderungsdynamik und ihre Antriebskräfte zu ermitteln.

Chapter 1 INTRODUCTION

1.1. Background and motivation

1.1.1. Overview

Forests are crucial to human survival and well-being. Therefore, human needs and sustainable development are the main perceptions directing forest sector development. These two principles are hardly interrelated for the attainment of balance between community's rising demands for forest good and services, and the conservation and development of forest resources. These concepts have been expressed in forest management by sustainability, which was defined by UNCD (1992) as "*Forest resources and forest lands should be sustainably managed to meet the social, economic, ecological, cultural and spiritual needs of present and future generations*".

The rural areas of Sudan, as well as much of its urban areas, rely on forests. Blue Nile region constitutes an important area of forest resources in the Sudan, where the forests play a significant roles in the economy through provision of a variety of goods and services. They are mainly source of sawn timber, fuel wood, charcoal, and construction materials from local to national levels, in addition to many other non-wood forest products as a main source of income and livelihood for the rural poor people (Deafalla, 2012). In spite of the fact that dry-land forests are not well-known for their export-oriented timber production; Sudan is a major producer of Gum Arabic for decades, producing more than 80% of the world market (Abdelgalil, 2005). Moreover, forests provide a variety range of environmental services (e.g. protection against desert creep, agricultural land deterioration, protection of the rivers and their tributaries against erosion, soil amelioration, wildlife sanctuaries, etc.), and are as well important for cultural and religious heritage and traditional practices.

There are several challenges the forest sector in the Sudan is facing which imposes the needs for well-designed information systems and management plans. One of these challenges are changes in land use/land cover (LU/LC) particularly due to deforestation and land degradation. In spite of LU/LC and its dynamics serves as one of the major input criteria for sustainable development

programs, currently, unregistered land covers almost about 85 to 90% of the land area in Sudan, while the remaining part is a private ownership, which is restricted to the registered rights offered before the implementation of the Unregistered Land Act in 1970. Before that time, the majority of the area was forest and grassland, which used communally for pasture and traditional farming under customary land laws (Agrawal, 2007). In this form of use, the right to cultivate an area of newly opened land became vested to the farmer who cleared it for use. This condition no longer exists, when the government disregarded the land used by customary laws, which were unregistered lands, forest and waste lands which the government managed. Subsequently, large areas were leased to individuals to be used for mechanized rain-fed agriculture, while majorities, whom used the land in the past for traditional farming, were not allowed to use the land. Since then, most of the natural land cover was dramatically destroyed as the issued act greatly influenced the exploitation of the land during the past decades (Elsiddig, 2004). Accordingly, as an absence of effective land-use plans are clear, an accurate, cost-effective and up to date knowledge about LU/LC patterns, in terms of their distribution, magnitude, and changing proportions, are highly demanded by legislators, planners, and local to national officials to construct better land use policy.

1.1.2. Deforestation and land degradation

The international concern about forest cover changes is motivated not only by the irretrievable imbalance in the natural environment, but also from the perspective that it is a destructive process in which the economic feasibility is lower than the environmental losses. Deforestation is a complex ecological and socio-economic process caused by a number of anthropogenic and natural factors. In present, global land cover is altered principally by people and their direct activities such as agricultural expansion, fuel wood collection, forest harvesting, mismanagement, urban and suburban construction and development (Myers, 1994). In Sudan, unsustainable wood harvesting and uncontrolled expansion of mechanized rain-fed agriculture inside forest land as well as a growing pressure on lands used for shifting cultivation has led to large-scale deforestation and land degradation. These changes in natural resources have gained attention as a result of the potential effects on climate change and subsequent desertification, erosion, increased run-off and flooding, increasing CO² emissions, climatological effects and biodiversity loss, in addition to other indirect impact such as migration and poverty (Mas, 1999; Williams, 2006).

As deforestation and land degradation are dynamic, interactive processes that grown and vary over time and place, the quantification and specifying the location of these dynamics remain an important aspect for such deteriorating regions. It is fundamental in forest management for the control of natural forest cover changes to identify the trends, rate, magnitude, and to specify the locations of these changes to find out how and why they developed (naturally or as a result of anthropogenic interventions) and to understand the specific driving forces, toward the best solutions to sustain our resources.

Based on the previous inventories conducted in order to study the extent, composition and changes of forest resources in Sudan, either partially conducted or are incomplete, it has been clearly observed that there an obvious change in the forest cover in the Sudan, and is evidently research has proven for declining forest resources and warned of expected bad consequences (e.g. FAO and FNC, 1998; Dawelbait *et al.*, 2006; FNC, 2007). Abdelgalil (2005) estimated the total decline in forest cover proceeds at a variable annual rate between 1-5% standing in an average rate for the past decade of -3% in the Sudan. A huge gap between afforestation and deforestation was also shown, which is expected to stand at 1:32 respectively. The most recent report available for the extrapolation of forests resources provided by FRA (2010), states that the forest area declined from 76.4 million ha in 1990 to 69.9 million ha in 2010, with an annual decline rate of -0.9% (table 1.1).

Table 1-1: Old united Sudan forest cover, source FRA 2010

Type of land/water	Area (000 ha)			
	1990	2000	2005	2010
Forest	76 381	70 491	70 220	69 949
Other wooded land	58 082	54 153	52 188	50 224
Other land	103 137	112 956	115 192	117 427
Inland water bodies	12 981	12 981	12 981	12 981
Total area	250 581	250 581	250 581	250 581
Forest area %	32.1	29.7	29.6	29.4
Annual deforestation rate	-959 -1.4%	-589 -0.8%	-589 -0.8%	-542 -0.7%

From the above mentioned statistics it has been clearly observed that the natural forests are being dramatically destroyed at an alarming rate threatening most of the local communities who rely almost totally on forests for their everyday life and income generation. Despite the importance of forests from one side, and the massive changes from the other side, Sudan has never conducted a complete national forest inventory. AFRICOVER was the only consistent formulated project to meet the demand of homogeneous database for African countries based on remotely sensed data and visual interpretation, which has been operational in the period 1995-2002 and was intended to cover ten countries. A local operational level there are the regular inventories of forest reserves as a basis for management plans, which are conducted utilizing conventional terrestrial sampling technique. The current status of natural forest cover can only be extrapolated from these uncertain surveys, as well as those made by FRA through FAO projects (1990, 2000, 2005 and 2010).

1.1.3. Remote sensing and forest resource assessment

As described above, typical updating of the LU/LC is still mainly based on costly and time consuming terrestrial sampling technique and visual and manual interpretation of remote sensing data as performed once for the part of the country in the 1990s by the AFRICOVER project, dealing with land cover at small scale, disregarding the operational at local scale level.

The challenge of image-based digital change analysis is the ability of the existing systems to automatically or semi-automatically determine, within specific time intervals whether there is change or not, and to locate the spatial distribution and the extent of the change as well as to quantify the trend and magnitude of the dynamics more or less precisely (Hall and Hay, 2003; Zhou *et al.*, 2008). The synthesis information needed for LU/LC change analysis is diverse. Although LU/LC changes can be monitored by conventional terrestrial inventories and surveys, space- and air-borne remote sensing facilitates a cost-effective way for detecting change, as it can explicitly reveal spatial patterns of LU/LC change over a large geographic area in a recurrent and consistent way (Zhou *et al.*, 2008). Thus, remote sensing provides a valuable contribution to document LU/LC changes at local, regional and global scales since the 1970s (Lambin *et al.*, 2003), as well as the potential capability for the identification of driving forces responsible for such changes.

Despite the importance of LU/LC change detection as an environmental variable which supports environmental planning, resources management, and public policy decision making, the scarcity of information about LU/LC and its dynamics is clear. Meanwhile, remotely sensed data are inherently suited to provide an accurate, cost-effective and up to date source of information about LU/LC and its dynamics. Therefore, this paucity is particularly related to the scarcity of efficient and accurate LU/LC information extraction methods (Foody, 2002; Estes and Mooneyhan, 1994). From the above mentioned perspective, it appears that an innovative approach for the interpretation of increasing availability of advanced remotely sensed data to provide valuable spatial information on change (Lu *et al.*, 2004; Rogan and Chen, 2004), and ultimately, this information into usable knowledge, is the highest priority for remote sensing applications (Franklin, 2001). Moreover, the development of the applications and interpretation approaches should follow the acceleration of advanced technologies and data available.

There are various tasks that can be accomplished in the visual interpretation that is performed manually by a human interpreter. Previous researchers such as Campbell (2002) and Lillesand *et al.* (2008) have sorted these tasks into classification “assigning objects, features, or areas to classes based on their appearance on the image”, detection “determining the presence or absence of a feature”, recognition “assigning an object or feature to a general class or category”, identification “specifying the identity of an object with enough confidence to assign it to a very specific class”, enumeration “listing or counting discrete items visible on an image”, measurement “dealing with objects and features measurement in terms of distance, height, volume or area, etc.”, and delineation “drawing boundaries around distinct regions of the image characterized by specific tones or textures”. Despite its diverse applications and precision, it is tedious and time consuming. Therefore, powerful line of thought in remote sensing is to develop interpretation approaches toward the automation of image interpretation process in a way that imitates human intelligence (Curran, 1985). Hence, many researchers (as e.g. Hay and Castilla, 2008; Lang, 2008; Blaschke, 2010) focused on a form of remote sensing known as an object-based image analysis (OBIA), that is methods and tools that adequately replicate human interpretation of remotely sensed data in automated/semi-automated ways. Recently, OBIA techniques have gained a lot of attention as an alternative analysis framework that can mitigate the weaknesses associated with the past dominant pixel based approach. It is based on the assumption that image objects offer features at hierarchical spatial levels, and exploit image

information more intelligently for mapping LU/LC, as it is much closer to real-world features than discrete pixels (Gamanya *et al.*, 2007).

As a result of the hierarchical nature of forest planning, LU/LC mapping has to be structured with certain amounts of detail at certain abstraction levels. Single-level approaches may be insufficient (Csaplovics, 1992), while a hierarchical approach is likely to be a more efficient way of producing adequate results at different levels of details. In the perspective of remote sensing as a primary data source to fully understand, monitor, model and manage the interactions between different levels, three elements are needed (Hay *et al.*, 2003):

- Remote sensing data contain sufficient details to identify surface features in a hierarchical manner;
- Methods and theories provide a capability to discover pattern components, real-world features at their respective scale of representation;
- Respective features can be connected in an appropriate hierarchical structure.

Therefore, an OBIA approach might provide a methodological framework of computer-based analysis for complex environment, possibly in a multi-level object hierarchy, based on spectral, spatial and structural information available on objects (Benz *et al.*, 2004; Lang, 2008).

Based on the previously mentioned background, the present study attempts to automate the interpretation process with its broad perspective (i.e. classification, measurement, enumeration, delineation, recognition, and identification) at various hierarchical levels of details. More specifically, rules to identify and classify real-world features at different abstraction levels of detail on the basis of human knowledge and data available, as well as models at the operational level to be used and generalized for the estimation of *Acacia nilotica* forest stand parameters will be developed. Criteria for the validation of the above mentioned methods will be based on thematic quantitative site-specific and non-site-specific measures as well as model validation based on an independent set of field survey data, respectively. As a special task of classification, object-based post classification change detection, which is crucial issue in the updating of the information for sustainable management, was also examined.

From the above mentioned perspective, pertinent research questions to be tackled by this research are:

- Could an OBIA approach provide advances in mapping and monitoring patterns of LU/LC using optical multispectral imagery?
- Could the study develop an accurate model at the operational level based on the extracted information from the object(s) values of remotely sensed data to predict *Acacia nilotica* forest stand parameters?
- Is OBIA inherently more precise at finer than at coarser spatial resolution? How do both pixel-based and OBIA approaches perform in the relative accuracy as a function of spatial resolution?
- Could the proposed approach to detect precisely the spatial distribution of hot spots of degraded and successfully recovered areas?
- What is the rate and magnitude of forest cover change in the region during the period of study?
- What are the driving forces of forest cover changes?
- What are the possible solutions that may stimulate the restoration of degraded areas?

1.2. Research hypotheses

1. OBIA approach provides accurate and precise results for mapping, monitoring and modeling forest cover at various abstraction levels of details.
2. The forest cover of the study area has been significantly changed (deforested and reforested) during the period of the study.
3. Deforestation is caused mainly by human factors (land clearance for mechanized agriculture, firewood, charcoal making and grazing in relation to population growth and poverty), meanwhile the stable and on the way to recover areas are

often as a result of specific methods of land management.

1.3.Objectives

On the basis of lack in knowledge and weaknesses in method previously mentioned, the research aimed to develop and assess OBIA as an effective tool for providing an accurate and up-to-date information at different levels, which support decision making, planning and sound management of forests on a sustainable basis.

More specifically, the aims of the study are:

1. To develop and evaluate an OBIA segmentation and classification approach for mapping natural forest cover of a wide area of the Blue Nile region based on optical multispectral imagery.

This objective will be achieved by hierarchical LU/LC classification. Object based image analysis approach will be performed using optical multispectral satellite imagery and *eCognition* software. Nine LU/LC classes needed to be identified, i.e. agriculture (rain-fed), bare-land, cropland, dense-forest, scattered-forest, grassland, orchard, settlements and water body. Different segmentation strategies will be applied based on the OBIA paradigm that might be effective to separate similar spectral values into a basic of unclassified image objects in groups of relatively homogeneous pixels, based on shape and compactness criterion at different scales. There are mainly two methods which will be examined (rule-based (RB) and nearest neighbor (NN) classifiers) to assign segmented objects to their corresponding class. The final results are shown in maps and figures (chapter 4).

2. To assess the OBIA approach versus the traditional per-pixel approach utilizing two different spatial resolutions.

A well-known maximum likelihood (ML) classification algorithm in pixel based approach will be applied to examine if the spectral properties of the discrete pixels alone can be used to discriminate between classes effectively. By a combination of remotely sensed data (i.e. Aster and RapidEye) and the field survey data, the nine respective LU/LC classes are distinguished. Training samples representing the typical spectral patterns for each LU/LC class will be defined. Then the quality of the results will be assessed by an independent set of test samples (chapter 4).

In order to assess the quality of the results obtained by the object based approach, the same set of testing samples which have been used to assess the above mentioned approach have to be introduced to the OBIA approach to generate Training and Test Area (TTA) Masks. Therefore, the classification results as well as the validation statistics are shown and compared.

3. To determine the magnitude and patterns of temporal LU/LC change.

This objective will be achieved by utilizing three consecutive optical multispectral images, two LANDSAT TM images of 1990 and 1999 as well as TERRA ASTER image of 2009 to evaluate forest cover dynamics during the period 1990 to 2009 (chapter 5). The method adopted in this research consists of a cross operation of classified images of different dates, which utilize the overlaying images for comparison towards change detection. A new layer of segments will be created represent the change areas as well as the overlapping areas of each pair of classified images. The proposed results might contain change “from-to” information classes. Moreover, the developed approach might allow the operator to effectively know the spatial pattern of change, the trend and magnitude of the dynamics of change which have occurred for each of the classified LU/LC classes. Subsequently, the change maps resulting from cross operation will be validated.

4. To identify key factors responsible for changes that may provide recommendations to formulate a recovery plan to restore deforested areas.

This objective will be achieved based on socio–economic data in form of social survey of households combined with spatiotemporal object based image analysis. Aggregated to the community-level, social survey of household data provides a comprehensive perspective to the Earth Observation (EO) data for a predetermined hot spots of degraded and successfully recovered areas. Thus, the study will utilize social survey of household through a well-designed questionnaire based on multi-choice and open ended questions in order to address the factors affecting land cover dynamics based on the perception of local communities. Population Proportional to Size (PPS) sampling technique has been applied to collect 120 questionnaires distributed on selected villages from the study area. These data are coded, interred and analyzed using the Statistical Package for the Social Sciences (SPSS) software.

5. To develop a model based on remotely sensed data to estimate *Acacia nilotica* pure stand structural attributes.

This objective will be achieved by an interactive processing of Aster and RapidEye imagery extracted metrics against forest inventory parameters at plot-level. Initially the image has to be segmented to achieve meaningful preliminary units. The following steps allow for the prediction of structural attributes of *Acacia nilotica* pure stands. Subsequently, two main sets of analyses will be undertaken. Firstly, based on the computed object features, the association between various image metrics and forest structural characteristics using Pearson's correlation coefficient will be addressed. Secondly focus will be laid upon the higher correlated forest attribute to develop a model by analyzing their relationship with the extracted image metrics using regression models. The selected models will be validated by randomly selected field survey data. In the final stage, the validated model will be used to produce the quantitative forest structure map.

6. To develop future forest planning in the study area by providing tools that facilitate forest management on a sustainable basis.

This objective will be achieved by providing recommendations for the legislators, planners, and local to national officials based on the potentiality of the expected output to be integrated in the future forest planning and decision making (chapter 8).

Chapter 2 STUDY AREA

2.1.Overview

This chapter provides a short description of the study area, which demonstrates the general characteristics of the Blue Nile region in means of its geographic location, climate, topography and vegetation cover, in addition to specific characteristics of the selected sites for the proposed study.

2.2.Introduction to the study area

2.2.1. General description

Sinnar state is one of the 16 states of the Republic of Sudan (figure 2.1). It has an area of 1,084,600 hectares, an estimated population of 1,270,500 capita according to the 2008 census, and is growing at the rate of 2.6% per annum. By projection, the present population was 1,402,000 capita. Sinnar is the capital of the Sinnar State. Another significant town is Sinja, which was the capital of the state till a few years ago. The main economic activity is cultivation within the irrigated schemes besides seasonal rained-fed agriculture. The state is located in the central-east of Sudan. It lies between latitude 12.5 – 14.7° N and longitude 32.9 – 35.4° E, it shares its borders with the Gezira State in the North, White Nile and South Sudan in the west, Gadarif State in the east and Blue Nile State in the South. The most important feature in the state is a Blue Nile valley (Arabic = Bahr Azraq), were the main forests, residential areas and horticultural land lie on the river banks along the basin from south-east to north-west.

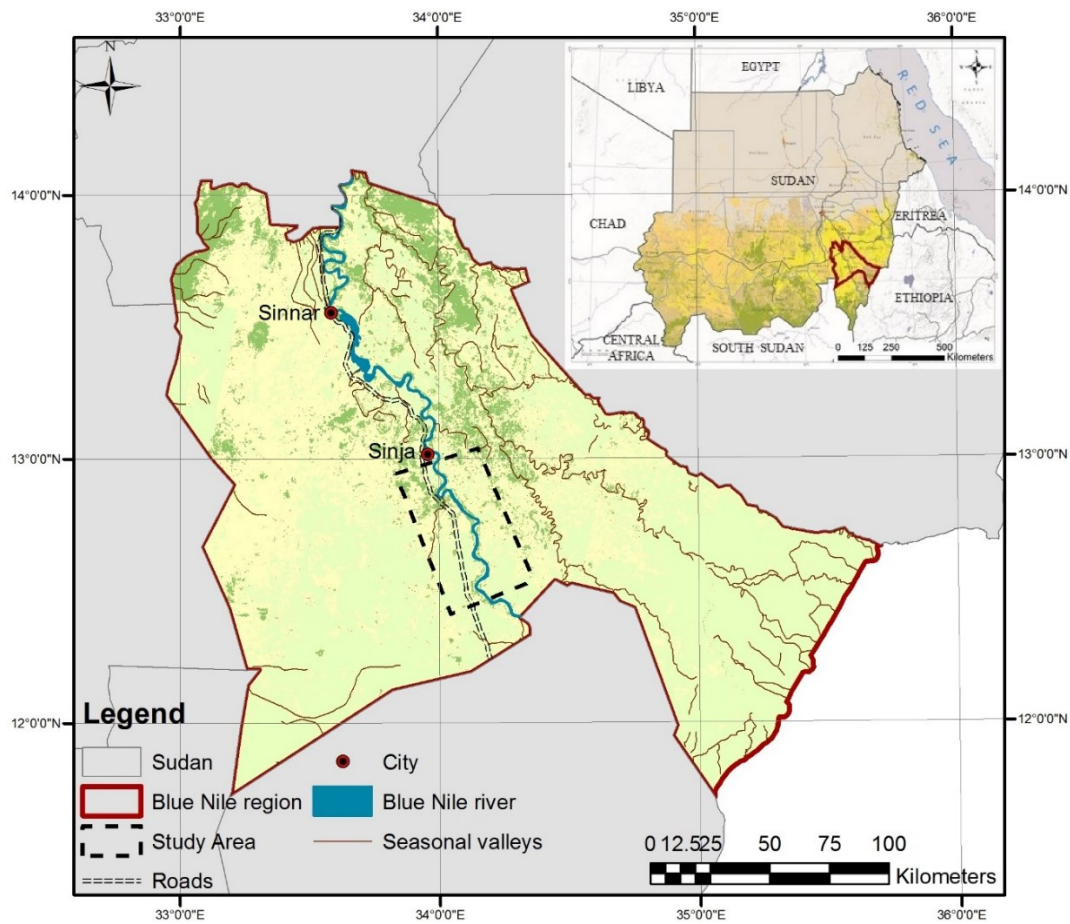


Figure 2-1: Location of the study area (developed by the author)

2.2.2. Vegetation

The most accurate and widely used classification of the vegetation cover of the Sudan was made by Harrison and Jackson (1958), while the general description of the ecological zones consists of; desert, semi desert, low rainfall savannah woodland, high rainfall savannah woodland, flooded areas and mountain vegetation. Sinnar State lies in the zone of a low rainfall woodland savannah. Accordingly the main vegetation communities of the study area are described as follow:

Bush land

1) *Acacia mellifera* and *Cadaba rotundifolia* often with association of mixed areas of *Cadaba rotundifolia* and *Boscia senegalensis*. The bushes and small trees of *Acacia mellifera* and the associated woody species range from 2 to 4 m height. Woody vegetation is generally open with scrubby patches and more or less extensive thickets separated by stretches of short grasses. The

common grasses are *Tetrapogon spathaceus*, *Sehima ischaemoides* and *Beckeropsis nubica*. *Acacia mellifera* may be locally absent. In this case *Cadaba rotundifolia* bush land or open grassland, composed mainly of the annuals *Cymbopogon nervatus* and *Sorghum purpureosericeum*, ranging from 0.6 to 0.9 m height, or on low-lying soils, of the perennial *Ischaemum afrum*, are found.

II) *Acacia nubica* bush land, often found with scattered *Calotropis procera*, distributed around the residential areas on upper part of *Blue Nile* valley (*Karab*). This form normally grows on clay plain soils. The bushy *Acacia nubica* stands raise 1.2 to 1.5 m height and the canopies frequently are closed gives a continuous low thicket. Its distribution seems clearly associated with disturbance, particularly with livestock movements.

III) Riverain thickets and bush land, mainly found along the bank of the *Blue Nile*, which occurs commonly on dark gray-brown sandy loams of the erosion slope (*Karab*) area close to the river. The species related to this area are *Ziziphus sp.*, *Cordia spp.*, *Cadaba rotundifolia*, *Crateva adansonii*, *Salvadora persica*, *Maytenus sp.*, *Piliostigma reticulatum*, *Grewia villosa*, *Balanites aegyptiaca*, *Boscia senegalensis*, *Maerua angolensis*, *Tamarindus indica*, *Ficus sp.* and *Gardenia sp.*

Woodland

I) This class of wood land is light and open, the dominant species is *Acacia senegal*. The trees are tapped extensively for gum (Gum Arabic) by the local people. The trees are 4-6m high, casting a tenuous shade, and are spaced 6-10m. The under storey of this class is similar to that of the above mentioned. This occurrence of *A. senegal* wood land has been noticed by Smith (1949) but is not recorded by Harrison and Jackson (1958).

II) The main species of this community are *Acacia seyal*, *Acacia fistula* and *Balanites aegyptiaca*, representing a wood land with areas of tall annual open grass land. This community was distributed mainly in the south of the state. It is wood land or sometimes wooded grass land (Gillman 1949) about 6-10m high with an understory of tall annual grasses ranging from 2 to 3 m height. This class found in the association of annual grasses include the tall (1-3 m) species *Sorghum purpureosericeum*, *Hyparrhenia confinis*, *Sorghum spp.*, *Cymbopogon nervatus*, *Rottboellia exalata*, *Barchiaria obtusiflora* and, in more dense wood land, *Beckeropsis nubica* and *Sehima ischaemoides*.

III) Broad-leaved deciduous woodland, being the characteristic vegetation on rocky hills and also occurs on the clay plain soils in the more southerly parts of the state, generally in areas where the slope of the terrain is more obvious than in the *Acacia seyal*, *Acacia fistiula* and *Balanites aegyptiaca* woodland. It may also occur in patches of more permeable (*Fuda*) soils in the *Acacia*-tall grass area.

Grassland

I) Wide shallow depressions of grey clay soil, annually flooded during the rainy season, consist mainly of open grassland of *B. obtusiflora* associated with the herbs *Ipomoea repens*, *Caperonia serrata*, *Cyperus spp.*, and the grasses *Eriochloa nubica*, *Panicum porphyrrhizos*, *Echinocloa colonum*, *Cloris gayana* and *Cynodon dactylon*.

Forest

I) *Acacia nilotica* forest. Single storey pure stands of *Acacia nilotica* about 15-20 m high, lie in seasonally flooded basins along the bank of the river and are sometimes found on similar flooded areas, such as drainage channels (*Khours*) and shallow surface catchment areas (*Hafirs*), on the clay plain inland from the Blue Nile. These forests, many of which are managed or regulated by the Forest National Corporation (FNC) for conservation objectives are as well of considerable economic importance as they provide hard wood round logs and sawn timbers.

2.2.3. Climate

The climate of the region is tropical and continental. The year is sharply divided between a very humid, rainy summer and autumn season and the intense dry winter and spring season. The winter months of December and January are relatively cold, with the average of 16° c to 35° c. while March to November are potentially very hot (20° c- 41° c) except in so far as the temperatures are reduced by evaporation in the rainy season (figure 2.2).

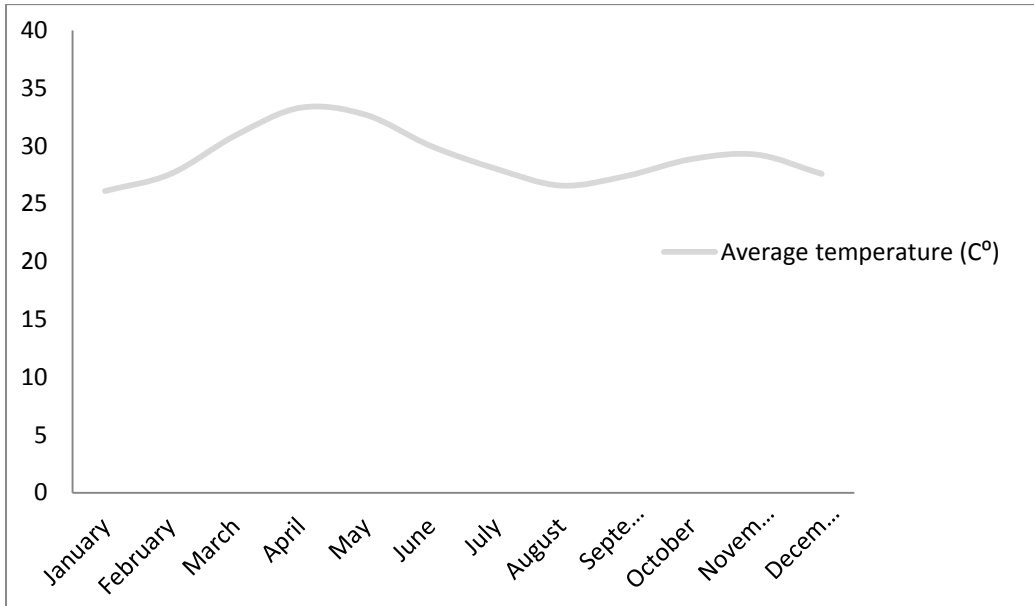


Figure 2-2: The average temperature during the year in the study area (source; NCDC)

The rainfall in the region comes as a result of the South Atlantic and Congo air masses, with little or no Indian Ocean influence. The study area lies in the zone in which rainfall increases to the south-east. The annual precipitation varies between 300mm to 500mm (figure 2.3) occurring between June to October and much heavily in August (figure 2.4).

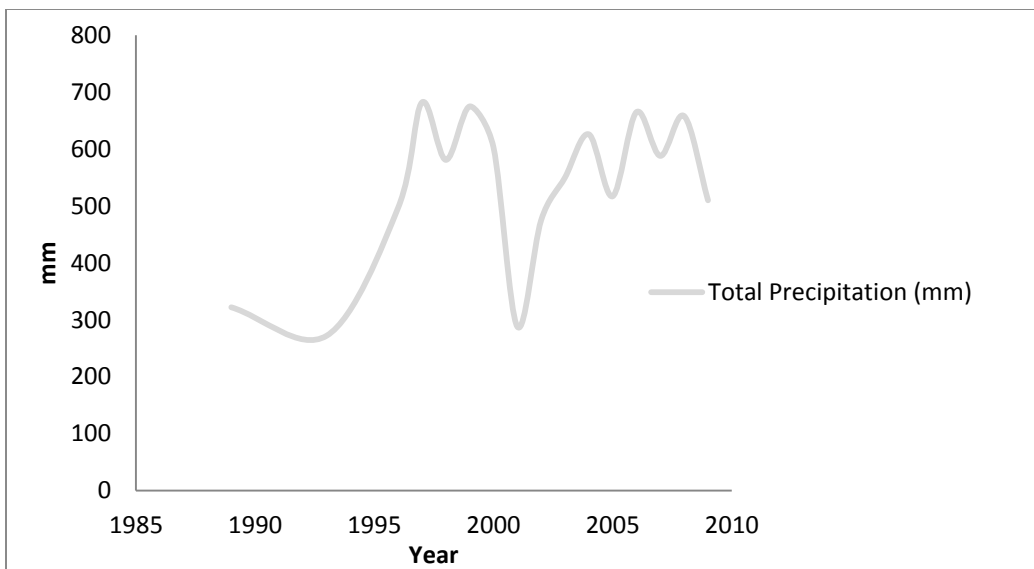


Figure 2-3: Rainfall pattern during two past decades in the study area (source; NCDC)

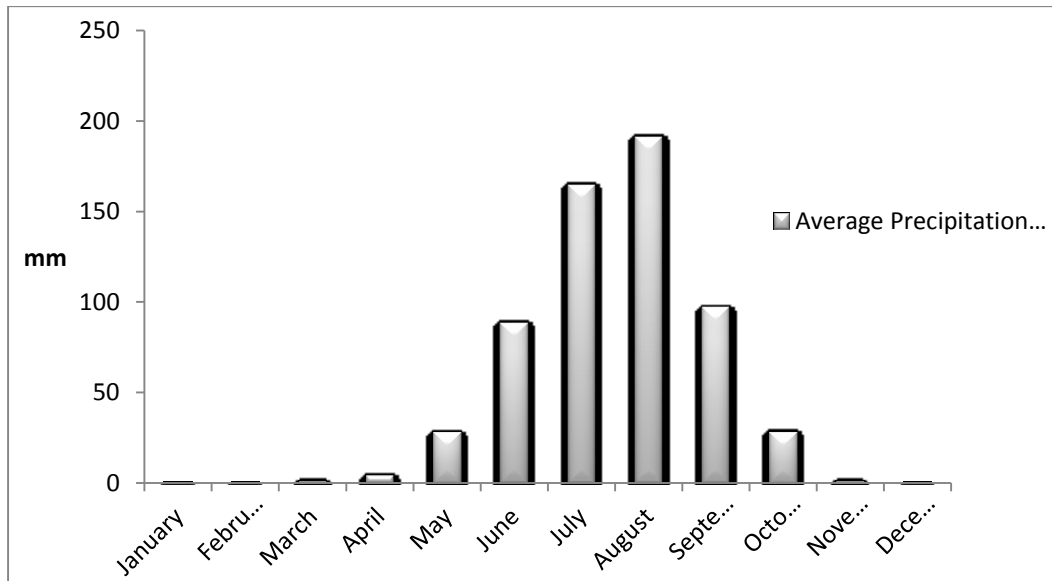


Figure 2-4: The average precipitation rate during the year in the study area (source; NCDC)

2.2.4. Topography and soil

The topography of the area is generally flat with some scattered mountain, of an altitude ranging from 1300 to 1500 feet above mean sea level.

The soil characteristics of the area in general are clays, alkaline dark coloured, which swells and sticky when it is wet, while it become cracks when it is dry. An exception was found in the slope (*Karab*) of the narrow eroded part of the Blue Nile River where the soils are sandy loams and clays, as well as permeable, fertile, sand-silt mixture (*Gerif*) in the nearest part along the banks of the Blue Nile valley.

2.3. Test sites

2.3.1. LU/LC level

The selected site, shown in figure 2.1 (site A), covers about 96.121 hectares, representing approximately 9 percent of the total area of the state, and is located in the centre of the state. This area covers most features in the state, which consist of; forests, horticultural land and settlements which lie near the bank of the Blue Nile River. Most of the entire area is grass land and rain-fed agriculture but it was dominated by natural forests till a few decades ago (figure 2.5). Many existing approaches of land cover extraction are based on spectral properties. The selected site

contains a large amount of entities that cannot be easily distinguished based on spectral properties. For instance, the main materials of buildings used are straw, wooden material and mud in addition to a large amount of trees grown in the settlements patches, which makes it difficult to separate them from other categories when using approaches based on pixel spectral value. Hence, the selected site provides a good opportunity to assess whether the proposed OBIA land cover mapping approach is more effective than other per pixel approaches such as the maximum likelihood algorithm.

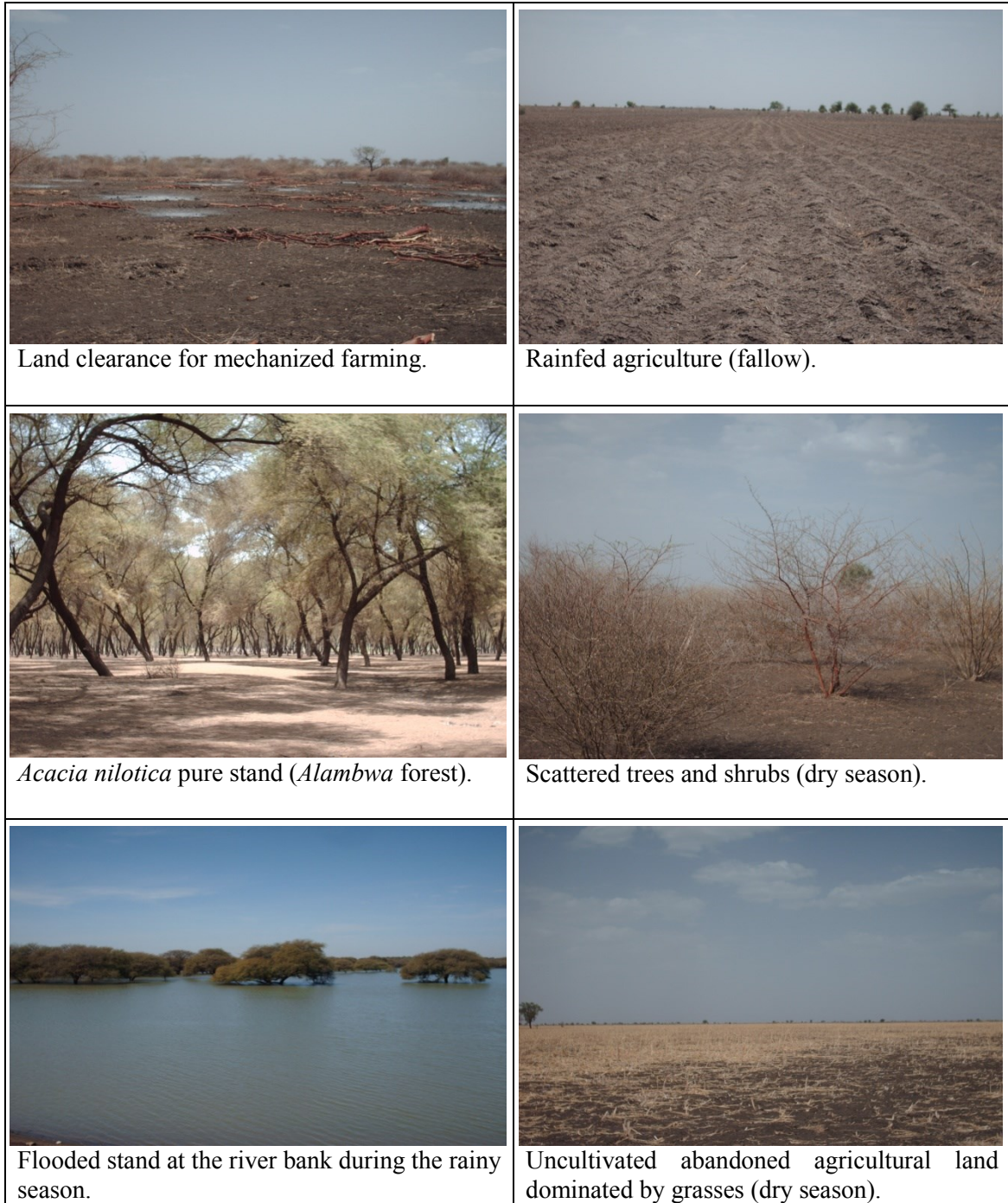


Figure 2-5: Some of the main features observed in the study area (photography taken by the Author)

2.3.2. Forest stand level

The second test site is *Alambwa* reserved forest, with an area of about 210 hectares (figures 2.1). The dominant species is *Acacia nilotica* “*Sunt*” trees, managed by FNC for thirty years sawn timber production. This forest stands like several other valuable neighbour stands distributed along with the Blue Nile valley, are affected by several factors like illegal cutting, expansion of horticultural land inside the forest area and by pathogen forest dieback. This dynamic situation needs up-to date and cost-saving methods to collect accurate information for reasonable management system. In this research EO data was used to evaluate the effectiveness of OBIA for forest stand parameters estimation, and assess the result versus collected field inventory data. A detailed description is given in section 4.3.6.

Chapter 3 THEORETICAL BACKGROUND OF OBIA APPROACHES AND FOREST RESOURCE ASSESSMENT

3.1.Overview

This part provides a background to the foremost theoretical and methodological contributions that correspond to the field of object based image analysis and its applications at different levels, i.e. small scale analysis of LU/LC pattern as well as forest structural attributes at stand level. Specific concern will be laid upon the focus on dry land forests of Sudan (i.e. Blue Nile region) and its dynamics based on the OBIA. The review focuses on topics that are of most significant for the study and within the sphere of responsibility of the sited authors.

3.2.Introduction

Remote sensing can be defined as studying an object without making any real contact with the object. More precisely, *“...remote sensing in the most generally accepted meaning refers to instrument-based techniques employed in the acquisition and measurement of spatially organized (most commonly, geographically distributed) data/information on some property(ies) (spectral; spatial; physical) of an array of target points (pixels) within the sensed scene that correspond to features, objects, and materials, doing this by applying one or more recording devices not in physical, intimate contact with the item(s) under surveillance (thus at a finite distance from the observed target, in which the spatial arrangement is preserved); techniques involve amassing knowledge pertinent to the sensed scene (target) by utilizing electromagnetic radiation, force fields, or acoustic energy sensed by recording cameras, radiometers and scanners, lasers, radio frequency receivers, radar systems, sonar, thermal devices, sound detectors, seismographs, magnetometers, gravimeters, scintillometers, and other instruments”* (Short, 2009).

This is a comprehensive definition of remote sensing in broad perspective. However, in this study remote sensing refers to imaging objects on the earth surface with the use of passive optical multi-spectral sensors (i.e. LANDSAT TM, TERRA ASTER and RapidEye). This study exclusively deals with the electromagnetic range of visible, near infrared and shortwave infrared radiation.

Meanwhile, the object based image analysis approach was introduced as a main processing method for the interpretation of natural features in the study area.

Previously image analysis techniques were solely based on pixel level which explores the spectral differences of various features of interest to be extracted as thematic information pixel per pixel. Due to complexity and spectral similarity in semi-arid areas, land cover mapping with remotely sensed data encounters serious problems when applying methods based on spectral information and ignoring spatial information. To overcome the failings of conventional pixel-based classification approach at facilitating precise LU/LC classification, researchers adopted a new method of remote sensing image analysis known as OBIA (Benz *et al.* 2004). Based on the assumption that the scene is composed of different sized real-world entities, and that a single resolution might not be appropriate to discriminate all classes within the image, OBIA was proposed to be an advanced solution to solve the issue (Gamanya *et al.*, 2007). The advantage of using OBIA is the capability to define rules for image object identification at various scales using spectral reflectance characteristics, as well as within object texture, shapes of features, context relationships, and ancillary thematic or continuous data of different spatial resolution. Recently, OBIA techniques gained a lot of attention as an alternative analysis framework that can mitigate the weaknesses associated with pixel based analysis, whereas the classification unit is a single pixel ignoring the spatial dimension of target feature under investigation. However, pixel-based image analysis experiences difficulties to discriminate between features that are significantly larger than pixel size (Aplin and Smith, 2008). In addition to the spectral properties of image pixels, the spatial extent of the feature under investigation is of great importance to the classification scheme (Flanders *et al.*, 2003; Hay and Castilla, 2006; Platt and Rapoza, 2008). A typical application observed in the study area involves extraction of features that are encompassing of multiple pixels from one hand (e.g. agricultural fields and Blue-Nile valley), and mixed with various entities from the other hand (e.g. residential areas and scattered forests). These features require classification of aggregative homogenous pixels that make up a feature. This is often defined as a segmentation process which is applied just before the classification (Martin *et al.*, 2001; Baatz *et al.*, 2004). Therefore, this study is an attempt to use the object based paradigm in order to group pixels of analogous spectral and spatial response, based on predefined criteria to extract features of interest.

3.3.Object based image analysis

OBIA approaches for analyzing remotely sensed data have been established and investigated since the 1970s, when pioneer researchers have been attempting to automate the object detection and feature extraction process. However rapid advances and its popularity have significantly increased in this field only over few past years (Opitz and Blundell, 2008; Lang, 2008; Blaschke, 2010). Main factor for the increasing interest in OBIA approaches include the growing availability of very high-resolution data and its associated huge amount of detailed features needed to be classified. Over the past decades, OBIA or other similar approaches have been mentioned by various acronyms; however the acronyms OBIA and GEOBIA (geographic object-based image analysis) are commonly used in recent literature.

OBIA provides a methodological framework of computer-based image analysis of a complex environment, possibly in a multi-level object hierarchy, based on spectral, spatial and structural information available in objects (Benz *et al.*, 2004; Lang, 2008; Niemeyer and Canty, 2003; Hay *et al.*, 2003). Objects are the primitives that form a scene, a photograph, or an image. For instance, when visualizing an image, it is explored by breaking it down into a variety of objects based on properties such as shape, texture, color, context, and others, in order to understand the content. The human brain has the innate capability to interpret the rich information content available in the scene and can intuitively identify various objects observed (in the scene). Several remote sensing techniques have been developed for analyzing images, such as supervised classification, texture analysis, contrast enhancement, and others that exploit the spectral responses of various features in different multispectral bands (Kumar, 2007). Significant progress has been made in the field of Artificial Intelligence (AI), fuzzy logic classification, rule-based (RB) classification from the expert systems domain, and neural nets by providing tools which emulate human perception and apply them to image analysis (Blaschke, 2010). Nowadays, most of these techniques are applied to pixels, limiting the use of these advanced technologies (Navulur, 2007). This study demonstrates how the newly developed object based paradigm can take advantage of these technologies and apply them to enhance the image analysis and interpretation process.

The idea behind object based image analysis is to develop and apply theory, methods, and tools for replicating and improving human interpretation of remotely sensed image data in an automated manner. Object based image analysis consists of aggregation of pixels into

homogenous segments. Subsequently these segments serve as input to a classification process, which utilizes spectral and spatial properties such as shape and object context to classify LU/LC (Blaschke *et al.*, 2011b). This means that the aggregated pixels directly influence the classification result although they might not represent the final features being investigated. The segments remain unchanged once they are created, and serve as basis for the subsequent step of classification (Baatz *et al.*, 2008). An object has, as compared to a pixel, in addition to spectral characteristics various other attributes such as shape, texture, and morphology, which can be used in image analysis (Navulur, 2007).

3.3.1. Image segmentation

Image segmentation is the first as well as the most important step in OBIA. The goal of this process is to divide the image into meaningful segments (or image objects). Moreover, image segmentation decreases the complexity by removing undesired details and then meanwhile provides a new vision of real-world objects which leads to an image with graspable objects. In remote sensing, the process of image segmentation is defined as “*an operation that creates new image objects or alters the morphology of existing image objects according to a given criteria*” (Darwish *et al.*, 2003). It is a preliminary step in object based image analysis. By image segmentation, the image is divided into meaningful, continuous, and contiguous segments. Segmentation principally means the grouping of picture elements by certain criteria of homogeneity. As the software deals with objects, not pixels, segmentation has to be made before the classification can be started.

The raw image data dose not contain explicit spatially discrete real-word entities. Instead, it is composed of pixel values, which maintain the latent attribute information of individual entities and the topological relationships in behind (Bassiri *et al.*, 2008). Despite this topological limitation of individual pixels, the segmentation process can cognitively cluster similar pixels based on their spectral and spatial properties into meaningful image-objects that correspond to real-world entities within the geographic extent of the image being investigated. In the object based approach, the image-objects assembled of individually resolvable entities occurred within an image which are perceptually produced by grouping the pixels. The definition of very high resolution satellite imaging systems is not fixed; it depends upon the application (Hay and Marceau, 1999). In other words, tens of meters may be described as a very high-resolution

satellite image, when the investigated feature is occurred within many pixels; in contrast low-resolution means that a single pixel is mixed with various entities of real-world features. In a remote sensing image, both cases occur concurrently. For instance, one meter spatial resolution may contain integrated reflectance from various tree components; in this context, it will be low resolution in relation to entities of individual tree measure. In contrast, even hundreds of meters may belong to high resolution in meteorological earth observation satellites; in this situation, each pixel is composed of more than one phenomenon. Consequently, a segmented image object tends to be an aggregation of harmonized pixels as a result of its unique source of investigated feature. Thus, when dealing with the issue of a fitting scale or the optimum resolution of image we must keep in mind what are the categories of target objects being investigated.

3.3.1.1. Image segmentation strategies

In general the segmentation techniques can be categorized into two main domains: knowledge driven (top down) methods and data driven (bottom up) methods. In top down approach the user already knows what he wants to extract from the image, but doesn't know how to perform the extraction. In this approach the input image is partitioned into many smaller homogeneous regions. By formulating a model of the desired objects, the system tries to find the best methods of image processing to extract them. Bottom-up methods assemble objects to create larger objects. As with clustering methods, in the beginning the generated segments are only image object primitives. It is up to the user to determine what kind of real world objects the generated image objects represent. Bottom-up methods perform a segmentation of the complete image. They group pixels to spatial clusters that meet certain criteria of homogeneity and heterogeneity (Baatz *et al.*, 2004).

Image segmentation may use thresholding (Weska, 1978), statistical classification, edge detection (Perkins, 1980), and region detection (Zucker, 1976), or any combination of these techniques. Each method has its own distinction, e.g., thresholding of the image pixels value is relatively simple, but ignores spatial information. In contrast, statistical approaches consider both the spectral and spatial information, but ignore spatial explicitness inherent in remote sensing imagery. Edge and region detection techniques are subjective which depends on the user's determination, while the integration of spatial properties is an advantage in both cases (Pavlidis and Liow, 1990).

As preliminary technique for image object information extraction, multiresolution segmentation algorithm was applied as a precursor to generate different abstraction levels. It is a bottom-up region-growing technique starting with one-pixel objects. In subsequent iterations smaller image objects are grown into larger ones (more pixels) based on the chosen scale, colour, and shape parameters, which control the limit of heterogeneity from the adjacent image objects. This procedure was developed to extract image objects at various ranges of resolutions (fine or coarse structures) in appropriate way. Moreover, it provides the ability to efficiently adapt the extraction of meaningful image object primitives to specific objectives and image data. This has the additional advantage that segments can not only be identified on basis of spectral properties but on a host of other features, as for instance geometrical, textural and class related features. In this sense, each image object has a large number of characteristic properties; the so-called object features or attributes, and moreover all the generated image objects are linked hierarchically to each other (Baatz *et al.*, 2004). The best segmentation result is that which provides optimal information for further processing (Gao *et al.*, 2007).

To obtain appropriate objects suited for the desired classification, the segmentation process can be controlled by defining which of the loaded layers are to be used with which weight and with inclusion of which of the following parameters (Willhauck, 2000; Hofmann, 2001):

- Weight of image layers; it can be used to more or less weight one or more image layers, influencing the creation of image objects.
- Scale parameter; it determines the maximum allowed heterogeneity within an object. For a given scale parameter, heterogeneous regions in an image will result in a higher number of objects as compared to homogeneous regions. The size of image objects can be varied by varying the scale parameter value.
- Colour; it defines the overall contribution of spectral values to define homogeneity. Moreover, it balances the colour homogeneity of a segment on one hand and the homogeneity of shape on the other.
- Shape; it is defined by the two parameters: smoothness and compactness. The smoothness factor can be used to optimize image objects for smoother borders, and compactness can be used to define the ratio between the perimeter of the

segment and the square root of its area (number of pixels it contains).

- Level; it determines whether a new generated image level will either overwrite a current level or whether the generated objects shall contain sub- or super-objects of a still existing level. The order of generating the levels affects the objects' shape (top-down vs. bottom-up segmentation).

3.3.2. Image objects hierarchy

Parametric statistical methods (e.g. maximum likelihood, minimum distance, Mahalanobis distance, etc.) are not designed to deal with data from different sources or at different hierarchical levels. Semi-arid areas are heterogeneous due to the overlap between land-cover features as well as the mixture between artificial and natural features. Advanced levels of structural information play a major role in LU/LC classification of such areas. Therefore, conceptual indicators have to be incorporated based on structural classification in order to achieve well-organized and accurate result.

One of the advantages of the object based approach is the possibility to build objects at various scales and extract features of interest at different resolutions. A practical example of such an approach would be classifying a large water body, such as the Blue Nile valley, at scale parameter of 20 and classifying other objects on 'land' parent class at much larger scales (i.e. 10 & 7), which allow for the separation of smaller water bodies related to other land-use classes. Using repeated segmentations with different weighting parameters, a hierarchical network of sensible image objects is assembled. Each object has knowledge of its neighbour-, sub- and super objects, which allows classification of relationships between objects at various levels. Ensuring hierarchical structure of the network, two rules are required (Willhauck, 2000);

- Object borders of higher levels are inherited by the sub levels.
- The segmentation process is bounded by super-object borders.

An early point for defining objects in LU/LC context may be to consider at which features are currently investigated. Many features with different sizes can be observed such as settlements, agricultural fields, roads, vegetative areas, water bodies, etc. However, some of these features are not likely to appear on a map with a unique round of segmentation and classification process. By

taking a close look at these objects, we can perceive that some of them are directly identified from their spectral attributes, such as vegetative areas and water bodies. Meanwhile, there are objects that consist of other conceptual characteristics, often extracted with thematically information developed by user's knowledge, such as residential areas, croplands and agricultural fields, which are commonly related to land use. A residential area may consist of mud and/or grass huts, concrete building, trees, footpaths, etc. It may be noticed that some objects can be treated based upon their spectral properties in some cases but considered by their conceptual characteristics in others. For instance, an immersed crop field can be misclassified as water based on its spectral properties, which can be reclassified in further processes by incorporation of textual and contextual properties. Therefore, since the spectral information alone is insufficient for classification of all LU/LC classes, spatial knowledge has to be introduced to enhance the resultant accuracy.

It is not easy task to understand the complex structure of natural systems. This structure, described as a “mosaic of patches”, requires a conceptual model identified by complex system theory (Hay and Marceau, 1999). Complex system theory is a way to explain the interaction of ecological systems are composed of large numbers of components which interact in a non-linear way and exhibit adaptive spatio-temporal properties (Hay *et al*, 2003). These components of complex systems are linked to each other in a hierarchical way in that they are built of sub objects and super objects, e.g. trees, compartment, stand, forest, vegetation type, etc. (Hay and Marceau, 1999). In perspective of a remote sensing as a primary data source to fully understand, monitor, model and manage the various interactions between these components, three elements are needed: (1) remote sensing data which contain a sufficient detail to identify surface features in hierarchical manner; (2) methods and theories which provide a capability to discover pattern components, real-world features at their respective scale of representation (Woodcock and Strahler, 1987); and (3) the potentiality to connect these features in appropriate hierarchical structure (Hay *et al*, 2003).

As a result of the hierarchical nature of forest planning, LU/LC mapping has to be structured with certain amounts of detail at certain abstraction levels. Single-level approaches may be insufficient, while a hierarchical approach is likely to be a more reliable way of producing an adequate result at different levels of details. On the other hand, the variation present within each level is usually significantly smaller than that between different strata. Hence, the hierarchical

classification improves classification performance by identifying the homogeneous classes with identical characteristics to be separated first and confused data later rather than classifying all classes at the same time.

Laliberte *et al.* (2007a) determined that the hierarchical segmentation approach is well suited for distinguishing features at different scales, where shrubs were segmented and classified at a fine scale and masked out, so that shrub-interspace vegetation could be analyzed at coarser scales. Other studies by Csaplovics (1992) and Gibbes *et al.* (2010) mention that the use of a hierarchical multi-scale approach for describing African savanna landscapes provides comprehensive and ecologically relevant information. On the other hand, sub-dividing the area into smaller homogeneous regions in a hierarchical approach minimises the risk of similarity-confusion among classes, which subsequently may increase the classification accuracy (Stewart and Lillesand, 1994).

3.3.3. Image object information extraction and feature measures

The synoptic view as well as large area coverage of remotely sensed data provides a complex scene content composed of target features in addition to an enormous amount of undesired information. In this point of view, feature extraction can be considered as the process of transforming high dimensional data into a low dimensional feature space based on an optimization criterion (Choi and Lee 2003). In other words, the non-representative features of the target objects, are disregarded while those which provide higher separability distances are maintained. Thus, great deal of interest was raised to manipulate the huge amount of data in image processing. The above mentioned methods of segmentation and hierarchical structuring of objects were applied to reduce the scene complexity, as far as possible, by matching the extracted information with real-world features.

In the context of LU/LC classification of semi-arid areas, many classes have similar spectral signatures, which stimulates the exploitation of other valuable information available in the images based on their spatial dimension. Conventionally, most of the digital image analysis approaches are performed only based on spectral information. Nowadays, high spatial resolution satellite imagery has become increasingly available. However, these data provide tremendous detail of surface features which complicates the analysis when using only spectral information.

Thus spatial information of the connected pixels has to be exploited. Therefore, it is not surprising that substantial research into integration of other reliable types of information into digital image analysis approaches has been promoted (Jensen, 2005). An astonishing advantage of the object based approach is related to the fact that it allows in addition to spectral properties to incorporate the spatial, contextual, textural and temporal properties for feature extraction based on image objects (Kumar, 2007). In this perspective, this information can be leveraged to improve/enhance the feature extraction process leading to a better discrimination of thematic information and to a more precise classification result. In summary, the object information about the target features may be obtained from imagery either on the basis of global image features, which describe an image as a whole (for example the number of image objects of a specific class) , or local features (for example the shape of an image object), which represent image object attributes (Benz *et al.*, 2004). Accordingly, the features used for classification can be divided into three main categories (Willhauck, 2000):

- Object features like colour, texture, form and area.
- Classification related features like relations to sub-objects, super-objects and neighbour objects
- Terms like Nearest Neighbour classifier or similarity to other classes.

The critical issue in image processing techniques is to manage the huge information available. In relation to the solely spectral information solely utilized in a per-pixel basis approach, the integration of the spatial dimension of the objects significantly expands the possibilities of image classification. Given the wide variety of potential features explains the object, it is indispensable to identify the most characteristic and significant features to describe the object classes of interest. Only a few object features describe a class and as the degrees of freedom increase, it become increasingly difficult to identify the optimum features among the massive number of available ones (Marpu *et al.*, 2008).

The determination of the appropriate object features in OBIA for class description can be based on previous user experience and knowledge (e.g. Laliberte *et al.* 2007a) or it can utilize feature reduction algorithms (e.g. Yu *et al.* 2006; Nussbaum *et al.*, 2006; Genuer *et al.* 2010; Tarantino and Figorito 2012). Pratt *et al.* (1997) divide features space reduction in two basic quantitative

groups: the prototype performance approach and the figure of merit. In the first case, the process consists of classifying segments using different combination sets of features. The best set of features is that which results in the highest classification accuracy. The inconvenience with the prototype performance is that many sets of features are possible and that the measure of performance indicators is dependent not only on the quality of the selected features but also on the classification and/or segmentation processes. In the second case, the method is related to the comparison of object separability by specific criteria. Here separability is evaluated by comparing sets of image object features, which involves the establishment of some functional distance measurements between sets of image features. Based on these approaches, several feature reduction or optimization methods have been used in conjunction with OBIA. Choi and Lee (2003), Herold *et al.* (2003) and Nussbaum *et al.* (2006) used the Bhattacharyya distance to assess the contribution by each feature, while Riedel *et al.* (2008) employed the Jeffries-Matusita distance for feature selection. Johansen *et al.* (2009) evaluated different visual and statistical assessment methods with various features for individual objects (i.e. feature space plots, box plots, band histograms, sample editor, feature viewer, and feature space optimization). Classification and regression tree algorithm for the selection of optimal features were applied by Yu *et al.*, (2006), Chubey *et al.*, (2006), and Laliberte *et al.* (2007a).

In addition, with spectrally homogeneous objects created by the segmentation process, both spectral values and spatial properties, such as layer values, shape, and texture can be explicitly exploited as object features to extract LU/LC classes.

3.3.3.1. Layer value features

As the main feature considered in this study is vegetation, and by reviewing the literature, the most prevalent method for discriminating vegetation classes from optical remote sensing data is through spectral properties. Plants have distinctive spectral signatures which are often modeled by combinations of reflectance measure, mainly in broad-band red and near-infrared channels (Csaplovics, 1984; Myneni *et al.*, 1995). Shape features can be very useful in urban image analysis (Thomas *et al.*, 2003), while vegetation cover in semi-arid areas are more defined by spectral and contextual features (Laliberte *et al.*, 2004). Spectral features provide information about the spectral response of segmented target objects, as detected by the sensor, and influenced by the segmentation process. This set of features initially constitutes the traditional information

derived from any type of optical satellite imagery. After the creation of image objects, the values of mean, standard deviation, minimum, maximum, range, sum and majority of the pixel values inside each object are obtained for each band in the input raster file (Ruiz *et al.*, 2010). In addition to the original spectral values, any combination, ratio, or transformation could be integrated as complementary thematic layers in the input image file to be analysed.

3.3.3.2. Texture features

The assumption behind methods applying texture technique is that the spectral properties of the adjacent pixels are highly correlated, and thus take superiority over those conventional techniques based on discrete pixel value, even with medium spatial resolution (e.g. Riggan and Weih, 2009; Fraser *et al.*, 2005; Whiteside *et al.*, 2011). Texture analysis is another means of integrating spatial information for identifying remotely sensed data. From the basic perspective, the concept is that textural and spectral features are highly correlated to each other. Spectral and textural features always exist in the image, although one property can dominate the other at times. The basic intuitively perceived relationships between these two features are the following. When a limited area patch of an image has slight variation (i.e., little variation of features of discrete brightness values) the dominant property of that area is spectral features. When a small area patch has a wide variation of features of discrete brightness values, the dominant property of that area is texture (Haralick *et al.*, 1973).

The texture of an image is related to the spatial intensity of the tonal values in the image, providing information about the spatial relationship between objects by means of brightness values. In different words, it determines the overall visual "smoothness" or "coarseness" of image patterns (Lillesand *et al.*, 2008). Features with similar spectral reflectance often can be discriminated based on their texture. An example would be the smooth texture of even-aged dense seedlings in *Acacia nilotica* forest as compared with the rough texture of uneven-aged/species natural forest.

3.3.3.3. Gray-level Co-occurrence Matrix (GLCM)

As a powerful source of information, texture features have been widely investigated in the field of remote sensing image analysis (Haralick *et al.*, 1973; Franklin *et al.*, 2000; Moskal and Franklin, 2002; Zhang *et al.*, 2004; Tzotsos *et al.*, 2008; Kim *et al.*, 2009). A considerable number

of quantitative texture features and approaches have been reported using different combinations of features and methodologies. Grey-level co-occurrence matrices (GLCM) got a lot of attention for deriving texture measures from images. A GLCM is a tabulation of how often different combinations of grey levels (brightness values) at fixed spatial relationship for a pair of pixels (reference pixel and neighboring) occur in an image (Haralick *et al.*, 1973). An initial assumption in GLCM is that all the texture information is contained in the spatial relationships between pixels of various grey level matrices. Therefore, all the textural features suggested are extracted from these gray level spatial-dependence matrices. Instead of window size in pixel based texture, and since an object based approach is used, it calculates all pixels of an image object. Only one GLCM is computed for each object, describing the co-occurrences of the pixel grey levels that are separated at a distance from the reference pixel inside the object, and considering the average value of four principal directions (0° , 45° , 90° and 135°). The measures more frequently exploited in GLCM include the angular second moment, entropy, standard deviation, contrast, correlation, and homogeneity (Jensen, 2005).

GLCM texture measures were widely investigated, especially with high resolution satellite imagery and aerial photos. As for example, Tuominen and Pekkarinen (2004) reported an enhanced classification accuracy over the method that utilize discrete spectral layers values. Moreover, Franklin *et al.* (2000) mentioned that the incorporation of texture measures improved the accuracy of higher resolution images more than lower resolution images.

3.3.3.4. Shape features

Based on the assumption, confusions might occur between spectrally generated classes as a result of similar spectral value, additional information is needed for their separability. One possibility is the incorporation of shape features. Shape feature refers to the general form, configuration, or outline of individual objects (Lillesand *et al.*, 2008), as for example asymmetry, border index, compactness, density, shape index, main direction, etc.). Shape features are highly considerable features which are very close to human perception. The majority of man-made features (e.g., agricultural fields, crop fields, residential areas, etc.) are characterized by a rectangular or quadratic shape with a specific range of lengths. However, a significant number of objects could be identified upon these feature types. One advantage for the object based approach is the fact

that, in many cases, the proposed result of most image analysis processes is the generation of real-world features, perfect in shape and perfect in classification.

As a result of fairly large pixel size in most of the dataset used in this study, the formation of fuzzy boundaries between neighboring objects became critical issue. Through the segmentation process the degree of brightness in most cases is an important criterion for creating meaningful objects. Hence, these fuzzy boundaries can be tackled with developed algorithms mainly based on brightness contrast of the objects of interest against their surroundings (Segl *et al.*, 2003).

3.3.4. Nearest neighbour classification

NN classifier is similar to supervised classification; the user should have a priori knowledge of the features present within an image. NN classifier utilizes the minimum distance to class means. With this classifier, training object is used only to determine class means for selected features; analysis is then performed by assigning an object to the nearest class mean (Kumar 2007). Therefore, representative training samples are required prior the implementation of classification process, guided with selected feature(s), normally multidimensional feature space, and the statistical analysis is performed on the multispectral bands data for each class.

Here the training samples are training objects (Yu *et al.*, 2006; Laliberte *et al.*, 2007a). As a result of uncertainty of small object samples to represent widely extended LU/LC classes, as well as the growing availability of multi-source data, the parametric classification schemes such as the well known ML classifier are not readily applicable in these cases (Srinivasan and Richards, 1990; Gong, 1996). From this point of view, in comparison to conventional pixel based approaches, NN classifier requires fewer training samples; one sample object already represents many typical pixel samples, and provides a new dimension of spatial relations between adjacent pixels for class description.

NN classifier supports an easy-click-and-classify approach guided by selecting typical objects as representative samples (Batz *et al.*, 2001), in so-called Training and Test Area (TTA) Mask. In other words, applying NN classifier as a classifier, image objects often have various membership values for more than one class, weighted from zero to one, and depending on the adjusted value of the nearest neighbor function slope, which calculates the fuzzy values depending on the distance of an image object to the nearest neighbour sample for each class. In this perspective,

classification result can be enhanced by editing the process; defining unclassified objects by declaring more object samples to represent correspondence classes, and correcting wrongly classified objects by add and/or remove samples from the feature space. Moreover, it has a considerable advantage of preserving the pixel value and its adjacent pixels relations of the original image which is useful for multi-levels of image classification. The use of NN classifier is well-suited to define multidimensional membership function when various features are intended to be utilized for a class description (Batz *et al.*, 2001). The perception behind that is: 1) NN classifier examines the relationship between object features favorably. 2) Increasing the feature dimensionality leading to overlap in the feature space which can be managed much easier with NN classifier. 3) NN classifier provides a quick and easy handling of multi-level class hierarchy.

LU/LC classification requires an easy-to-use, appropriate, transparent, and transferable utilization of remote sensing data. Therefore, an object-based NN classifier reported as a potential for novel approaches toward automation and standardization of the analysis of remote sensing data. In this perspective, a study conducted by Walker and Blaschke (2008) mentioned that the NN classifier provides an accurate classification scheme that was intended to be transferable to other area in the image or to other images with similar characteristics, in which slightly lower accuracies were achieved from the standardized classification results in eight test sites. Ivits and Koch, (2002) mentioned the capability of NN classifier toward automatic and standardized methodology for land cover classification in different regions, in their study they forced to utilize a modified set of training samples to optimize the result of misclassified areas, which they attributed that to the use of small size of the test areas and the spatial resolution of the LANDSAT TM images uses. Study conducted by Aguilar *et al.*, (2012) for land cover classification utilizing pansharpened and panchromatic GeoEye-1 very high spatial resolution imagery, reported that a percentage of 10% of training object samples for each class was sufficient for gaining good accuracies applying object-based supervised classification with the NN classifier.

Since samples are required for different classes in order to assign membership values, normally multidimensional feature space, therefore stepwise refinement strategy (elimination Strategy) was considered as a well-suited strategy with NN classifier method to reduce the number of required features to identify the target pair of classes. With this strategy less detailed classes with coarser resolution are identified first (see figure 5.4 in chapter 5), frequently with spectral features, and then deduce more detail classes from the coarse parent classes (see Lillesand *et al.*,

2008). Most likely this strategy leads to complete classification of all objects, but makes it required to describe all classes which it may not of main focus in the study (see for example Hofmann, 2001; Laliberte *et al.*, 2007b).

When the user has not experienced enough about the area under investigation to describe feature spaces, *eCognition* software provides a data mining functionality called Feature Space Optimization (FSO) so as to identify the best parameters useful for classification, relying on training samples. An appropriate range of features are required as an input, relying on the assumption that there is no correlation between the input variables (Kumar, 2007). This tool is an algorithm that compares the features of the selected classes finding an optimized combination of features which producing the largest average minimum distance between the training samples of different classes (user guide). Object statistics of the optimized selected features space are calculated based on the selected samples for each class, which are then applied for classifying all image objects based on their nearest Neighbor sample (Baatz *et al.*, 2001).

FSO tool provided the best combination of features for land cover classification, without setting thresholds (Tarantino and Figorito 2012). It is important to mention that this tool requires a predefined set of input features as well as representative training samples for well representation in the classification process. From this standpoint, the optimized features are directly affected by the selection of samples and object features; therefore the best classification result with NN classifier has to be achieved through an iterative procedure (Benz *et al.*, 2004; Baatz *et al.*, 2008; San Mlguel-Ayanz and Blging, 1996).

3.3.5. Rule based classification

Alternatively, instead of supervised classification based on training samples, the user's knowledge is used in rule based methods to perform a fuzzy or soft classification approach, which permit an object to be assigned to more than one class but with varying membership values (see Benz *et al.*, 2004; Baatz *et al.*, 2008; Kumar, 2007). A fuzzy rule-base is an arrangement of fuzzy rules, which combine different fuzzy sets. The simplest fuzzy rules are built by only one fuzzy set. The perspective behind this method assumes that the entire process of image analysis is characterized by the transformation of knowledge, and the class description of the image objects should meet the user's conceptual criteria generated from the real-world features (Lang, 2008).

RB method is a flexible way of classification which allows incorporating multisource information as guidance in the interpretation process (e.g. ancillary thematic or continuous layers and human knowledge). For example Xu and Yaping, (2010) incorporate Normalized Difference Vegetation Index (NDVI) to extract various vegetation classes. Geneletti and Gorte, (2003) combine aerial photographs with LANDSAT TM image to generate detailed land cover classes. While the high-resolution orthophotos were used to automatically identify and delineate suitable segments, the LANDSAT TM satellite image was used as a reference to classify the segments. Other study conducted by Jie Shan and Ejaz Hussain, (2010) using high-Resolution imagery for LU/LC mapping concluded that the better classification accuracy attributed to the use of meaningful objects combined with addition geographic information system (GIS) layers, which enhanced the result from 71.45% and 74% to 85.5% and 81.4% for the user and producer accuracies respectively. Moreover, the basis is available to analyze not only images but also texts from many different domains in addition to integrate the knowledge from various sources to support decision makers (Benz *et al.*, 2004; Zhang *et al.*, 2008).

A fuzzy expression in rule based method is frequently formulated with single-dimension membership function. This ambiguous labeling allows for various assignments of the objects (Mather, 2006). Whereas, an object has no match to necessary class description or it is not closely enough to the proposed class, then it should be described further with other conceptual condition to fulfill the requirement of the class criterion, if not, then assigned to different class later (Baatz *et al.*, 2001). Therefore, if a class of interest can be separated from other classes with a single or a few conceptual criteria, the application of rule based method is suggested otherwise multidimensional feature space based on samples with NN classifier is appreciated.

From the above mentioned perspective, unlike elimination strategy adopted with NN method, here each class depicted directly utilizing specific rule(s) to describe a class as accurate as possible. Therefore, the so-called “selective” strategy has to be utilized in this case to generate classes of interest, giving a fuzzy indication of whether an object belongs to the target class or not (Lillesand *et al.*, 2008). In different words, in this case only the classes of interest are described, while all other objects which do not meet the conditions of the described classes remain unclassified (e.g. Hofmann, 2001). Civanlar and Trussel, (1986) mentioned that the better knowledge about the real world features being modeled by the membership function, leads to better final classification result.

3.3.6. An application of object-based approach for mapping earth surface features

Since the 1970s remote sensing and GIS are becoming very popular and handy tools, at various levels, for resources monitoring, evaluation, planning and detection of the change of forest areas to meet the human demands and interests by sustainable management (Lepers *et al.*, 2005). To achieve sustainability, Franklin (2001) categorizes the applications in four themes that include classification of forest cover type, estimation of forest structure, forest modeling, and forest change detection. Therefore, this information it can be anticipated to be in ready-to-use format meeting the strategic, tactical, and operational planning from the regional to local scale. As forest management decisions are required at various levels, methods should be developed to provide unique discrete partitions of coarser scale land covers to be linked with individual forest stand structure. Nevertheless, most of the previous studies were performed to address each of these levels separately, while a little has been done to develop approaches that provide a well-structured levels of information in which way that coincide with its real world representation, and covers different points of view.

In the past few years a revolution of object based image analysis has been observed. The applications of this approach have been extended in various fields. It has been applied for forest mapping (Lennartz and Congalton, 2004; Johansen *et al.*, 2007; Kim *et al.*, 2009; Kim *et al.*, 2011), mapping of forest species composition (Leckie *et al.*, 2003), forest structural attributes estimation (Ozdemir *et al.*, 2008; Pascual *et al.*, 2008), mapping of agricultural fields (Geneletti and Gorte, 2003; Mueller *et al.*, 2004), urban area mapping (Hofmann, 2001; Segl *et al.*, 2003; Herold *et al.*, 2003; Thomas *et al.*, 2003; Blaschke *et al.*, 2011a), mapping of arid and semi-arid grasslands (Laliberte *et al.*, 2004), as well as at coarser scale LU/LC classifications (Gamanya *et al.*, 2007; Riggan and Weih, 2009; Huth *et al.*, 2012). The main matched findings of these studies were that OBIA classification:

- enables analysis and classification of surface features at hierarchical network with different object levels of different resolutions,
- mitigates confusion occurred in generated classes as a result of homogeneous image objects introduced to the classifier which reduce spectral variability within

land-cover classes (reducing salt-and-pepper effect), and

- enhances classification accuracies because of the capability to incorporate additional information such as temporal, morphological, contextual and textual object features in addition to spectral information

3.3.6.1. Land use/land cover (LU/LC) level

Land cover describes the biophysical characteristics of the Earth's surface such as different types of vegetation, soil, man-made features, and water body. On the other hand, land use describes the anthropogenic activities to modify, manage and use specific type of land cover such as agricultural use, residential use, and industrial use (Jensen, 2000; Brown and Duh, 2004). Comprehensive knowledge about the LU/LC pattern considered as a foundation stone toward many planning and management activities of the earth's surface features (Lillesand *et al.*, 2008). LU/LC are typical example of addition value for extracting information, which can be derived from EO data.

Ideally land use should be mapped separately from land cover, but for practical reasons both are frequently merged together in a single LU/LC information map (e.g. Chen, 2002; Aitkenhead and Dyer, 2007; Huth *et al.*, 2012). Recent advances in remote sensing techniques deal with different levels of detail at the same time in a hierarchical network. Hence, the scene is composed of different sized real-world entities which necessitates hierarchical segmentation and classification process, which mitigates the confusion of class description, especially in transition and overlapping areas. Land cover is in most cases extracted directly utilizing spectral characteristics, while land use classes may be inferred by conceptual arrangements of spatial relations (Barr and Barnsley, 1997; Zhan *et al.*, 2002). From this perspective, based on the level of mapping details, as an example of vegetative area, its land cover could be categorized as vegetation land cover in super level, while it may contain different land use and/or cover classes in the sub-level (e.g. agricultural fields, orchard, grasses, forests, etc.).

Some previous study of land classification schemes have been developed and promulgated to act as standards (Jensen, 2005). Anderson *et al.* (1976) considered as one of the first widely implemented standard scheme which sponsored by United States Geological Survey (USGS). This classification scheme was designed in hierarchical levels and combines both land use and

land cover classes. Africa shows a severe scarcity of quantitative and qualitative information on LU/LC at local, national and regional levels. The dominant method of collecting data about the land use and land cover is a time consuming ground surveys, which involves enumeration and observation samples in some accessible areas. AFRICOVER was the only consistent formulated project to meet the demand of a homogeneous database for African countries based on remotely sensed data. The project has been operational in the period 1995-2002 and was formulated by ten countries: Burundi, Democratic Republic of Congo, Egypt, Eritrea, Kenya, Rwanda, Somalia, Sudan, Tanzania and Uganda (FAO, 1995). Main limitations present in the application and interpretation of this project are; incomplete data coverage, varying data age and season, and implementation of incompatible classification systems. In addition, it focuses mainly on land cover at one level of detail, disregarding the highly demanded land use classes. Most of the above mentioned problems were also encountered by other projects such as the first harmonized land cover classification system in Europe (i.e. CORINE), for example generalizations were performed for areas less than 25 ha (Heymann *et al.*, 1993).

Successful utilization of remotely sensed data for LU/LC studies demands careful selection of an appropriate dataset and of image processing technique(s). The common approaches of extracting thematic information from remotely sensed data for decades are based upon the use of the pixel as a basic processing unit (Curran, 1985; Lillesand *et al.*, 2008). These approaches are only applicable if the target themes are unambiguous and could be explicitly separated by their own spectral responses. This is in general an acceptable hypothesis in the case of land cover classes, whereas land use comprises a complex spatial assemblage of land cover categories with varying spectral values which require addition information to infer the complexity of indirect land use classes (Wharton, 1982; Barnsley and Barr, 1996). In addition, most of the automated classifiers would be unable to assign pixels with similar spectral value to different classes, which it may possibly refer to different land use classes (Gurney, 1981). This suggests that, to explicitly separate structural land cover from functional land use classes in digital remotely sensed data, a conceptual iterative hierarchical system has to be adapted rather than linear, that is capable to integrate multiple sources of data, and to exploit a varying range of available information.

Promising attempts have been done by many researchers to infer land use in this way, utilizing different set of data in various regions. Zhan *et al* (2002) applied object based hierarchical scheme at two levels utilizing IKONOS imagery and airborne LIDAR data, whereas land use objects

have been inferred at higher level based on land cover objects level and structural information. Bock *et al.* (2005) conducted a study for habitat mapping at regional and local scales using medium spatial resolution LANDSAT TM/ETM scenes combined with ancillary data sources. Their study mentioned the well-capability of the OBIA with EO data for habitat mapping at the range of different scales.

The characterization of finer hierarchical levels, such as land use themes, requires additional contextual features, which are easily delineated by visual interpretation but are confused when automatically interpreted. This arises when investigating geographical entities that exhibit conceptual borders more willingly than spectral ones. Therefore, it is advisable to develop region- (or domain-) specific multi-scale strategy and knowledge-based configuration of coarser level objects as spatially and thematically defined reference units for finer scale(s) (Burnett and Blaschke, 2003; Tiede *et al.*, 2008). Therefore, domain-specific modeling allows users to tailoring transformation of the input data contents into ready-to-use information based on the required field and detail level. Moreover, it supports integrating multisources of information addition to EO data (Tiede *et al.*, 2006; Zhang *et al.*, 2008).

3.3.6.2. Forest structural attributes level

Despite the different generations and types of satellite sensors that have been launched over the past decades, no single sensor presently covers absolutely the requirements of the entire levels of a forest resource assessment system (Boyd and Danson, 2005). Hence, multisource EO data considering each desired level of forest resource information are required, as well as appropriate approaches which efficiently manipulate this variety of information sources commissioned for use.

The categorical result from a classification process considered as one of the main information products about forest condition that generated from remotely sensed data. The second set of forestry information products is produced by continuous variable estimation procedures (Franklin, 2001; Boyd and Danson, 2005). Beside forest type and species composition forest structural attributes might include; forest crown closure, diameter at breast height (DBH), height, number of trees per unit area (density), volume, age, stage of development, roughness, leaf area, and biochemical or nutrient status (Tokola *et al.*, 1996; Franklin, 2001). Unlike classification, rather than a discrete categorization, forest inventory parameters frequently have been driven by

empirical or semi-empirical estimation models (Stenberg *et al.*, 2008). These models describe the statistical relationship between the forest condition of interest as independent variables, and the information available about that condition from remotely sensed data as dependent variable. If all of these variables can be controlled, then an accurate and precise predictive model can be constructed by which the forest structural attribute(s) can be applied to predict the extracted features from remotely sensed data. Subsequently, the model can be reversed and generalized to predict forest structural attributes over large areas of forest based on the selected features of the remotely sensed data (Franklin, 2001).

Forest is defined by the FAO through FRA (2005) programme as; “*land spanning more than 0.5 ha with trees higher than 5 meters and a canopy cover of more than 10%, or trees able to reach these thresholds in situ*”. The traditional operational unit for forest structure is the stand. Therefore, precise and consistent measurements of forest structural attributes are required for decision makers as well as the forest planner in order to make sound decisions for efficient and sustainable uses. Particularly, in semi-arid areas the transferable, automated and accurate detecting methodologies are urgently needed to update the information for sustainable management of these rapidly deteriorated ecosystems (Deshayes *et al.*, 2006). Although, the conventional approaches of gathering stand structural attributes through manual interpretation of aerial photographs and ground-based sampling measures provides high level of detail, it has great deficiencies (e.g. costly, subjectivity, and low spatial and temporal coverage). In Sudan, so far, the continuous forest stand information are mainly based on a systematic terrestrial sampling design of field plots using hand-held equipments with area ranging from 0.1 to 0.5 ha for each sample, in which basic tree attributes DBH, height, crown diameter, stem number, etc. are measured. Subsequently, other structural attributes are calculated at field plot mean values such as dominant height, basal area, and volume, and then generalized at stand-level average values. It has long been anticipated that those conventional forest inventory procedures will be superseded by semi-automated computer-assisted, satellite-based remote sensing approaches that offer several attractive characteristics including consistency, large area coverage, and efficiency in terms of time and resources (Pitt *et al.*, 1997; Franklin, 2001; Levick and Rogers, 2008).

Nowadays, the precise estimation of forest volume and its distribution is the most important structural attribute for various applications, from the merchantable use of wood (Morgan and Moss, 1985; Henry *et al.*, 2011), to the global carbon sequestration (Bombelli *et al.*, 2009). Stand

volume is arguably the crucial variable in *Acacia nilotica* forests of Sudan. However, these forests are managed for fuel wood and sawn timber production. In regardless of the applications, the empirical models for the estimation of the structural attributes based on remotely sensed data are remaining fairly standard. So far, in Sudan stand volume has been estimated by field survey sampling for planning purposes. However, the method is tedious, costly and time consuming. In contrast, satellite-based remotely sensed data supplemented by low intensity field survey (Rahman *et al.*, 2005), or coarser scale low-cost satellite imagery combined with very high resolution imagery as sample (Stojanova *et al.*, 2010), can provide relatively cost-effective and fast estimation.

Optical multispectral remote sensing data provide a continuous view of moderate resolution (30-15 m) and broad scales with a relatively low cost (Hyyppa *et al.*, 1998), which have shown promising results to estimate various horizontal structural attributes, such as stand density, age and tree species composition (Wulder and Seemann, 2003). These structural attributes are frequently derived at the forest, stand, and tree patches scale rather than tree-level, because the spatial resolution of such sensors is not fine enough to characterize individual tree structural attributes. In past decades various studies have shown the potential of using optical multispectral data for extracting of forest structural attributes. For example, SPOT satellite data was used by Wolter *et al.* (2009) to estimate a large set of forest structural attributes in northeast Minnesota, Levin *et al.* (2007) showed that there are great agreements between plant species richness and the NDVI of TERRA ASTER imagery ($R^2=0.87-0.89$, $p<0.01$), even with LANDSAT TM; it has the ability to measure forest structural attributes at large scale with strong correlations in some bands (see Cohen *et al.*, 1995; Puhr and Donoghue, 2000), for the reason that such sensors have wide spectral sensitivity to various stand components (i.e. overstory, understory, soil, and shadow (Scarth *et al.* 2001; Lillesand *et al.*, 2008). Although, those passive optical multispectral sensors were successfully examined for estimating forest structural attributes, some deficiencies were mentioned such as difficulty penetration beyond top canopy layers (Weishampel *et al.*, 2000), and an ideal spectral response is difficult to attain if it is not impossible due to various extraneous factors, as for example; background reflectance, stand structure, and atmosphere (Danson, 1995; Gemmell *et al.*, 2001). Therefore, to meet these challenges, recent researches are focused on the integration of additional information in the image in excess of spectral properties for the estimation of forest structural attributes (Hay and Castilla, 2008; Blaschke, 2010).

OBIA has been proven as an effective solution for analyzing remotely sensed data by incorporating analyst's knowledge and complimentary ancillary data, in a way that simulates human intelligence for image interpretation as a real-world formulation of feature (e.g., based on shape, size, position, color, texture, etc.), more efficiently than discrete spectral pixels values (Hay and Castilla, 2008; Blaschke, 2010; Chen *et al.*, 2011). Thus, over the last years there has been an obvious shift in the analysis of EO data from the conventional per-pixel multispectral-based approaches towards the promising application of object-based multi-scale data processing strategies, allowing for integrating various ranges of image features (Hay *et al.*, 2003; Levick and Rogers 2008; Lang, 2008). Additionally, the analysis can be performed combining a multisource of information getting an advantage of each image commissioned for use. For instance, although it is cost effective estimating these parameters using only optical scenes, model accuracies are lower than those using very high resolution airborne lidar data (Chen *et al.*, 2012). Therefore, some recent researcher utilized optical scenes that provide large scale horizontal forest attributes features, combined with small-area lidar transects, that are used as a substitution for at plot-level forest parameters measure (Holmstrom, 2002; Wulder and Seemann, 2003; Stojanova *et al.*, 2010; Chen and Hay, 2011). In the research conducted by Chen, *et al.*, (2012) utilizing OBIA, strong relationship was achieved with the use of lidar transects, whereas a high estimate was observed ($R = 0.85$) when the model was generalized over the whole area with only 7.6% a lidar transect sample. Even with coarser resolution such as LANDSAT ETM+ optical scenes, whereas a similar research methodology by Stojanova *et al.*, (2010) in different geographical zone, reported a correlation of 0.885 and Residual Mean Square Error (RMSE) = 2.25 m for vegetation height and a correlation of 0.861 and RMSE= 0.17 for canopy cover. Nevertheless, quite limited number of studies has investigated the potential of using medium spatial resolution optical data (e.g., 15 meter spatial resolution of visible and near infrared bands of TERRA ASTER and 30 meter LANDSAT TM imagery) to estimate vertical forest stand structural attributes such as tree height (Hudak *et al.* 2002, Wulder and Seemann 2003; Gebreslasie *et al.*, 2008).

3.3.6.3. An object based approach for change detection

Accurate, cost-effective and up to date information about LU/LC patterns is highly demanded for land management decision making. The challenge in digital change analysis techniques is the ability of the existing systems to automatically determine, within specific time intervals whether there is change or not, and to locate the spatial distribution and the extent of the change as well

as to quantify the trend and magnitude of the dynamics precisely (Hall and Hay, 2003; Zhou *et al.*, 2008). Although LU/LC changes can be monitored by conventional terrestrial inventories and survey, space- and air-borne remote sensing facilitates a cost-effective way for detecting the change, as it can explicitly reveal spatial patterns of LU/LC change over a vast geographic area in a recurrent and consistent way (Zhou *et al.*, 2008).

Digital change detection has been defined by Rogan and Chen (2004) as a process of “determining and/or describing changes in land-cover and land-use properties based on co-registered multitemporal remote sensing data”. Various techniques have been applied using remotely sensed data for LU/LC change detection for many decades (Singh 1989; Lambin and Ehrlich 1997; Lunetta and Elvidge, 1999; Lu *et al.*, 2004; Rogan and Chen 2004). Basically, these techniques can be grouped into the following categories: algebra (differencing, rationing, and regression), change vector analysis, transformation (e.g. principal component analysis, multivariate alteration detection, and Chi-square transformation), classification (e.g. multi-temporal clustering, post-classification comparison, expectation maximization algorithm, and neural networks) and hybrid methods (Niemeyer *et al.*, 2008). To simplify, based on Johnson and Kasischke (1998), two broad approaches are common:

- Data transformation (e.g., image differencing, PCA),
- Change labeling (e.g., regression, classification).

Basically, the detection of continuous (transformation) and categorical (labeling) changes are also known as pre-classification and post-classification methods respectively. Pre-classification techniques operate on raw imagery, while post-classification comparison methods detect land cover change by overlaying independent sets of classified imagery of different dates (El-Abbas and Csaplovics, 2012). Although the various studies attempted to evaluate these techniques for decades (see for example Weismiller *et al.* 1977; Singh 1989; Lu *et al.*, 2004), the research of change detection techniques is still a challenging task, and innovative approaches are required to effectively utilize the increasingly availability of advanced remotely sensed data (Lu *et al.*, 2004; Rogan and Chen, 2004).

The reason behind the effectiveness of the post-classification approach is that the thresholds applied for assigning the segmented objects to the same class vary between different acquisition

dates as a result of altered surface features (e.g. phenological variation in vegetation and soil moisture), and atmospheric effect (Franklin, 2001). Singh (1989) mentioned that, some of these differences may be partially reduced by selecting coincided data type and season. However, it may be extremely difficult to acquire multi-temporal data for the same geographical location in the same season of the year. Therefore, methods mitigate the influences of multisource imagery and acquisition differences are appreciated. As the post-classification approach is less sensitive to these variations and robust to radiometric differences between scenes, by independently placing the spectrally derived objects in the appropriate classes before considering the information acquired from other scenes (Duggin and Robinove, 1990). Therefore, each scene must be manipulated separately to achieve optimum classification, and then compare the results for an accurate “from-to” change information (see Jakubauskas *et al.*, 1990; Im and Jensen, 2005; El-Abbas and Csaplovics, 2012). Many authors such as Stow (1999), Mas (1999), Foody (2002), and El-Abbas and Csaplovics (2012) mentioned that, the produced change “from-to” map of two classifications most probably exhibits accuracies analogous to that produced from the multiplying of the accuracies of each individual classified map.

The second approach of change is the continuous one, known also as spectral change detection techniques, where changes occurring in the amount or intensity of some features of the LU/LC are (continuously) measured (Coppin and Bauer, 1996). It involves subtracting one image date from another that has been precisely co-registered to each other. A main finding from Townshend *et al.* (1992) was that the miss-registration effects on change detection based on this approach were greatest for multi-temporal datasets of regions that were spatially heterogeneous. Moreover, these techniques generally generate “change” vs. “no-change” maps, but do not specify the type of change “from-to” maps (Singh 1989; Lu *et al.*, 2004; Im and Jensen, 2005; Jensen 2005). However, the simple detection of change in most cases is inadequate in itself; information is generally required to quantify the detailed LU/LC changes as well as to specify its spatial distributions (Zhou *et al.*, 2008). Due to the heterogeneous features of dry-land region combined with increasing availability of very high resolution image data (Benz *et al.*, 2004), too many changes are detected which may not be of interest for the particular application. Not only with continuous approach, this drawback appears as well in post-classification comparison with the use of pixel-based approach, which leads salt and pepper effect (Niemeyer *et al.*, 2008). Meanwhile, as described earlier, OBIA can exploit the changes of shape values as well as other

contextual features to generate precise and accurate change map near to the real-world-features. Therefore, OBIA approaches for remotely sensed data information extraction meets a lot of concern in a few past years for the application to the research of LU/LC change.

3.3.7. Quality assessment

There is no doubt that an accurate spatial extent of LU/LC data and its dynamics are required. Despite the importance of LU/LC as an environmental variable that supports environmental planning, resources management, and public policy decision making, the paucity of information about LU/LC and its dynamics is clear. Understanding the importance of LU/LC and forecasting the effects of its dynamic is particularly limited by the scarcity of precise and accurate LU/LC data (Foody, 2002; Estes and Mooneyhan, 1994). Remotely sensed data are inherently suited to provide an attractive source of information about LU/LC and its dynamics, and the thematic maps are the common form of extracted information to the end users based on continuously developed classification approaches. Meanwhile, the classification is not complete until its accuracy assessed (Lillesand *et al.*, 2008). Thus, an accurate mapping is an important and complex issue that not yet reached to the satisfaction and acceptable level.

Various methods to assess the accuracy of the resultant maps derived from remotely sensed data analysis have been discussed in the literature, whether they are positional or thematically derived methods (e.g., Hammond and Verbyla, 1996; Koukoulas and Blackburn, 2001; Foody, 2002; Skirvin *et al.*, 2004; Congalton and Green, 2009). The most widely accepted and applied method for LU/LC accuracy assessment is the thematic quantitative site-specific, well-known as error matrix or confusion matrix (Khorram, 1999; Congalton and Green, 2009). An error matrix is a cross-tabulation that expresses the number of reference units assigned to a particular label in one classification compared to the number of reference units assigned to a particular label in another classification, assuming that the reference units are correct. Unfortunately, there is no unique accepted standard or universal measure for maximum allowable error. The most widely promoted and utilized cutoff between the acceptance and rejection of the result proposed by Anderson *et al.* (1976) is 15% allowable error (i.e., 85% overall accuracy), however, there are nothing logical or even particularly significant to rely on it. Therefore, it has been recommended that accuracy assessment reports must indicate the entire raw error matrix of computed assessment values (Congalton and Green, 2009). These related specific assessment values that are used to evaluate

the probability of correct class assignments are error of commission, error of omission, and kappa coefficient as a compensation for the chance in agreement, in addition to the overall precision or reliability of a classification result (Lang, 2008). Indeed, these values provide the basis to describe the classification precision and the errors as well (Foody, 2002).

The collection of a considerably high number of ground truth data is not economically feasible and is time consuming. Therefore, the sample size must be kept as small as possible. Thus, performing the accuracy assessment with an improper sampling design will generate misleading validation results. However, many studies provided good suggestions for designing an effective and efficient sample strategy to collect valid reference and map accuracy (e.g., Hammond and Verbyla, 1996; Deppe, 1998; McCoy, 2005; Köhl *et al.*, 2006; Congalton and Green, 2009), with a consideration to; distribution of the thematic classes across the landscape, types and number of samples to be taken, and choice of a sampling strategy for selecting the representative samples. Based on the above mentioned perspective, it will be possible to evaluate the uncertainty associated with the decisions based on these results.

Chapter 4 DATA AND RESEARCH APPROACHES

4.1. Overview

As the study area is composed of different sized real-world entities, and a single resolution might not be appropriate to discriminate all classes within the image, a synthesis of multisource data and integrated research approaches was applied to achieve the objectives. This chapter provides a brief description of the technical details of various types and sources of the datasets used, as well as of the data collection strategies. Subsequently, the up-to-date and most promising approaches adopted for the study were expressed. Prior to the implementation of analyses to the multisource and multitemporal EO data, geometrical, radiometrical and atmospheric corrections were required. The utilization of the field surveyed data are shown, which encompasses the preprocessing, main analyses techniques, the integrated model approaches and result validation. The development of the rules through the complementary ancillary data and user's expert knowledge were also shown. For better understanding of the change dynamics as an interactive process, local community perceptions were integrated into the EO data, which provide insight into how and why the changes occur and to find potential solutions for restoration.

4.2. Data

4.2.1. Earth observation data

A series subsets of multi-temporal satellite imagery subsets, acquired at the same season, were used to examine the proposed OBIA for coarser scale LU/LC mapping and change analysis, as well as at a forest stand level to estimate forest stand structural attributes.

4.2.1.1. TERRA ASTER data

The satellite was launched at the end of 1999 as part of NASA's Earth Observing System (EOS). TERRA ASTER (Advanced Space borne Thermal Emission and Reflection Radiometer) which is a joint project between NASA, Japan's Ministry of Economy, Trade and Industry (METI) and Japan's Earth Remote Sensing Data Analysis Center (ERSDAC).

Table 4-1: Specifications of TERRA ASTER image used for the study

Satellite	TERRA (ASTER)		
Acquisition date	13.03.2009		
Scene Size (km)	60 x 60		
Sensor	VNIR	SWIR	TIR
Band	1- 3	4-9	10-14
Spectral Range (μm)	0.52-0.86	1.60-2.43	8.12-11.65
Spatial Resolution (m)	15	30	90

One TERRA ASTER free cloud image of the study area was obtained on March 13th, 2009 (Annex 4), and was used to generate accurate thematic LU/LC classes for the test site “A” with an area of about 111,000 ha, as well as forest parameter estimation for the selected site “B” (Alambwa forest) with an area of about 210 ha, based on image object feature extraction at plot-level forest inventory data. The scene is located in path 172 and row 52. It consists of fourteen bands allocated in three spectral regions as follow; visible and near-infrared (VNIR) (bands 1–3) with 15-m resolution, short wave infrared (SWIR) (bands 4–9) with 30- m resolution and thermal infrared (TIR) (bands 10–14) with 90-m resolution, as illustrated in table 4.1. Nine bands were chosen for the analysis (VNIR, SWIR); the thermal infrared bands were excluded.

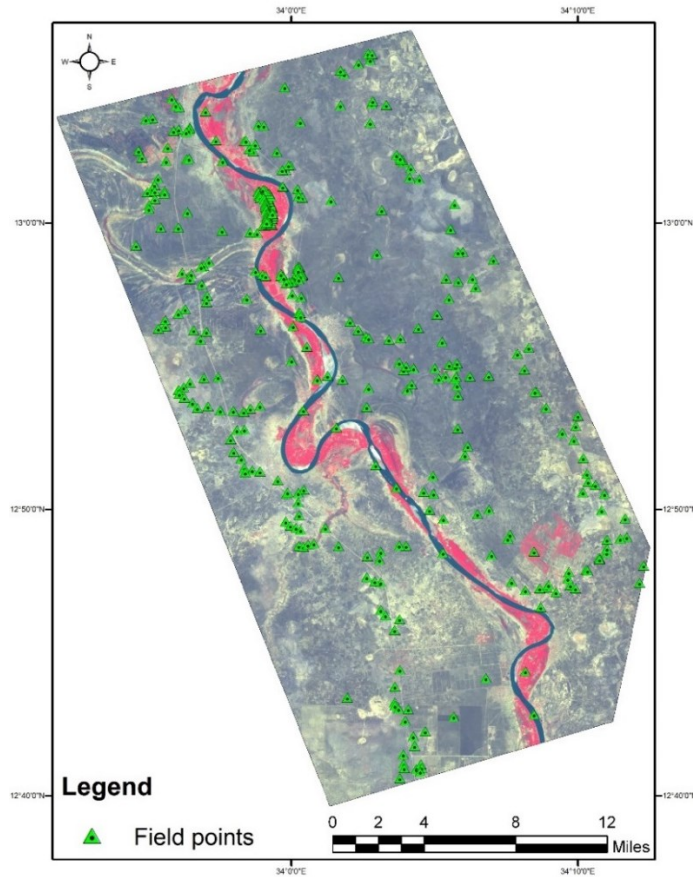


Figure 4-1: Spatial distribution of the ground truth data collected during the field visit (colour infrared composition of RapidEye imagery)

4.2.1.2. LANDSAT -5 Thematic Mapper (TM) data

For the study, two LANDSAT TM images were also allocated from the United States Geological Survey (USGS) archive, located at path 172 and row 051, acquired in March 26th, 1999 and January 4th, 1990 (Annex 4), which aim to estimate the dynamics of LU/LC over time in selected site “A” (same area of interest for the selected TERRA ASTER data mentioned above in figure 4.1). The LANDSAT TM imagery is part of the LANDSAT 5 mission, launched in March 1, 1984 by NASA. The sensor observes the Earth's surface in seven spectral bands that range from visible to thermal infrared regions, these bands that simultaneously record emitted or reflected energy from the Earth's surface in the blue-green (band 1), green (band 2), red (band 3), near-infrared (band 4), mid-infrared (bands 5 and 7), and the thermal (band 6) portions of the electromagnetic spectrum. The study used bands 1, 2, 3, 4, 5 and 7, although the thermal band was excluded. Each LANDSAT TM scene covers an area 185 km by 172 km, with each pixel in

the scene representing an area of 30 m by 30 m, except the thermal band with 120 m spatial resolution. A detailed description of the LANDSAT TM imagery was given in table 4.2.

Table 4-2: Specifications of LANDSAT TM images used for the study

Satellite	LANDSAT 5 (TM)			
Acquisition date	26.03.1999 and 04.01.1990			
Scene Size (km)	170 x 185			
Sensor	VS	NIR	MIR	TIR
Band	1,2& 3	4& 5	7	6
Spectral Range (μm)	0.45–0.69	0.76–1.75	2.08–2.35	10.4–12.5
Spatial Resolution (m)	30	30	30	120

4.2.1.3. RapidEye data

Recently, the study succeeded in acquiring high resolution data for the study area from the RapidEye EO mission. The scene located in path 172 and row 051, taken on January 4th, 2010 (Annex 4), aimed to address the issue of spatial resolution compared to the coarse spatial resolution of Aster data. The RapidEye is a commercial remote sensing mission by the German company RapidEye AG, launched in August 29th, 2008. The sensor observes the Earth's surface in five spectral bands that range from visible to near IR regions, these bands that simultaneously record the reflected energy from the Earth's surface in the blue (band 1), green (band 2), red (band 3), red edge (band 4) and near-infrared (band 5) portions of the electromagnetic spectrum. The study utilizes in this study only the visible bands 2, 3, and the NIR band number 5 for consistent comparison, the blue and red edge bands were excluded. All satellite sensors have a pixel size represents an area of 5 m by 5 m spatial resolution. A detailed description of the RapidEye imagery is given in table 4.3.

Table 4-3: Specifications of RapidEye data used for the study

Satellite	RapidEye				
Acquisition date	04.01.2010				
Swath Width (km)	77				
Sensor	Blue	Green	Red	Red Edge	Near IR
Band	1	2	3	4	5
Spectral Range (μm)	0.44–0.51	0.52–0.59	0.63–0.685	0.69–0.73	0.76–0.85
Spatial Resolution (m)	5	5	5	5	5

4.2.2. Field survey data

Several datasets used for this research work applied in two test sites (i.e. LU/LC level and forest structural attribute level). However, in addition to the EO data as a main source of data used in this research, Global Positioning System (GPS) to collect field check points and ground control points as well as forest inventory data were also used. The field survey data were collected during the field visit in April 2010 which coincided with the season of acquisition in order to eliminate the variation in natural phenological status and allow for same atmospheric and environmental conditions. The collected data are used for various purposes including; TTA masks and training samples, that were created as a reliable guidance in the analytical process to support NN and ML classifiers, as well as to evaluate and assess the results obtained based on EO data. In addition, Ground Control Points (GCPs) were collected for image rectification (figure 4.1).

4.2.2.1. Ground control points

GCP could be defined as a point on the Earth's surface of known location which is used to rectify the image data. The GCPs or ground reference points were collected during the field visit, using handheld GARMIN eTrex Venture HC GPS device to record coordinate position for each visited point. The points were collected at 27 locations, from pre-defined areas that were easy to access in the ground and could be very clearly identified from the satellite image, such as roads, bridge, forest boundaries, towns and other key features.

4.2.2.2. Land Use/ Land Cover (LU/LC) data

Stratified random field sampling design was used with a proportional allocation strategy, which has been established from spectral classes generated from unsupervised classification, to ensure a sound distribution of represented field samples relating to identified LU/LC class categories. These samples were collected in two main forms. The first sampling design, the inner coordinates of selected pure segments (polygons), achieved from *eCognition* software to make TTA Masks to be used in subsequent steps of OBIA paradigm. The second sampling design was the coordinates of selected pixel samples, with at least 20 m by 20 m dimension size. In the study area a number of 85 polygon samples were collected (inner coordinates) to eliminate the intersected areas, in addition to 409 point samples for the analysis and validation of the proposed innovative OBIA as well as a ML classifier as an assessment method (Annex 1). The

classification scheme utilized nine LU/LC classes, representing agriculture (rain-fed), dense-forest, grassland, orchard, irrigated crop-land, bare-land, scattered-forest, settlements, and water body (table 4.4).

Table 4-4: Land Use/ Land Cover (LU/LC) patterns of the study area

Class	Description
Agriculture (rain-fed)	This class includes the lands which are used or cleared to be utilized for seasonal crop production in the rainy season.
Dense-forest	Land spanning more than 0.5 hectares with trees higher than 5 meters and a canopy cover of more than 10 percent, or trees able to reach these thresholds in situ. It does not include land that is predominantly under agricultural or urban land use.
Grassland	Includes all vegetation features that are not typically wood-land or cropped areas.
Orchard	Includes all trees and annual plants which are planted for fruits commercial production. Mainly; <i>Mango</i> , <i>Citrus</i> , <i>Guava</i> and <i>Banana</i> .
Crop-land	Includes the areas of irrigation schemes, where the land is used for commercial seasonal crops.
Bare-land	Most often degraded areas with no vegetation cover and have not been developed for other uses.
Scattered-forest	Land not classified as “Dense-forest”, spanning more than 0.5 hectares; with trees higher than 5 meters and a canopy cover of 5-10 percent, or trees able to reach these thresholds in situ; or with a combined cover of shrubs, bushes and trees above 10 percent. It does not include land that is predominantly under agricultural or urban land use.

Table 4-4: Land Use/ Land Cover (LU/LC) patterns of the study area (continue)

Class	Description
Settlements	This class representing residential areas ranging from local building material to concrete and bricks houses, trees and small gardens inside the villages are included.
Water	The main feature of the class is Blue Nile river. Other seasonal river tributes (khour) are excluded, which are normally covered by trees during the dry season.

4.2.2.3. Forest inventory data

The forest inventory data collected during the field visit in Alambwa *Acacia nilotica* pure stand forest to collect at plot-level information of forest parameters information such as age (Y, year), tree height (H, meter), DBH cm, stand density (D, number of trees per unit area), in addition to the general characteristics of the stand has been observed (Annex 2). Systematic sampling design was applied to a total of 104 sampling units to be used for forest parameters estimation and model validation, and the handheld GPS device was used to determine the center location of each target unit. The sample plot area was estimated using the Townshend *et al.* (1992) equation (Equation. 4.1).

$$A = S(1 + 2R) \quad (4.1)$$

Where:

A = Minimum site dimension

S = Single pixel dimension

R = Estimated positional accuracy in number of pixels

Subsequently, and according to the input data used, and registered with RMSE less than 0.5 of pixel, the sample area calculated to be 0.09 of a hectare (Equation 4.2).

$$A = 15(1 + 2 \cdot 0.5) = 30 \text{ m} \quad (4.2)$$



Figure 4-2: Collection procedure of plot level forest inventory data

4.2.2.4. Socioeconomic data

Aggregated to the community-level, social survey of household data provides a comprehensive perspective in addition to the EO data, investigating predetermined hot spot degraded and successfully recovered areas. Hence, the study utilized a social survey of household through a well designed questionnaire based on multi-choice and open ended questions to address the factors affecting LU/LC dynamics based on local community's perception. Population Proportional to Size (PPS) sampling technique was applied to collect 120 questionnaires distributed in 6 villages in the study area (Annex 3). The interviews were carried out through personal contact, which was enumerated by the author himself, and the interviews considered the local community language, which was conducted in Arabic language.

Data collected from interviews were coded, interred and analyzed using the SPSS software. And the descriptive statistic analysis was applied to explain the local community perceptions about different aspects of changes dynamics.

4.2.2.5. Ancillary data

Ancillary data were collected from different sources to enhance the data processing framework. The other data used in this research were the meteorological information, census of population information, records and reports about rain-fed agriculture, *Acacia nilotica* forest stand stock maps and historical records about silvicultural operations.

4.3. Methodology

4.3.1. Atmospheric correction

The image pixel value recorded in remotely sensed data (must be only) is a function of the signal detected by the sensor. As a result of atmospheric interference, this detected value is affected by the combination of the target surface object and the atmosphere itself. The importance for atmospheric correction depends on the quality of the image (for example, an image displaying high haze effects and clouds) and the purpose for which the image will be used. In the simplest study, where a single image is being processed and there is no need to match the results with other remotely sensed data (different sensor, season and location), it is feasible to proceed with the analysis process with digital number (DN) without conversion to radiance and/or surface reflectance. Multi-sources and multi-temporal data used in the present study require atmospheric correction to reduce the atmospheric effect for accurate quantitative analyses to insure the differences obtained as a result of image difference rather than atmospheric conditions.

The FLAASH (Fast Line-of-sight Atmospheric Analysis of Spectral Hypercubes) atmospheric correction method in ENVI 4.5 software input image requires to be calibrated into spectral radiance in units of $\mu W/(cm^2*sr*nm)$.

Subsequently, the solar and atmospheric effects have been eliminated through a process of conversion at-satellite radiance to surface reflectance. The spectral reflectance obtained from multi-spectral satellite image data used was retrieved using Moderate Resolution Atmospheric Transmission (MODTRAN) model atmosphere and aerosol types, which is applied to eliminate the atmospheric effect from calibrated data (Schmidt *et al.*, 2009).

FLAASH starts from a standard equation for spectral radiance at a sensor pixel, “T” that applies to the solar wavelength range and flat, Lambertian materials or their equivalents. The equation is as follows (Alder-Golden *et al.*, 1999):

$$T = \left(\frac{A\rho}{1-\rho_e S} \right) + \left(\frac{B\rho_e}{1-\rho_e S} \right) + T_a \quad (4.3)$$

Where:

ρ Pixel surface reflectance

ρ_e An average surface reflectance for the pixel and a surrounding region

S Spherical albedo of the atmosphere

T_a Radiance back scattered by the atmosphere

A and B are coefficients that depend on atmospheric and geometric conditions but not on the surface

FLAASH atmospheric correction model input parameters require scene and sensor information, such as scene center location, the average ground elevation of the scene, the sensor type, the sensor altitude, and the flight date and time. These parameters estimate the sun location in the sky and the path of radiation took through the atmosphere to the sensor. In addition to estimating the water vapor amount and surface temperature is estimated through the selection of one of the standard MODTRAN model atmospheres. The study select Tropical (T) with estimated water vapor 4.11 g/cm² and surface air temperature 27°C (figure 4.3).

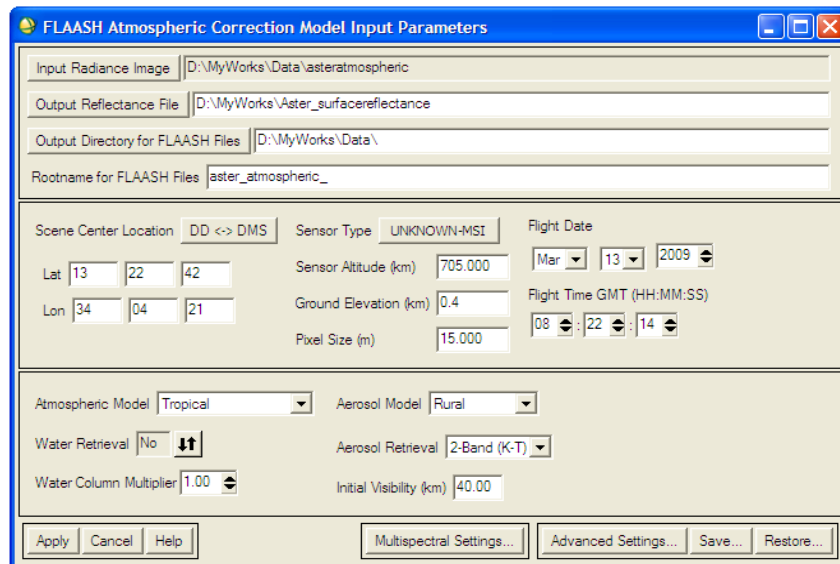


Figure 4-3: FLAASH atmospheric correction model input parameters window in ENVI software

4.3.2. Geometric correction

Geometric correction of remotely sensed data involves modeling the spatial position of the satellite imagery in relation to its actual ground location (Bruce and Hilbert, 2004). In multi-

temporal analysis, the classification accuracy of the thematic output is directly affected by the registration precision of input datasets. Such accuracy is also required when combining EO data with forest stand parameters at plot-level forest inventory data. Each of the proposed results of the current study (LU/LC mapping, multi-temporal analysis and forest stand parameters estimation) depend on field survey data based on GPS coordinates and/or other reference map. Therefore, the validity of the intended output highly depends on appropriate geometric correction results.

Firstly, the GCPs covering distinguishable features in the study area were collected during the field visit and used as control and check points. Images have been co-registered in ERDAS Imagine 8.7 software with 27 GPS points. The RMSEs achieved in all cases are less than 0.5 of pixel size, which illustrates a high adequate precision of rectification. The RMSE was calculated using the following formula:

$$RMSE = \sqrt{\frac{1}{n} * \sum_{i=1}^n (\varepsilon_i)^2} \quad (4.4)$$

Secondly, image-to-image registration technique was then applied based on georeferenced TERRA ASTER image (2009) using the Polynomial geometric model, so that the geometry of LANDSAT TM images (1990 and 1999) is normalized accordingly (Appendix 5).

When geometric correction has been implemented to retrieve displacement in images as described above, Bilinear Interpolation resampling method was applied to each of the image individually. The output maps projection was Transverse Mercator Projection (UTM/ zone 36 WGS 84). The RMS error achieved was less than 0.5 of pixel size for all input images.

The spatial dimension of the image used is as follows; the TERRA ASTER image provides 15 X 15 m spatial resolution, and LANDSAT TM 30 X 30 m spatial resolution. The TERRA ASTER image has been resampled by a scale factor of 2 to create 30 m dimension size in ENVI 4.5 software to match the LANDSAT TM data.

4.3.3. Image classification

The essential task in the present study is to manage the huge information derived from multi-spectral imagery in the form of spectral value in addition to shape, texture and context of the

image segment. In general, the overall objective of the image classification process is to automatically cluster all image pixels into meaningful land cover class categories (Lillesand *et al.*, 2008).

In this study two classification approaches were implemented for LU/LC classification. Firstly, the innovative OBIA utilizing NN and RB classifiers and secondly the traditional per-pixel approach to evaluate the performance of the proposed newly developed OBIA approaches.

The main difference between the two approaches is that firstly, in object based approach the process units are image objects, rather than discrete pixels. Secondly, the classifiers that are based on fuzzy logic which utilize the membership functions to express the assignment of an image objects to a specific group. The membership values lie between 1.0 and 0.0 where 1.0 represent a full assignment to a class and 0.0 expresses absolutely non-membership (Geneletti *et al.*, 2003).

4.3.3.1. OBIA approaches

In recent years considerable advancements in computer processing imaging techniques alternative strategies have been proposed, particularly the use of fuzzy logic, and the incorporation of additional information such as shape, texture and context. In this study, an object-based approach was proposed for discriminating different LU/LC classes at coarse level as well as forest parameters estimation of forest stand level.

The basic processing unit in OBIA is a meaningful segment, which means that the image segmentation is considered as a preliminary step toward the subsequent process. Multiresolution segmentation strategy was applied in OBIA paradigm that might be effective to separate similar spectral values into preliminary unclassified image objects of groups of relatively homogeneous pixels based on the shape and compactness criterion at different scales. Subsequently, segmented objects were assigned to different classes by RB and NN classifiers implemented in *eCognition* software using knowledge-based and minimum distance measures derived from randomized TTA Mask respectively.

Image Segmentation

Dealing with meaningful image objects in the classification process, rather than individual pixel, distinguish OBIA from most of the other classification paradigms. Segmentation algorithms

utilized in OBIA approaches subdivide the entire image at any primitive desired objects, or re-segment specific image objects from another domain, which enables multi-cycles of data processing strategy. The approaches vary from very simple algorithms, such as chessboard segmentation, to very complicated approaches such as a multiresolution segmentation, which it has been applied in different fields, and the typical examples of the appropriate uses of this algorithm are as follows (Baatz *et al.*, 2004):

- Extracting features that are identified not only based on spectral value but also by shape criteria.
- Extracting land use classes or man-made features from remotely sensed data.

Accordingly, the multiresolution segmentation algorithm was applied to the dataset in the present study as a preliminary step of OBIA approaches to create meaningful unclassified image objects (object primitives). This segmentation algorithm characterized as a bottom-up pair wise region merging technique, applying a threshold optimization procedure for image segments, which categorizes the image objects according to a maximum acceptable heterogeneity based on defined threshold to maximize their respective similarity (Baatz *et al.*, 2004). To obtain appropriate segments of the desired class, the segmentation process was performed for the selected bands and thematic layers. Moreover, a careful selection of scale factor and homogeneity criteria must be considered to achieve the desire level (figure 4.4).

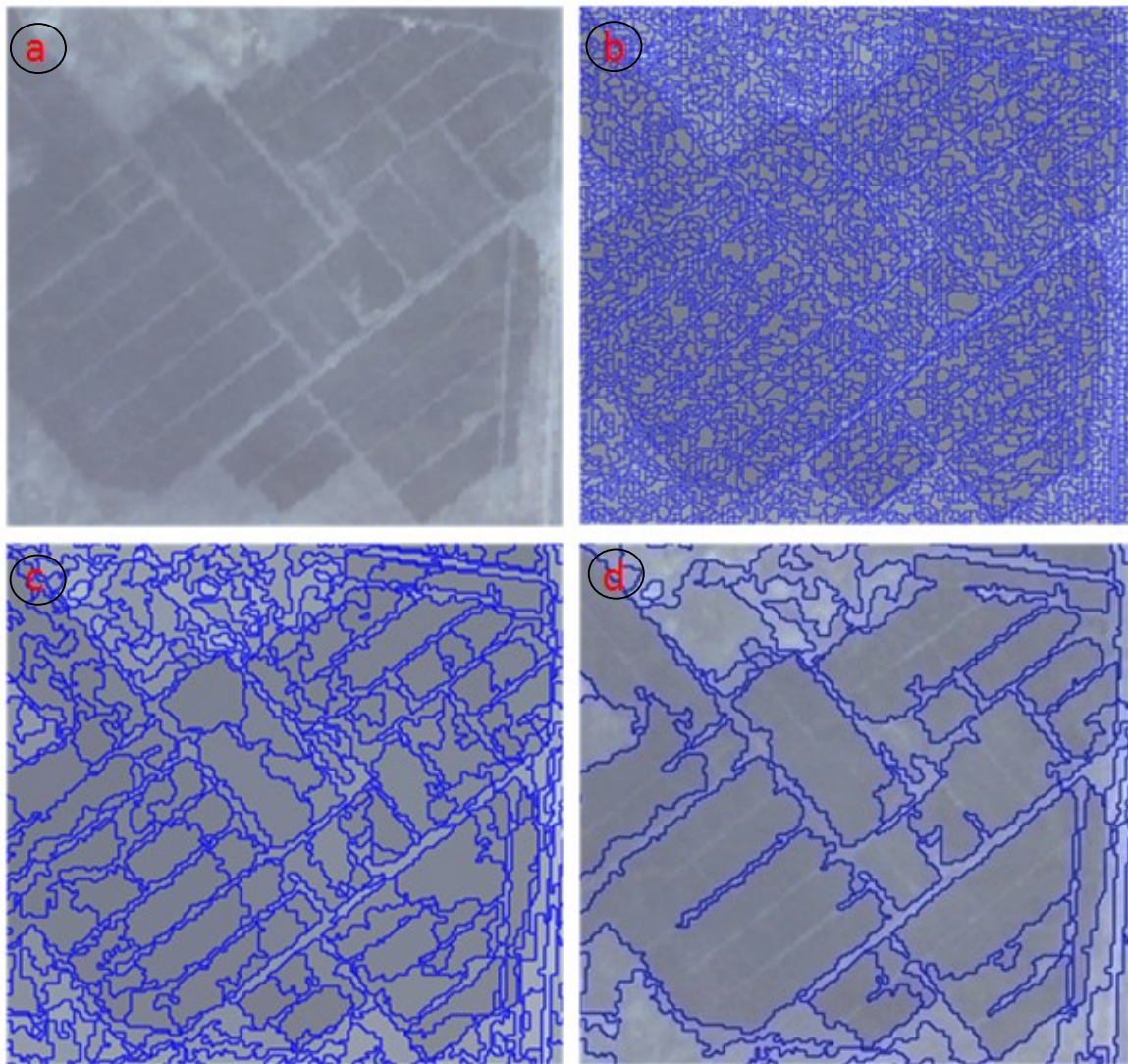


Figure 4-4: Comparison of different experimental segmentation results with different scale factors; a) Original image (without segmentation), b) segmentation result with scale parameter of 5, shape 0.3, smoothness 0.4, c) scale parameter of 10, shape 0.3, smoothness 0.4, d) scale parameter of 20, shape 0.3, smoothness 0.4

The shape heterogeneity is determined by two values, the compactness, which can be derived from the object extent x and the size n , and the smoothness, which is given by the object extent x and the extent of the minimum surrounded rectangle r , parallel to the image raster (Equations 4.6 and 4.7).

$$h_{comp} = \frac{x}{\sqrt{n}} \quad (4.6)$$

$$h_{smooth} = \frac{x}{r} \quad (4.7)$$

The colour heterogeneity is given by following equation:

$$h_{colour} = \sum_{c=1}^n w_c * \sigma_c \quad (4.8)$$

Whereas c is the n band, σ_c the spectral standard deviation of the band c and w the weighting of the n band analogue to the equation above.

The approach applied to determine these parameters have been trial and error until satisfactory features are achieved. The following table (table 4.5) shows the different parameter values applied to the entire classification of the proposed approach.

Table 4-5: Levels of segmentation parameters applied to the input dataset for LU/LC analysis

Criterion	Coarse level		
	Level 1	Level 2	Level 3
Class hierarchy			
Scale	20	10	7
Shape	0.1	0.3	0.3
Color	0.9	0.7	0.7
Smoothness	0.5	0.4	0.4
Compactness	0.5	0.6	0.6

Hierarchical classification

Multiresolution OB segmentation algorithm has been performed at all levels with different scales to create objects that are connected to each other in the class hierarchy of contextual features. These connections can be achieved between super and sub-objects as well as at the same level. Each hierarchical level contains groups of objects, which are created to maximize the variability between different levels while minimizing the variability within them (Baatz *et al.*, 2004). Moreover, each level contains different information details which have been achieved by suitable scale parameters at each level (table 4.5). That allowed to express each class and/or object in the respective level by one or more fuzzy sets.

An image object domain has been used to link between the segmented object and the classification scheme through defined level, objects and fuzzy sets. There are two fuzzy sets applied, multidimensional features and membership function to be used for the NN classifier and RB method respectively.

A hierarchical system is proposed to attain LU/LC classes at three levels. The first level was created to discriminate between water and land (non-water) parent classes. Subsequently, the second level aimed to separate vegetation from non-vegetation classes, which allowed for the separation of five vegetation and three non-vegetation LU/LC child classes in the third level (figure 5.4).

Nearest neighbour classifier

NN classifier is similar to supervised classification, when training objects contain predefined features that are required prior to performing the classification. By executing the process for the entire image or specific image object domain the algorithm starts to search for the nearest object in the feature space and declare the image segments to be significant members of a precise class. For the NN function slope a parameter of 0.1 is set as a membership value at standard deviation.

As shown in figure 4.5, if an image object “A” is nearest to sample object “T”, then an image object “A” will be assigned to the class category “T”.

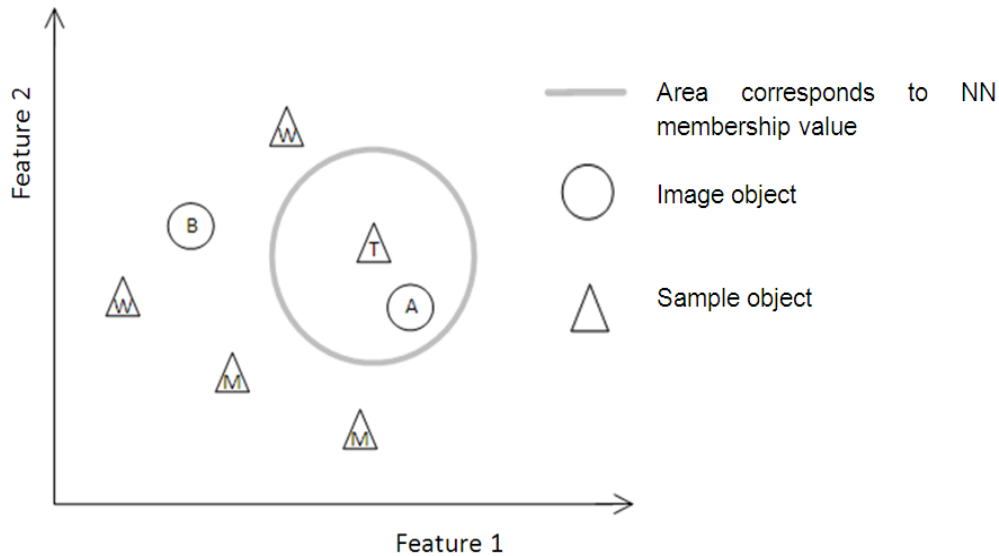


Figure 4-5: The nearest neighbour classification principle; represent class assignment in two dimensions

The classification process with NN classifier has been performed through data fusion, segmentation, creation of class hierarchy, selection of training object(s), define feature space, and calculation of the optimum feature(s). All these must be considered to distinguish between different classes in the image object domain.

The process projects were created in Definiens *eCognition* with the aggregation of multispectral imagery and thematic layers of TTA Mask.

Training and Test Area Mask

For the purpose of OBIA using the NN classifier, the TTA Mask for each class was generated from collecting ground truth field survey data (section 4.2.2.2). Subsequently, data were transformed to shapefile format, and then introduced to *eCognition* software in the form of thematic layer as training and testing objects to guide the process (figure 4.6).

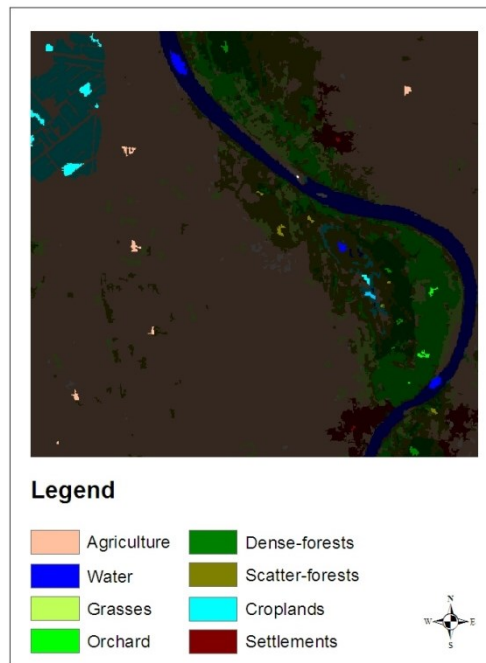


Figure 4-6: Part of the training and test area mask introduced to eCognition software for training

To generate sample objects from the TTA Mask, sample objects were defined by the threshold of 0.90, which mean that 90% of an image object has to be overlapped by the sample area for specific class category derived by the TTA Mask to create a class sample.

In the NN classification approach, these objects utilize user-defined features to supervise the classification, and then training objects has been declared by selecting representative samples containing meaningful spectral and spatial properties for each class, and the confused training objects (critical samples) eliminated (figure 4.7).

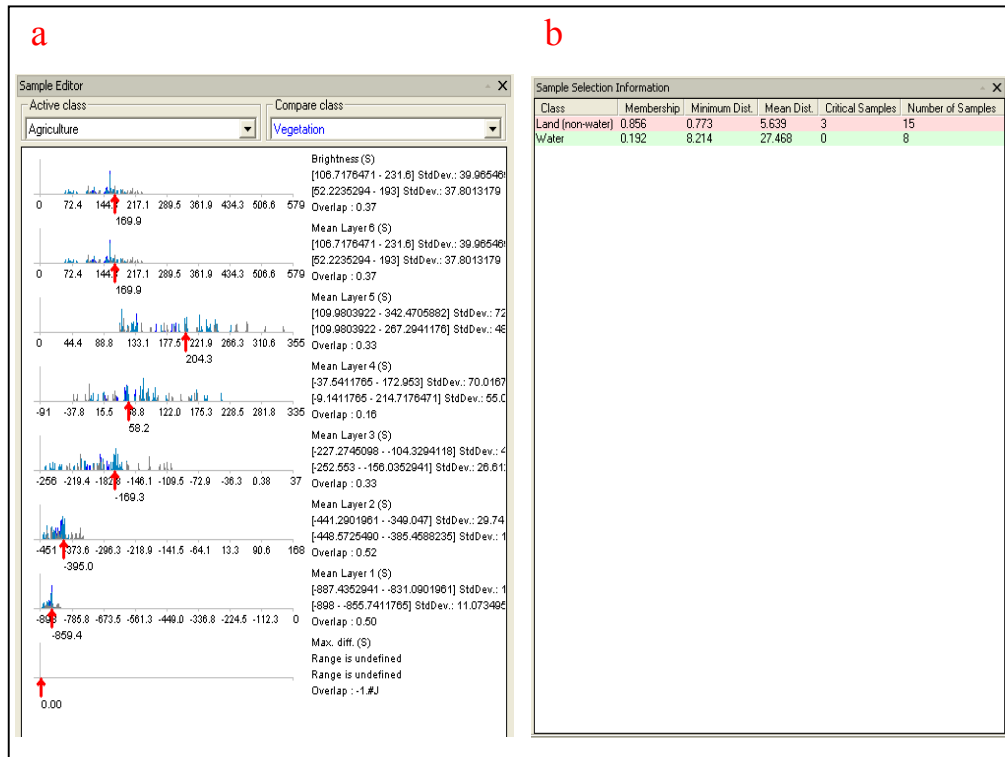


Figure 4-7: a) The sample editor window showing the histogram of the selected TTA Mask for the currently active class, b) sample selection information window to assess the quality of the selected TTA Mask applied in eCognition software

Image object features

OBIA utilizes spectral, shape, and hierarchical characteristics, which is similar to human perception. These features are used as sources of information to define the parameters used to classify image objects.

There are two major types of features (Baatz *et al.*, 2004):

- Object features, which are attributes of image objects such as the geometrical features of each image object.
- Global features, which are not represented by an individual image object such as the number of image objects of a certain class.

To cope with rich information is contained in multispectral data, layer values are considered as one of the most important feature used to discriminate between most of the patterns observed in

the study. Separability between vegetation from non-vegetation as well as water body from other land cover class categories common commonly use these object features.

Due to the complexity and spectral similarity in semi-arid areas, introducing spatial information in addition to spectral information to the classification hierarchy provides valuable features which allow for separation of spectrally similar objects. Utilization of these features was applied mainly to discriminate between different types of vegetation cover and to separate settlements from confused relevant objects such as grasses and scattered-forest classes (section 5.4.2).

Feature space optimization

The huge number of image features used lead to slow computation processes and the classification became more complicated without the sound increase in the result quality (Francois, 2004). Hence, a feature space optimization function in *eCognition* software was provided as an appropriate method to mathematically calculate the best combination of features in the feature space, which are most suitable to separate between classes. The “*eCognition*” tool used to calculate the best separation distance was performed using the following formula (Batz *et al.*, 2004):

$$d = \sqrt{\sum_f \left(\frac{v_f^{(s)} - v_f^{(o)}}{\sigma_f} \right)^2} \quad (4.9)$$

Where:

d : distance between sample object s and image object σ ;

$v_f^{(s)}$: feature value of sample object for feature ;

$v_f^{(o)}$: feature value of image object for feature ;

σ_f : standard deviation of the feature values for feature f

Figure 4.8 a. shows the feature space optimization window with the user defined features for respective classes and the result of optimized feature space. The advanced information of the result is shown in figure 4.8 b. window which displays all feature combinations and their corresponding distance values for the closest samples of the classes. The result chart shows the

calculated maximum distances of the closest samples along the dimensions of the feature spaces, performed in *eCognition* software project.

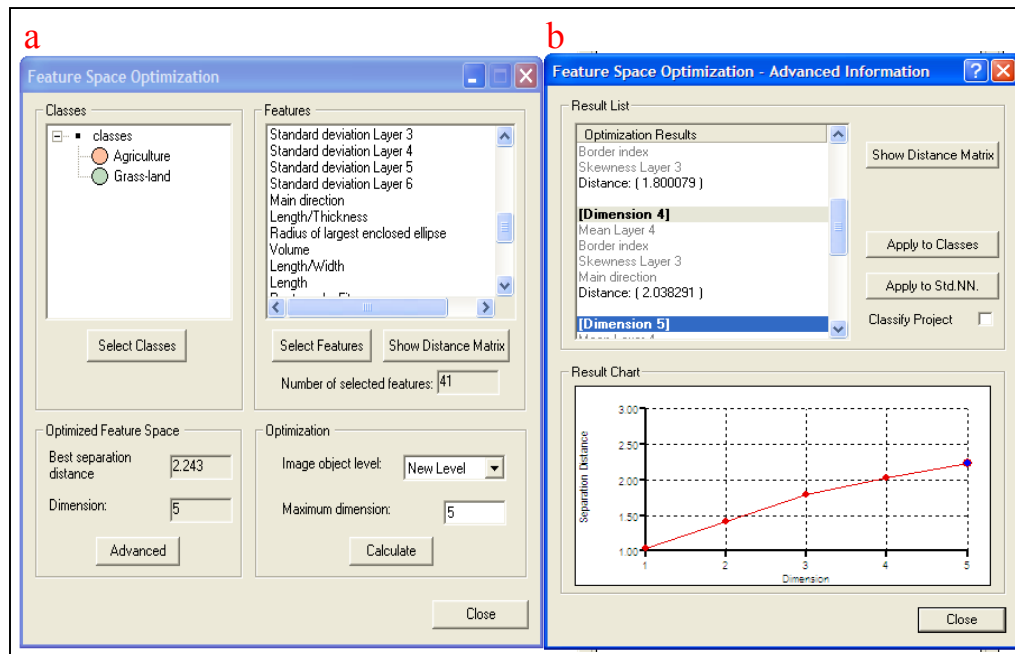


Figure 4-8: a) The feature space optimization input parameters, and b) advance information dialog box in *eCognition* software

Rule-based method

The process starts with primitive image objects achieved by multiresolution segmentation as described earlier. An appropriate segmentation algorithm leads to meaningful image objects which are directly linked to real-world objects under investigation. The study utilizes physical and spatial properties derived based on user's expert knowledge to generate LU/LC classes by combinations of rules to interpret objects of interest, which it has been well-known as rule-sets in *eCognition* software.

The RB emulates human logical thinking. The study visually investigates represented image objects to take a decision for the best features that should be considered to discriminate respective classes. Accordingly, the mean layers values have been selected as main features to discriminate between most of the investigated objects. An exception was made using subsequent rules such as geometrical features and texture values, which effectively optimize or correct most of misclassified objects. For example, due to the different phenological stages of cropped area, the

class has various spectral values; these objects were solved in the proposed approach with the condition that all vegetation classes and/or objects that are completely enclosed by croplands occupying an area less than “n” pixels have to be classified as “croplands”.

4.3.3.2. Pixel-based approach

In pixel-based image analysis approaches the main idea of image classification strategy is to categorize all pixels in an image into a homogeneous LU/LC classes based on pixel-by-pixel spectral properties (Lillesand *et al.*, 2008).

The process in the approach is represented by a hard classifier. Each pixel only belongs to one class. In the present study, two basic kinds of pixel based classification approaches have been applied for different purposes, i.e. supervised classification and unsupervised classification.

Unsupervised classification

An unsupervised classifier is normally utilised where no reference data or previous knowledge is presented as the basis for LU/LC classification. Alternatively, this classifier involves testing algorithms for the unknown pixels in an image and aggregates them into a number of thematic classes representing natural clusters of the image values (Lillesand *et al.*, 2008).

In the early stages of this work, unsupervised classification was applied to classify the image into different strata to be used for determination of representing field survey samples based on proportional allocation strategy.

There are various clustering algorithms that can be used in the unsupervised classifier to calculate the natural groupings present in a dataset (Lillesand *et al.*, 2008). The study performed the classifier based on K-means approach performed in ERDAS IMAGINE 8.7 software, the process proceeds with predefined eleven clusters that have been located in the data. The algorithm then arbitrarily locates that number of cluster centers in the multidimensional measurement space. Each pixel in the image is then assigned to the cluster whose arbitrary mean vector is nearest. After all pixels have been classified in this manner, revised mean vectors for each of the clusters are manipulated. The revised mean is then used as the basis to reclassify the image data. The procedure continues until there is no significant change in the location of cluster mean vectors

between successive iterations of the algorithm (Lillesand *et al.*, 2008). Once this point is achieved, the identity of each proposed class category was specified.

Supervised classification

The study applies supervised classifier as a traditional per-pixel approach based on spectral properties to evaluate the effectiveness of introducing image feature information like shape and texture measures provided by the proposed innovative OBIA approaches.

ML classifier was selected as one of the commonly used methods, when it quantitatively evaluates both the variance and covariance of the category spectral response patterns classifying an unknown pixel (Lillesand *et al.*, 2008). The study utilises the training samples that were collected during the field survey mission to assemble a set of statistics to describe the spectral response pattern for each class category to be classified in the image.

As described in figure 4.9, the maximum likelihood classifier delineates ellipsoidal “equiprobability contours” through a scatter diagram. The probability density functions are used to classify pixel 1 by computing the probability of the pixel value belonging to each category. After evaluating the probability, the pixel was assigned to the highest probability value of class category “2”. Otherwise it can be labeled as “unclassified” if the probability values of all categories were below a threshold defined by user (Lillesand *et al.*, 2008).

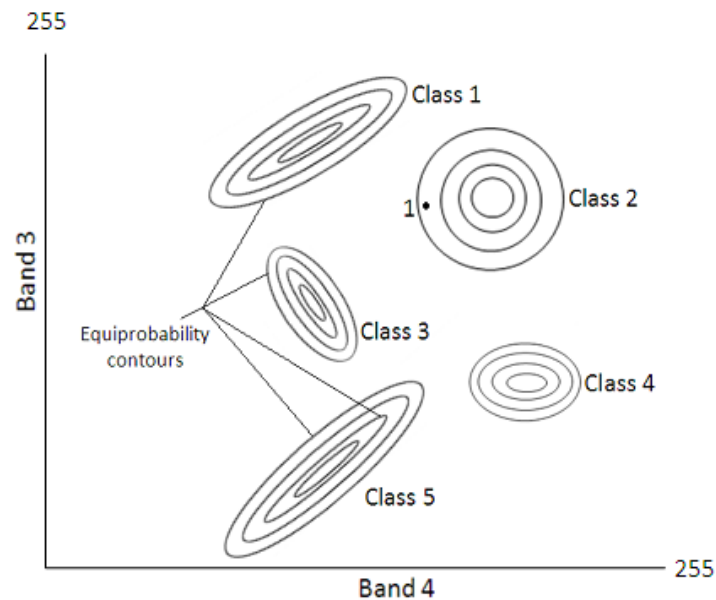


Figure 4-9: Equiprobability contours defined by a maximum likelihood classifier

4.3.4. Change detection

Multi-temporal analysis of the classified imagery was applied by utilizing OB fused image data. In order to perform an appropriate multi-temporal analysis, post change detection technique might reduce the possible effects of atmosphere, sun angle, seasonal variation of acquired date and multi-sensor variability (Singh, 1989). However, rather than using multi-spectral imagery, the classified images were used. In addition, the post-classification comparison provides class changes from-to as well as a change matrix.

OB post-classification comparison was applied between the dates 1990 and 1999 as well as 1999 and 2009. Each pair of classified images was overlaid, segmented and reclassified. Simple change analysis (each pair of image separately) was applied due to the rapid changes observed in the study area during the past decades, which obtain a very heterogeneous result if more than two images were overlaid.

Multiresolution segmentation algorithm was applied to create objects with restricted boundaries that separate different LU/LC classes generated from bi-temporal thematic layer. In other words, the segmented objects were not allowed to move over any of the borders of other LU/LC categories.

The change analysis utilizes the information on segmented LU/LC classes to be attached to each of the image objects. Subsequently, series of rule sets were developed to discriminate between LU/LC change classes. The rule sets were structured based on mean layer values as follows: if mean layer values of " t_0 " image objects \neq mean layer values of " t_1 " of that location, the output class is recorded as a change class " $t_0 - t_1$ ". The rule sets for "no-change" corresponded to: if mean layers value of " t_0 " image objects = mean layer values of " t_1 " of that location. The final change maps "from-to" with the 61 and 62 change categories as well as the classes of no-change were created for the periods 1990 to 1999 and 1999 to 2009 respectively.

In object-based post-classification comparison a hierarchical system provides a tool to enhance the quality of the results according to the research objective. Hence, some aggregated change categories were generated from a single process trend in child classes to be represented by enhanced parent change class categories in the class hierarchy window. For example, "Deforestation" (Def.) category represents all dense or scattered forest class categories that were converted to any non-forest class categories and the reverse was applied to the "Reforestation" (Ref.) parent class.

The post-classification method for LU/LC change detection depends directly on the accuracy of individual classification results (Foody, 2002). Hence, the accuracy assessment of the post-change classified maps could be roughly estimated by multiplying the accuracies of each pair of individual classification, which often reveals accuracies highly relevant to the product of the input classified dataset used (Mas, 1999). Moreover, the generated results from the change detection were compared and assessed with independent set of field data.

4.3.5. Classification accuracy assessment

In order to assess the quality of the classification results, stratified random field survey samples were selected to create an error matrix also referred to as confusion matrix or contingency table. An error matrix is a square assortment of numbers defined in rows and columns that represent the number of sample units (pixel in our case) assigned to a specific class as represented in the classification result relative to an actual class as defined on the ground. The rows in the matrix represent the LU/LC classified maps (figure 6.2), while the columns represent the reference values (ground truth) that were collected during the field mission (section 4.2.2). These tables

produce many statistical measures of thematic accuracy including KIA statistic, producer, user, hellden, short and overall classification accuracies.

The accuracy assessment is directly affected by the number of test samples. Therefore, a minimum number of 20 field samples was proposed for each class to achieve a representative error matrix, resulting in a minimum of 180 sampling units that should be considered (Congalton and Green, 2009). These criteria are met by 82%, as 148 samples were applied for result validation.

The imagery classified by the OB approach were defuzzified to be mutually exclusive, that means each mapped unit was assigned to that class which represents the higher membership value (Congalton and Green, 2009).

4.3.6. Forest parameters estimation and model validation

The study utilized multi-spectral remotely sensed satellite imagery analysed by OBIA versus per-pixel classification for forest parameters estimation. OBIA approaches provides additional information that can be derived from a homogeneous group of pixels such as object mean layers value, standard deviation, area, shape and texture measures rather than DN information available from each pixel separately.

In particular, the study aims to develop and validate a model for extracting forest stand parameters such as volume, basal area, height and stand density based on the relationship between plot-level forest inventory data and the information derived from TERRA ASTER and RapidEye multi-spectral imagery.

4.3.6.1. Image object information

A multiresolution segmentation algorithm was performed. By a bottom-up pair wise region merging technique applied in *eCognition* software to the image data of the study area the images were segmented into groups of homogeneous objects. The user can influence the result of the segmentation process through determination and weighting of input data and definition of parameters affecting the shape, size, spectral and spatial homogeneity of the resulting image segments. In terms of spatial characteristics, the TERRA ASTER VNIR and SWIR (Visible Near Infrared and Short Wave Infrared) bands, with a spatial resolution of 15 and 30 m respectively

captures more spatial detail than the 90 m TIR (Thermal Infrared) data. Although data layers of differing spatial resolutions can be used simultaneously in *eCognition*, the study utilized the highest resolution as input layers in Aster while the visible bands were used in RapidEye.

The segmentation parameters were set as described in table 4.6 which allowed for the creation of appropriate image objects. These image objects have to be calculated on multiple rounds of levels following an iterative ‘trial and error’ process to result in final image objects representing the single objects of interest as much as possible (Mueller *et al.*, 2004). The segmentation results were evaluated by the visual inspection of the quality of the output image segments (Mathieu *et al.*, 2007).

Table 4-6: Segmentation parameters applied for forest stand level

Criterion	Forest stand level
Input	TERRA ASTER & RapidEye
Layers	Green, red and NIR
Scale	7
Shape	0.8
Color	0.2
Smoothness	0.5
Compactness	0.5

The metrics information was derived from the segmented image and calculated by *eCognition* software for each image object. Several types of metrics can be used to describe the objects. The study utilized object layer value and texture measures based on OBIA, as well as DN from an individual pixel in pixel based approach.

Textural attributes of each segment were calculated based on VNIR bands, while the SWIR and TIR bands were excluded. The GLCM was used for evaluating the image texture of an object. GLCM is an approximation of the joint probability density function of pixel pairs, and it is fairly insensitive to outlier values (Herold *et al.*, 2003). The study measured one of the first-order textural attributes (mean object layer value “OLV”) and four of the second-order textural attributes (angular second moment, homogeneity, dissimilarity, and correlation). First-order textural attributes indicated the likelihood of observing a gray value at randomly chosen locations in an image and can be computed from a histogram of pixel intensities in the image (Tuceryan *et*

al., 1998). While second-order textural attributes define the likelihood of observing a pair of gray values at the ends of a dipole of random length placed at a random location and orientation (Tuceryan *et al.*, 1998). The mean of the DNs of the objects represents the intensity of spectral bands in the object. Angular second moment is the measure of the density distribution of co-occurrence matrix parameters. Homogeneity is the measure of image homogeneity and is sensitive to the presence of near-diagonal elements in the GLCM. Dissimilarity is a measure of the total variation present in each image object. Correlation is the measure of gray-tone linear dependencies in an image. These four second-order textural attributes used are mathematically calculated as follows;

Angular second moment:

$$\sum_{i,j=0}^{N-1} P_{i,j}^2 \quad (4.10)$$

Homogeneity:

$$\sum_{i,j=0}^{N-1} \frac{P_{i,j}}{1 + (i - j)^2} \quad (4.11)$$

Dissimilarity:

$$\sum_{i,j=0}^{N-1} P_{i,j} |i - j| \quad (4.12)$$

Correlation:

$$\sum_{i,j=0}^{N-1} P_{i,j} \left[\frac{(i - \mu_i)(j - \mu_j)}{\sqrt{(\sigma_i^2)(\sigma_j^2)}} \right] \quad (4.13)$$

Where

i : the row number

j : the column number

$P_{i,j}$: the normalized value in the cell i, j

N : the number of rows or columns

4.3.6.2. Field-plot data analysis

The field-plot measures described in section 4.2.2.3 were analyzed to estimate; tree volume per unit area, height, density based on number of trees per unit area and basal area.

The calculated number of trees in each sample plot was multiplied considering the sample area (0.09 ha) by estimating the stand density per hectare. The height was estimated by measuring three representative trees (the lowest, middle and highest stem diameter) in each sample plot. The average DBH was used to calculate the average basal area per unit area by using the Equation 4.14 While the volume (m³/ha) was calculated (Equation 4.15) by multiplying the Equation 4.14 with average sample height (m) (El Tayeb *et al.*, 2006), and the form factor of *Acacia nilotica* plantation ($f= 0.5$) as reported by FAO and FNC, (1998).

$$b = \pi * \frac{d^2}{4} \quad (4.14)$$

$$v = b * h * f \quad (4.15)$$

Where:

- b Basal area (cm)
- d Diameter at breast height (cm)
- v Volume (m³)
- h Height (m)
- f Form factor

4.3.6.3. Statistical analysis

In order to generalize at plot-level forest parameters information obtained from a small area in the entire study area (*Alambwa* reserved forest), TERRA ASTER subset imagery was used to simulate extracted parameter variability obtained from forest inventory data. In the OBIA and

the pixel-based approaches, independent texture attributes and DN values were sampled from a single object and a single pixel on the plot locations, respectively. The forest inventory data were used to extract dependent variables, including Basal Area (BA), Height (H), Density (D), and Volume (V). Pearson's correlation coefficient was applied to determine the relationship between forest metrics obtained from TERRA ASTER imagery data, including the above-mentioned textural attributes and the DN values from on side and the plot-level forest inventory data from the other side.

Subsequently, regression analysis was applied to model and analyzed the numerical independent texture attributes and DN values with forest parameters as dependent variables. Regression analyses were performed using linear, logarithmic and inverse models (Equations 4.16-4.18). Pearson's correlation coefficient and regression analyses were performed using the statistical package for the social sciences (SPSS) software for Windows.

Linear:
$$Y = b_0 + b_1x \quad (4.16)$$

Logarithmic:
$$Y = b_0 + b_1 \ln(x) \quad (4.17)$$

Inverse:
$$Y = b_0 + b_1/x \quad (4.18)$$

Where:

- Y Tree parameter
- b_0 A constant
- $b_{1...n}$ Regression coefficient
- x Variable (image metric at specific band)
- \ln The natural log base

4.3.6.4. Model validation

70 percent of the forest inventoried data were randomly selected for extraction of the forest dependent variables, while the entire 30 percent was used for model validation.

The RMSE has been used to measure the differences between values predicted by a model and the values actually observed or modeled. On the other hand, the determination coefficient (R^2) is indicative of the proportion of variability between prediction and estimation of a model. Both of them were used to evaluate the performance of the regression model and to estimate the accuracy of the results obtained, based on various link functions applied. Hence, the higher R^2 and the lowest RMSE represents the best fitted model (Equations 4.19 and 4.20).

$$R^2 = 1 - \frac{\sum_{i=1}^n (y_i - \hat{y}_i)^2}{\sum_{i=1}^n (y_i - \bar{y})^2} \quad (4.19)$$

$$RMSE = \sqrt{\frac{\sum_{i=1}^n (y_i - \hat{y}_i)^2}{n - 1}} \quad (4.20)$$

Where:

- \hat{y}_i Modeled value
- y_i Observed value
- \bar{y} Mean of the observed value
- n Number of the test parameters

Chapter 5 LAND USE/ LAND COVER ANALYSES

5.1.General overview

Due to the complexity and spectral similarity in semi-arid areas, LU/LC mapping with remotely sensed data encounters serious problems when applied to the methods based on spectral information and ignore spatial information. This chapter aims to evaluate the effectiveness of OBIA versus pixel-based classification approaches to generate LU/LC thematic maps in the Blue Nile region of Sudan based on TERRA ASTER and RapidEye multi-spectral imagery. Nine LU/LC classes are needed to be identified i.e. agriculture (rain-fed), bare-land, crop-land, dense-forest, scattered-forest, grassland, orchard, settlements and water body. ML Classifier was applied to examine if the spectral properties of the selected classes alone can be discriminated effectively. In contrast, different segmentation strategies were applied with the OBIA paradigm that might be effective to separate similar spectral values into a basic unclassified image objects in groups of relatively homogeneous pixels based on the shape and compactness criterion at different scales. The segmented objects were assigned to LU/LC classes with the method of Rule-Based (RB) and NN Classifier. Therefore, the classification results as well as the validation statistics are shown and compared (figure 5.1).

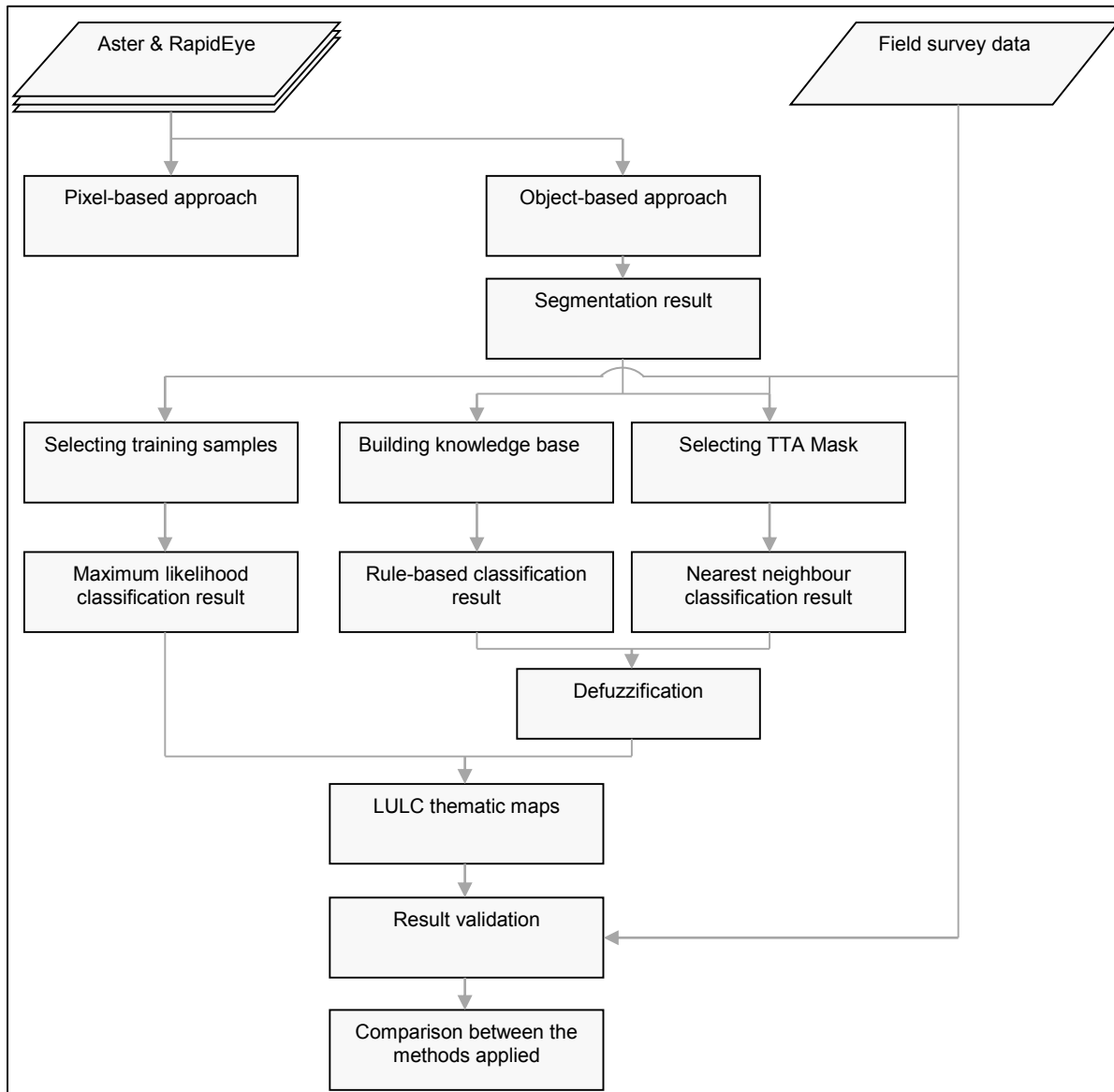


Figure 5-1: Structure of the results achieved from LU/LC image analysis

5.2.Pixel-based classification of Aster imagery by maximum likelihood (ML) classifier

The conventional per-pixel approach based on ML classifier was performed according to the spectral information of TERRA ASTER imagery data. The classification unit is a single pixel, and one pixel only belongs to one class. Training samples representing the typical spectral pattern for each LU/LC class were defined. By using a combination of TERRA ASTER nine spectral bands (VNIR+ SWIR) and the field survey data, the nine LU/LC classes are needed to be

distinguished. Then the quality of the results has to be assessed by an independent set of testing samples.

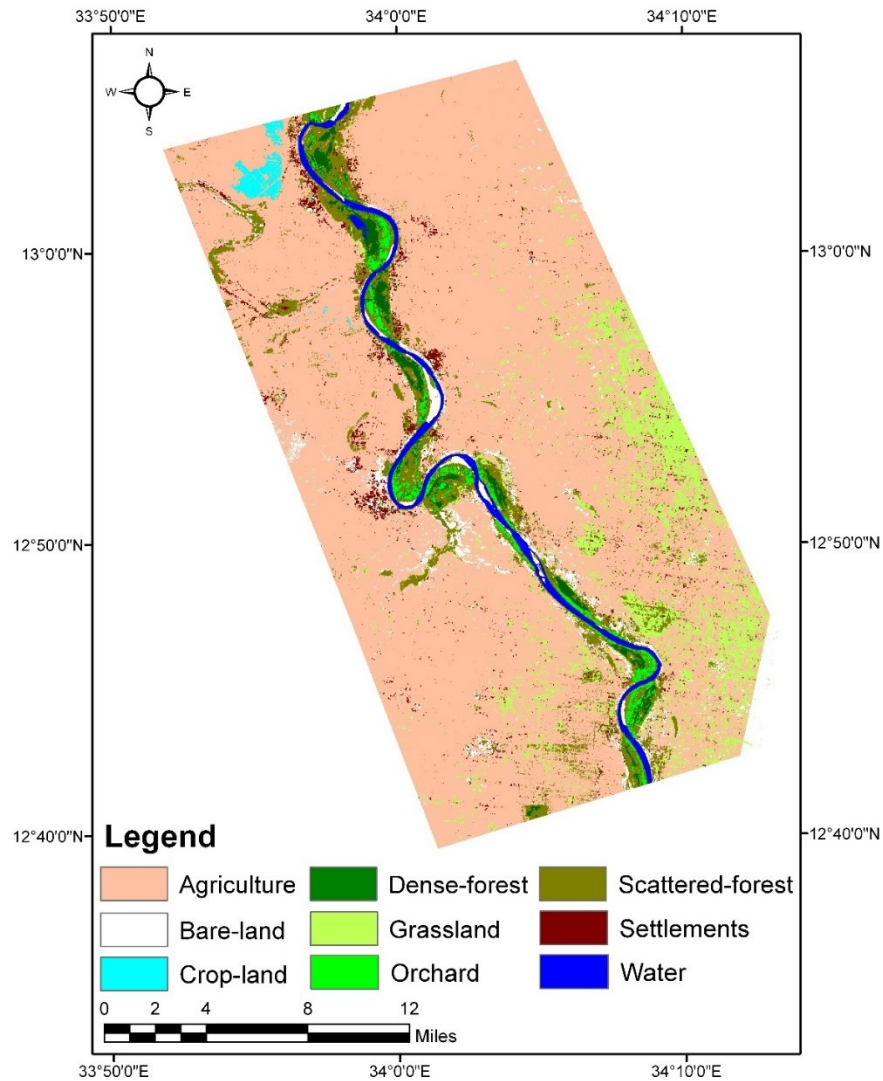


Figure 5-2: Thematic map of study area developed from 2009 TERRA ASTER scene using maximum likelihood classifier and nine LU/LC classes

Table 5-1: Error matrix of maximum likelihood classification ($k=0.79$)

Category	Reference									User's accuracy
	1	2	3	4	5	6	7	8	9	
1. Agriculture	13	0	1	1	0	0	0	0	1	0.81
2. Bare-land	1	14	0	0	0	0	0	0	0	0.93
3. Water	0	0	15	0	0	0	0	1	0	0.94
4. Grassland	2	0	0	11	0	0	0	2	1	0.73
5. Orchard	0	0	0	0	14	2	0	0	0	0.88
6. Dense-forest	0	0	0	0	2	14	0	0	0	0.88
7. Scat.-forest	1	0	0	1	0	1	16	1	3	0.73
8. Crop-land	0	0	1	1	0	0	0	12	0	0.86
9. Settlements	0	2	0	2	0	0	2	0	12	0.67
Producer's accuracy	0.76	0.88	0.88	0.69	0.88	0.82	0.89	0.86	0.71	
Overall accuracy = 0.82										

As expected earlier, due to the closer spectral distances of different classes, and groups of pixels that correspond to the same class did not have identical spectral information on the others, confusions were observed in most of the LU/LC classes in the study area by using this method. The best classification results achieved by this approach are shown in figure 5.2 and the incorporated error matrix is highlighted in table 5.1. The overall classification accuracy is 82% (Kappa 79%), however some classes performed better than others. The lowest accuracy has been observed in settlements class. The producer's and user's accuracy ranged from 71% to 67% respectively. This classification method experiences difficulties in discriminating among agricultural fields (rain-fed) and grassland especially when the agricultural fields are fallow during the dry season. The error of commission obtained from agriculture and grassland classes were 19% and 27%, while the error of omission was 24% and 31%, respectively. The confusion occurred also in crop-land class, where irrigated croplands are wrongly classified as other vegetation types due to the stage variability and different types of crop cultivated. The water body obtained a higher user's accuracies (94%) as a result of the uniqueness of its spectral value compare to other LU/LC class categories.

From the previous discussion, it can be pointed-out that the conventional per-pixel approach is confused in classification of semi-arid areas, since the approach is not capable to deal with spectrally similar features. Therefore, produced a thematic map of this approach has confused accuracy due to the fact that various areas have spectrally similar features while it belongs to different classes.

5.3.OBIA approaches

OBIA is a technique that basically relies on fuzzy logic, which is used to translate the feature values of arbitrary range into fuzzy values ranging from 0 to 1, representing the degree of membership to a specific class or more.

Classification is the process of connecting the LU/LC classes with well-defined image objects. There are two fuzzy sets applied in the present study to discriminate between these classes; user defined features and membership function to be used for the NN classifier and RB method respectively.

5.3.1. Segmentation result

The image in OBIA approaches is segmented into meaningful objects is treated as a whole in the classification process. Dealing with meaningful image objects in the classification process, rather than with individual pixel values, distinguishes OBIA from most other classification paradigms. Segmentation algorithms utilized in OBIA approaches subdivide the entire image at any primitive desired objects, or re-segment specific image objects from other domain, which allows for hierarchical data processing strategy. However, the best segmentation result is the one that proposed to be the optimum information for the subsequent classification level. In the present study, several experimental trials of segmentation processes were performed utilizing small representative image subsets of the study area. These trials aimed to experiment the various scale factors and weighting parameters to visually evaluate their effects on output segmentation results. The selected criteria were applied later to the entire study area image subsets which resulted in the final output as shown in figure 5.3.

When performing a segmentation and classification processes over large area with OBIA paradigm, the process of various functions leading to slow or completely stuck the computation process. Therefore, several loops of segmentation and classification which are generated at each scale in the class hierarchy must be considered to deal with tremendous information in multi-spectral imagery. In different words, dealing with larger segmentation scale with restricted level of information as much as it provides satisfactory results rather than looking constantly for high level of details.

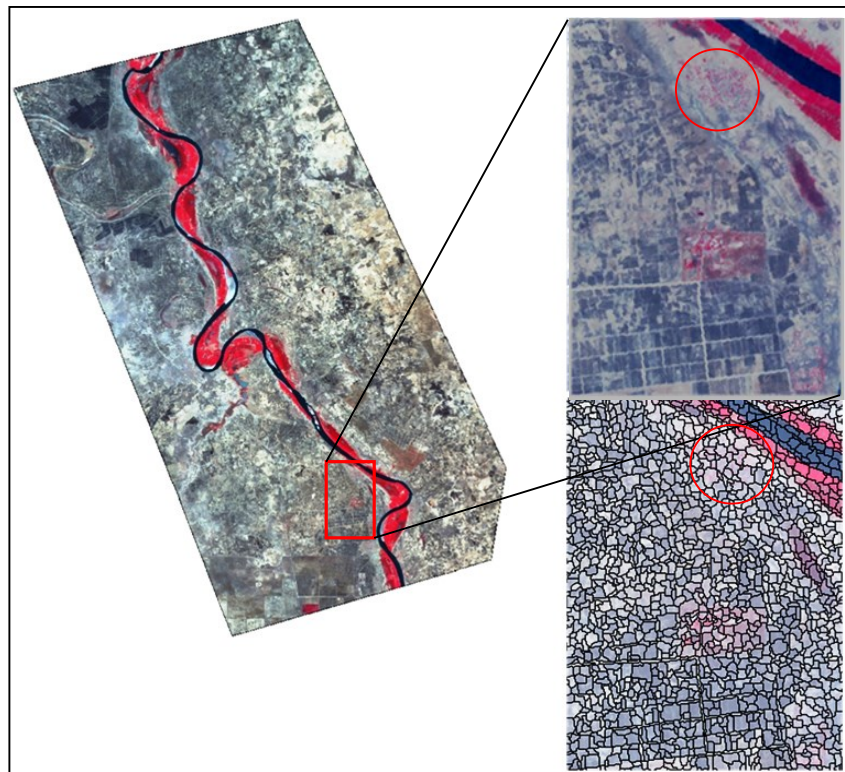


Figure 5-3: Final segmentation result of TERRA ASTER imagery used for classification at scale level 1. Subset of the entire study area (right); portion site used to train segmentation processes (upper right); final segmentation result of that level (lower right)

5.3.2. Hierarchical classification

As can be seen from figure 5.3, the segmentation result at this level creates coarse objects that is sufficient to discriminate between classes of this level. While, for example the red circle represents settlements area that are unable to be distinguished using this level of segmentation. Thus, a hierarchical system is proposed to attain LU/LC classes at three levels. The first level

was created to discriminate between water and land (non-water) parent classes. Subsequently, the second level aimed to separate vegetation from non-vegetation classes, which allowed for further separation of five and three LU/LC child classes respectively in the third level (figure 5.4).

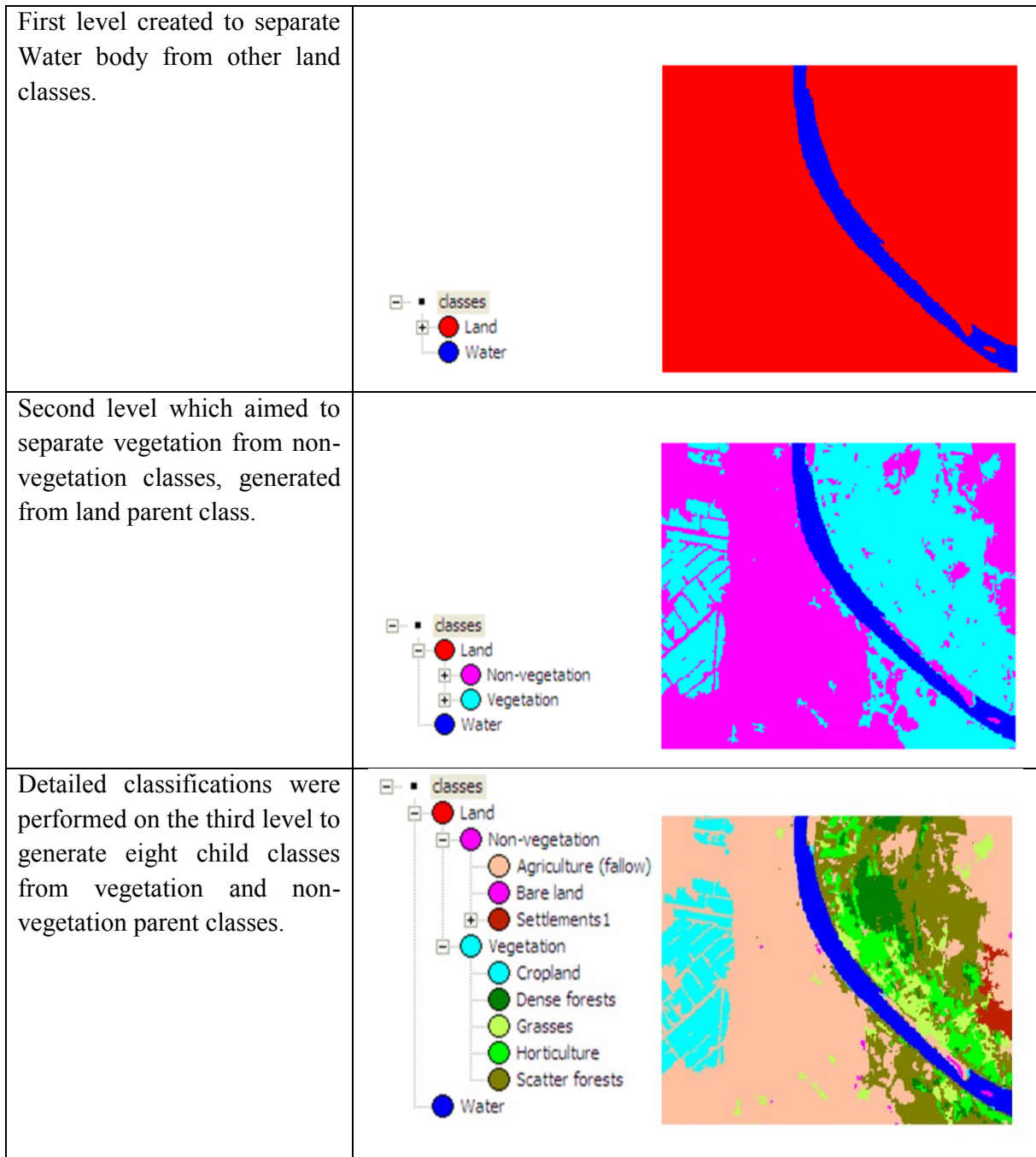


Figure 5-4: A hierarchical classification system applied to generate LU/LC classes in OBIA approaches. A figure extracted from eCognition viewer and its associated class hierarchy window

5.3.3. Object-based classification of Aster imagery by Nearest Neighbor (NN) classifier

In OBIA paradigm, the classification unit is a meaningful object and not the discrete pixel as in per-pixel approaches. The classified image objects do not belong to only one class, but also have a range of membership values, and the image object is assigned to one of the classes contains in the class hierarchy based on the highest membership value. As a result of complexity and spectral similarity in semi-arid areas, there were highly needed to test many variables of image objects for training. In NN classifier, after deciding how many classes are needed to be identified according to the classification objectives, sets of training objects are needed to be introduced. Accordingly the image object was assigned to specific class categories using optimal features is defined in *eCognition* software. In order to perform LU/LC classification based on this method, a combination of broad sets of image object features was applied for class description explained as follows:

- Layer value of respective band:
 - Mean brightness and layer values
 - Standard deviation
 - Mean difference to neighbor objects
- Texture value of respective band:
 - GLCM after Haralick (dissimilarity, homogeneity, entropy etc.)
- Object geometry:
 - Extent of object area in number of pixel
 - Extent of border length
 - Length/thickness
 - Shape features (compactness, density, main direction, roundness etc.)
 - Distance to super-object center
 - Based on skeleton (average branch length, average area represented by segments, length of main line etc.)
- Object position:
 - Distance to scene border

Applying NN as the classifier is similar to supervised classification and therefore training objects have to be selected. Accordingly, TTA Masks were generated based on the field survey data and were used for each LU/LC class to train the classifier. After performing the classification, classification results were visually assessed, and the process was edited by adding or removing some of the sample objects until obtaining a good classification result. Figure 5.5 shows the best classification result of TERRA ASTER VNIR and SWIR spectral bands using NN classifier to identify nine LU/LC classes.

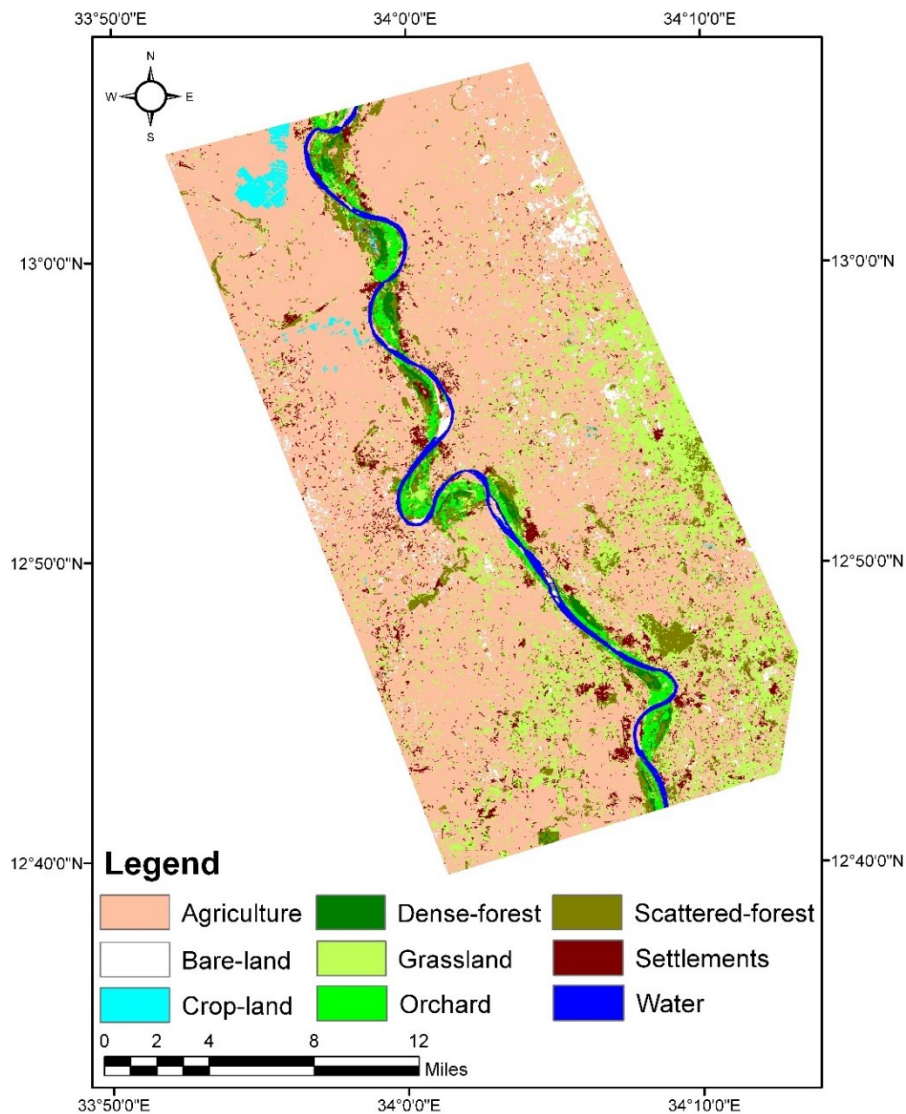


Figure 5-5: Thematic map of study area developed from 2009 TERRA ASTER scene using NN classifier and nine LU/LC classes

In order to assess the quality of the results obtained by this method, a same set of testing points used to assess the previous approach were introduced to *eCognition* software to generate TTA Mask. After defining the TTA Mask for each class an error matrix table was generated as shown in table 5.2 below.

Table 5-2: Error matrix of nearest neighbour classification ($k=0.88$)

Category	Reference									User's accuracy
	1	2	3	4	5	6	7	8	9	
1. Agriculture	14	0	0	1	0	0	0	0	0	0.93
2. Bare-land	1	15	0	0	0	0	0	0	0	0.94
3. Water	0	0	17	0	0	0	0	1	0	0.94
4. Grassland	2	0	0	13	0	0	0	1	0	0.81
5. Orchard	0	0	0	0	14	2	0	0	0	0.88
6. Dense-forest	0	0	0	0	2	15	0	1	0	0.88
7. Scat.-forest	0	0	0	1	0	0	16	0	1	0.89
8. Crop-land	0	0	0	1	0	0	0	13	0	0.93
9. Settlements	0	1	0	0	0	0	2	0	16	0.84
Producer's accuracy	0.82	0.94	1.00	0.81	0.88	0.88	0.89	0.87	0.94	
Overall accuracy = 0.89										

From the table 5.2 it can be seen that the overall classification accuracy was enhanced to 89% and that the kappa coefficient was 0.88, compared to the above mentioned ML classifier. Higher producer's and user's accuracies was achieved in most LU/LC classes and similar only in a water body. The clear difference between the classification accuracy of the two methods is observed in settlement class where the producer's accuracy improved from 71% in ML classifier to 94% in NN classifier, while the user's accuracy improved from 67% to 84% respectively. Most of the confusion detected in ML method was reduced by the incorporation of secondary information such as texture and context features provided by training objects applied to these classes which are crucial while it has similar spectral characteristics (Baatz *et al.*, 2004).

Considering more careful inspection to the accuracy matrix table, most of the confusion can be observed in grassland (81%), which is mainly confused with agricultural patterns. Reason for this is; the fact that object information contained in these classes is indistinguishable. Even through the field visit, we faced some difficulties to differentiate between these classes. Confusion was also observed in settlement class. 16% of the field survey data of settlement class was incorrectly classified as scattered forest. As discussed with the previous method, a considerable number of trees grown and protected by the local communities in between their buildings were the reason of the confusion as a result of unique spectral properties between these classes. In this classification method, due to the limited number of training objects especially in class orchard, a considerable weight was given to the spectral layer values in objects. This reason could explain the 12% confusion that was observed between orchard and scattered-forest.

5.3.4. Object-based classification of Aster imagery by rule-based (RB) method

The classification of the image objects in order to define LU/LC classes is accomplished with this method with the use of a fuzzy logic rule base. Also, the user expert knowledge is crucial for the quality of results. However, it depends on the best separation features defined by users rather than training sets in the above mentioned methods. The following examples describe the features and thresholds applied to calculate the membership value for the LU/LC classification:

- Agriculture at New Level, enclosed by Water: Bare-land
- Agriculture with GLCM Contrast Layer 1 (all dir.) ≤ 4092 at New Level: Grassland
- Scattered-forest Mean Layer 3 ≤ 2310 at new level: Croplands
- Unclassified with Mean Layer 3 $< > 3115-3310$ at Level 1: Orchard

The RB classification result is shown in figure 5.6. table 5.3 shows the error matrix associated with this classification. In the class orchard the confusion with grassland and scattered-forest categories observed in the above mentioned method was reduced due to specific geometrical features which allow distinction of orchard from grassland and scattered-forest. Hence, the producer's and user's accuracies increased from 88% to 100% and 94% respectively. There was also a great advantage as observed in the settlement class by the use of rule sets developed with a combination of user expert knowledge. These developed rules applied to settlement class

achieved high producer's and user's accuracies (94%), compared to 94% and 84% in NN method and 71% and 67% in ML classifier respectively.

The superior overall classification accuracy was achieved by the use of this method. The overall classification accuracy reaches 95% by improvement of 6% and 13% for NN and ML methods respectively. Meanwhile the reported kappa coefficient value is 0.94. The only slightly lower user's accuracies were produced by scattered-forest and grassland (89% and 88% respectively).

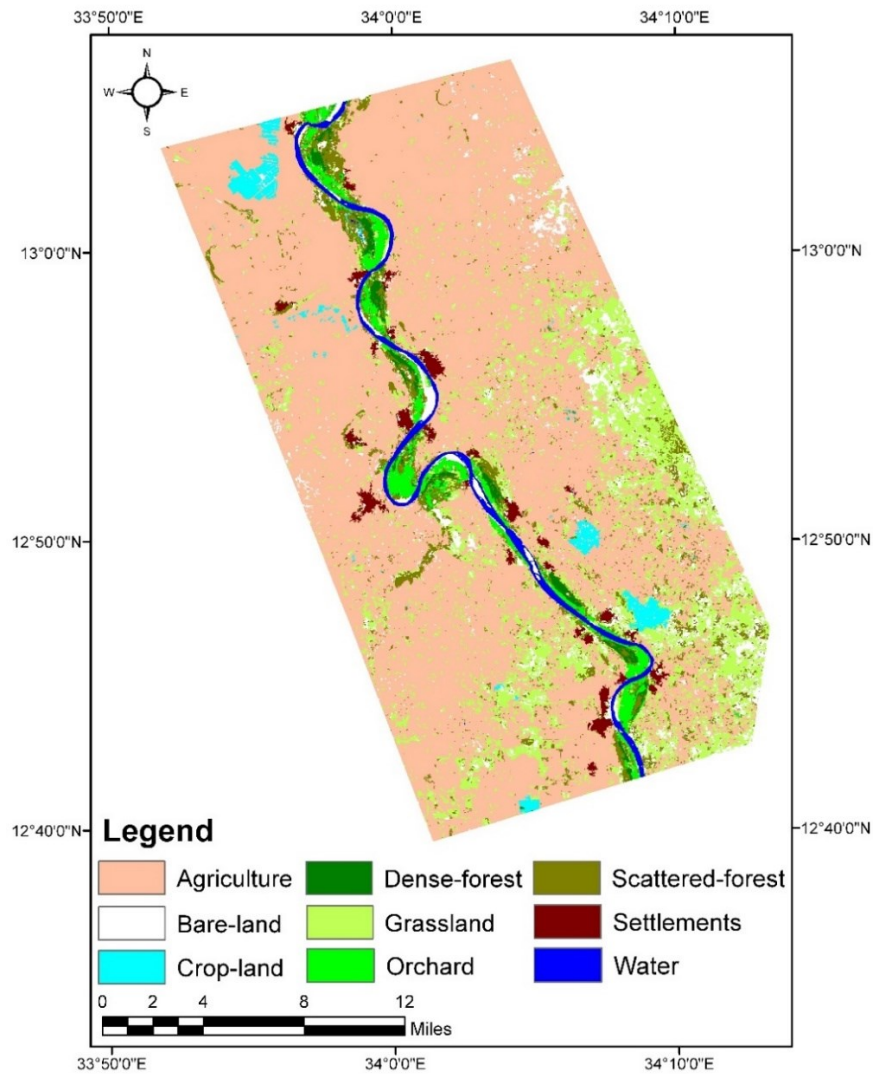


Figure 5-6: Thematic map of study area developed from 2009 TERRA ASTER scene using rule-based classifier and nine LU/LC classes

Table 5-3: Error matrix of rule-based classification ($k=0.94$)

Category	Reference									User's accuracy
	1	2	3	4	5	6	7	8	9	
1. Agriculture	15	0	0	1	0	0	0	0	0	0.94
2. Bare-land	1	16	0	0	0	0	0	0	0	0.94
3. Water	0	0	17	0	0	0	0	0	0	1.00
4. Grassland	1	0	0	14	0	0	0	1	0	0.88
5. Orchard	0	0	0	0	16	1	0	0	0	0.94
6. Dense-forest	0	0	0	0	0	16	0	0	0	1.00
7. Scat.-forest	0	0	0	1	0	0	17	0	1	0.89
8. Crop-land	0	0	0	0	0	0	0	15	0	1.00
9. Settlements	0	0	0	0	0	0	1	0	16	0.94
Producer's accuracy	0.88	1.00	1.00	0.87	1.00	0.94	0.95	0.94	0.94	
Overall accuracy = 0.95										

5.4.OBIA vs. per pixel classification

This section presents a comparison of results of accuracy assessments performed based on the three methods applied to nine TERRA ASTER imagery VNIR and SWIR bands, followed by some interpretation of the results and discussion of likely causes of mis-classified areas highlighted in the sample details of the output maps.

The classification approaches of OBIA and pixel-based were used to compare the performance of different methods applied, which focused on the extraction of nine LU/LC classes, representing agriculture (rain-fed), dense-forest, grassland, orchard, irrigated croplands, bare-land, scattered-forest, settlements, and water body, figures 5.2, 5.5, and 5.6 (see above) show the results of classification. The results of each method have been assessed by generating the error matrix utilizing the same testing samples as reference data. Figures 5.7 and 5.8 summarize the statistics of the producer's and user's accuracies of RB and NN from OBIA as well as the ML classifier which represent pixel-based approach. An OBIA achieved higher overall classification accuracies and higher individual LU/LC classes ("producer's accuracy" and "user's accuracy")

in spite of the method applies when compared with ML classifier of pixel-based approach. More specifically, in OBIA approaches an expert knowledge introduced to RB method improves the classification of NN classifier for most of LU/LC classes.

A better representative value to evaluate the classification accuracy performance is the Kappa statistic, which shows the measure of agreement between the classification result and the reference data, i.e. overall accuracy, and the chance agreement (Jensen, 2005). A Kappa statistic of > 80% suggests a strong agreement, while 40% to 80% is a moderate agreement. Thus, strong agreements were achieved in OBIA methods, while a moderate agreement was observed in pixel-based method.

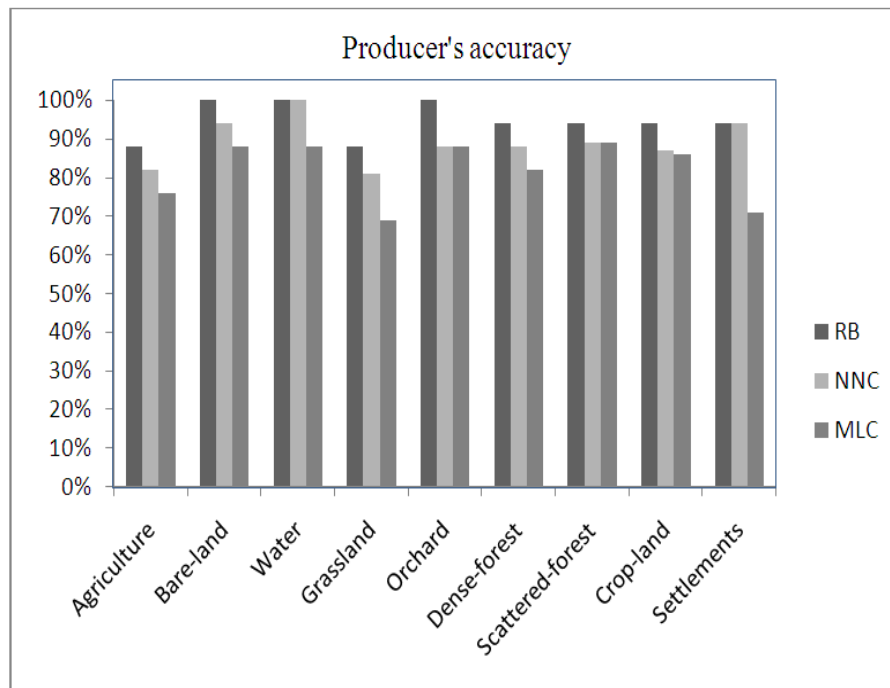


Figure 5-7: Summary statistics of producer's accuracy for each class category obtained from the different methods applied

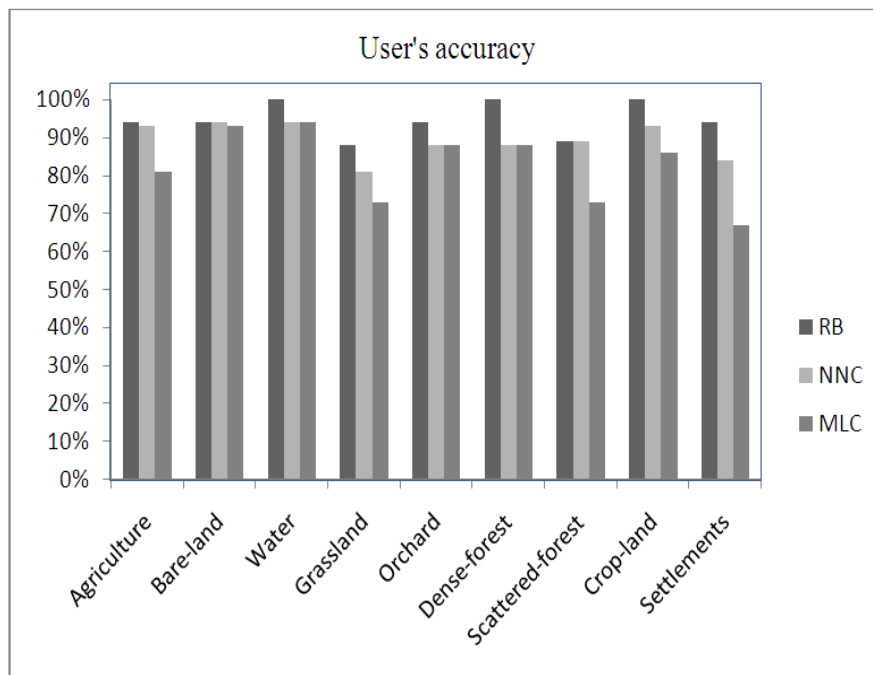


Figure 5-8: Summary statistics of user's accuracy for each class category obtained from the different methods applied

By looking at the summary statistics of LU/LC classification results as shown in table 5.4, the classification results obtained from different methods were compared. It can be seen that about two third of the area was classified as agricultural, while the rest shares the remaining portion. In NN classifier, the classes grassland and settlements were overestimated, which was represented by the higher error of commission, while a high error of omission was observed in agriculture class as shown in table 5.2.

Table 5-4: Quantitative results of the LU/LC classes achieved from different method applied

Class name	Rule-based		Nearest neighbour		Maximum likelihood	
	Area (ha)	%	Area (ha)	%	Area (ha)	%
Agriculture	73851.6	66.21	71033.9	63.68	73633.0	66.01
Bare-land	2882.9	2.58	6269.0	5.62	6485.4	5.814
Water	1881.2	1.69	4696.2	4.21	4820.0	4.321
Grassland	20625.3	18.49	16152.2	14.48	12459.9	11.17
Orchard	2182.4	1.96	3045.3	2.73	2721.8	2.44
Dense-forest	1109.4	0.99	1829.4	1.64	1963.2	1.76
Scattered-forest	6612.2	5.93	4673.9	4.19	6514.4	5.84
Crop-land	886.4	0.79	1524.9	1.367	1483.6	1.33
Settlements	1516.8	1.36	2320.2	2.08	1472.4	1.32
Total	111548.2	100	111544.9	100.00	111553.8	100

5.4.1. Classification of agricultural land

The field visit was conducted in the dry season which coincided with the season of EO data acquisition. Agricultural land is cultivated during the rainy season and harvested in November. Thus, the cultivated lands were observed clear and open during the field visit (figure 5.9). What makes the agriculture class perform poorly is that the class is confused especially with area of failure un-harvested crops, which become similar to other LU/LC classes like grassland. Moreover, difficulties were experienced to identify some pockets or strips of scattered trees and shrubs that were left intentionally by farmers, inside the agriculture class, as there are same spectral properties in the dry season, which results in inconsistency of classification in some areas. For this reason, even through the field visit, it appeared to be difficult to separate this class from grassland and scattered-forest classes in several areas.



Figure 5-9: A typical form of semi-mechanized rainfed agricultural field in dry season (Photograph was taken by the author)

As can be seen from the figures 5.7 and 5.8, this class was one of the most confused LU/LC classes. The producer's accuracy (omission) ranges from 76% in ML classifier to 88% in RB method, while the user's accuracy (commission) varied from 81% in ML classifier to 94% in RB method. The variation between user's and producer's accuracy could be explained by the limited number of reference points used to validate the result. Nevertheless, this trend of different methods applied coincided with the results achieved from all other LU/LC classes.

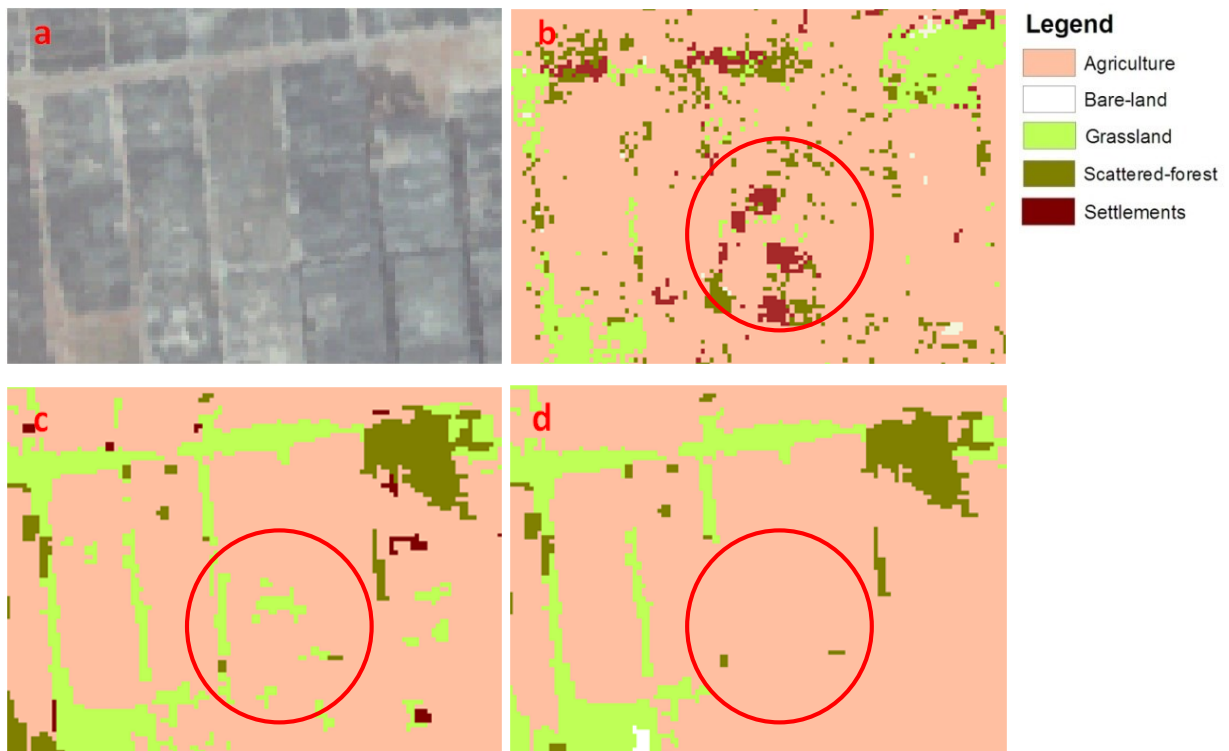


Figure 5-10: Misclassified areas in agricultural field. A) Unclassified scene, b) maximum likelihood classifier, c) nearest neighbour classifier, and d) rule-based classifier

Figure 5.10 was taken from the central part of the subset imagery. Undertaken more emphasis to the spatial and textural properties in OBIA methods, enhancement is observed in the methods of OBIA (figure 5.10 c and d), compared to the misclassified areas of pixel based approach (figure 5.10 b). The abandoned agricultural areas were recovered in most cases by grasses and scattered trees and shrubs from the dormant seed bank, which results in no pure objects these classes. Thus, this phenomenon impedes the classification and reduced the accuracy of the produced maps in most cases.

By the incorporation of user expert knowledge, some membership functions (e.g. “area” and “enclosed by class”) were used in d) to eliminate the presence of minor objects of the misclassified area as shown under the red circles.

5.4.2. Classification of residential areas

Due to the similarity of the spectral signature of settlements because of building materials (straw, wooden material and mud) and the dried-out vegetative areas (grassland class), there were spaces

between the housing pattern and agriculture fallow class, as well as due to the presence of trees in the villages confusion with scattered-forest class. Therefore, considering the 15 meter spatial resolution of Aster data, few pure pixel were found, therefore interferences occurred at the classifier which leads to inaccurate results in these classes. Figure 5.11 shows a typical form of housing pattern in the study area.



Figure 5-11: Partial view of housing pattern in Umbnean village in the study area (left) (Photograph taken by the author), Google earth view of the area (right)

From the figures 5.7 and 5.8, it can be seen that the classification accuracies were varied between the methods applied. Considering the user's accuracy and producer's accuracy of individual classes, for the settlements, the lowest accuracy was 67% and 71% respectively obtained from the ML classifier, while the gradual improvements were obtained in OBIA methods, which achieved 84% and 94% in NN classifier and 94% for both in RB method, respectively. In different words, that means only 67% of the area that is classified as settlement is truly in this category and also 71% of the settlements is correctly identified. While in OBIA paradigm, by the incorporation of user expert knowledge of RB method, 94% of the area were truly identified.

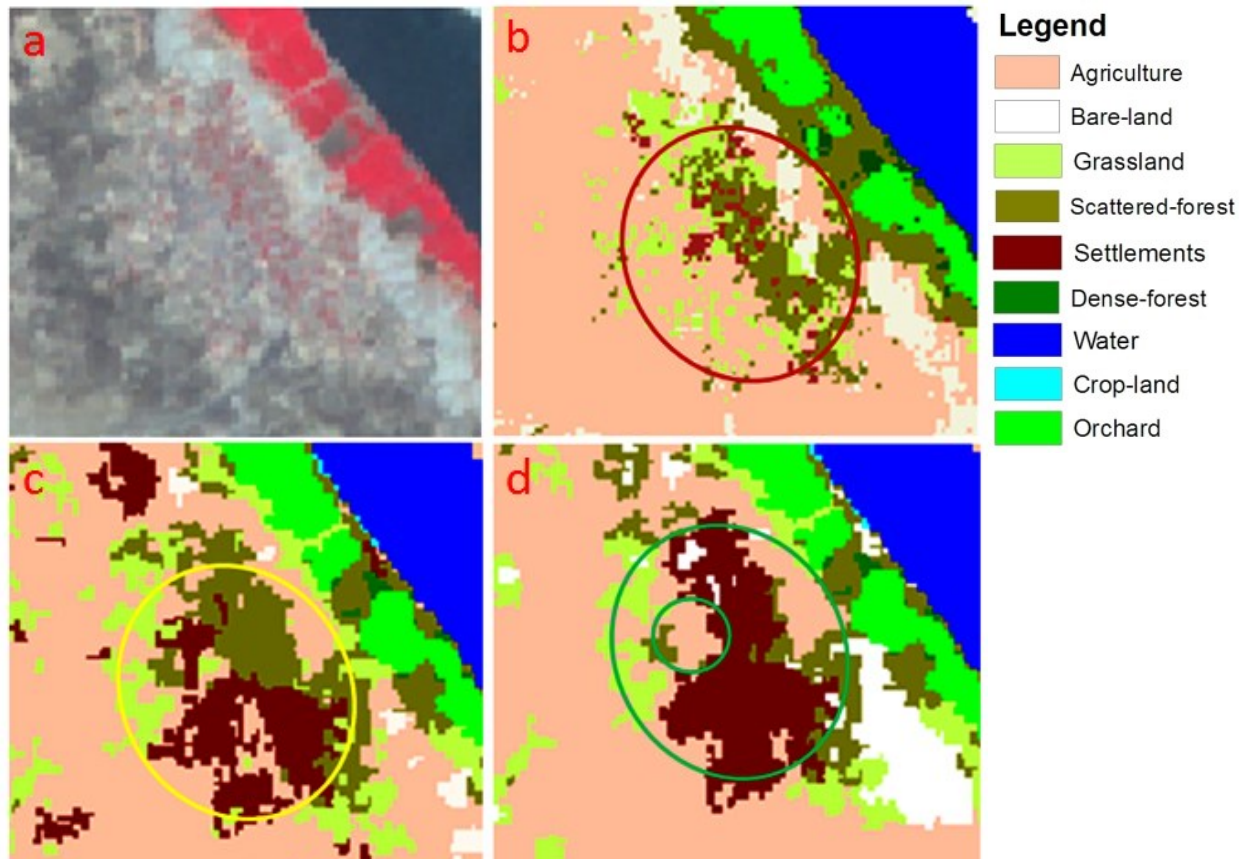


Figure 5-12: Misclassified areas of Merau village in the study area. A) Unclassified scene (colour infrared Aster imagery), b) maximum likelihood classifier, c) nearest neighbor classifier, d) rule-based classifier

Figure 5.12 was taken from the central part of the subset imagery. In pixel-based approach, a significant confusion exists (red circle) between settlement, grassland, scattered-forest, and agriculture. As discussed earlier, the missing of pure pixels and similarity (in spectral value) with the above mentioned classes leads to misclassifications in that area. In contrast OBIA leads to an improvement (yellow circle) as training objects were introduced under an appropriate segmentation level selected. However, the incorporation of textural features in addition to the spectral layer values leads to satisfactory results in most cases.

Comparing the methods applied in OBIA, accurate results were observed in RB method as shown under the green circle. An enhancement of this method was achieved by the use of a special set of conditions. For the example in order to describe the settlements class, beside the layer values of respective band, texture value (GLCM), object geometry (extent of object area in number of pixels, length/thickness, density, and roundness etc.) and enclosed by class were used

in an iterative process to deal with confused objects. Thus, a considerable amount of settlements was extracted and classified correctly, but under the small green circle there were still some objects which were wrongly classified as agriculture because the very low density of houses. Nevertheless, a superior result was achieved by the RB method.

The training objects used to classify the image in “c” might not be the appropriate for discriminating settlements from agriculture as shown under the black circles. Thus, an error of commission is relatively high as shown in figure 5.8. One of the reasons that could affect the classification accuracy in NN classifier is that a limited number of training objects selected to supervise the classifier, as well as the lack selection of representative meaningful objects prior the field visit, which could be also another reason for misclassifications in this method.

5.4.3. Discrimination of vegetation classes

The classification approaches were performed in different ways. In pixel based approach, by using field training data of the LU/LC distribution in the study area and in the image classification, classes were grouped into 9 spectral LU/LC class categories; five out of which were vegetation classes, i.e. grassland, cropland, scattered-forest, dense-forest and orchard. While in OBIA approaches, classes were achieved in editable and iterative processes as sub-child classes from vegetation parent class in the third level of the class hierarchy (figure 5.4). Accordingly, this advantage allowed for dealing with misclassified objects to be edited in the form of multidimensional feature in the feature space with different set of training objects in NN classifier or combinations of conditions to redefine the wrongly classified objects based on user expert knowledge in RB method. The agriculture class was excluded from this group, which was categorized under the non-vegetation parent class because it was uncultivated fallow land during the field visit as well as the EO data acquisition date.

By looking at the classification accuracy as shown in figures 5.7 and 5.8, and error matrices in tables 5.1, 5.2 and 5.3, it can be seen that the classification accuracies vary between the methods applied. Concerning the overall accuracy of vegetation classes, in RB method and NN classifier, the classification accuracies were 94% and 87% respectively, which is slightly lower than the results of the overall accuracy of all classes. This is probably due to the considerable number of objects occurring within the critical range of separation distances between these classes. On the

other hand, the vegetation classes in the pixel-based approach equally shared the confusion with other non-vegetation classes, whereas the vegetation classes show 82% classification accuracy. Coincided with results for other classes, superior accuracy was observed in RB method followed by NN classifier in OBIA, while the lowest accuracy was obtained from ML classifier in pixel-based approach.

Considering the user's accuracy and producer's accuracy of individual vegetation classes, the class grassland represents the lowest accuracy between the vegetation classes in all cases. Moreover, it is the lowest accuracy over the all classes in object-based methods, while it ranked as the second lowest accuracy in pixel-based approach after settlements class. The producer's accuracy and user's accuracy were found to be 87%, 88% and 81% in RB method and NN classifier respectively. While, the producer's accuracy and user's accuracy in pixel-based approach was found to be 69% and 73% respectively. As discussed earlier, this confusion could be explained by the unavailability of pure pixel, where the grassland commonly found in the association of scattered trees and shrubs. Moreover, the low density of grassland permits the reflection of soil cover led to confused result with agriculture class.

Giving more careful inspection to the classification accuracies, it can be seen that the error of commission in scattered-forest class is relatively high (73%) and is omitted from settlements, agriculture and grassland classes. One thing which should be considered that might affect the classification result is the high variability in this class, ranging from bush land (pure and mixed) near the Blue Nile valley, although it is tributaries to wood land in the south. Thus, the ML classifier experiences difficulties in discriminating between these classes. Meanwhile, in OBIA, the error of commission was reduced by 16% in both methods.

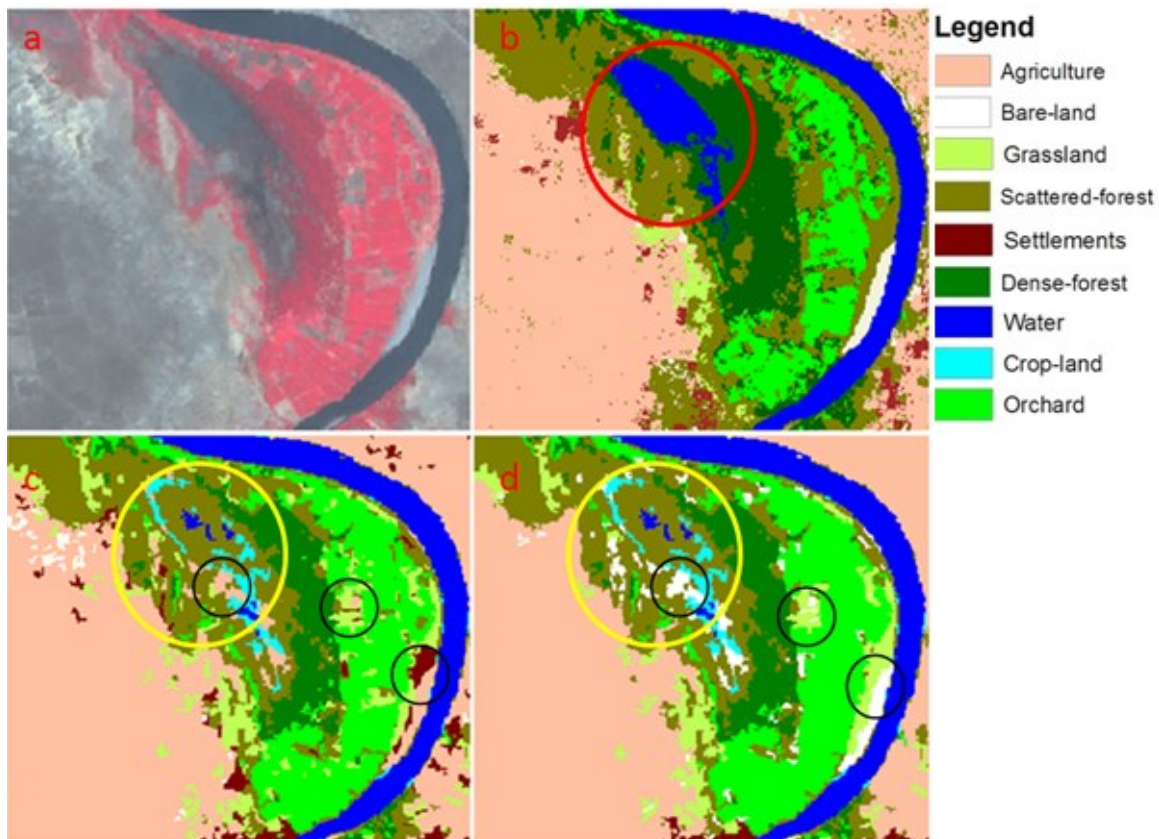


Figure 5-13: Misclassified areas of vegetation classes in the study area. a) Unclassified scene (colour infrared Aster imagery), b) maximum likelihood classifier, c) nearest neighbour classifier, and d) rule-based classifier

The figure 5.13 was taken from the upper part of the subset imagery. It shows a typical form of the Blue Nile valley in the region, with orchards near the riverbank, followed by *Acacia nilotica* pure stand forest in flooded areas of depressions, and scattered trees and shrubs in the upper part of the valley. The scattered-forest class under the red circle in b) was wrongly classified by the ML classifier as water body, which could be due to the presence of water in depressed areas. The misclassifications of that area were enhanced by the NN classifier in c) and RB method in d) as shown under the yellow circles.

As shown in the figure 5.13, confusions were observed under the yellow circles of c) and d) between scattered-forest, crop-land, bare-land and agriculture classes. The appearance of crop-land in the reserved forest area could be due to the *Tongya* system (after flood cultivation), which is adopted in Sudan to establish tree plantations in a clear cut area, where farmers are encouraged to cultivate primary crops after the rainy season (September to January) with full care of the tree

plantation during the first years of establishment. As shown in the figure 5.14 the red circle represents the *Acacia nilotica* seedlings while the green is the cultivated crop.



Figure 5-14: Reestablishment of *Acacia nilotica* plantation using “Tongya” system in the study area, (photograph taken by the author, summer 2008)

The incorporation of the RB method in d) reduced the misclassifications of the areas of “bare-land” class under the dark circles. The presence of the agriculture and settlements classes under the dark circles in c) may be attributed to the limited number of training objects, which affects the ability for extraction of additional information that might be available in the image objects.

5.5. Scale issue and hierarchical OBIA for mapping LU/LC

5.5.1. Overview

For simplicity’s sake, the term ‘scale’ referring to the spatial resolution, is used although it is worth mentioning that image scale has additional components (Warner *et al.* 2009). In most of the previous studies, when studying the issue of scale, scientists only investigating a specific geographical environment (a scene), such as a forest land, an urbanized zone, or an agricultural field. They also searched for the most appropriate unique spatial resolution for their particular concern. It was rarely considered that the scene was composed of different sized real-world entities, and that a single resolution might not be appropriate to discriminate all classes within the image. Fine spatial resolution imagery is assumed to provide detailed attribute

characterizations, meanwhile within class variances of the spectrum is subsequently increased, which leads to confused results in most cases. Therefore, an implicit assumption of the OBIA literature is that the analysis and classification based on contiguous segmented homogeneous pixels (i.e. image objects) is more accurate than pixel-based methods for high spatial resolution, since the objects efficiently suppress this local variability in the final thematic map product (Johansen *et al.* 2009; Kim *et al.* 2011). However, questions arise whether OBIA is inherently more precise at fine spatial resolution than coarser resolution, and how both pixel-based and OBIA approaches are compared in the relative accuracy as a function of spatial resolution. This section investigates these assumptions within the context of a case study of LU/LC classification system for use with optical multispectral satellite data in the Blue Nile region of Sudan. A RapidEye scene data of 2010, with 5 meter spatial resolution, were used to generate thematic nine LU/LC classes. The image was classified using both maximum likelihood as a common method of pixel-based, as well as OBIA. The results were compared with the classified maps of coarser resolution achieved from Terra Aster image data, with 15 meter spatial resolution, utilizing the same spectral regions, unique approaches and an identical set of training samples. Field survey validation points were implemented to assess the quality of results achieved based on confusion matrices. Consequently, in this section we discussed the characteristics of the hierarchical ecosystem of LU/LC classifications based on the different spatial resolutions of the image sensors utilized.

5.5.2. Pixel-based classification of higher resolution RapidEye scene

The conventional per-pixel approach based on ML classifier was performed based on spectral information on Rapideye imagery data. The classification unit is a single pixel, and one pixel only belongs to one class. Training samples representing the typical spectral pattern for each LU/LC class were defined. The classes were discriminated based on four spectral RapidEye bands (VNIR) aided with the field survey data. Subsequently, the quality of the results was assessed by an independent set of testing samples.

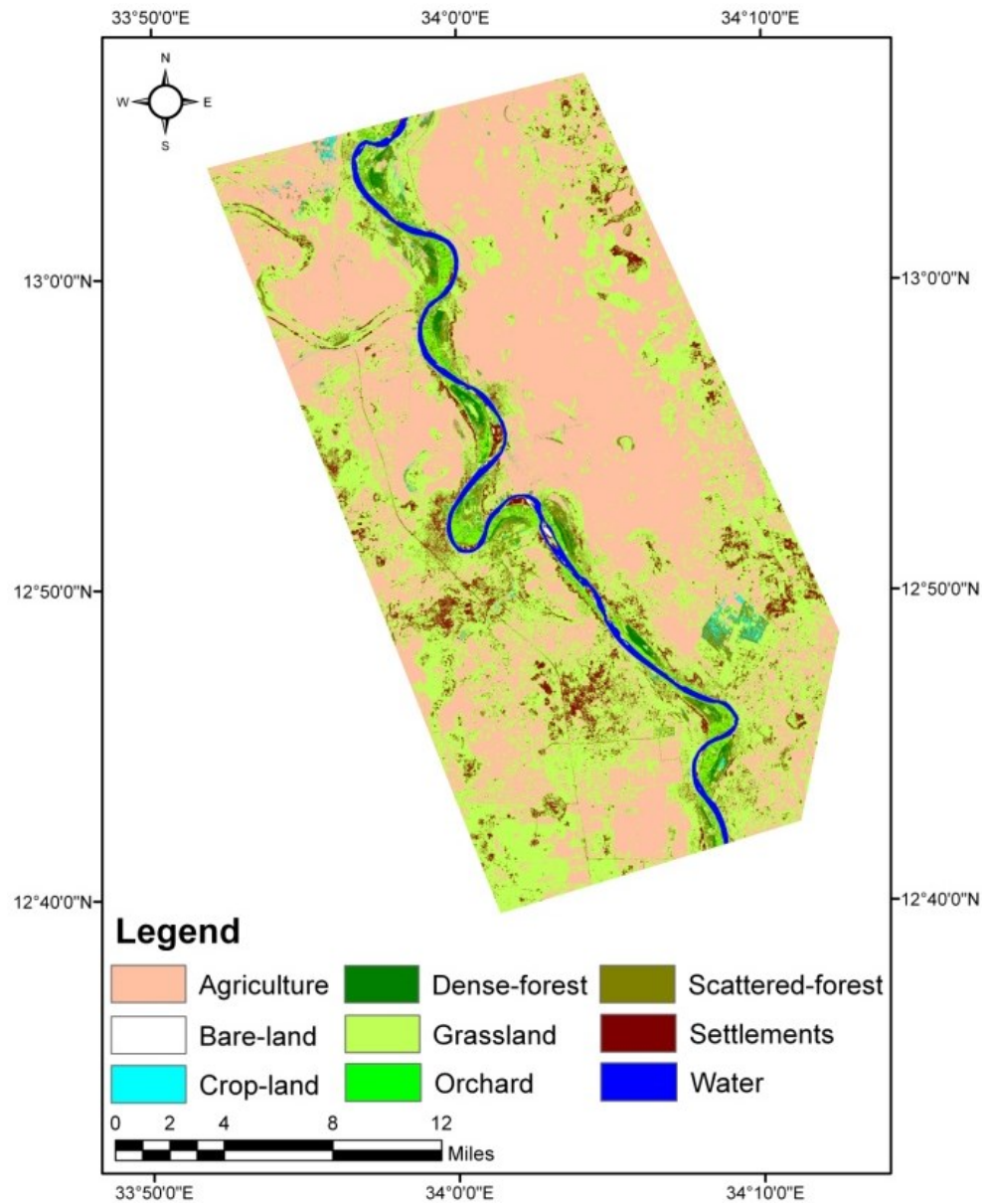


Figure 5-15: Thematic map of study area developed from 2010 RapidEye scene using maximum likelihood classifier and nine LU/LC classes

Table 5-5: Error matrix of maximum likelihood classification ($k=0.84$)

Category	Reference									User's accuracy
	1	2	3	4	5	6	7	8	9	
1. Agriculture	12	1	0	0	1	0	0	0	0	0.86
2. Bare-land	0	13	0	0	0	0	0	0	0	1.00
3. Water	0	1	11	0	0	0	0	0	0	0.92
4. Grassland	3	0	0	13	0	0	0	1	0	0.73
5. Orchard	0	0	0	0	15	0	0	0	0	1.00
6. Dense-forest	0	0	0	0	2	14	1	0	0	0.82
7. Scat.-forest	0	0	0	0	0	2	18	3	1	0.75
8. Crop-land	0	0	0	0	0	0	0	11	0	1.00
9. Settlements	1	0	0	3	0	0	0	0	10	0.71
Producer's accuracy	0.75	0.87	1.00	0.69	0.88	0.88	0.95	0.69	0.91	
Overall accuracy = 0.85										

The best classification results achieved by this approach were shown in figure 5.15 while the accuracy results as error matrix were represented in table 5.5. As anticipated, confusion matrix was observed in many areas by the use of this approach. Overall accuracy for pixel-based image classification is 85% (Kappa 84%), however some classes performed better than others. Water body Class has higher accuracy (100% producer's accuracy and 92% as user's accuracy) which is attributed to the uniqueness of its spectral value as the remaining areas of the image represent very different spectral information compared to this class. The lowest accuracy has been observed in grassland class which is confused with agricultural fields and settlement class, while the reported accuracies are between 69% as producer's accuracy and 73% as user's accuracy. This confusion attributed to units of pixels within the same class have heterogeneous values due to the increased class variances of spectrum in high resolution imagery. This classification method experienced difficulty in discriminating among agricultural fields (rain-fed), settlements and grassland especially when the agricultural fields are fallow during the dry season. The error of commission obtained from agriculture, settlements and grassland classes were 14%, 29% and 27%, while the error of omission was 25%, 9% and 31%, respectively. The confusion occurred also in crop-land class, where irrigated croplands are wrongly classified as scattered-forest due to the stage variability and different types of crop cultivated. It is expected that different soil type

must have a different digital number to easily be distinguished in a unique class. Because in the study area; the bare-land class is distributed within or around other land cover types and vary within the year. The ML classifier for this specific class is confused with agricultural fields and water body as a result of seasonal variations in the acquisition period of validation points and/or the registration error.

From the previous discussion, it can be pointed-out that the conventional per-pixel approach is confused in classification of semi-arid areas regardless of the scale applied, since the approach is not capable to deal with spectrally similar features of different classes or to deal with the issue of within class spectral variability.

5.5.3. Object-based classification of higher resolution RapidEye scene

As mentioned earlier, in the OBIA paradigm, the classification unit means the full object rather than individual pixels as in conventional per-pixel approaches thus classified image objects do not belong to only one class, but have a range of membership values, and the image object is assigned to the class contained in the class hierarchy which shows the highest membership value. The classification of the image objects to define LU/LC classes is accomplished in this approach with the use of a fuzzy logic rule-based. The user expert knowledge is crucial for the quality of the results; however it depends on the best separation features and distances defined by the user rather than training set utilized in the above mentioned method. In this section the best classification results (figure 5.16) are presented and discussed based on confusion matrix (table 5.6).

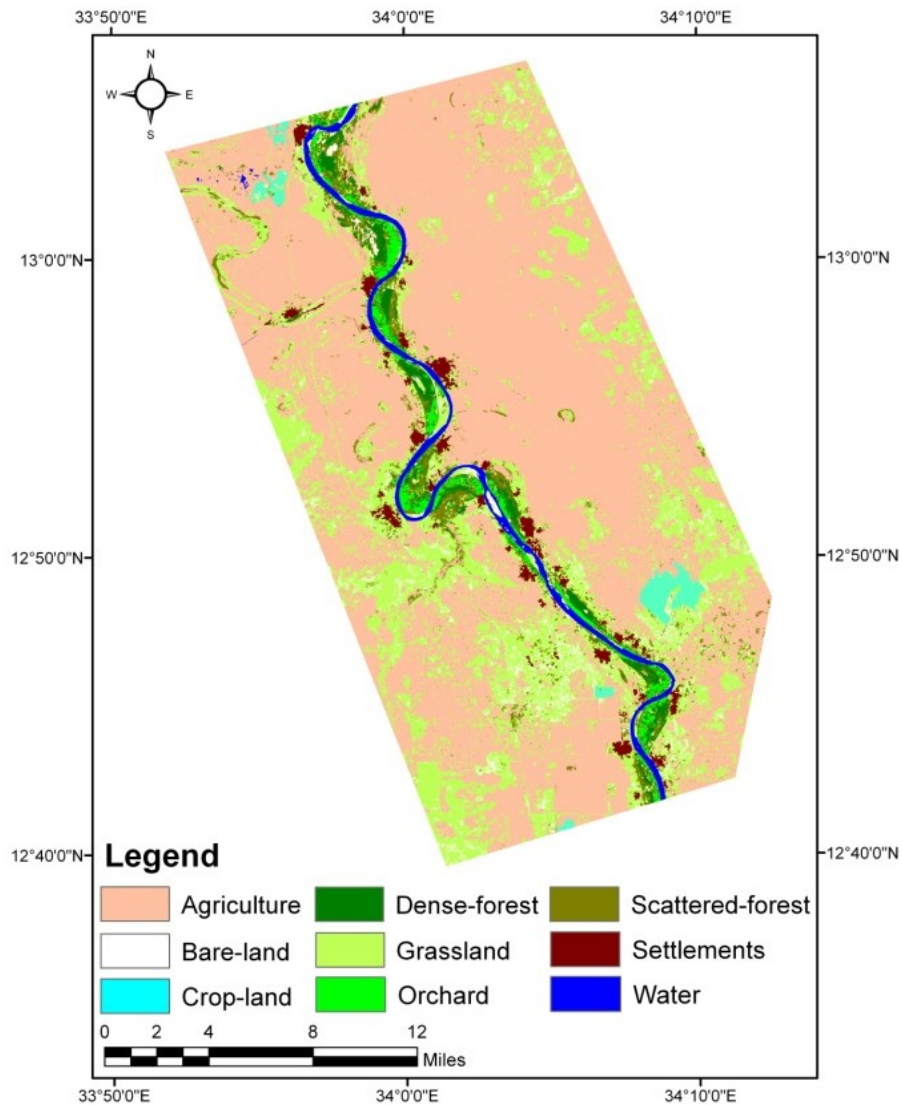


Figure 5-16: Thematic map of study area developed from 2010 RapidEye scene using rule-based classifier and nine LU/LC classes

The quality of the results obtained by this approach are validated utilizing an identical set of testing samples used to assess the previous approach. TTA Mask was used in *eCognition* software to generate an error matrix table as shown in table 5.6 below.

Table 5-6: Error matrix of rule-based classification ($k=0.96$)

Category	Reference									User's accuracy
	1	2	3	4	5	6	7	8	9	
1. Agriculture	29	0	0	0	0	0	0	0	0	1.00
2. Bare-land	0	21	0	0	0	0	0	0	0	1.00
3. Water	0	0	29	0	0	0	0	0	0	1.00
4. Grassland	1	1	0	29	0	0	0	0	2	0.88
5. Orchard	0	0	0	0	35	1	0	0	0	0.97
6. Dense-forest	0	0	0	0	0	27	0	0	1	0.96
7. Scat.-forest	0	0	0	1	0	0	27	1	0	0.93
8. Crop-land	0	0	0	0	0	0	0	29	0	1.00
9. Settlements	0	0	0	0	0	0	1	0	28	0.97
Producer's accuracy	0.97	0.95	1.00	0.97	1.00	0.96	0.96	0.97	0.90	
Overall accuracy = 0.97										

From the table 5.6, it can be seen that the overall classification accuracy was significantly enhanced to 97% and kappa coefficient to 0.96, compared to the above mentioned ML classifier, which achieved higher producer's and user's accuracies in most LU/LC classes. The lowest accuracy has been observed in grassland class which is confused with settlements class which contains heterogeneous entities that is unable to be discriminated with simple knowledge as an identical class. The best reported accuracies in this class is 97% as producer's accuracy and 88% as user's accuracy. Most of the confusions detected in ML method was reduced by the incorporation of secondary information such as texture and context features which were crucial to reduce within the class variability of the spectrum.

5.5.4. Overall assessment of the approaches based on the two selected scales

The accuracies of classification approaches at different scales are depicted in figure 5.17. The peak is always located where the object-based method applied and much precisely in most cases at the finer spatial resolution of RapidEye scene. It was found that using pixel-based approach, whether at the fine or coarse scale, only with multi-spectral properties for classification do not

lead to satisfactory results of LU/LC, because the differentiation between LU/LC classes is performed not only with the aid of spectral information, but also with textural and contextual information of the image objects. The same colors in a dataset might show different objects (e.g. construction materials of rural settlements are very similar in color to the grassland class), the expressiveness are ambiguous. Only the incorporation of additional textural and contextual information could lead to unambiguous discrimination. Therefore, produced thematic maps of this approach have confused accuracy due to the fact that various areas have spectrally similar features while it belongs to different classes.

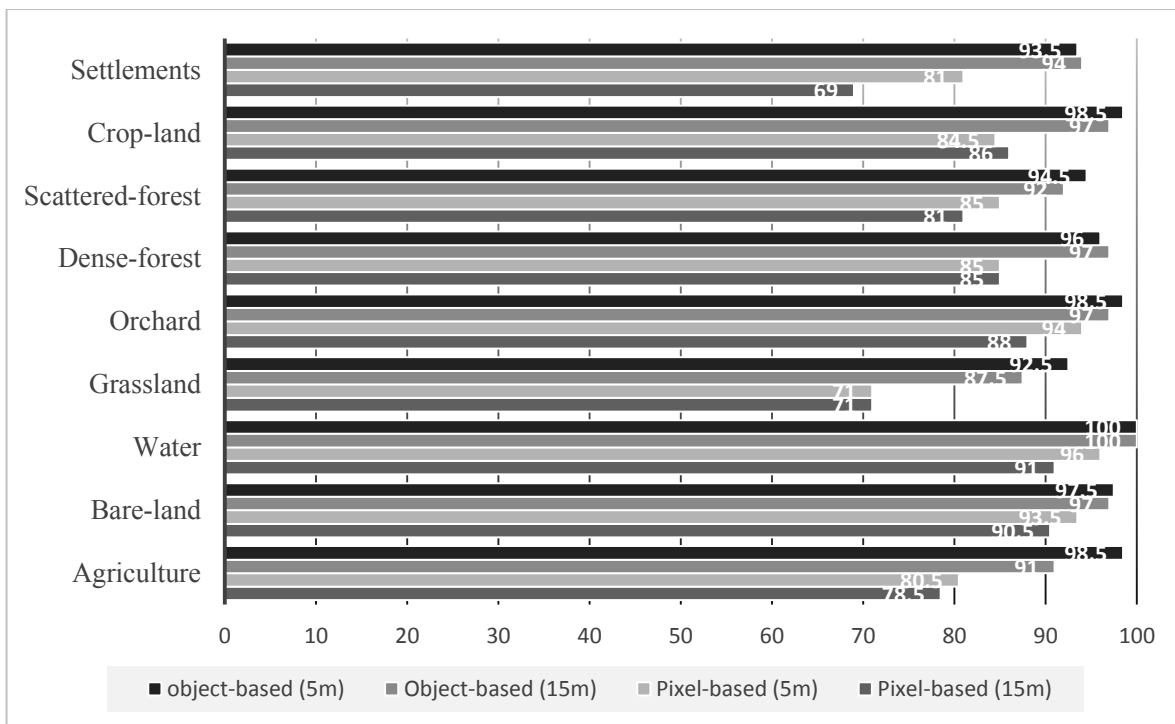


Figure 5-17: Overall accuracy comparison of LU/LC maps for pixel-based and object-based classification methods of the two spatial resolution applied.

Although, the transition from 15 m to 5 m did in fact result in an enhancement of the classification accuracies in most cases, the judgment is still critical since the method applied play the cornerstone for the characterization of class entities at both resolutions. The peak is always located where the object-based method applied, and much precisely at the finer spatial resolution of RapidEye data. Therefore a purified pixel utilized in the classification of Rapideye scene reveals enhanced accuracies in most cases even with pixel-based approach. Inspecting the figures 5.15 and 5.16 closely reveals that, the discrimination of individual scattered trees and shrubs

became possible with 5 meter RapidEye scene. Because in the region this class is distributed within or around other classes, namely agriculture and grassland, enhanced accuracies were achieved in scattered-forest and accordingly in agriculture, grassland classes. In the study area the concern that selective removal of individual trees is occurring could be quantified and monitored using an object based classification and RapidEye data with a high degree of precision.

5.6. Summary

The major contribution of the research presented in this chapter is the development and testing of OBIA image techniques as well as conventional per-pixel approaches to define and map LU/LC patterns in Blue Nile region of Sudan. Different resolutions of Aster and RapidEye multispectral satellite imagery were examined to achieve this objective. As anticipated, this work emphasized that the OBIA approach is proposed to be an advanced solution for image analysis, since the accuracies were improved at different scales applied compared with those of pixel-based approach. Meanwhile, the results reported for the two approaches were consistently high at the finer spatial resolution, and much significantly enhanced with OBIA.

Initially, different image processing techniques were applied based on Aster data in order to achieve a better fitted method for accurate LU/LC mapping for the subsequent spatiotemporal analysis. The obtained results from various methods were validated with same independent set of field data. Strong agreements were obtained in OBIA, while a moderate agreement was observed in pixel-based approach. Giving more detailed inspection to the classification accuracy, the Producer's accuracy for the pixel-based classification results varied from 69% to 89%, while the Producer's accuracy of the object-based classification ranged from 100% in RB method to 81% in NN classifier. The User's accuracy for the pixel-based classification varied from 67% to 94%, while the User's accuracy for the object-based classification ranged from 100% in RB method to 81% in NN classifier.

RapidEye data were integrated and compared with the previously mentioned results to answer the questions whether OBIA is inherently more precise at fine spatial resolution than coarser resolution, and how both pixel-based and OBIA approaches are compared in relative accuracy as a function of spatial resolution. Although, confusions were observed in pixel-based method, overall classification accuracy was slightly enhanced from 81% with Aster data to 85% when the

RapidEye data introduced. Regardless to the enhanced results achieved in OBIA with the use of Aster data, the overall classification accuracy enhanced from 95% with Aster to 97% with RapidEye.

The quality of the results in OBIA approaches largely relies on repetitively modifying segmentation parameters, training sets, and/or testing different combinations of features as trial-and-error processes. Due to the hardware and software limitations, the process of iterative adaptation of functions led to a slowdown or complete stinking of the computation process. Therefore, different levels of segmentation and classification are generated in the class hierarchy to deal with tremendous information in multi-spectral imagery data. The parameters used for the three levels of segmentation were found to be in general appropriate criteria toward obtaining accurate results.

In pixel-based approach, the multispectral digital number (DN) values were found to be not optimal in the separation of LU/LC classes in different cases. The approach experienced difficulties in discriminating between agriculture, grassland and scattered-forest classes. The settlements class was found as the most confused feature due to the spectral similarity to other LU/LC classes. Accordingly, the separation of these LU/LC classes based on spectral behaviors were not performed well.

In contrast, for both the spatial resolutions, the object-based image processing techniques overcome these difficulties by utilizing spectral and spatial information as well as the texture and context information contained in the image (Flanders *et al.*, 2003). Accordingly, two selected methods were tested in *eCognition* software to generate LU/LC classes, and the RB classifier was found to be the best fitted approach.

The multidimensional features used to define LU/LC classes in NN classifier were found not also to be optimal in separation of the classes, while more set of features were needed to discriminate between classes. The feature space was optimized by selecting the features that represent the maximum separation distance from the training objects, accordingly the result enhanced sharpness compared to the pixel-based approach. Nevertheless, these features were confused and the misclassifications were not avoided in several cases. In fact, this approach largely depends on the experimental objects used, which the successful results attributed to the careful selection

of training objects (Yang, 2011). The mismatching between the TTA mask boundaries and the field surveyed data might be considered as a key factor that affects the quality of the result in this method. As an example, the extraction of the grassland class was found to be very complex as shown by the relatively low separation distance, which is confused mainly with agriculture and settlements LU/LC classes.

In RB image-processing strategy, the operator needs to have a considerable knowledge of the area of interest to select the best set of rules to identify and classify the segments (de Kok, 1999). The operator must be aware of the spectral and spatial properties of the area of interest in addition to the base information to define the rules. This ideal situation does not exist at all, which is considered as a common drawback of this method. Moreover, the extraction of LU/LC classes was found to be very complex and time consuming. After a series of trial-and-error processes, a final set of rules which confused the least between the LU/LC classes were achieved (Annex 5). Nevertheless, the superior optimal results were obtained by using this method, whether with Aster or RapidEye data.

Most of the confusion observed in conventional per-pixel approach were enhanced by the two selected methods in OBIA, where the most of the confused pixels were extracted correctly by the incorporation of the spatial information as well as the texture and context information of image objects. The study pointed out that the OBIA yielded more accurate results than the classical per-pixel approach especially when analyst's expert knowledge is presented.

To conclude, although the transition from 15 m to 5 m did in fact result in an enhancement of the classification accuracies in most cases, the judgment is still critical since the method applied play the cornerstone for the characterization of class entities at both resolutions. However, broad set of rules was inserted to differentiate between the LU/LC classes, which result in very complex and time consuming processes. Moreover, the RB method requires considerable a prior knowledge of the area under investigation. In contrast, the classification accuracies with RapidEye data confused the least, and moreover the developed rules have less complexity. From this point of view and considering the slight difference between the results obtained in NN and RB methods, the NN classifier with more careful selection of representative meaningful training

objects might be more realistic with a coarser spatial resolution than time consuming RB method, especially with the absence of user expert knowledge.

Nevertheless, for the both resolutions examined, the object-based classification approach provides significantly more accurate LU/LC classification results than the conventional per-pixel approach (i.e. maximum likelihood classifier). Finally, with both imagery resolutions applied in this study, the mapping of LU/LC patterns in the Blue Nile region of Sudan was generated with a high degree of precision.

Chapter 6 SPATIOTEMPORAL OBJECT-BASED IMAGE ANALYSES AND DRIVING FORCES

6.1. General overview

The challenge in digital change analysis techniques is the ability of the existing systems to automatically determine, within specific time intervals whether there is change or not, and to locate the spatial distributions and the extent of the change as well as to quantify the trend and magnitude of the dynamics precisely (Hall and Hay, 2003; Zhou *et al.*, 2008). In this chapter efforts were carried out to provide a comprehensive knowledge on the rapid forest cover loss (El-Abbas, 2006), integrating rates and spatial distribution of the change with other LU/LC patterns in the Blue Nile region of Sudan. Moreover, some investigations were performed to address the driving forces that might be associated with these dynamics. Therefore, three multi-spectral satellite images were used; two LANDSAT TM of 1990 and 1999 as well as TERRA ASTER of 2009, in addition to socio-economic data in form of social survey of households, climatic data and reports were used as well to achieve these goals. Figure 6.1 summarize the structure of the results achieved in this chapter.

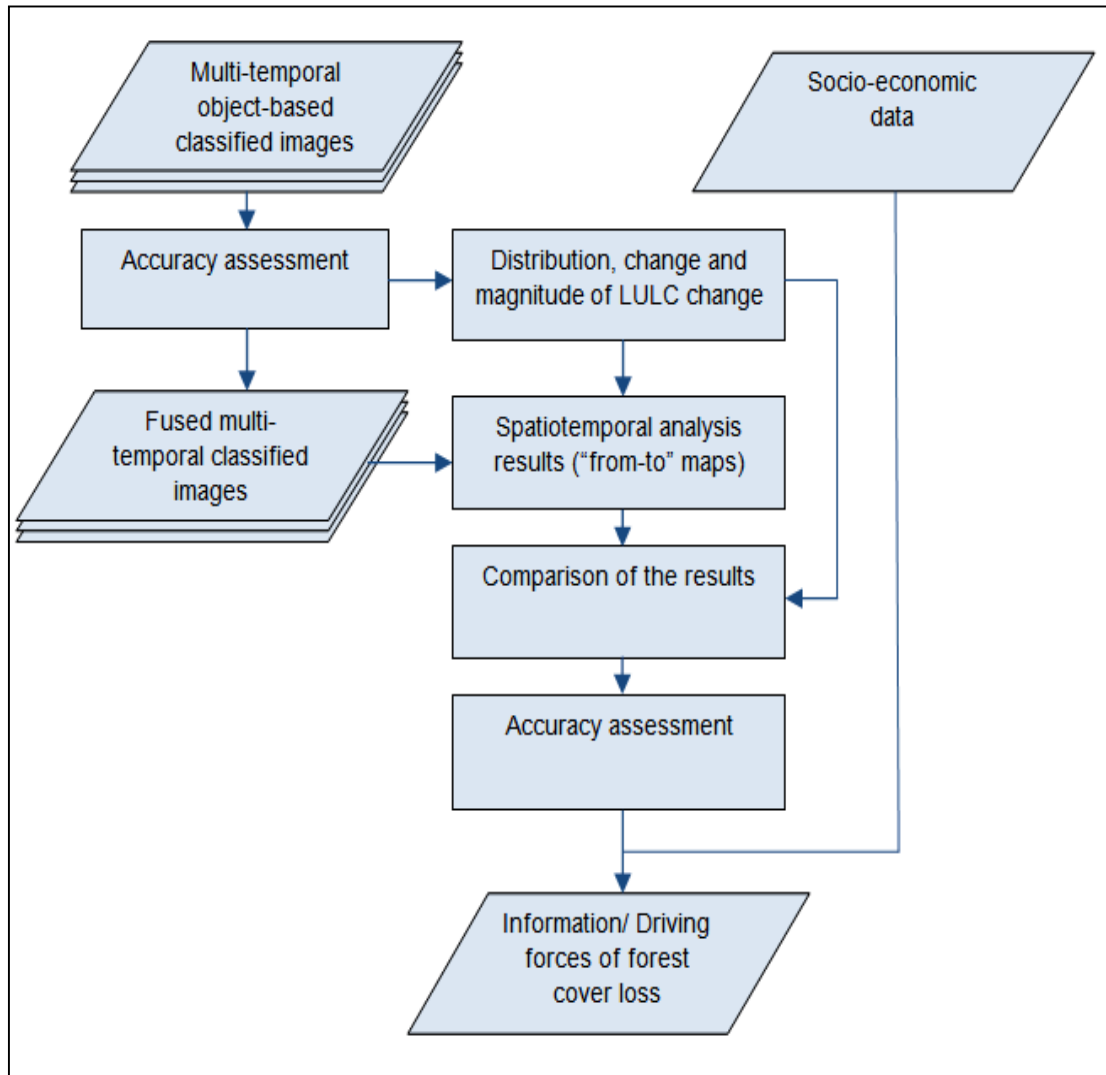


Figure 6-1: Structure of the results for spatiotemporal OBIA analysis and driving forces

Various techniques have been applied using remotely sensed data for LU/LC change detection for many decades (Singh 1989, Lu, *et al.*, 2004; Rogan and Chen, 2004). Those techniques may be generally be sorted into two main groups; i.e. pre-classification change detection and post-classification comparison. Pre-classification techniques operate on the raw images, while post-classification comparison methods detect LU/LC change by overlaying independent set of classified images from different dates. The post-classification change detection technique was performed in the present study. This technique was adopted here for the following reasons:

- To eliminate the atmospheric effects and spectral variation in vegetation classes due to the different phenological properties since each image was classified

separately and later those classifications were overlaid to describe LU/LC dynamics.

- To locate whether there is a change or not, but also to provide detailed change (from-to) information classes.
- To reduce the variations of image characteristic acquired from different satellite sensors.

The rapid changes observed during the periods 1990 to 1999 and 1999 to 2009 result in very complicated and numerous LU/LC change classes. Hence, simple technique of post-classification comparison for the subsequent dates of each couple of images (1990 to 1999 and 1999 to 2009) was performed, which results in “from-to” change classes.

6.2.Land use/ land cover classification and accuracy assessment

For the purpose of post-classification change detection technique, classified maps for corresponding dates were required. The two well known image classification approaches (object-based and pixel-based) were performed to address the ability of each to generate accurate LU/LC class categories (chapter 5). Based on the best classification accuracies, in addition to unavailability of neither aerial photograph nor field survey data to be used as training areas for the LANDSAT TM images 1990 and 1999, the RB method in OBIA was found as the best fitting method to classify the images required for post-classification change detection. The classifications were intended to generate thematic maps of nine LU/LC classes for the corresponding dates, “from-to” change detection maps and LU/LC matrices and dynamics.

Prior the implementation of the post-classification change detection process, it is essentially to validate the results against any reference data or field survey data. Due to the dramatically changes observed in the region, the topographic maps are not suitable for result validation. Instead, the accuracy of LANDSAT TM 1990 and 1999 classified images was assessed by visual selection of random points from the raw image data.

6.2.1. Land use/ land cover classification

In the present study, the post-classification change analysis technique was undertaken by developing separate classification protocols for LANDSAT TM (1990 and 1999) as well as TERRA ASTER (2009) multispectral imagery. Classification of LANDSAT TM imagery was performed by utilizing a combination of 6 bands (VIS, NIR and MIR), and so the TIR band was excluded, while the VNIR and SWIR bands were utilized for the classification of TERRA ASTER data. All images were acquired in dry season to eliminate the phenological variability in the vegetation patterns as well as to guarantee for low atmospheric effects, since all images were cloud free. However, to deal with the spectral variations within each class, the classification was performed to identify LU/LC classes by combining sets of rules for each class and/or object(s) within the classification hierarchy based on user expert knowledge. User's experience was obtained through other studies performed to that area previously, e.g. FAO and FNC, (1998); El-Abbas (2006) as well as many previous field visits to the study area which enhances the analyst knowledge. The *eCognition* software was used to classify the images into nine LU/LC classes, i.e. Ag. (rain-fed), Br., Cr., DF, SF, Gr., Or., St., and W. (figure 6.2).

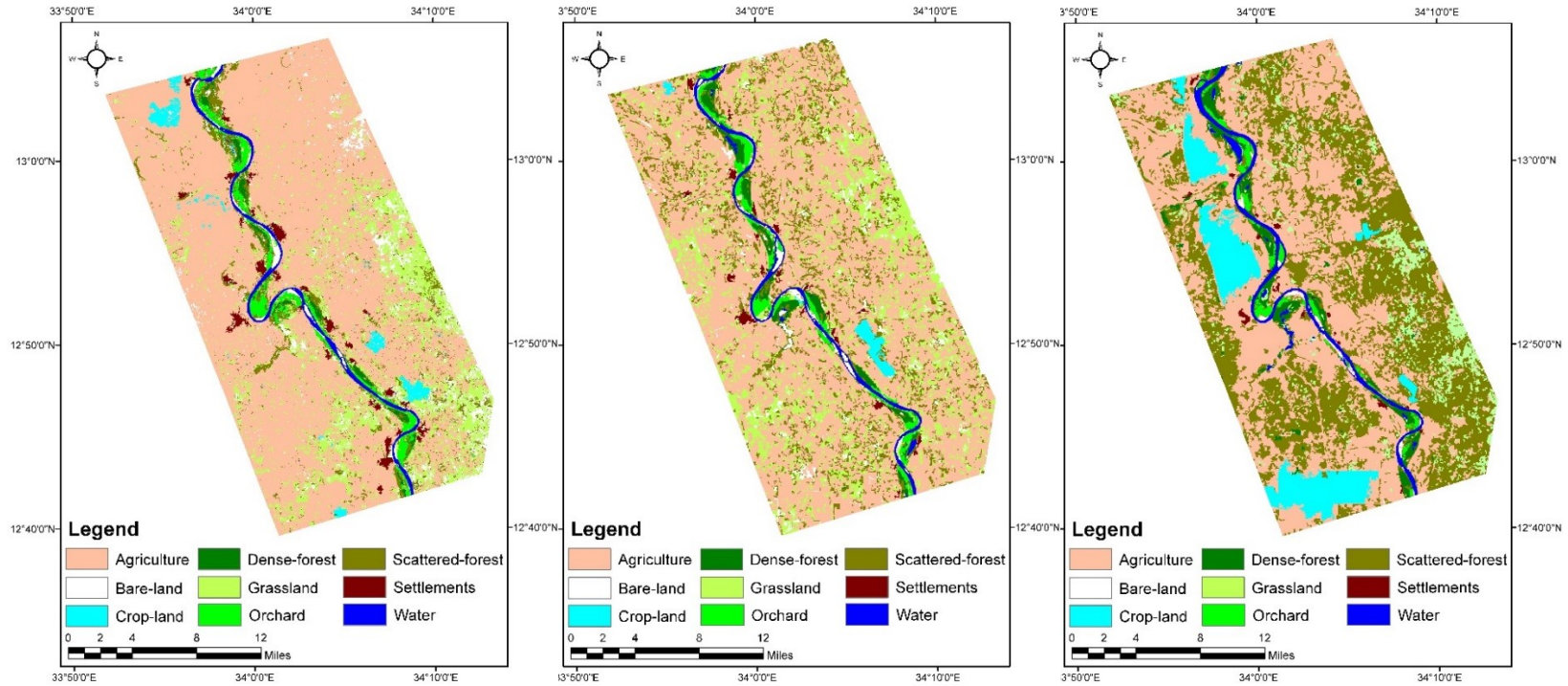


Figure 6-2: LU/LC maps of the study area developed from TERRA ASTER 2009 and LANDSAT TM 1999 and 1990 (from the left to right respectively)

6.2.2. Accuracy assessment based on error matrix

The classification accuracy of each image separately is the cornerstone toward any post-classification change analysis technique. The classification accuracy was assessed by cross tabulating the reference data and the classified maps into matrices, well known as error matrix. The accuracy assessment was carried out separately for the three dates. Since the classification accuracy for Aster was already assessed in section 5.3.4, overall comparison is needed to compare between the different dates. A stratified random sampling design was applied to generate the random points which was introduced as thematic layer to the *eCognition* software. The overall accuracy and kappa statistics as well as producer's accuracy and user's accuracy were generated to assess the quality of the classification maps. Producer's accuracies were calculated as the number of correct objects in a category divided by total number of reference testing objects (measure of omission error), while the user's accuracies were calculated as the total number of correct objects in a category divided by total number of objects that were actually classified in a category (measure of commission error, is that several of the testing objects are being placed into incorrect category). From the figure 6.3, it can be seen that the producer's accuracy is relatively low in agriculture class. Discriminating agricultural fields from grassland, dense-forest and settlements experienced difficulties, this could be explained by the misleading of training objects, since they were acquired from visual interpretation of unclassified LANDSAT TM 1990 and 1999 images as well as limited number of field points used for widely extended agriculture class in the classification of 2009 TERRA ASTER image. User's accuracy is relatively poor for grassland, scattered-forest and bare-land (figure 6.4) since they are overlapped and confused each other. Discriminating dense-forest from crop-land also experienced difficulties in some areas leading to misclassifications on that areas. Nevertheless, by using, either multispectral LANDSAT TM or TERRA ASTER imagery data, the clear distinctions were observed between most of the LU/LC classes, since spatial information as well as the texture and context information contained in the image were introduced to discriminate between spectrally similar objects.

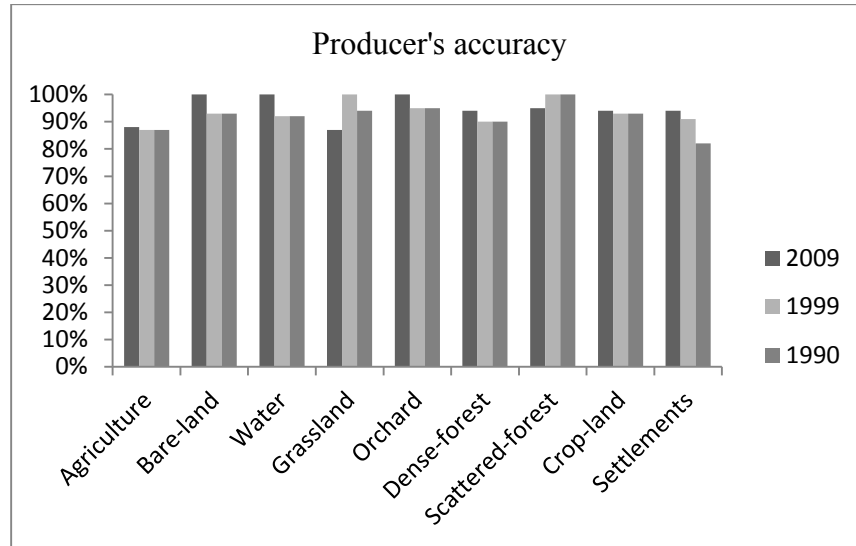


Figure 6-3: Producer's accuracy of the selected results obtained from rule-based method

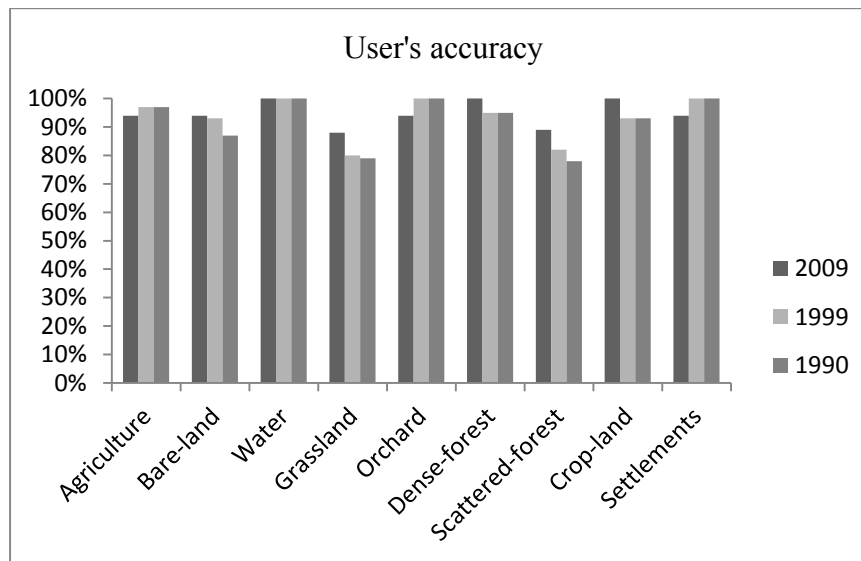


Figure 6-4: User's accuracy of the selected results obtained from rule-based method

The overall accuracy and kappa coefficient of classification results achieved from TERRA ASTER 2009 were 0.95 and 0.94, while LANDSAT TM 1999 and 1990 achieved overall accuracy of 0.93 and 0.91 and kappa index of 0.92 and 0.90, respectively (table 6.1). A good evaluation of the classification accuracy performance is the Kappa statistics, which computes the agreement between the classification result and the reference data (Jensen, 2005). A Kappa statistics of >80% suggests a strong agreement. Accordingly, strong agreements were achieved from these classifications. For more details about the classification accuracies, the confusion matrix tables were presented in the table 5.3 and annex 6.

Table 6-1: Overall accuracy and kappa index of the best classification results

	1990	1999	2009
Overall accuracy	0.914	0.926	0.947
Kappa coefficient	0.901	0.915	0.940

6.2.3. Accuracy assessment based on best classification result

As a result of the fuzzy classification concept, an image object has memberships in one or more classes. Accordingly, the classification with the highest assignment value is considered as the best classification result. Therefore, the accuracy assessment based on best classification result was considered to assess the quality of the results achieved from different dates. This method represents the minimum, maximum as well as the mean of all membership values for each class. The sum of standard deviation of each classified category was also presented.

Table 6.2 is the accuracy assessment for classification result of LANDSAT TM image (1990) based on the best classification result. As shown clearly in this table, for the minimum membership values there were confusion observed in some objects in all classes. Nevertheless, considering the overall classified objects, the mean membership values and the standard deviations of the best classification results show that most of the objects for all LU/LC classes were assigned with high membership values.

Table 6-2: Accuracy assessment of the classified LANDSAT TM image (1990) by best classification result

Class	Objects	Mean	Std. Dev	Minimum	Maximum
Agriculture	4491	0.94	0.06	0.15	1.00
Bare-land	43	0.90	0.10	0.67	1.00
Water	505	0.88	0.11	0.48	1.00
Grassland	1806	0.97	0.07	0.24	1.00
Orchard	429	0.83	0.12	0.31	1.00
Dense-forest	981	0.93	0.10	0.45	1.00
Scattered-forest	6650	0.94	0.09	0.27	1.00
Crop-land	1476	0.89	0.11	0.10	1.00
Settlements	80	0.96	0.04	0.86	1.00

Table 6.3 is the accuracy assessment for classification result of LANDSAT TM image (1999) based on the best classification result. Similar to the previous one, the mean membership values and standard deviations of the best classification results indicate that most of the objects were classified with high membership values, ranging from 0.99 in bare-land, scattered-forest and crop-land to 0.72 and 0.78 for water and dense-forest respectively.

Table 6-3: Accuracy assessment of the classified LANDSAT TM image (1999) by best classification result

Class	Objects	Mean	Std. Dev	Minimum	Maximum
Agriculture	14343	0.90	0.06	0.78	0.99
Bare-land	1484	0.99	0.05	0.33	1.00
Water	429	0.72	0.08	0.25	0.82
Grassland	4451	0.93	0.09	0.25	1.00
Orchard	699	1.00	0.00	1.00	1.00
Dense-forest	565	0.78	0.12	0.36	0.99
Scattered-forest	3443	0.99	0.03	0.74	1.00
Crop-land	134	0.99	0.02	0.90	1.00
Settlements	154	0.94	0.07	0.77	1.00

Table 6.4 is the accuracy assessment for classification result of TERRA ASTER image (2009) with VNIR and SWIR spectral region based on the best classification result. We can confirm from this table, that the best classification values for all LU/LC classes are significantly high. As well the minimum membership values are not less than 0.62. The mean membership values for the assignment of these classes are very high, which ranges from 1.00 to 0.96.

Table 6-4: Accuracy assessment of the classified TERRA ASTER image (2009) by Best classification result

Class	Objects	Mean	Std. Dev	Minimum	Maximum
Agriculture	25058	1.00	0.00	1.00	1.00
Bare-land	9484	0.99	0.02	0.80	1.00
Water	1403	1.00	0.00	1.00	1.00
Grassland	2229	0.99	0.02	0.79	1.00
Orchard	6338	0.96	0.04	0.71	1.00
Dense-forest	2415	0.97	0.03	0.88	1.00
Scattered-forest	11693	0.99	0.02	0.87	1.00
Crop-land	841	0.99	0.01	0.94	1.00
Settlements	3405	0.98	0.02	0.62	0.98

By looking at the summary statistics of LU/LC classification accuracy assessment results as shown previously, and as the classified images need to be validated prior the post-classification comparison, the results obtained from different dates were validated which were found to consistently have high degree of precision. All in all, the class assignment is significant. Hence, these classification results were approved in this study to be used for the subsequent step of post-classification comparison as well as an input layers for object-based post-classification change detection technique.

6.3. Distribution of LU/LC during the periods 1990, 1999 and 2009

The static LU/LC distributions for each category in the study area are presented in table 6.5. With reference to these classifications, the most dominant pattern observed in the area is the rainfed agriculture, which covers an area of about 47809.1 ha (42.88 %), 66468.3 ha (59.53 %) and

73851.55 ha (66.21 %) for the years 1990, 1999 and 2009 respectively. This pattern of use is located in different soil properties and topographic conditions. These agricultural fields are cultivated during the rainy season with different cash crops mainly *Sorghum*, *Millet* and *Sesame*. The other form of LU/LC is the irrigated crop-land occupying about 8627.49 ha (7.74 %) in 1990, although this scheme collapsed and the area decreased to 857.07 ha and 886.41 ha which represents only 0.77 % and 0.79 % from the total area of the selected site for the years 1999 and 2009 respectively.

The study clarifies that, in the early 1990s, forest occupied more than one third of the study area (38.87 %), covering an area of about 43341.15 ha ranging from even stand dense forest near the river bank with an area of about 3381.75 ha to scattered trees and shrubs distributed widely among the area with different forms of associations and structures with an area of about 39959.4 ha. Chapter 3 gives more details on the forest cover structure and association in the Blue Nile region. The above mentioned statistics do no longer exist, where the forested area occupied only 15958.35 ha and 7721.62 ha which declined by 14.29 % and 6.92 % in 1999 and 2009 respectively. The most associated class to the scattered trees and shrubs is the grassland, leading to difficulties during the classification processes to discriminate between these patterns. Nevertheless, the grassland occupied only 6.15 % of the total area from the selected site in 1990, while it covers 19575.1 ha and 20625.28 ha representing 17.53 % and 18.49 % for the years 1999 and 2009 respectively.

The other forms of patterns prevalent in the area are associated with the Blue Nile valley is small sandy islands (bare-land) mainly due to the river movements, orchard and residential areas. The Blue Nile river covers an area of about 2808.9 ha, 2036.7 ha and 1881.20 ha for the years 1990, 1999 and 2009 respectively. One of the most important patterns in the area is the settlements class. It represents less than one percent in the years 1990 and 1999, although it is about to be doubled in the year 2009, with area of about 403.74 ha, 851.94 ha and 1516.82 ha respectively. The orchard covers an area of about 1394.28 ha, 2079.81 ha and 2182.43 ha for the years 1990, 1999 and 2009 respectively. By visual interpretation, the classifications of 1999 and 2009 show that the proliferation of bare-land patches are not observed earlier.

Table 6-5: Land use/ land cover distribution during the period 1990- 2009

Class	1990		1999		2009	
	Area (ha)	Area (%)	Area (ha)	Area (%)	Area (ha)	Area (%)
Agriculture	47809.1	42.88	66468.3	59.53	73851.55	66.21
Bare-land	261.99	0.23	3824.46	3.43	2882.93	2.58
Crop-land	8627.49	7.74	857.07	0.77	886.41	0.79
Dense-forest	3381.75	3.03	2219.85	1.99	1109.43	0.99
Grassland	6851.61	6.15	19575.1	17.53	20625.28	18.49
Orchard	1394.28	1.25	2079.81	1.86	2182.43	1.96
Scattered-forest	39959.4	35.84	13738.5	12.30	6612.19	5.93
Settlements	403.74	0.36	851.94	0.76	1516.82	1.36
Water	2808.9	2.52	2036.7	1.82	1881.20	1.69
Total	111498.26	100	111651.73	100	111548.24	100

6.3.1. Trend, rate and magnitude of land use/ land cover changes

The differences between the classified maps are quantified for each class as shown in table 6.6. The result of the change detection analysis exhibits significant changes of LU/LC patterns. The trend generally shows an increasing degradation from the period between 1990 to 2009 as well as for each pair of images i.e., from 1990 to 1999 and 1999 to 2009. The most interesting fact is that the trend of change is always similar; when the forest areas are decreased, and the agricultural land is expanded. The study also shows that, bare-land and settlements as well as orchard categories have been significantly increased during the study period. The magnitude of increases in grassland was questionable. However, that could be due to the removal of natural forest covers.

Giving more inspections to the table 6.6, the study indicates that the forests were being degraded and completely deforested in some areas, e.g. dense-forest in the study area lost about one third of its cover during the first period of study and also the same rate was observed in the second time interval. Meanwhile, the scattered-forest in the study area covers an area of about 39959.4 ha in 1990 which decreased sharply to 13738.5 ha and 6612.19 ha in 1999 and 2009 respectively.

Very interestingly, the annual rate of change is coincided between agriculture and scattered-forest categories, while the agricultural land increased by 1.85 % and 0.66 %. In like manner, the scattered trees and shrubs decreased by 2.61 % and 0.64 % during the first and second study periods respectively. The fact is that the average annual rate of loss during the whole study period for scattered trees and shrubs (1755.12 ha) is more than the annual rate of area cleared for mechanized farming (1370.66 ha), which indicates that there are another factors in the deforestation and degradation processes. Therefore, these issues will be addressed afterward in section (6.5).

Another form of degradation is the appearance of bare-land patches with an increasing annual rate of about 137.94 ha during the study period from 1990 to 2009. Moreover, by looking at the trend and magnitude during the two time interval, the grassland increasing rate is coincided with the forest cover loss, which indicates that the grassland class is the turning point toward land degradation rather than a recovery process. Other thing that it maybe significant to mention in that most of the negative changes observed during the period 1999 to 2009 when compared with the first period of study coincided with the dramatically increase of settlements. Therefore, the explosion in residential areas that were observed during the study periods (1990 to 1999 and 1999 to 2009), represented by 448.2 ha and 664.88 ha respectively, could be one of the important factors that must be considered to address the land degradation and dynamic processes.

The variations in water body, which decreased by 772.2 ha and 155.50 ha for the two time intervals respectively, could be due to the amount of river flow controlled in Aldamazeen dam. Hence, this could not be an eventual value of the real amount of the Blue Nile stream. Therefore, more analyses with more time intervals during the year maybe needed to quantify this pattern.

During the first period of study the irrigated agricultural schemes collapsed. 7770.42 ha in the study area were lost from the total of 8627.49 ha classified in that class earlier, which represents 6.97 % out of 7.74 % that was classified as crop-land in 1990. As a result, this deterioration leads to high pressure on natural resources from the local communities seeking sources for income generation.

Giving more emphasis on neighbour classes i.e. orchard and dense-forest, interestingly the only way of orchard expansion is on the Blue Nile forests. Therefore we can roughly estimate the

deforestation in *Acacia nilotica* forests as a function of illegally expansion of orchard class by 685.53 ha and 102.62 ha for the two time intervals respectively (table 6.6).

Table 6-6: LU/LC change; trend, rate and magnitude (1990- 2009)

Class	1990- 1999				1999- 2009				1990- 2009			
	Change (total)		Annual rate		Change (total)		Annual rate		Change (total)		Annual rate	
	Area (ha)	%	Area (ha)	%	Area (ha)	%	Area (ha)	%	Area (ha)	%	Area (ha)	%
Agriculture	18659.20	16.65	2073.24	1.85	7383.25	6.62	738.32	0.66	26042.45	23.35	1370.66	1.23
Bare-land	3562.47	3.19	395.83	0.35	-941.54	-0.84	-94.15	-0.08	2620.94	2.35	137.94	0.12
Crop-land	-7770.42	-6.97	-863.38	-0.77	29.34	0.03	2.93	0.00	-7741.08	-6.94	-407.43	-0.37
Dense-forest	-1161.90	-1.04	-129.10	-0.12	-1110.42	-1.00	-111.04	-0.10	-2272.32	-2.04	-119.60	-0.11
Grassland	12723.49	11.39	1413.70	1.27	1050.18	0.94	105.02	0.09	13773.67	12.35	724.93	0.65
Orchard	685.53	0.61	76.17	0.07	102.62	0.09	10.26	0.01	788.15	0.71	41.48	0.04
Scattered-forest	-26220.90	-23.53	-2913.40	-2.61	-7126.31	-6.39	-712.63	-0.64	-33347.21	-29.89	-1755.12	-1.57
Settlements	448.20	0.40	49.80	0.04	664.88	0.60	66.49	0.06	1113.08	1.00	58.58	0.05
Water	-772.20	-0.70	-85.80	-0.08	-155.50	-0.14	-15.55	-0.01	-927.70	-0.83	-48.83	-0.04

6.4. Spatiotemporal object-based post-classification analysis

The net change of the values of t_0 and t_1 were useful only as an eventual result, but this value did not necessarily indicate the real change in each category (Pontius *et al.*, 2004). In order to achieve a comprehensive description of forest cover dynamics during the period of study, a newly developed object-based post-classification change analysis was addressed.

Following the same procedure of OB classification, the initial step in OB post-classification change detection was to perform image segmentation. For the purpose of change detection with OB approach, the adopted novel procedure applied in this study is the fusion of classified thematic maps for t_0 and t_1 as input layers in OBIA project when performing the segmentation. Following the available classified maps generated for the study area for the years 1990, 1999 and 2009 (figure 6.2), segmentation was performed for each pair separately (i.e., 1990 to 1999 and 1999 to 2009). The images were fused to generate a new level of objects differing from those in the original images, as shown in a figure 6.5. However, the intersections between the change “from-to” information classes were automatically delineated with controlled scale and shape parameters, which were weighted as follows: Scale Factor= 5, Color: Shape= 9: 1, and Compactness: Smoothness= 5:5. The total number of generated objects in the first phase (1990-1999) is 32,964 objects while in the second period (1999-2009) rose to 75,766 objects.

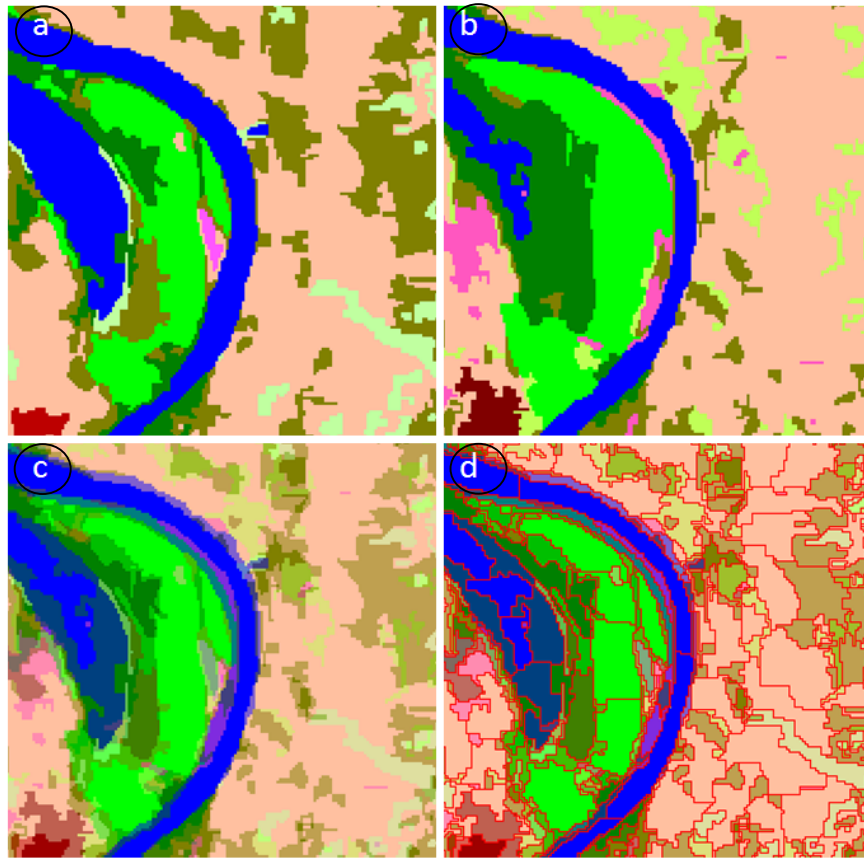


Figure 6-5: a) and b) illustrate a selection of the classified maps (1990 and 1999) used as input layers, c) fused layers, and d) the segmentation result of the fused images

In the second step, TTA Masks were created and coded with the observed change found between t_0 and t_1 . Subsequently, as shown in figures 6.8 and 6.11 as well as the associated matrix tables 6.7 and 6.8, out of 81 possible probabilities according to the nine classes, 61 change “from-to” information classes were identified in the first time interval, while 62 classes were generated from the analysis of second time interval. The no change classes were found for all categories in the two time intervals except “crop-land” class in the first time interval since all areas of that class were converted to other LU/LC classes.

Important aspects which must be considered in change detection analysis techniques are detecting the changes that have occurred, identifying the nature of changes, measuring the spatial extent of the change, and assessing the quality of the result (Macleod *et al.*, 1998). Thematic maps describing LU/LC changes “from-to” information and its dynamics in the study area were obtained for the periods 1990- 1999 and 1999- 2009 respectively, by means of the OB post-classification change detection approach. These change maps not only show where LU/LC

changes occurred, but also illustrate the spatial location of the changes between each of the nine LU/LC classes of the two time intervals. Furthermore, associated matrices quantify the magnitude and shift “from-to” each class category, which were derived from the fused t_0 and t_1 classified maps.

The OB post-classification change detection approach effectively illustrates the detailed “from-to” as well as no change classes as presented in figures 6.8 and 6.11. For more visible results, and following the research objective, the above mentioned classes were aggregated to seventeen and eighteen parent classes for the first and second period of study respectively as shown in the figures 6.6 and 6.9. The change to the respective class represents all gained areas to that class except the gain and loss in forest classes (i.e. Dense-forest and Scattered-forest), which were aggregated under “deforestation” and “reforestation” parent classes.

6.4.1. Forest cover change dynamics 1990- 1999

For the LU/LC change analysis between 1990 and 1999, the dark-orange areas in the map (figure 6.6) reveal an intensive clearance of natural forest cover, and as shown in table 6.7, 36585.11 ha representing 32.72 % were converted from forest to other LU/LC class categories. The occupancy of the mechanized rain-fed agriculture expanded over the natural forest land represents 23636.19 ha, which is 35.53 % of the total gained areas obtained from the forest land. The recovered area represents only 7.88 %, mainly from abandon agricultural field (5.10 %). Therefore, evidence is clear for the potentiality of the area to recover if manmade impact is well-controlled. It is worth mentioning that an area which constitutes 8.35 % was converted from Scattered-forest to grassland. This change could be explained by the practice of shifting cultivation in forest land. This issue was supported by the coincided statistics of the areas that were converted from agriculture to grassland as well as the areas that were re-utilized from grassland (table 6.7). However, other factors that could be leading to forest cover loss were addressed and discussed in section 6.3.

Interestingly, most of the unchanged areas were observed near the Blue Nile valley, representing an area of about 38.93 %, rain-fed agriculture occupied an area of about 29.20 % of this portion. Linking these areas with landownership system may provide an answer, where these areas are managed under clear property rights and ownership conditions in relation to other areas.

Therefore, land tenure could play an indispensable role in the stability of these areas (Robinson *et al.*, 2011).

Table 6-7: LU/LC change matrix of fused images 1990-1999 (ha)

Class	1	2	3	4	5	6	7	8	9	Total Area 1999
1-Agriculture	32649.75	-	5825.88	361.86	4199.56	-	23274.33	113.35	96.95	66521.68
	29.20 %	-	5.21 %	0.32 %	3.76 %	-	20.81 %	0.10 %	0.09 %	59.49 %
2-Bare-land	1325.64	111.73	217.97	119.48	237.61	98.94	1282.93	36.22	398.36	3828.88
	1.19 %	0.10 %	0.19 %	0.11 %	0.21 %	0.09 %	1.15 %	0.03 %	0.36 %	3.43 %
3-Crop-land	609.39	-	-	-	8.11	-	240.58	-	-	858.08
	0.54 %	-	-	-	0.01 %	-	0.22 %	-	-	0.77 %
4-Dense-forest	33.97	2.16	-	1445.03	72.99	202.20	283.29	-	178.23	2217.87
	0.03 %	0.002 %	-	1.29 %	0.07 %	0.18 %	0.25 %	-	0.16 %	1.98 %
5-Grassland	6930.85	61.18	1473.41	197.24	1465.93	119.93	9336.76	12.80	24.87	19622.97
	6.20 %	0.05 %	1.32 %	0.18 %	1.31 %	0.11 %	8.35 %	0.01 %	0.02 %	17.55 %
6-Orchard	129.84	26.22	-	497.83	10.99	865.47	389.17	-	162.64	2082.16
	0.12 %	0.02 %	-	0.44 %	0.01 %	0.77 %	0.35 %	-	0.15 %	1.86 %
7- Scattered-forest	5704.69	36.94	1069.47	614.70	853.75	74.34	5104.49	45.95	257.07	13761.4
	5.10 %	0.03 %	0.96 %	0.55 %	0.76 %	0.07 %	4.56 %	0.04 %	0.23 %	12.30 %
8-Settlements	554.69	-	50.19	-	-	-	68.93	220.85	-	894.66
	0.50 %	-	0.04%	-	-	-	0.06 %	0.20 %	-	0.80 %
9-Water	96.41	24.06	-	201.30	11.35	27.93	-	-	1678.04	2039.09
	0.09 %	0.02 %	-	0.18 %	0.01 %	0.02 %	-	-	1.50 %	1.82 %
Total Area 1990	48035.23	262.29	8636.92	3437.44	6860.29	1388.81	39980.48	429.17	2796.16	111826.8
	42.97 %	0.23 %	7.72 %	3.07 %	6.13 %	1.24 %	35.75 %	0.38 %	2.51 %	100 %

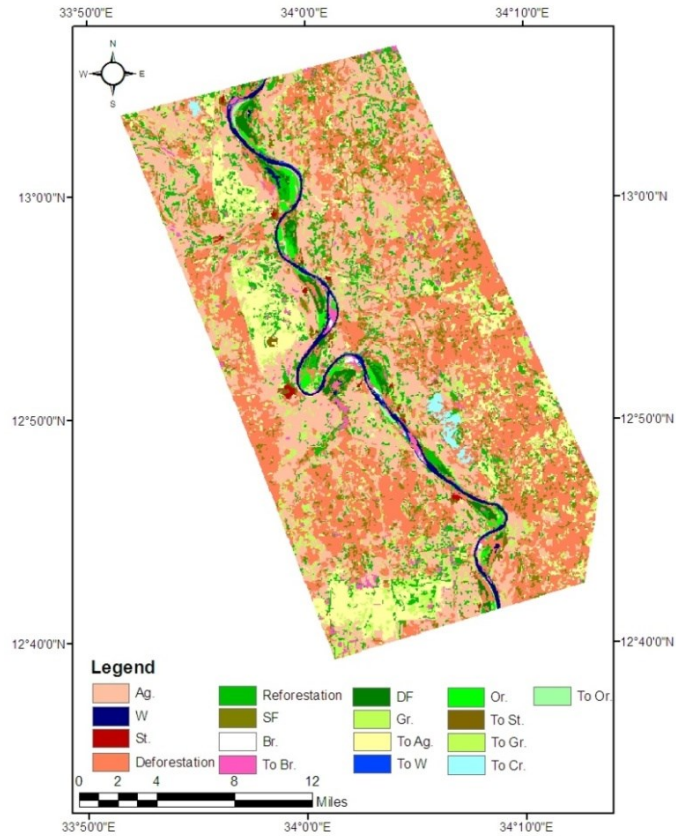


Figure 6-6: Change map “from-to” parent classes generated from overlaid classified images 1990 and 1999 (figure 6.2)

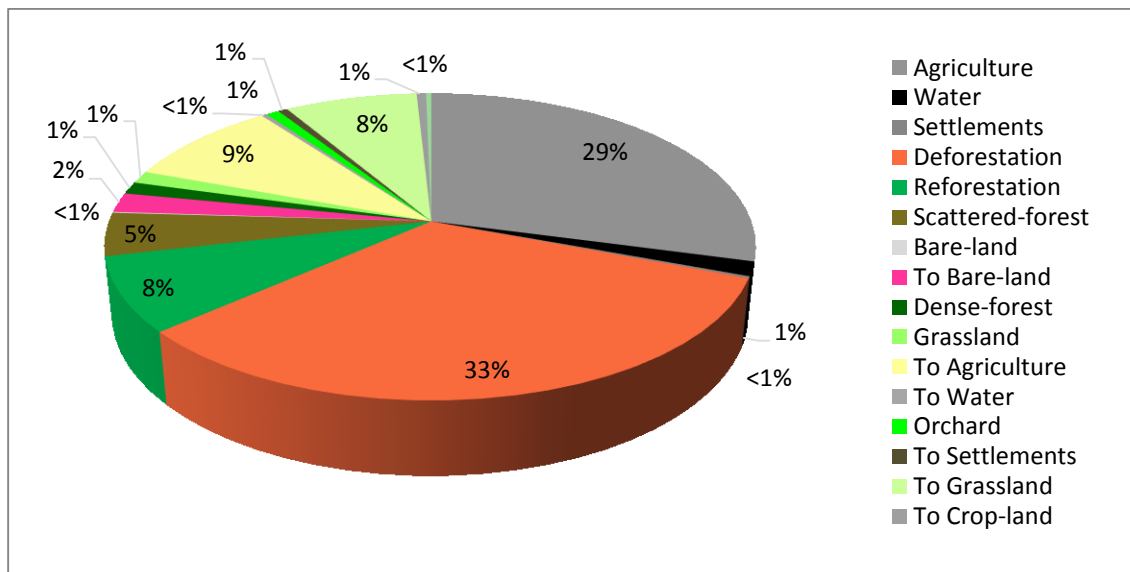


Figure 6-7: Change area “from-to” parent classes generated from overlaid classified image 1990-1999

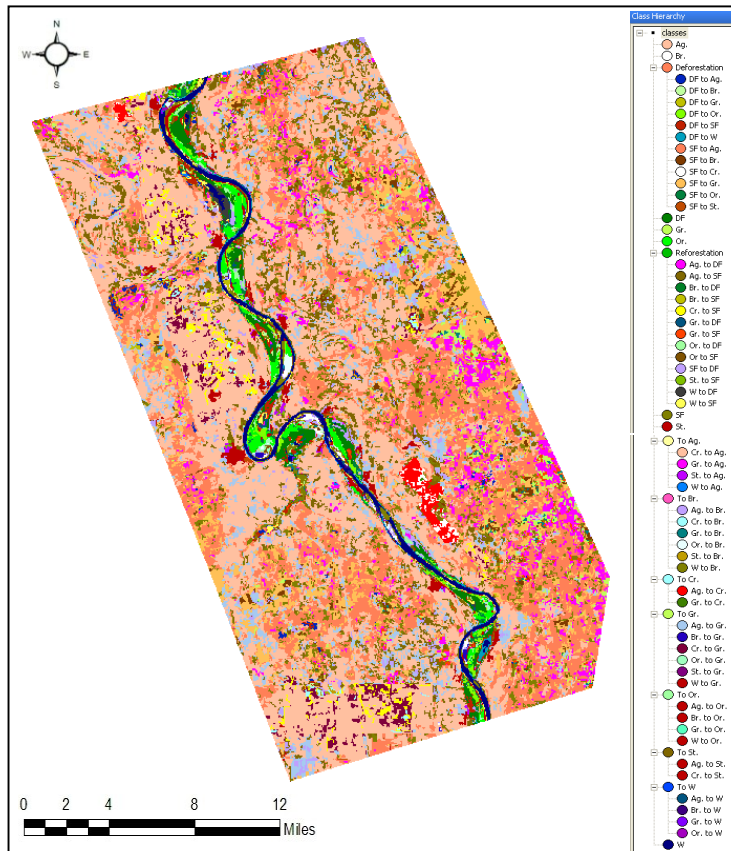


Figure 6-8: Change map “from-to” child classes generated from overlaid classified images 1990 and 1999 (figure 6.2)

6.4.2. Forests cover change dynamics 1999- 2009

Regarding the LU/LC analysis between 1999 and 2009, about half of the area (51.79 %) remained unchanged, mostly agricultural fields which represent 48913.58 ha (43.80 %). One of the major class category observed during this period of study is the deforestation parent class, which occupies 13857.56 ha (12.41 %) of the total area, mostly as a result of rain-fed agriculture expansion over the forest areas (8.16 %), as shown in the magnitude of child class scattered-forest to agriculture (table 6.8).

Table 6-8: LU/LC change matrix of fused images 1999-2009 (ha)

Class	1	2	3	4	5	6	7	8	9	Total Area 2009
1-Agriculture	48913.58	2073.69	723.82	-	12815.94	-	9108.62	335.00	146.85	74117.50
	43.80 %	1.86 %	0.65 %	-	11.48 %	-	8.16 %	0.30 %	0.13 %	66.37 %
2-Bare-land	1515.81	203.42	15.54	76.10	616.77	69.68	262.76	26.04	118.90	2905.02
	1.36 %	0.18 %	0.01 %	0.07 %	0.55 %	0.06 %	0.24 %	0.02 %	0.11 %	2.60 %
3-Crop-land	524.12	14.53	6.19	15.05	168.30	-	137.62	-	21.67	887.48
	0.47 %	0.01 %	0.01 %	0.01 %	0.15 %	-	0.12 %	-	0.02 %	0.79 %
4-Dense-forest	-	60.49	-	714.85	-	103.51	164.99	-	-	1043.84
	-	0.05 %	-	0.64 %	-	0.09 %	0.13 %	-	-	0.91 %
5-Grassland	12045.55	726.18	-	186.39	4503.99	324.62	2308.11	125.75	234.08	20454.67
	10.79 %	0.65 %	-	0.17 %	4.03 %	0.29 %	2.07 %	0.11 %	0.21 %	18.32 %
6-Orchard	40.86	115.83	15.99	381.88	188.26	1047.11	183.42	-	211.78	2185.13
	0.04 %	0.10 %	0.01 %	0.34 %	0.17 %	0.94 %	0.16 %	-	0.19 %	1.96 %
7- Scattered-forest	2694.49	282.51	110.11	751.96	928.66	355.79	1170.69	80.71	377.08	6752.00
	2.41 %	0.25 %	0.10 %	0.67 %	0.83 %	0.32 %	1.05 %	0.07 %	0.34 %	6.04 %
8-Settlements	711.84	-	-	-	247.80	-	158.75	326.82	-	1445.21
	0.64 %	-	-	-	0.22 %	-	0.15 %	0.29 %	-	1.30 %
9-Water	242.17	201.17	-	94.77	-	195.67	192.13	-	952.99	1878.91
	0.22 %	0.18 %	-	0.08 %	-	0.18 %	0.17 %	-	0.85 %	1.68 %
Total Area	66688.42	3677.82	871.65	2126.23	19469.72	2383.29	13494.96	894.32	2063.35	111669.76
1999	59.72	3.29	0.78	1.90	17.44	2.13	12.08	1.85	0.80	100 %

Giving more inspection to the change analysis results as shown in figure 6.9 and its associated table 6.8, it very important to be mentioned that is a proliferation of “bare-land” patches in areas intensively used for mechanized farming. The study proves that the agricultural expansion reached its peak period during the past decades. As a result of intensive cultivation, eventually crop yield decrease, and farmers are forced to abandon parts of the land and to open new fertile forest land. As a result, 5158.34 ha of the total area of the study was reforested, mostly from agriculture class represented by 2694.49 ha as shown in the child class agriculture to scattered-forest (table 6.8). Most of the lost area from agriculture class converted to grassland class, representing 67.77 % of the total abandons area. Interestingly, this figure coincided with the area that was reutilized from grassland to agriculture, as observed also in the first period of study. Therefore, less than ten years abandon period is too short since the natural forest cover needs addition period to recover.

We can achieve from the above mentioned analyses, the deforestation process occurring at semi-steady rate. However, when shifting cultivation practices in unsustainable forms, natural forest covers disappears permanently. Extrapolation of reforestation process dynamics indicates that natural forest cover has a potentiality to recover if the rain-fed agriculture is managed in sustainable manner, considering the succession period needed for natural forest cover. Therefore, the abandonment period of the agricultural field is a vital conservation strategy to promote restoration of natural resources in degraded land (Asefa *et al.*, 2003).

The settlements areas were increased rapidly during the period of study as a result of population growth in the region (Annex 7). These residential areas increased by 673.81 ha during the first period of study while the new residential areas reached 1118.39 ha during the second period of study. The total increasing rate for the settlements area is 673.81 ha and 1118.39 ha for the first and second period of study respectively. This increase in population combined with collapse in agricultural schemes (7741.08 ha) has led to more pressure on natural resources to cover there direct needs, i.e.; foods, energy, building materials and to feed their animals.

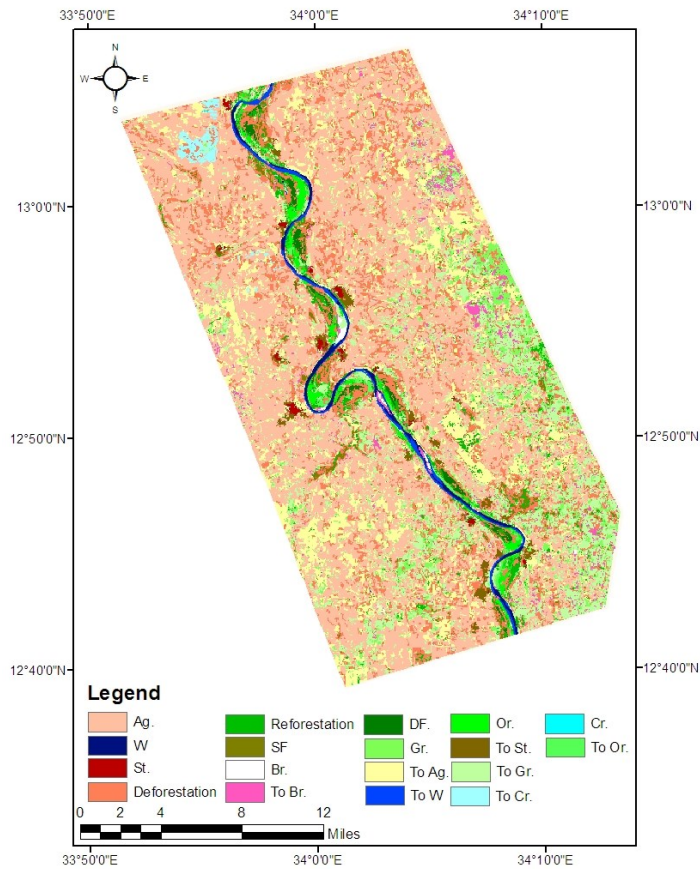


Figure 6-9: Change map “from-to” parent classes generated from overlaid classified images 1999 and 2009 (figure 6.2)

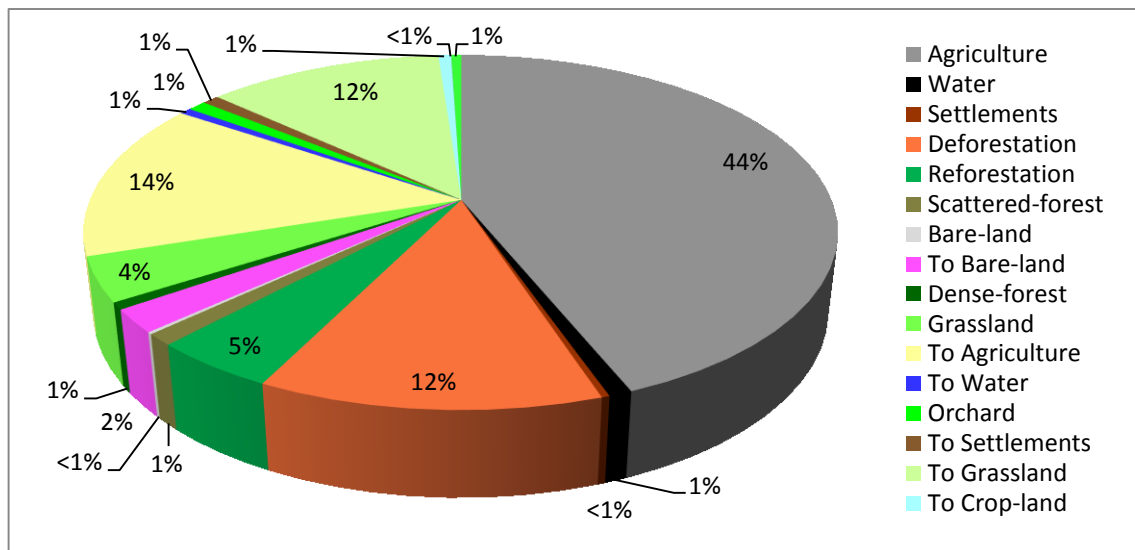


Figure 6-10: Change area “from-to” parent classes generated from overlaid classified image 1999-2009

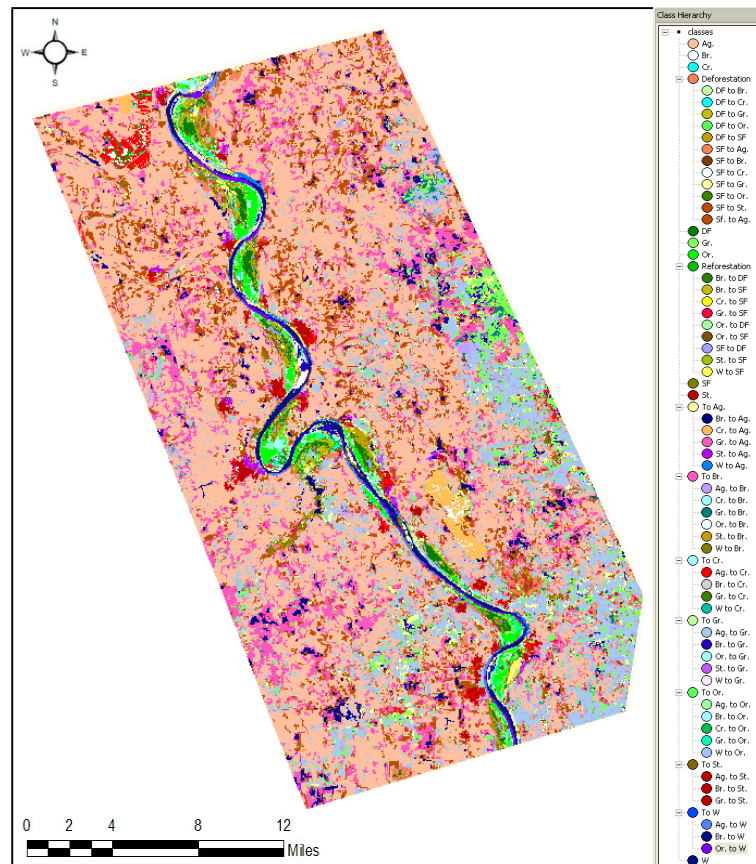


Figure 6-11: Change map “from-to” child classes generated from overlaid classified images 1999 and 2009 (figure 6.2)

According to the above mentioned results, we can confirm that the LU/LC structure in Blue Nile region of Sudan is mostly composed of seasonal rain-fed agriculture (figure 6.7 and 6.10). Therefore, the past decades were considered as a golden period for the mechanized rain-fed agriculture in the region, when the new opened land gained high profitability ratio combined with the benefits from selling the harvested woods. However, the selling of woods takes several forms; e.g. firewood, furniture, local building materials and charcoal (figure 6.12).



Figure 6-12: Land clearance for mechanized farming, traditional method adopted in the region for charcoal making in harvested areas (photograph taken by the author, summer 2004)

6.4.3. Overall evaluation of the adopted approach in mapping forest cover change dynamics

Accurate spatial registration is crucial for any reliable and accurate change detection technique (Townshend *et al.*, 1992 and Singh, 1989). The multi-temporal image fusion analysis can be used as an assessment method, since the fixed areas between the overlaid images can be compared and measured with different geometrical features via OBIA. Thus, the measured differences between the two objects in different dates for the same pattern can be reported as a registration error. Ground control points could be added as a thematic layer, if available, for the correspondent date, and could be also used to assess the registration quality of each image as well as the change analysis result. Fortunately, the RMS errors reported were negligible (< 0.5 pixel). Hence, the above mentioned processes were not performed in the present study. The accuracy assessment achieved in this case indicates only the level of membership assignment for each change “from-to” information class.

A wide range of change-detection techniques has been developed, but little has been done to assess the quality of these techniques. The expected accuracy of the post-classification change detection can be roughly estimated by simply multiplying the accuracies of each individual classification (Singh, 1989). However, in order to quantitatively evaluate the accuracies of the

change maps, the accuracy assessment based on best classification results were performed in *eCognition* software.

The accuracies of the change maps resulting from the OB post-classification method are summarized in table 6.9 and 6.10. The lists of the best classification membership values for all parent change classes were generated for each couple of overlaid images. Also, the detailed child change classes were shown in figures 6.8 and 6.11 Most of the change areas as well as the overlapped (no change) areas have mean membership values accurately assigned to the class with not less than 0.99. The lowest accuracy between all parent change classes is the “reforestation” class in the second time interval with mean membership value of 0.94.

Table 6-9: Accuracy assessment based on the best classification result for the change map of 1990-1999

	Class	Objects	Mean	Std. Dev.	Minimum	Maximum
No Change	Ag.	4633	1.00	0.00	1.00	1.00
	Br.	38	1.00	0.00	1.00	1.00
	DF	249	0.99	0.02	0.84	1.00
	Gr.	1107	1.00	0.00	1.00	1.00
	Or.	116	0.99	0.02	0.79	1.00
	SF	2961	0.99	0.01	0.86	1.00
	St.	32	1.00	0.00	1.00	1.00
	W	147	1.00	0.00	1.00	1.00
Change	Def.	11049	0.99	0.06	0.30	1.00
	Ref.	4872	0.99	0.03	0.12	1.00
	St.	118	0.95	0.14	0.51	1.00
	W	195	0.99	0.03	0.77	1.00
	Ag.	2338	0.99	0.02	0.59	1.00
	Br.	1190	0.99	0.03	0.57	1.00
	Gr.	3624	0.99	0.04	0.57	1.00
	Cr.	68	0.98	0.14	0.18	1.00
	Or.	227	1.00	0.00	1.00	1.00

Table 6-10: Accuracy assessment based on the best classification result for the change map of 1999-2009

	Class	Objects	Mean	Std. Dev.	Minimum	Maximum
No Change	Ag.	15041	0.99	0.00	0.89	1.00
	Br.	333	1.00	0.00	1.00	1.00
	DF	8	1.00	0.00	1.00	1.00
	Gr.	467	1.00	0.02	1.00	1.00
	Or.	5332	1.00	0.00	1.00	1.00
	SF	483	0.99	0.01	0.81	1.00
	St.	2171	0.99	0.01	0.87	1.00
	W	148	1.00	0.00	1.00	1.00
Change	Def.	231	1.00	0.00	1.00	1.00
	Ref.	17502	0.99	0.04	0.38	1.00
	St.	5692	0.94	0.17	0.40	1.00
	W	652	1.00	0.00	1.00	1.00
	Ag.	600	0.97	0.11	0.11	1.00
	Br.	9256	0.99	0.05	0.60	1.00
	Gr.	4794	0.99	0.02	0.58	1.00
	Cr.	11795	0.99	0.02	0.58	1.00
	Or.	664	1.00	0.00	1.00	1.00

Moreover, the swap area between LU/LC classes may show slight difference in the mean of their mismatching between two dates. For this reason, quantitative statistical analysis was performed to calculate the area of each LU/LC class from the change maps based on the static area from the reference classified data (i.e. non site specific accuracy assessment) as shown in table 6.11. All in all, the classification accuracy achieved from the change maps indicates that the change classes as well as the overlapped area were clearly identified with high degree of precision.

Table 6-11: Non-site specific accuracy assessment for the change maps (1990-1999 and 1999-2009) based on the reference data of classified images 1990, 1999 and 2009

Class	1990				1999				2009			
	Ref. Area (ha)	Est. Area (ha)	Error (ha)	Error (%)	Ref. Area (ha)	Est. Area (ha)	Error (ha)	Error (%)	Ref. Area (ha)	Est. Area (ha)	Error (ha)	Error (%)
Agriculture	47809.10	48035.23	226.13	0.47	66468.30	66521.68	53.38	0.08	73851.55	74117.50	265.95	0.36
Bare-land	261.99	262.29	0.30	0.11	3824.46	3828.88	4.42	0.12	2882.93	2905.02	22.09	0.77
Crop-land	8627.49	8636.92	9.43	0.11	857.07	858.08	1.01	0.12	886.41	887.48	1.07	0.12
Dense-forest	3381.75	3437.44	55.69	1.65	2219.85	2217.87	-1.98	-0.09	1109.43	1043.84	-65.59	-5.91
Grassland	6851.61	6860.29	8.68	0.13	19575.10	19622.97	47.87	0.24	20625.28	20454.67	-170.61	-0.83
Orchard	1394.28	1388.81	-5.47	-0.39	2079.81	2082.16	2.35	0.11	2182.43	2185.13	2.70	0.12
Scattered-forest	39959.40	39980.48	21.08	0.05	13738.50	13761.40	22.90	0.17	6612.19	6752.00	139.81	2.11
Settlements	403.74	429.17	25.43	6.30	851.94	894.66	42.72	5.01	1516.82	1445.21	-71.61	-4.72
Water	2808.90	2796.16	-12.74	-0.45	2036.70	2039.09	2.39	0.12	1881.20	1878.91	-2.29	-0.12

6.5. Major driving forces of forest cover loss and restoration problems

6.5.1. Deterioration of forest cover in the area

The social survey of households was intended to be used as an evaluator of the change dynamics as well as to understand the underlying forces that lead to forest cover loss. The study indicates that the deforestation in the area was estimated to occur at a rate of about 2.38 % per annum. Therefore, as shown in table 6.12, great percentage of local communities indicates that many of the goods and services obtained from the forest in the past are currently no longer available. 91 respondents out of 120 indicate that they used to obtain benefits from the forest in the past. For those community members, combinations of these goods and services are widely used in a few past decades. However, 87 % of the respondents indicate that they lost their ability to collect woody product for direct need as cooking energy, building materials and furniture. The second most important is the non-wood forest products as pointed out by 78 % of those respondents. One of the most important products is the *Gum Arabic* from *Acacia senegal* and *Acacia seyal*, where the area was rich in this species in few past decades.

Table 6-12: Percent and total of local communities indicating goods and services attained from the forest in few past decades but which are no longer available

Obtained value	Number of responses	Total respondents (%) (N= 91)
Woody products¹	79	87
Non-woody products²	71	78
Associated with forest³	67	74
Climate control	45	49
Recreation	19	21

Note:

¹Charcoal, firewood, building materials, furniture.

²Gums, Fruits, seeds, oils.

³Hunting, wild honey, grazing.

6.5.2. Driving forces of forest cover loss

Table 6.13 illustrates community perception of the underlying forces of forest cover loss. From the analysis of this result, land clearance for mechanized farming seems to be the major cause of deforestation in the study area, which was indicated by 97 % of the total respondents. Cultivation expansion leads to removal of natural woody vegetation and this conversion on land leads to deforestation. Accordingly, vast areas were converted to agricultural land under intensive cultivation. Moreover, as a result of high profitability gained from selling woody products from a new opened land, high percentage of respondents indicated that the harvesting of woody products is considered as the second force of deforestation. Many authors have agreed on those subjects, Abdallah (1991) and Elmoula (1985) noted that the illegal cutting for energy purpose (fuel wood, charcoal making) as well as excessive clearance for mechanized rain-fed agriculture has decimated the forest resources in the study area.

Other form of deforestation was observed in *Acacia nilotica* pure stand forests. As shown in tables 6.7 and 6.8, these forests shrinkage by 497.83 ha and 381.88 ha for the first and second time intervals respectively, as a result of orchard expansion. Furthermore, the dense forests have become more fragmented and exposed. 614.70 ha from the first period of study as well as 751.96 ha from the second period of study were transformed from dense-forests to scattered-forests. Because the local communities no more look at the forest as their own, they have commenced to practice all their activities in the forests as illegal. Subsequently, the forest resources have become increasingly vulnerable to unsustainable practices. Somewhat, this behavior is further enhanced by the restrictive Sudan's Forest Act of 1989. However, inevitably the forest resource based on the study area has decreased rapidly because of lack of public concern and an increase in overexploitation and illegal activities.

Table 6-13: Local community's perception about the causes of forest cover loss

Factors	Number of responses	Total respondents (%) (N= 117)
Agricultural expansion	113	97
Harvesting of woody products	88	75
Manmade fire	34	29
Natural phenomena	14	12

The annual precipitation rate was proposed as one of the causes of forest cover loss in the area. As shown in figure 6.13, which is coincided with the local community perception, there is very weak relation with the deforestation process. From the table 6.13, only 12 % of the respondents indicate that some years of drought were responsible for this deterioration.

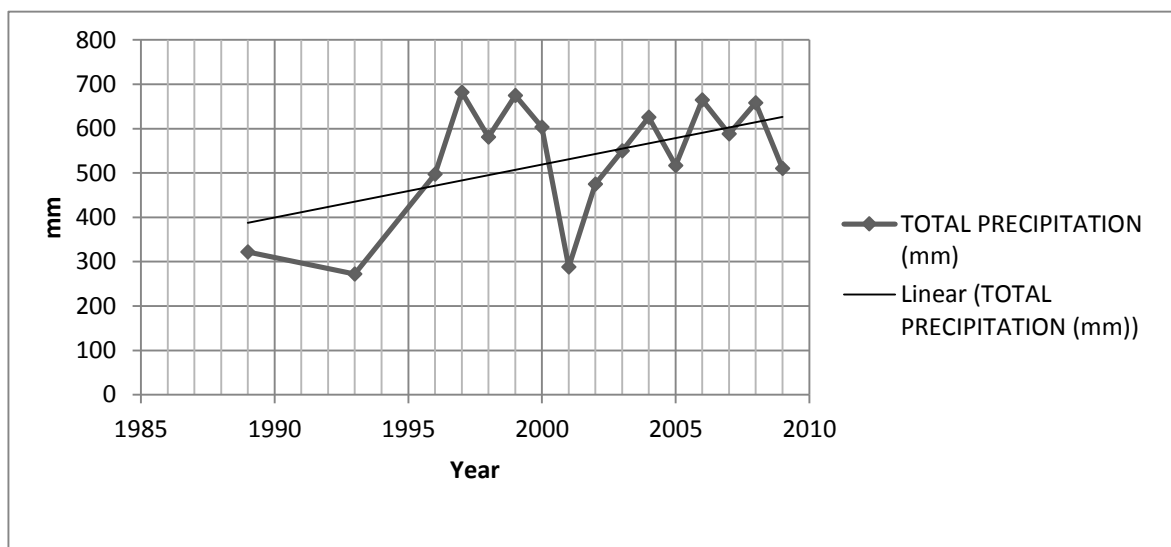


Figure 6-13: Total annual precipitation in the study area (Abunama station)

6.5.3. Restoration of destroyed forests

Before the 1970s, majority of the area was forest and grassland, which was used communally for pasture and traditional farming under customary land laws (Agrawal, 2007). In this form of use, the right to cultivate an area of newly opened land became vested in the farmer who cleared it for use. Since 1980 the government disregarded the land used by customary laws and then the unregistered lands became government owned. Subsequently, vast areas were leased to individuals to be used for mechanized rain-fed agriculture, while majority of the local farmer are

not allowed to use the land. This might be one of the main causes that lead to illegal degradation, as shown in table 6.14, 80 % of the respondents declared that land ownership system is considered as a prime factor of forest cover loss. The difference between the two systems is that, by customary law, the farmers maintain the land for sustainable use by shifting cultivation, which gives chance for the forest to recover, while the leaser, looks for high profitability ratio with intensive cultivation (figure 6.15). As a result, the seed bank becomes bankrupted and the ability for the natural forest to recover may be lost for ever (Miller, 1999). Additionally, the crop productivity ratio of the area has been reduced as stated in figure 6.14.

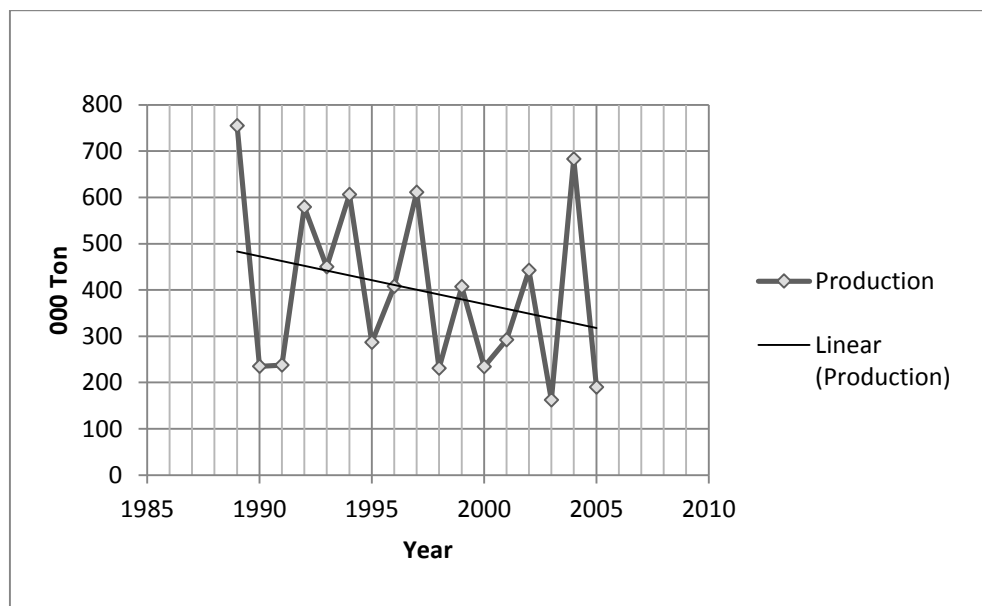


Figure 6-14: Total production of cereal crops in Sinnar state. Source: GAPE (2009)

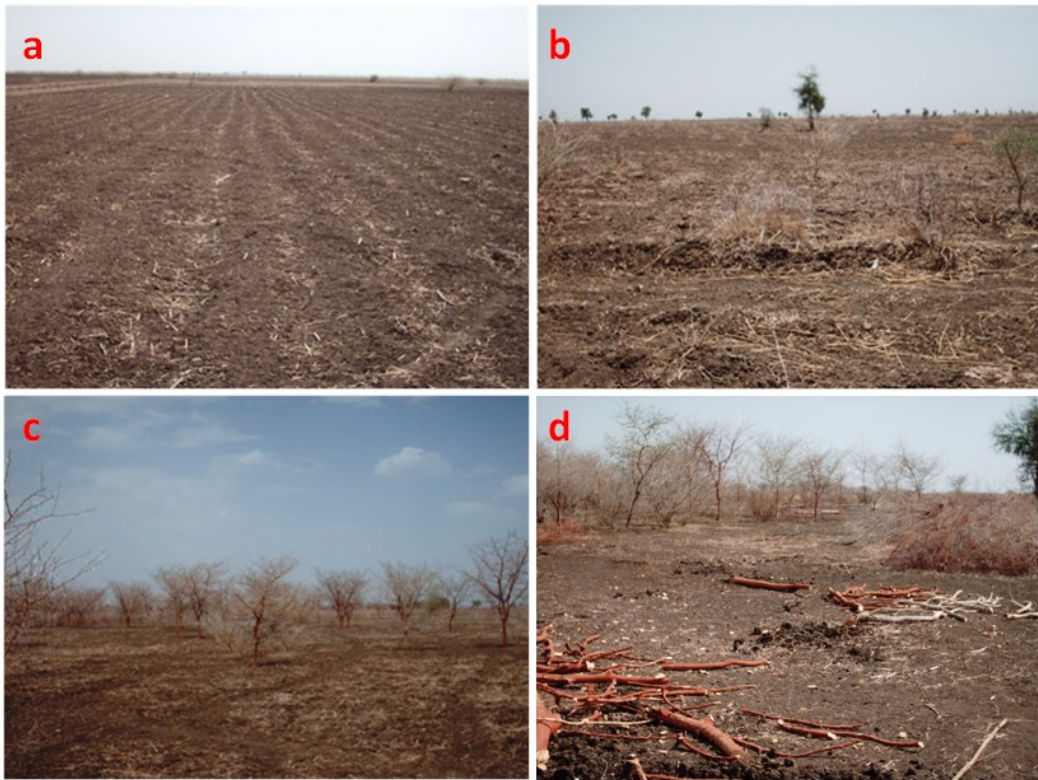


Figure 6-15: A typical pattern in dry season of abandoned agricultural land rotation ; a) currently in use, b) recently abandoned, c) abandoned recovered land (*Acacia seyal*), and d) land clearance for cultivation (Photographs taken by the author, winter 2010).

As an effort to stem the deforestation in the study area, several initiatives have been undertaken at the state and national levels. Accordingly, some areas were successfully reserved and recovered, additionally community forests were established in the state as a joined program between the local communities and the government represented by FNC; while the FNC provides the financial support and extension, the local communities perform the silvicultural operation and protect the forest, and eventually the revenue is mainly for the local communities. As a result, in 1990s progressive increase in reforested areas was observed (figures 6.6 and 6.7).

Moreover, majority of the people in these communities are unemployed poor subsistence farmers. As a result of losing their ability to cultivate the lands by late 1980s, as well as the collapse which occurred in the irrigated agricultural schemes in early 1990s, more pressure on natural forest occurred, and the local community became highly dependent on natural resources for their everyday needs and income generation. Therefore, when we asked the local communities about their perception on this, 71 % of the respondents think that creating a diverse set of economic

opportunities and jobs for local people may conserve the forests as well as restore those that were exposed.

Table 6-14: Local community's perception about the mission that it may stimulate the recovery process

Mission	Number of responses	Total respondents (%) (N= 108)
Land tenure	86	80
Afforestation & reforestation	69	64
Job opportunities	77	71
Awareness programs	14	13

6.6. Summary

Considering the dramatic change which has occurred and still occurs in the Blue Nile region of Sudan, this study is of great value for developing a method to monitor changes over time. The study utilizes three consecutive optical multispectral images, two LANDSAT TM images of 1990 and 1999 as well as TERRA ASTER image of 2009 to evaluate forest cover dynamics during the period between 1990 to 2009. The method adopted in this research consists of cross operation of classified images of different points in time, which utilizes the overlaid classified images to be compared to change detection. New layer of segments were created representing the change areas as well as the overlapped areas of each pair of classified images. As the fundamental stage, smooth and accurate classified images are very essential for any post-classification change detection technique, which were typically achieved by OBIA with overall accuracy 91 %, 93 % and 95 % for the years 1990, 1999 and 2009 respectively. Nine LU/LC classes were generated from each, therefore, and considering the dramatic change observed in the area, the operation results initially in quite numerous change “from-to” information classes, which allows for aggregation of these classes at any hierarchical level of details. Moreover, the developed approach allows the operator to effectively know the spatial pattern of change, trend and magnitude of the dynamics which occurred in each of the classified LU/LC classes.

While many change-detection techniques have been developed, little has been done to assess the quality of these techniques. Hence, the change maps resulting from cross operation were

assessed, which reveals that the accuracies of the change maps for the two time intervals were consistently high (tables 6.9 and 6.10). Most importantly is to be noted that the classification accuracy is affected by the minor area change classes that were observed in some segments, which experience difficulties to be visually interpreted. For example, change in bare-land to dense-forest for the first time interval; the change is 0.002 % which is negligible (table 6.7), thus the system calculates the error in this class regardless of its real representation portion in the change map. For practical comparison, the statistics of the swap area of each LU/LC class derived from overlaid maps were compared with static classes area derived from each classified image separately as reference data. Hence, post-classification comparison might be able to mitigate the problem of getting accurate registration of multi-temporal image analysis (Singh, 1989). As a result of efficient co-registration as well as the appropriate method adopted in this research, in most cases, and considering the large area coverage, negligible differences in area were observed.

The results achieved from the change detection analysis exhibit significant changes of LU/LC in the study area during the two distinctive periods (from 1990 to 1999 and 1999 to 2009). The most interesting fact is that the trend and magnitude of change for the two time intervals coincide in most cases. The quantitative result of the change detection reveals that the forest cover has dramatically been shrunked and destroyed. As it can be obviously noted from the change maps, the expansion of rain-fed agriculture is the main driving force leading to forest cover loss. During the first period of study (table 6.7), all areas of irrigated schemes collapsed. Interestingly, the settlements area doubled in each time interval. During the second period of study (table 6.8), there was proliferation of bare-land patches, where the rain-fed agriculture was intensively practiced (figure 6.9). Giving more inspections to the change analysis results during the first period of study, there was light at the end of the tunnel where the capability of the area to recover was obviously shown for abandoned agricultural fields (figure 6.6 and table 6.7). It must be considered that most of the stable area observed includes the land managed under clear property rights (i.e.; dense-forest and orchard patterns), which coincided with the result achieved from the social survey of households (table 6.14).

In conclusion, the present study exhibits a great potential for accurate LU/LC change detection when utilizing OB post-classification technique with optical multispectral satellite imagery. The proven capability of the adopted method for gaining knowledge of the change dynamics and its

driving forces was also shown. Moreover, the results of the combined analysis indicate that the mechanized rain-fed agriculture was the major force which led to forest cover loss.

Chapter 7 OBJECT-BASED TEXTURE MEASURES AND FOREST INVENTORY

7.1. General overview

Sustainable forest management requires flexible, reliable and up-to-date information. A possible solution for updating the Blue Nile *Acacia nilotica* structural attributes in Sudan is the application of object-based texture measures, which is presently being investigated. TERRA ASTER and RapidEye data are being considered as a data source to cover large areas rather than the conventional forest inventory method. *Alambwa* forest is one of the several *Acacia nilotica* pure stand forests managed for timber production. These forests are located alternately along the riverbanks, therefore the dispersal of these forests did not allow for aggregation of those forests to be mapped all together. Therefore, samples in this study do not consider the entire area of the Blue Nile forests. The field survey has been carried out in *Alambwa* forest in order to collect data concerning tree volume estimation (V) such as diameter at breast height (DBH), tree height (H), stand density (D), and basal area (BA), which are currently being examined by a combination of object-based and pixel-based image metrics extraction. Remote sensing is often the only reliable source of information on these variables over large areas, particularly in semi-arid regions with inaccessible areas in most cases. In OBIA the object layer value (OLV) of the digital numbers of image segments in addition to textural attributes described by grey-level co-occurrence matrices (GLCM) were calculated for the objects corresponding to field samples, while in pixel based approach the DN was extracted from each pixel to assess the object-based metric estimates.

The processes of image metrics feature extraction and methods of forest parameters estimation were discussed in chapter 4. In this chapter interactive processes were performed between Aster (VNIR bands) and the visible bands of RapidEye extracted metrics from one side and at plot-level forest inventory parameters from the other side. Initially the images were segmented to achieve preliminary meaningful units. Steps were followed to predict each of *Acacia nilotica* pure stand plantation structural attribute. Subsequently, two main sets of analyses were undertaken. Firstly, based on the computed object features, the study addresses the association between various image metrics and forest structural characteristics using Pearson's correlation

coefficient (section 7.4). Secondly a focus is laid upon volume (higher correlated) estimation by analyzing its relationship with the extracted image metrics using regression model (section 7.5). The selected models were validated by randomly selected field survey data (section 7.5.1). Finally, the validated model was used to produce a forest structure map (section 7.6). The data used and the methodological steps applied are presented in figure 7.1.

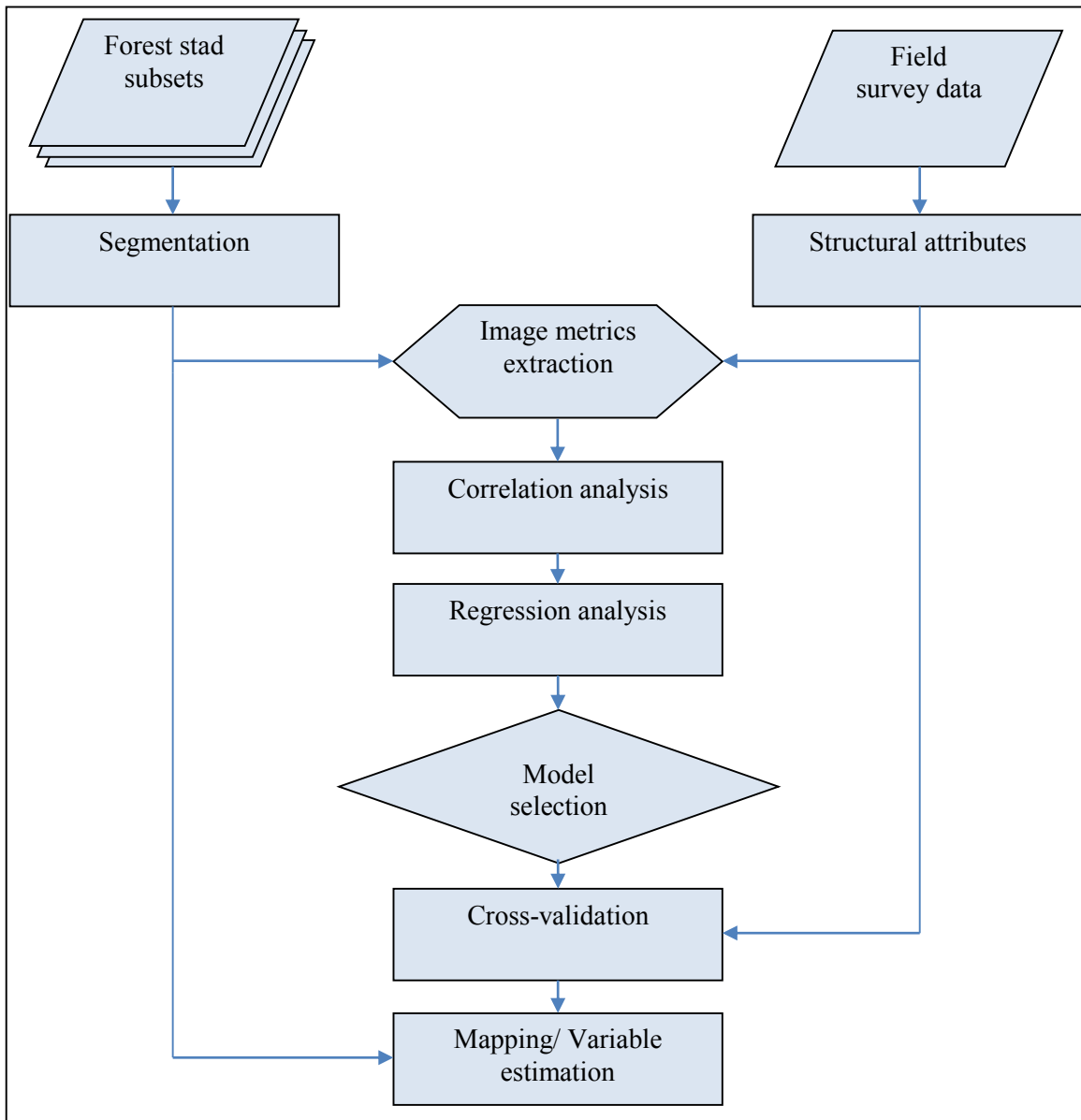


Figure 7-1: Modeling steps to estimate *Acacia nilotica* structural attributes

7.2. Segmentation

Segmentation of imagery was performed using *eCognition* software, version 8.0. Multiresolution segmentation algorithm was applied to generate preliminary meaningful objects. Best segmentation results were achieved by setting the parameters algorithms with trial and error procedure (Mathieu *et al.*, 2007). As shown in table 4.6, after experience of several combination sets of segmentation parameters, a scale parameter of 7 was considered as optimal for Aster and RapidEye imagery. The composition of homogeneity criteria for color and shape were set at 0.8 and 0.2 respectively. While the shape criteria, smoothness and compactness, were set equally as 0.5. The total number of image objects obtained by the above mentioned criteria were 2,472 and 9,394 image objects for Aster and RapidEye subsequently.

7.3. Descriptive analysis of field data

In total, forest stand parameter data of 24,251 trees were collected from 104 surveyed plots in the stocked area of Alambwa forest. Unstocked and regeneration areas were excluded in this study (Annex 2). The measured stands age from 9 to 21 years and consist of *Acacia nilotica* pure stand plantations was managed for 30 years in timber production. All the trees with dbh ≥ 5 cm were measured in the established systematic sample plots. Additionally, number of trees per unit area and average tree height for each sampled area were measured. Tree basal area was calculated from the field measurements (Equation 3.14), while the volume was estimated from the above measured variables using an equation described in chapter 4 (Equation 4.15).

The average total of forest stand parameters in each volume class is given in table 7.1. More than half of the area has an average range of stand volume between 50 to 150 m³/ha (58%), while only about 7% have volume more than 200 m³/ha. The mean value of tree diameter at breast height equal or more than 5 cm was approximately 36.14 cm with a standard deviation of 11.65 cm. The means of the total basal area, density and tree height were 0.0359 m²/ha, 347.00 trees/ha and 20.76 m with a standard deviation of 0.0208 m²/ha, 175.47 trees/ha and 5.52 m, respectively. While the total average of stand volume was found to be directly correspond to the above mentioned parameters.

Table 7-1: Statistical summary of stand parameters for each volume class and its total

Volume classes (m³/ha)	<50	50-100	101-150	151-200	>200	Total
Average diameter (cm)	17.8	34.4	38.3	44.8	49.4	36.140
SD of diameter	5.65	5.80	7.47	6.31	11.14	11.650
Avg. of total BA (m ² /ha)	3.36	8.35	11.06	12.17	18.40	9.8680
SD of total BA	0.28	3.01	1.955	1.37	1.96	4.3269
Average density (No./ha)	509.7	309.8	349.6	255.6	328.5	347.00
SD of density	200.8	157.8	177.7	75.4	122.1	175.47
Average height (m)	14.44	18.41	21.67	25.61	25.50	20.760
SD of height	4.81	4.93	4.42	2.18	1.29	05.520
Average volume (m ³ /ha)	25.9	77.1	125.6	167.2	253.0	114.91
SD of volume	7.53	18.89	14.31	9.86	23.99	62.610

Measurements of forest stand parameters (basal area, number of trees per unit area, tree height, and volume) were analyzed and presented by box-plots shown in figure 7.2 for the entire collected dataset.

As can be seen, average basal area measured ranging from 3.3 to 25 m²/ha are the minimum and maximum values respectively, while the median is approximately 16 m²/ha. However, the stand density has a median estimate of 430 trees/ha and the minimum to maximum values of 150 to 860 trees/ha, respectively. The stand tree height minimum value is 8 m and 37 m as a maximum value. While the volume value which combined the above mentioned parameters ranged from 63 m³/ha to 335 m³/ha, although the median is approximately about 177 m³/ha.

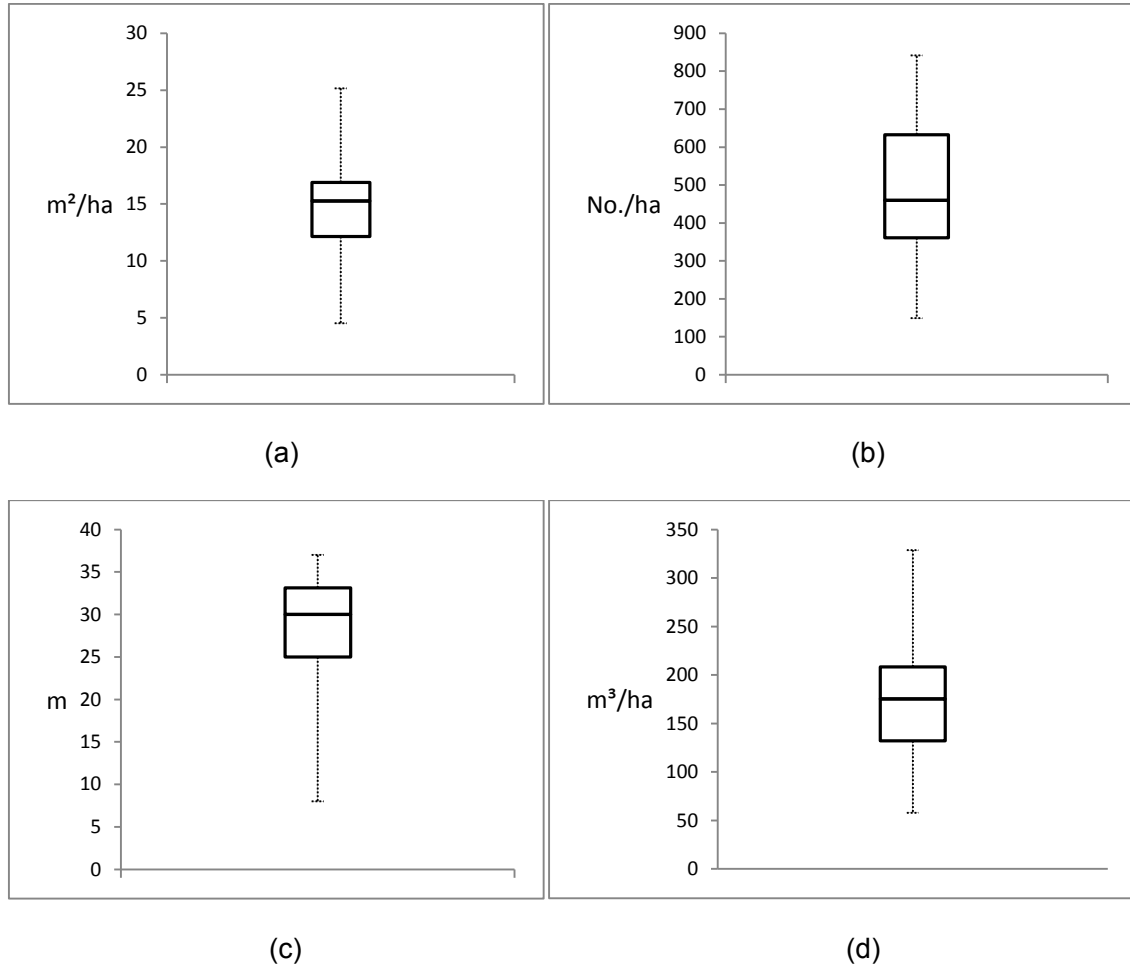


Figure 7-2: Average tree basal area (a), total number of trees per unit area (b), average stand height (c), and average stand volume based on sampled areas (d)

The total stand volume in the study area was estimated to 29937.93 m³. Pearson's correlation coefficient was applied to address the association between forest stand variables measured and estimated (table 7.2). The major difference in the volume values was observed due to the average variation of tree basal area (0.98). While the higher variation in stand density results in low negative correlation with average stand volume (0.73). The negative correlation attributed to the thinning operation applied to the stand ends up with low number of mature commercial volume.

Table 7-2: Pearson's correlation coefficient matrix for *Acacia nilotica* plantation average stand variables

	Height	Volume	Diameter	Density	Basal area
Height	1	.792**	.733**	-.689**	.696**
Volume	-	1	.946**	-.731**	.977**
Diameter	-	-	1	-.771**	.978**
Density	-	-	-	1	-.730**
Basal area	-	-	-	-	1

***. Correlation is significant at the 0.01 level (2-tailed).*

7.4. Image metrics and forest inventory

7.4.1. Volume

The link between *Acacia nilotica* stand volume and each of the extracted image metrics (i.e.; OLV, GLCM, and DN), which were derived from TERRA ASTER and RapidEye VNIR bands were analyzed using Pearson's correlation coefficient (table 7.3).

Table 7-3: Pearson's correlation coefficient between image metrics and stand volume

Method	Image metric	Band 1		Band 2		Band 3	
		5m	15m	5m	15m	5m	15m
OB	Mean object value	.794**	.770**	.794**	.786**	.783**	.819**
	SD of object value	-	.753**	-	.669**	-	.628**
	Homogeneity	.007	.374**	.229	.568**	.337**	.453**
	Contrast	-	.430**	-	.538**	-	.396**
	Dissimilarity	.520**	.501**	.266*	.561**	.531**	.465**
	Entropy	-	.006	-	.185	-	.277*
	Ang. 2 nd moment	-	.305*	-	.518**	-	.251*
	Correlation	.040	.715**	.173	.684**	.060	.563**
PB	Digital number	.635**	.497**	.682**	.666**	.658**	.554**

***. Correlation is significant at the 0.01 level (2-tailed).*

**. Correlation is significant at the 0.05 level (2-tailed).*

The calculated results of the correlation between data of total average stand volume for each plot and the extracted image metrics gave high correlation in most of the image metrics for all tested bands. Exceptions were found in "entropy" and "ang. 2nd moment" of Aster as well as green and red bands of "homogeneity" and the all bands of "correlation". The highest correlation (P-value

≥ 0.01) was observed in mean of the object value among the other tested metrics. However, at this metric, no significant difference was observed at the both resolutions for all bands, while the NIR band of Aster has the superior correlation (0.819). A high correlation was also observed in object-based textural attribute “correlation” of Aster in all bands with values 0.715, 0.684 and 0.563 respectively. “Dissimilarity” has a good correlation with no significant difference except the lower correlation observed in red band of RapidEye (0.266), while “homogeneity” has good correlations except green and red bands of RapidEye. Moreover, the DN of all bands in pixel-based approach shows a good correlation (P-value ≥ 0.01), varying from 0.497 as a lowest value and 0.682 as a higher value represented by the red band of RapidEye scene.

7.4.2. Height

The Pearson’s correlation calculated results between data of the average of each plot height and image metrics based on the two selected resolutions are shown in table 7.4.

Table 7-4: Pearson’s correlation coefficient between image metrics and stand height

Method	Image metric	Band 1		Band 2		Band 3	
		5m	15m	5m	15m	5m	15m
OB	Mean object value	.916**	.632**	.917**	.643**	.915**	.718**
	SD of object value	-	.627**	-	.513**	-	.486**
	Homogeneity	.095	.307**	.232	.414**	.350**	.278*
	Contrast	-	.319**	-	.397**	-	.285*
	Dissimilarity	.569**	.388**	.357*	.392**	.583**	.377**
	Entropy	-	.167	-	.004	-	.142
	Ang. 2 nd moment	-	.268*	-	.372**	-	.191
	Correlation	.135	.601**	.295*	.520**	.115	.404**
PB	Digital number	.669**	.528**	.692**	.583**	.701**	.407**

***. Correlation is significant at the 0.01 level (2-tailed).*

**. Correlation is significant at the 0.05 level (2-tailed).*

High correlation coefficient between forest stand height and image metrics derived from remotely sensed data among all investigated bands was observed. Overall metrics attributes measured with stand height, the highest correlations with 0.92 were observed in OLV of RapidEye scene. However, an exception was found in some bands of textural attributes metrics. Hence, there is no correlation observed in “ang. 2nd moment” as well as the 1st and 2nd bands of “homogeneity” and

the green and NIR bands of “correlation” in RapidEye scene., “contrast” in NIR band and “ang. 2nd moment” textural attribute green band with positive correlation 0.278, 0.285 and 0.268, respectively (P-value \geq 0.05). Moreover, there was no correlation observed between forest stand height and “entropy” in all bands, as well as “ang. 2nd moment” NIR band. Moreover, the DN of all bands in pixel-based approach shows a good correlation (P-value \geq 0.01), while the highest correlations were observed in NIR, red and green bands in RapidEye scene represented by 0.701, 0.692 and 0.669 respectively. Therefore, the DN of Aster has a correlation with degraded value when compared with the above mentioned metrics (0.528, 0.583 and 0.407 for the green, red and NIR bands respectively).

7.4.3. Density

The association of stand density and image metrics measures for each plot was analyzed using Pearson’s correlation coefficient for all plots measured from the field as shown in the table 7.5 below.

Table 7-5: Pearson’s correlation coefficient between image metrics and stand density

Method	Image metric	Band 1		Band 2		Band 3	
		5m	15m	5m	15m	5m	15m
OB	Mean object value	.632**	.282*	.636**	.313**	.606**	.453**
	SD of object value	-	.288*	-	.197	-	.240*
	Homogeneity	.058	.054	.173	.152	.267*	.031
	Contrast	-	.117	-	.170	-	.013
	Dissimilarity	.382**	.143	.170	.081	.415**	.282*
	Entropy	-	.249*	-	.100	-	.050
	Ang. 2 nd moment	-	.038	-	.116	-	.022
	Correlation	.026	.305*	.071	.250*	.082	.070
PB	Digital number	.549**	.203	.626**	.218*	.570**	.296*

***. Correlation is significant at the 0.01 level (2-tailed).*

**. Correlation is significant at the 0.05 level (2-tailed).*

The weakest correlation among all forest structural attributes and image metrics was observed in stand density with remotely sensed measured metrics. The highest correlation was obtained by the mean layer value of the object at red band in RapidEye scene with a value of 0.636, while there is no significant difference at this image metric in all bands either for Aster or RapidEye, except the red band of Aster image which has lower correlation (P-value \geq 0.05). But in the DN

in pixel-based approach there was no significant difference observed at higher resolution (i.e. RapidEye), when compared with object layer value for the selected segmentation level. Meanwhile, among all other textural attributes metrics, high correlation (P-value ≥ 0.01) was observed only in “dissimilarity” green and NIR bands of RapidEye scene with values of 0.382 and 0.415. With exceptions in “dissimilarity” NIR band and the green band in “entropy” of Aster as well as green and red bands in “correlation” of Aster data, no correlation was observed in other textural attributes.

7.4.4. Basal area

Like the above mentioned forest structural parameters, the Pearson’s correlation coefficient was also applied to address the association between forest stand basal area for all plots measured with each of the TERRA ASTER VNIR bands image metrics(OLV, GLCM and DN) as shown in table 7.6.

Table 7-6: Pearson’s correlation coefficient between image metrics and stand basal area

Approach	Image metric	Band 1	Band 2	Band 3
Object-based	Mean object value	-.717**	-.720**	.761**
	SD of object value	-.709**	-.629**	.595**
	Homogeneity	.354**	.517**	.431**
	Contrast	.418**	.511**	.373**
	Dissimilarity	-.498**	-.543**	-.472**
	Entropy	.057	.264*	.324**
	Ang. 2 nd moment	.284*	.480**	.260*
	Correlation	.685**	.691**	.576**
	Pixel-based	Digital number	-.508**	-.669**

***. Correlation is significant at the 0.01 level (2-tailed).*

**. Correlation is significant at the 0.05 level (2-tailed).*

Strongest correlation between forest stand volume and basal area (table 7.2), substantiate the results of the correlation between basal area and image metrics, which directly correspond to the correlation results obtained from stand volume and the image metrics (table 7.3). Hence, highest correlation was observed in mean layer value of NIR band (0.761), followed by red and green bands with 0.720 and 0.717, respectively. Moreover, most of the measured metrics are highly correlated with stand basal area at 0.01 level of significance. While “ang. 2nd moment” was correlated at 0.05 level of significance in green and NIR bands. There was no correlation

observed in “entropy” at the green band, and weak correlation found in red band. Among the image textural values “dissimilarity” and “correlation” as well as the DN in pixel-based approach, there were no significant difference observed at all bands.

7.5. Development of the regression model to estimate *Acacia nilotica* stand volume

From the previous results, there was an obvious trend in the ability of each forest structural attribute to be explained by the imagery in most cases (tables 7.3, 7.4, 7.5, and 7.6). By performing the correlation analysis prior fitting the regression models, best sets of variables were extracted for the modeling. A great number of explanatory variables were eliminated (18 out of 34) from the candidate models in subsequent stage due to its weak association (Annex 9).

The study found clear differences among the image metrics applied for their ability to predict forest structure variables (section 7.4). The various image metrics applied were ranked with respect to their relative ability to estimate *Acacia nilotica* structural attributes. This was achieved by the selection of the highest coefficient of determination (R^2).

According to the above mentioned assessments and tests, the study concludes that the range of predictability of variables varies based on the image metrics and on respective resolution on the one side and forest structural attributes on the other side. Among all forest stand structural attributes, in general the forest stand volume gives more reliable estimates with most of the investigated metrics (table 7.3). Regardless of the highest correlation observed in RapidEye OLV with stand height at all bands, OLV with stand volume was found to have much significantly stable and constant statistics at all resolutions. In contrast, a variable like stand density shows much lower sensitivity to the metrics being used for prediction (table 7.4). Therefore, application of statistical regression analyses using forest stand volume and image metrics will be performed in the subsequent step.

The same models and estimation approaches were applied to the forest stand volume data to determine which function model in conjunction with each of the selected image metric will fit well. If tree attributes are to be estimated from metrics derived from the RapidEye and ASTER imagery, models have to be empirically built based on field measurements. The relationship between forest stand volume of each plot and extracted image metrics derived from the different

resolutions dataset (OLV, GLCM and DN) was analyzed as dependent and independent variables respectively with simple regression models. Among 104 randomly located training points, two third of the randomly selected points were used to develop the estimation models, which predicted average stand volume per hectare (m^3 per 0.09 ha), in each sampled area.

Three types of link functions were used, linear, logarithmic and inverse. The regression models were developed using the image metrics independent variables and *Acacia nilotica* stem volume dependent variable. The coefficient of determination (R^2) values, p-level for the model, and RMSE were calculated to ensure finding the best fit models. The model which meets the above mentioned requirements should be selected as the best fitted model for *Acacia nilotica* pure stand structural attributes estimate. Table 7.7 summarizes the relationship between modeled forest stand volume and the variables associated with the imagery bands.

Table 7-7: Summary table of generated models and statistics for the forest stand volume and the derived metrics from the VNIR of ASTER and RapidEye data

Method	Metric	Model	ASTER						RapidEye					
			Green		Red		NIR		Green		Red		NIR	
			R ²	RMSE	R ²	RMSE	R ²	RMSE	R ²	RMSE	R ²	RMSE	R ²	RMSE
OB	Mean	Linear	.59**	2621	.62**	2456	.67**	2121	.63**	2189	.63**	2193	.61**	2296
		Log.	.60**	2550	.64**	2346	.64**	2310	.66**	2045	.68**	1920	.69**	1858
		Inverse	.61**	2489	.65**	2259	.60**	2554	.68**	1905	.72**	1661	.75**	1497
	Homog.	Linear	.14**	5529	.32**	4356	.21**	5113	.00	5935	.05	5624	.11**	5260
		Log.	.44**	3573	.48**	3345	.24**	4902	.00	5923	.03	5787	.19**	4822
		Inverse	.45**	3547	.40**	3889	.03	6212	.01	5890	.00	5917	.11	5307
	Dissim.	Linear	.28**	4663	.24**	4881	.22**	5038	.27**	4331	.07*	5516	.28**	4259
		Log.	.28**	4622	.24**	4899	.20**	5138	.30**	4165	.08*	5470	.27**	4313
		Inverse	.27**	4668	.22**	4992	.17**	5316	.31**	4094	.08*	5442	.25**	4432
	Corr.	Linear	.51**	3147	.47**	3421	.32**	4390	.00	5926	.03	5757	.00	5914
		Log.	.51**	3159	.44**	3616	.34**	4247	.00	5930	.01	5875	.00	5933
		Inverse	.45**	3535	.26**	4746	.33**	4327	.00	5935	.00	5933	.01	5898
PB	DN	Linear	.25**	4840	.44**	3578	.31**	4455	.40**	3540	.47**	3176	.43**	3367
		Log.	.26**	4762	.45**	3538	.30**	4483	.42**	3443	.46**	3203	.44**	3354
		Inverse	.27**	4691	.45**	3520	.29**	4657	.42**	3430	.44**	3316	.42**	3423

** Correlation is significant at the 0.01 level (2-tailed).

* Correlation is significant at the 0.05 level (2-tailed).

Regression models which were calculated using forest stand volume as the dependent variable and all other extracted metrics attributes as independent variables. Among all variables based on the two selected approaches, the regression model of inverse equation in OLV of RapidEye NIR band was found to be the best fitting model, which is represented by the highest coefficient of determination ($R^2= 0.75$) and lowest residual mean square error (RMSE= 1497). Moreover, all tested equations in all band resolutions showed higher correlations regarding that image metric than all other metrics attributes as highlighted in table 7.7. The second best predicted variable is the “correlation” in second order textural attribute by the use of linear equation in green band of lower resolution Aster data ($R^2= 0.51$ and RMSE= 3147.5), whereas no correlations were observed mostly in textural attributes of higher resolution RapidEye scene. This in fact is attributed to the highest segmentation level selected, whereas the selected level helps the estimation for individual trees supported by the higher correlations observed in OLV and DN metrics rather than tree batches as is the case with Aster data with textural attributes.

The inverse type of equation was the best fit for the pixel-based approach in Aster data, with the highest $R^2= 0.45$ and the lowest RMSE= 3520.8 which was observed in red band. Meanwhile the linear equation of RapidEye red band provides the highest score in pixel-based approach for both image data. However, this showed degraded result in correlation with forest stand volume if compared with the previous result of OLV in object-based approach.

Regression models were developed using the object-based attributes and DN of pixel as independent variables, as well as field measured volume, basal area, height, and stand density as dependent variables. From the adoption criterion for model selection, the mean object layer value of Aster NIR band using linear model and the OLV of RapidEye NIR band based on inverse model were selected for the subsequent stage (highest $R^2= 0.67$ and 0.75 , and lowest RMSE= 2121 and 1497 subsequently).

7.5.1. Model validation

For the validation of the best fitted model, independent data was used to validate the constructed stand volume equation in *Alambwa Acacia nilotica* forest. The estimated and measured forest stand volume (m^3/ha) were cross validated against each other based on 34 randomly selected field points, and the coefficient of determination (R^2) was calculated as shown in figure 7.3 and figure

7.4. The estimated volume for each plot was predicted using extracted statistics (table 7.8) from linear and inverse functions of mean layer value (NIR band). The confident interval of the model was considered with 0.05 level of significance (95% confidence).

Table 7-8: The coefficients of the best fitted models equation with stand volume

Model	Unstandardized Coefficients		Standardized Coefficients	t	Sig.
	B	Std. Error	Beta		
OLV 3 (RapidEye)	792747.5	55839.3	.865	14.197	.000
(Constant)	-94.036	16.467		-5.711	.000
OLV 3 (Aster)	.132	.011	.819	11.753	.000
(Constant)	-191.926	28.987		-6.621	.000

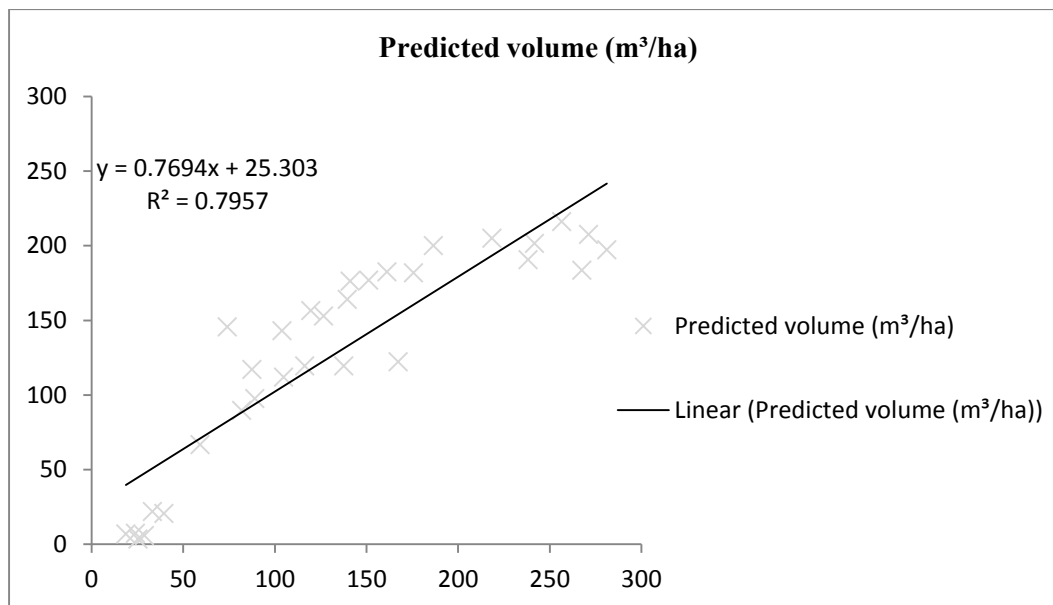


Figure 7-3: Observed vs. predicted forest stand volume (m³/ha) based on RapidEye data

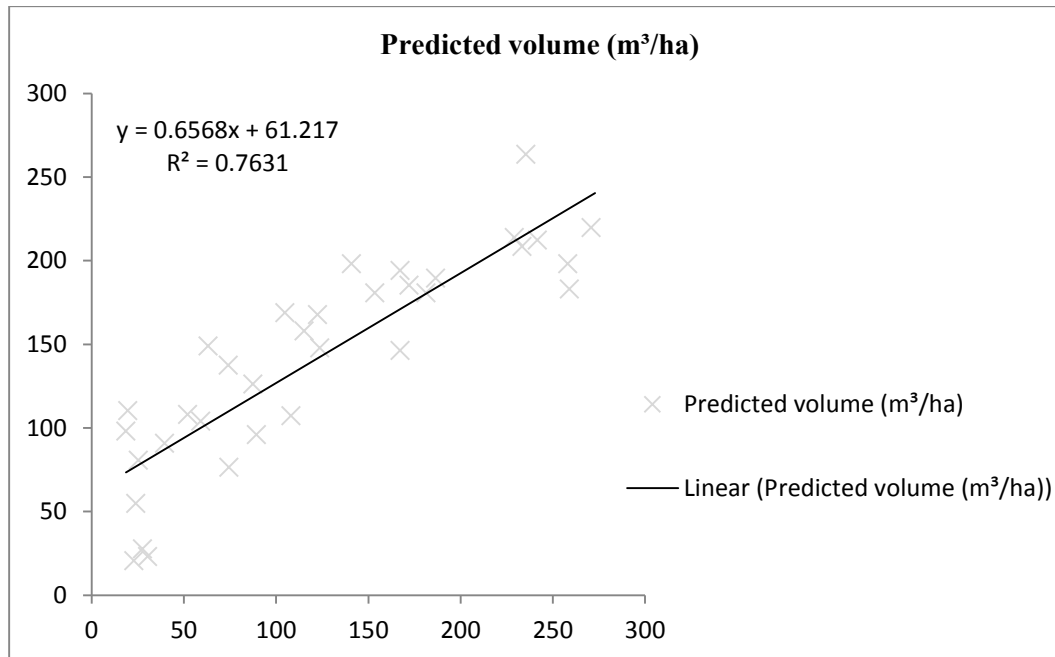


Figure 7-4: Observed vs. predicted forest stand volume (m³/ha) based on Aster data

It was clear from the figures that the selected regression models using the mean layer value of NIR band in both resolutions were effective to predict the volume in *Acacia nilotica* pure stand forests. The model validation lines show that about 80% of field plots were explained by the predicted value with the use of RapidEye data, meanwhile about 76% of the validation data were explained based on the predicted value of Aster NIR band. The smallest stand volume values in both figure 7.3 and figure 7.4 were overestimated, while most of the highest stand volume values were underestimated, and the middle range was overestimated in most cases with moderate error. In general, the average stand volume was overestimated with Aster data by about 19 m³/ha (122.9 m³/ha and 141.9 m³/ha for the measured and predicted volume respectively). On the contrary, it was underestimated by about 5 m³/ha with the use of RapidEye data (134.4 m³/ha and 128.7 m³/ha for the measured and predicted volume respectively).

It is worth noting that the proposed regression models developed to estimate forest structural attributes, such as forest stand volume, make it promising to approximate this variable based on the object-based measure over largely distributed *Acacia nilotica* forests in the region with high level of precision.

7.6. Mapping forest stand volume in Alambwa *Acacia nilotica* pure stand

As a final step, the linear regression model was decided to estimate *Acacia nilotica* volume classes at *Alambwa* forest following the equation (7.1).

$$Y = -94.037 + 792747.5/x \quad (7.1)$$

Where:

Y: Estimated forest stand volume (m³/ha)

X: Mean of the object value extracted from RapidEye band 3

As a result, the developed linear regression model was applied to the TERRA ASTER subset data over the entire stocked area of *Alambwa* reserved forest to produce classified image of estimated volume (figure 7.5).

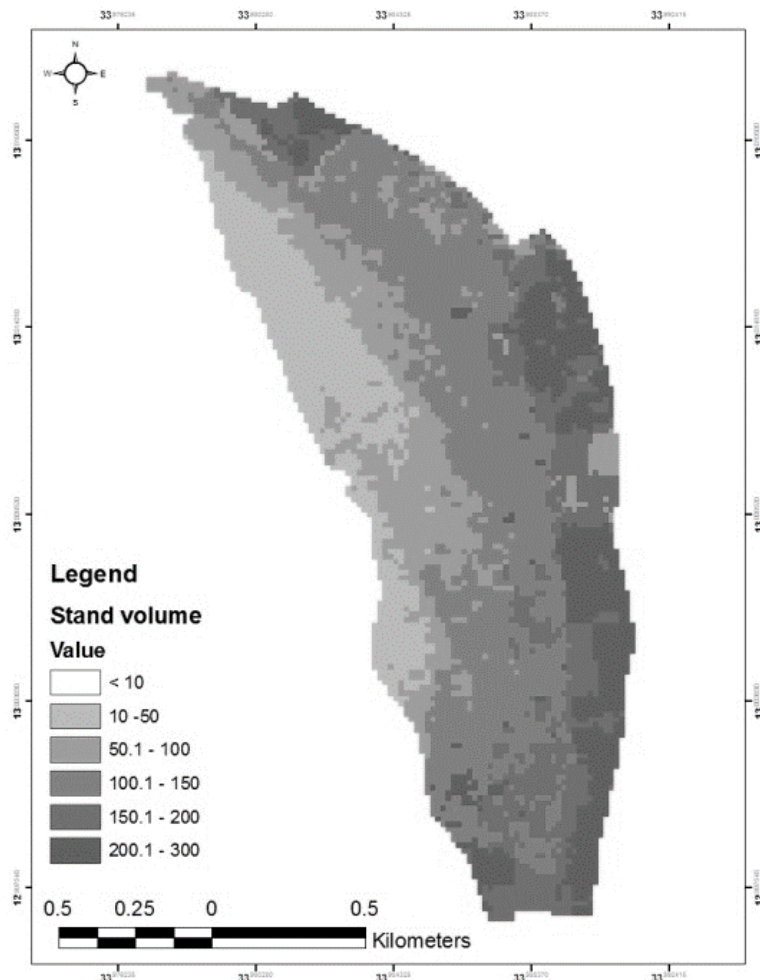


Figure 7-5: Map of estimated volume (m^3/ha) in Alambwa reserved forest

As the forest stand volume has to be estimated from the remotely sensed data (RapidEye data), six ranges of classes were generated for better visualization of the stand volume distribution. As one of the limitation of the generated predicted volume map with simple regression the model was only based on the selected highly correlated attribute (i.e. OLV of NIR band), which disregards the penifits of utilizing multispectral imagery. However, the developed methodology to predict forest structural attributes based on both selected datasets reveals high degree of precision, and thus most accurate maps can be achieved with the use of combined layers in multiregression models.

7.7. Summary

The study aims to develop a regression model as a possible solution to predict forest structural attributes such as basal area, stand density, tree height and volume with reasonable degree of precision in Blue Nile forests. The models formulated are based on the relationship between at plot-level forest inventory data and two different resolution metrics achieved from TERRA ASTER and RapidEye satellite imagery. Initially, the study found that there were a great associations between the forest stand structural attributes itself. A positive correlation was observed between forest stand volume, basal area, height and tree diameter (DBH). The strongest one was observed between measured average tree diameter and estimated volume ($R^2=0.978\text{m}^3/\text{ha}$). While moderate negative correlation was observed between stand density and all textural attributes measured and estimated. This negatively correlated trend is referred to the thinning line or the maximum-density line in even-aged stand (Reineke, 1933). Hence, measuring any of the structural attributes could represent the other to some extent.

The correlation analysis was applied between the forest structural attributes of *Acacia nilotica* pure stand and images metrics based on the object-based and pixel-based approaches. So far, there are very few existing studies that addressed Aster and RapidEye imagery data for forest structural attributes in dry-lands. Moreover, the study revealed that there were strong correlations between forests structural attributes and most of the imagery metrics measured (i.e. OLV, GLCM, and DN). Therefore, this study indicates the potentiality of replacing the conventional costly at plot-level forest inventory methods to estimate biophysical parameters.

In regard to the forest stand variables used, the highest accuracy achieved was the mean OLV (band 3) obtained through object-based method. The superior one was observed with average stand height in red band of RapidEye data ($R^2=0.917$). Meanwhile in sum the average stand volume gave more accurate and consistent results. In contrast, the overall assessment indicate that the lowest accuracy was observed with average stand density, which might be attributed to the high variation in stand density as a result of irregular execution of thinning operation and the effect of illegal cutting. Accordingly, the study points out that the mean OLV in image objects was more appropriate for forest structural attributes estimation, especially with forest stand volume, than the GLCM textural attributes of the image objects and the DNs of pixel-based method.

Most of the image metrics measured were highly correlated with the forest stand structural attributes (section 7.4). An exception was found in the GLCM textural attributes and much precisely with RapidEye data. This in fact is attributed to the highest segmentation level selected, whereas the selected level led to higher estimation for individual trees supported by the higher correlations observed in OLV and DN metrics rather than tree batches as the case of Aster data with textural attribute.

For *Acacia nilotica* the inverse regression model, which was computed from RapidEye mean OLV of NIR band, was found to be the best estimator of forest stand volume at plot-level among all other tested image metrics ($R^2 = 0.75$, RMSE = 1497; table 7.7). Between the GLCM, the linear regression model of the correlation Aster green band textural attribute, was found to be the best fit of the forest stand volume at plot-level ($R^2 = 0.51$, RMSE = 3147.5) when compared with other GLCM textural attributes. While in pixel-based the linear model of red band, was found to be the best estimator of forest stand volume at plot-level ($R^2 = 0.47$, RMSE = 3176) when compared to other tested bands.

The study points out that the results of the forest structural attributes estimation models were fairly good. Our case study was only performed in only one tested site (*Alambwa* forest) with single-phase sampling design considering the area as one stratum. This circumstance could give rise to a high variation result especially in forest stand density. Therefore, there is a need to stratify the forest into different class categories with more numbers of training points (Kasischke *et al.*, 1997).

The selected model was cross-validated with independent thirty four randomly selected field points. The result confirmed that there was a good agreement between those points and the predicted forest stand volume achieved from the best fitted models ($R^2 = 0.80$ and 0.76 for the both resolutions of RapidEye and Aster data respectively; figures 7.3 and 7.4). In fact, if only the thirty four validation points had been taken for model validation, significantly higher value of R^2 would definitely be achieved (Salvador and Pons, 1998).

The R^2 value observed in the present study was in fairly good agreement with most of the previously published studies, such as Kajisa (2009), showed that there was a high R^2 achieved based on the first-order textural attributes (the mean of the digital numbers of image objects) and the DNs of green band. Also a study conducted by Salvador and Pons (1998) using LANDSAT

TM imagery for estimating forest variables, stated that there is a clear possibility of using satellite information to estimate forest structural attributes by means of regression models. In contrast, this study was in disagreement with a study conducted by Gebreslasie *et al.* (2008) using TERRA ASTER to estimate homogenous Eucalyptus plantation forest attributes in South Africa, he found that the reflectance values recorded by the TERRA ASTER satellite sensor are somehow weakly related and not useful for prediction of forest structural attributes.

Hence, according to the previous result and discussion, the relationships between *Acacia nilotica* structural attributes, such as forest stand volume, and imagery most of the examined extracted metrics based on the both resolutions can be used for prediction of forest stand volume with high degree of precision. The models were developed based on data acquired in dry season when most of the water from depression areas (*Mayaa*) is dried. Accordingly these models could be applied for prediction of volume in Blue Nile forests only in dry season.

Chapter 8 CONCLUSIONS, RECOMMENDATIONS AND FUTURE WORK

8.1. Conclusions

8.1.1. Overview

The spatial heterogeneity and rapid changes observed in the Blue Nile region of Sudan motivate the inspection for more efficient, reliable and accurate methods to update the required information for sustainable development. Currently, planners and decision makers are not provided with automated data sources of the desired information levels. Over large areas, field surveys are often tedious and time consuming and other innovative methods of gathering the information need to be developed. In this sense, and in following the main goal earlier mentioned, the study reveals that OBIA has proven its capability as an efficient and accurate methodological framework for gaining knowledge about the land features, whether it is operational forest attributes or categorical LU/LC features. As no single sensor presently covers absolutely the requirements of the entire levels of forest resource assessment, advances of incorporating different forms of data and knowledge were also shown. Moreover, the methodological approach exhibits a potential solution to attain precise facts and figures about the change dynamics and its driving forces. Since an object is a basic processing unit, among various segmentation criteria tested, the study formed different segmentation results convenient for each level in the process hierarchy. Subsequently, optimum features were extracted and rules as well as models were developed for each particular level.

Following the specific objectives, the study can draw the following conclusions:

8.1.2. Land Use/ Land cover categorical level

Among the methods applied in OBIA and the most popular ML classifier from pixel-based approach, both RB and NN classifiers outperform the conventional per-pixel approach when conducting hierarchical classification, providing insight into how image segmentation levels and object features directly improved the LU/LC classification results. Results of the LU/LC maps

and statistics were shown and assessed. Consequently, the validation statistics exhibits strong agreements from object-based methods, while a moderate agreement was observed in pixel-based approach. Giving more inspection to the validation statistics, the overall accuracy was improved from 82% in pixel-based approach to 89% and 95% for NN and RB classifiers respectively, in OBIA.

As a result of multidimensional features used to define LU/LC classes based on NN classifier, complex variables were introduced to discriminate between classes. Despite the fact that optimized feature selection in NN classifier leads to outperform the conventional per-pixel classifier, misclassifications are not avoidable in several cases. Therefore, further analysis was performed to develop rules in RB classifier by incorporating analyst's expert knowledge, which enhances the results effectively. In that way, the extraction of LU/LC classes was found to be very complex and time consuming, since a series of trial-and-error processes were applied to achieve a final set of rules which confused the least between the classes. Nevertheless, the optimal results to categorize LU/LC in Blue Nile region of Sudan were obtained by the use of RB classifier.

Moreover, the following important questions were answered; firstly is OBIA inherently more precise at fine spatial resolution than coarser resolution, and secondly how do both pixel-based and OBIA approaches compare in relative accuracy as a function of spatial resolution. The peak accuracy is always located where the OBIA method is applied and much precisely in most cases at the finer spatial resolution of RapidEye scene. It was found that using pixel-based approach, whether at the fine or coarse scale, only with multi-spectral properties for classification doesn't lead to satisfaction results of LU/LC, because the differentiation between LU/LC classes were performed not only with the aid of spectral information, but also with textural and contextual information of the image objects. Giving more inspection to the validation statistics, the overall classification accuracy was improved in OBIA to 97% when the finer spatial resolution RapidEye data used, meanwhile the classification accuracy in pixel-based method was enhanced slightly from 82% to 85% when the transition from 15 m to 5 m spatial resolution applied.

To sum it up, at these levels some advantages of OBIA have been shown:

- The capability to discriminate between spectrally similar classes was observed (e.g. agriculture, grassland, scattered-forest and settlements classes), in way that mimic human

intelligence for image interpretation as a real-world representation of feature more willingly than discrete pixel value.

- Explicitly the separation of structural land cover from functional land use classes, through adoption of hierarchically conceptual iterative segmentation and classification procedure rather than linear manner, where the developed region- (or domain-) specific multi-scale strategy and the configured knowledge of land cover objects level have been used and defined as spatially and thematically reference units to infer land use classes.
- The analyses were performed not only with multisource imagery; different forms of ancillary data and analyst's knowledge were also introduced.
- Spatial heterogeneity of the region produced salt and pepper effect when utilizing pixel-based approach especially with the use of finer spatial resolution RapidEye data, however this effect was efficiently reduced by OBIA since the classification scheme utilized homogeneous meaningful objects.
- Land features were extracted at different scales from the same scene, e.g. categorical vegetation parent class at higher level analyzed further to generate child classes at sub level such as dense-forest, which has been utilized later for the estimation of continuous structural attribute parameters at operational level.

8.1.3. Integrated framework of change analysis

Considering the area heterogeneity, rapid changes and the variation in data source and season, post-classification were allocated for the change analysis rather than transformation spectral methods. Thus, detailed change “from-to” information classes as well as changes statistics were generated.

At fundamental level, smooth and accurate classified maps were very essential for any post-classification change detection technique, which were typically achieved by object-based approaches. Hence, previously advantages mentioned about OBIA are also pertinent and directly interlinked with the post-classification change analysis (e.g. effective extraction of respective classes, reducing salt and pepper effect, hierarchical structure providing different levels of details, etc.).

The most challenging tasks in change analysis techniques are how to reduce the influences of differences in acquisition system parameters (e.g. spatial resolution), and variations irrelevant to the target under investigation (e.g. atmospheric effect). These issues were significantly solved respectively by object-based post-classification change analysis as follow; firstly, the minimum mapping units were larger than the vertical variations between input layers, and secondly, the target features were extracted separately incorporating various datasets and knowledge eliminating to some extent the irrelevant variation effects.

While many change-detection techniques have been developed, a little has been done to assess the quality of these techniques. Hence, the change maps resulting from the change analyses were assessed (non-site specific methods), which reveals that, the accuracies of the change maps for the two time intervals were consistently high.

The fact achieved from the study is that the forest areas were drastically decreased, while there were still light at the end of the tunnel, where the capability of the area to recover was obviously shown in the case of abandoned agricultural fields.

The integrated analyses of the change maps and the socio-economical and socio-ecological data reveal that the crucial human intervention was found to be the main force for forest changes, quantitatively as well as qualitatively. More precisely, land clearance for mechanized farming and harvesting of woody products respectively are considered as direct causes of deforestation. Meanwhile, the improper policy and legislation of land management system was the major underlying cause of deforestation, since most of the stable areas on the change maps were observed where the land managed under clear property rights and ownership system, were fairly confirmed by the social survey of households.

Therefore, EO data aggregated to the community-level might provide comprehensive perspective for and insight into change dynamics and its driving forces as well as provide possible solutions to restore exposed areas.

8.1.4. Continuous forest structural attributes level

At the operational level at individual trees or aggregated tree patches, the study intends to predict continuous forest structural attributes of *Acacia nilotica* pure stand based on two selected

resolutions (i.e. 15 m Aster as well as 5 m RapidEye imagery), which reveals a potential solution to overcome the drawbacks of costly and time consuming at plot-level terrestrial forest inventory methods.

The study showed that there was fairly good correlation between forest structural attributes and most of the imagery metrics measured (i.e. OLV, GLCM, and DN).

In regard to these variables tested, the highest correlation was observed between the object layer value of red band and average stand height ($R^2 = 0.917$). Nevertheless, in sum the average stand volume gave more accurate and consistent results.

Fortunately, since the volume attribute achieved high and consistent results as well as it is the most important attribute for various applications, from the merchantable use of wood, to the global carbon sequestration, the study concluded that for *Acacia nilotica* forest structural attributes estimation, the inverse regression model, which was computed from RapidEye mean object layer value of NIR band, was found to be the best estimator of forest stand volume ($R^2 = 0.75$, RMSE = 1497).

The best fitted models for the two resolutions were reversed for cross-validation with independent set of randomly selected field points. The result confirmed that there were good agreements between those points and the estimated forest stand volume achieved from the overall best models ($R^2 = 0.80$ and 0.76 for the both resolutions of RapidEye and Aster data respectively).

Therefore, the study can confirmed that OBIA outperformed the Pixel-based approach at the operational level for both resolutions examined.

8.2.Recommendations

- Advanced technology combined with new imagery data should be integrated for future forest planning in the region as an effective and accurate tool that support planners and decision makers for sustainable development.

- OBIA could be used as an efficient solution to extract and update the required information in Blue Nile region of Sudan at various abstraction levels of details, utilizing optical multispectral imagery.
- The RB classifier requires considerable pre-knowledge for the area under investigation to achieve a satisfaction result. From this point of view and considering the slight difference between the results achieved in NN and RB methods, the multidimensional NN classifier with more careful selection of representative meaningful training objects is recommended rather than relatively time consuming RB classifier.
- Fusion of different combinations of imagery in addition to other forms of available datasets to facilitate each level with its required details, rather than feeding the analytical process with a uniform data source.
- It is advisable to develop region- (or domain-) specific multi-scale strategy and knowledge-based configuration of coarser level objects as spatially and thematically defined reference units for finer scale(s).
- The study observed that the process of various functions over vast areas lead to slow performance or even to completely get stuck of the computation process. Therefore, different levels of segmentation and classification which are generated at each scale in the class hierarchy must be considered to deal with tremendous information in multispectral imagery.
- The relationships between *Acacia nilotica* structural attributes, such as forest stand volume, and both the resolutions Aster and RapidEye imagery extracted metrics can be applied for the prediction of forest stand volume with high degree of precision.
- Since the finer spatial resolution RapidEye data outperformed the lower resolution Aster data whether at the categorical LU/LC level or operational level forest structural attribute, it would be recommended to use finer spatial resolution (i.e. RapidEye data), especially if the target feature is urbanization activities or fragmented forests and trees outside forest.
- Clear legislative framework for partnerships in forest management is required.

- Abandonment of agricultural fields for sufficient period is strongly recommended to achieve sustainability, whether sustainable production or maintenance of natural habitats.

8.3.Limitations

- The common criticism of OBIA is that the operator must be aware of the spectral and spatial properties of the area of interest in addition to the base information to define the rules.
- The study faces difficulties in scaling from field observations as point or single pixel coverage to meaningful real-world segments specifically with coarser resolution.
- The absence of historical data and information reduce the consistency of the analyses and assessment of the old satellite images compared to the recent one.
- The study points out that the developed models were fairly good. Our case study was performed only in one tested site (Alambwa forest) with single-phase sampling design considering the area as one stratum. This circumstance resulted in high variation result especially in forest stand density. Therefore, there is need to stratify the forest into different class categories with more numbers of training points (Kasischke *et al.*, 1997), and examine different sites for accurate estimation.
- Despite a good agreement achieved for forest structural attributes estimation of tree patches, the ground element dimensions of 15mx15m of Aster data was not sufficient for *Acacia nilotica* individual tree estimation that expanded over these dimensions, which may face difficulties especially in estimation for heterogeneous stand structure.

8.4.Future work










Despite a great potential of the adopted approach toward the automation of the interpretation process, this work is still a prototype and further investigations are needed: 1) to discover different sites in the region and its variations, 2) test different combinations of imagery in addition











to other forms of data sources (e.g. integrates very high resolution imagery with penetration capability through tree canopy as a substitution for costly and time consuming field survey methods to measure vertical in addition to horizontal forest attributes, which can be used to develop models for forest structural attributes over large areas), 3) rules need to be developed considering an effective knowledge and features variability within the region, and between the regions for transferability issue, 4) segmentation strategies need to be assessed for optimal segmentation scale and criteria for each respective level, 5) investigate other optimization techniques of features reduction for efficient extraction without significant information loss.











The preliminary attempt in this study was to perform the examination of spatial relations between the change dynamics and various associated factors that might cause deforestation. The achieved results eliminated from this study exhibit no or very weak relations in most cases, which is attributed to the limited site dimensions (El-Abbas *et al.*, 2013). Therefore, spatial analysis with full-scale research project and fairly large area coverage to discover most features in the region should be done for better understanding of the changing dynamics and its drivers, in addition to simulate the changes and provide suitability maps to manage the LU/LC effectively.












Last but not the least, further investigations to improve the use of OBIA with increasingly available high resolution satellite imagery data poses unique challenges that require advances of interpretation procedures have to be done.











REFERENCES














-  Abdallah, H., 1991. Energy potential from economically available crop residues in the Sudan. *Oxford*. 16 (8), 1153-1156.
-  Abdelgalil, E. A., 2005. Deforestation in the dry lands of Africa: Quantitative modelling approach. *Environment, Development and Sustainability* 6, 415-427.
-  Adler-Golden, S. M.; Matthew, M. W.; Bernstein, L. S.; Levine, R. Y., Berk, A.; Richtsmeier, S. C.; Acharya, P. K.; Anderson, G. P.; Felde, G.; Gardner, J.; Hoke, M.; Jeong, L. S.; Pukall, B.; Ratkowski, A. and Burke, H. H., 1999. Atmospheric correction for short-wave spectral imagery based on MODTRAN4. *SPIE proceedings on imaging spectrometry* 3753, 61–69.
-  Agrawal, A., 2007. Forests, Governance, and Sustainability: Common property theory and its contributions. *International Journal of the Commons* 1(1), 111-136.
-  Aguilar, M. A.; Vicente, R.; Aguilar, F. J.; Fernandez, A. and Saldana, M. M., 2012. Optimizing object-based classification in urban environments using very high resolution Geoeye-1 imagery. *ISPRS Annals of the Photogrammetry, Remote Sensing and Spatial Information Sciences* I (7).
-  Aitkenhead, M. J. and Dyer, R., 2007. Improving land-cover classification using recognition threshold neural networks. *Photogrammetric Engineering & Remote Sensing* 73(4), 413–421.
-  Ali, M. H.; Mohamed, A. O.; Ibrahim, S. M.; Elamin, F. M., 2008. Evaluation and adjustment of the 2008 census data. *CbS, Sudan*. <http://www.cbs.gov.sd/en/node/6>.
-  Anderson, J. R.; Hardy, E. E.; Roach, J. T. and Witmer, R. E., 1976. A land use and land cover classification system for use with remote sensor data (Geological Survey Professional Paper 964). Washington DC: USGS.
-  Aplin, P. and Smith, G. M., 2008. Advances in object-based image classification. *The International Archives of the Photogrammetry, Remote Sensing and Spatial Information Sciences* XXXVII (B7), Beijing.












-  Asefa, D. T.; Oba, G.; Welad B.; and Colman, E., 2003. An assessment of restoration biodiversity in degraded high mountain grazing lands in Northern Ethiopia. *Land Degradation Development*. 14, 25–38.
-  Baatz, M.; Heynen, M.; Hofmann, P.; Lingenfelder, I.; Mimier, M.; Schape, A.; Weber, M. and Willhauck, G., 2001. *eCognition User Guide 2.0 : Object oriented image analysis*. Definiens Imaging GmbH, Trappentreustrasse 1, 80339 München, Germany.
-  Baatz, M.; Benz, U.; Dehghani, S.; Heynen, M.; oltje, A. H.; Hofmann, P. and Lingenfelder, I., 2004. *eCognition professional user guide, version 4.0*. Definiens Imaging GmbH. Munchen, Germany: Definiens.
-  Baatz, M.; Hoffmann, C. and Willhauck, G., 2008. Progressing from object-based to object-oriented image analysis. In: Blaschke, T.; Hay, G. & Lang, S. (Eds.): *Object-Based Image Analysis - Spatial concepts for knowledge-driven remote sensing applications*. Lecture Notes in Geoinformation & Cartography (LNG&C), Springer, Berlin: ISBN 978-3-540-77057-2, 29-42.
-  Bassiri, A.; Alesheikh, A. A. and Malek, M. R., 2008. Spatio-temporal object modeling in fuzzy topological space. *The International Archives of the Photogrammetry, Remote Sensing and Spatial Information Sciences XXXVII (B2)*, Beijing.
-  Barnsley, M. J. and Barr, S. L., 1996. Inferring urban land use from satellite sensor images using kernel-based spatial reclassification. *Photogrammetric Engineering and Remote Sensing* 62, 949–958.
-  Barr, S. and Barnsley, M., 1997. A region-based, graph- theoretic data model for the inference of second-order thematic information from remotely-sensed images. *Int. J. Geographical Information Science* 11(6), 555–576.
-  Benz, U.C.; Hofmann, P.; Willhauck, G.; Lingenfelder, I.; and Heynen, M., 2004. Multiresolution, object-oriented fuzzy analysis of remote sensing data for GIS ready information. *ISPRS Journal of Photogrammetry & Remote Sensing*, 58, 239–258.
-  Blaschke, T., 2010. Object based image analysis for remote sensing. *ISPRS International Journal of Photogrammetry and Remote Sensing* 65(1), 2–16.
-  Blaschke, T.; Hay, G. J.; Weng, Q. and Resch, B., 2011(a). Collective sensing: Integrating geospatial technologies to understand urban systems—an overview. *Remote Sens.* 3, doi:10.3390/rs3081743, 1743–1776.











-  Blaschke, T.; Johansen, K. and Tiede, D., 2011(b). Object based image analysis for vegetation mapping and monitoring. In Qihao Weng (Ed.), *Advances in environmental remote sensing: Sensors, algorithms, and applications* United States: CRC Press, Taylor and Francis, 141–266.
-  Bock, M.; Xofis, P.; Mitchley, J.; Rossner, G. and Wissen, M., 2005. Object-oriented methods for habitat mapping at multiple scales - Case studies from Northern Germany and Wye Downs, UK. *Journal for Nature Conservation* 13, 75-89.
-  Bombelli, A.; Avitabile, V.; Belelli Marchesini, L., Balzter, H., Bernoux, M.; Hall, R.; Henry, M.; Law, B.E.; Manlay, R., Marklund, L.G. and Shimabukuro, Y.E., 2009. Assessment of the status of the development of the standards for the terrestrial essential climate variables: Biomass. Food and Agriculture Organization – Global Terrestrial Observation System, 18.
-  Boyd, D. S. and Danson, F. M., 2005. Satellite remote sensing of forest resources: three decades of research development progress. *Physical Geography* 29 (1), 1–26.
-  Brown, D.G. and Duh, J.-D., 2004. Spatial simulation for translating from land use to land cover. *Int. J. Geogr. Inf. Sci.*, 18, 35–60.
-  Bruce, C. M. and Hilbert, D. W., 2004. Pre-processing methodology for application to Landsat TM/ETM+ imagery of the wet tropics. Cooperative Research Centre for Tropical Rainforest Ecology and Management. Rainforest CRC, Cairns. 44.
-  Burnett, C. and Blaschke, T., 2003. A multi-scale segmentation/object relationship modeling methodology for landscape analysis. *Ecological Modelling* 168, 233–249.
-  Campbell, J.B., 2002. *Introduction to remote sensing*, Third edition, London, Taylor and Francis, 621.
-  Chen, G. and Hay, G. J., 2011. An airborne lidar sampling strategy to model forest canopy height from Quickbird imagery, lidar transects and GEOBIA. *Remote Sensing of Environment* 15 (6), 1532–1542.
-  Chen, G.; Hay, G. J.; Castilla, G.; St-Onge, B. and Powers, R., 2011. A multiscale geographic object-based image analysis to estimate lidar-measured forest canopy height using Quickbird imagery. *International Journal of Geographical Information Science* 25(6), 877–893.











-  Chen, G.; Hay, G. J. and St-Onge, B., 2012. A GEOBIA framework to estimate forest parameters from lidar transects, Quickbird imagery and machine learning: A case study in Quebec, Canada. *International Journal of Applied Earth Observation and Geoinformation* 15, 28–37.
-  Chen, X., 2002. Using remote sensing and GIS to analyse land cover change and its impact on regional sustainable development. *International Journal of Remote Sensing* 23(1), 107–124.
-  Choi, E. and Lee, C., 2003. Feature extraction based on the Bhattacharyya distance. *Pattern Recognition* 36 (8), 1703–1709.
-  Chubey, M. S.; Franklin, S. E. and Wulder, M. A., 2006. Object-based analysis of Ikonos-2 imagery for extraction of forest inventory parameters. *Photogrammetric Engineering and Remote Sensing* 72(4), 383–394.
-  Civanlar, R. and Trussel, H., 1986. Constructing membership functions using statistical data. *IEEE Fuzzy Sets and Systems* 18, 1 –14.
-  Cohen, W.B.; Spies, T.A. and Fiorella, M., 1995. Estimating the age and structure of forests in a multiownership landscape of western Oregon, USA. *International Journal of Remote Sensing* 16, 721–746.
-  Congalton, R. G. and Green, K., 2009. *Assessing the accuracy of remotely sensed data - principles and practices*. 2nd edition, CRC Press, Taylor & Francis Group, Boca Raton, Florida, 183.
-  Coppin, P. and Bauer, M., 1996. Digital change detection in temperate forests. *Remote Sensing Reviews* 13(3-4), 207–234.
-  Csaplovics, E., 1984. A Practical Application of Colour Infrared (IR) Image Interpretation - The Classification of the Reed of Lake Neusiedl (Austria). *ISPRS Archive XXV (A7)*, 143-152.
-  Csaplovics, E., 1992. *Methoden der regionalen Fernerkundung- Anwendungen im Sahel Afrikas*. Springer, Berlin Heidelberg New York, 219.
-  Curran, B. J., 1985. *Principles of remote sensing*. Longman, New York.

-  Danson, F. M., 1995, Developments in the remote sensing of forest canopy structure. In *Advances in Environmental Remote Sensing*, F. M. Danson and S. E. Plummer (Eds.), Chichester: John Wiley & Sons, 53-69.
-  Darwish, A.; Leukert, K. and Reinhardt W., 2003. Image segmentation for the purpose of object-based classification. *Geoscience and Remote Sensing Symposium, IGARSS 03. Proceedings 2003 IEEE International 3*, 2039-2041.
-  Dawelbait, N.; Yousif, S.; Branthomme, A.; Elmahi, A. G.; Lungo, A. D. and Abdelnour, H., 2006. Global forest resources assessment 2005: estimating forest cover and forest cover change in Sudan. FRA Working Paper 109/E. FAO, Rome.
-  Deafalla, T. H. H., 2012. Non wood forest products and poverty alleviation in semi arid region. ISBN: 978-3-659-16411-8, 59-66.
-  De Kok, R.; Schneider, T. and Ammer, U., 1999. Object based classification and applications in the Alpine forest environment. In *Fusion of sensor data, knowledge sources and algorithms*, Proceedings of the Joint ISPRS/EARSel Workshop, 3–4 June 1999, Valladolid, Spain. *International Archives of Photogrammetry and Remote Sensing 32 (7-4-3 W6)*.
-  Deppe, F., 1998. Forest area estimations using sample surveys and Landsat MSS and TM data. *Photogrammetric Engineering & Remote Sensing 64(4)*, 285–292.
-  Deshayes, M.; Guyon, D.; Jeanjean, H.; Stach, N.; Jolly, A. and Hagolle, O., 2006. The contribution of remote sensing to the assessment of drought effects in forest ecosystems. *Ann. For. Sci. 63*, 579–595.
-  Duggin, M. J., and Robinove, C. J., 1990. Assumptions implicit in remote sensing data acquisition and analysis. *International Journal of Remote Sensing 11*, 1669–1694.
-  El-Abbas, M. M., 2006. Forest cover change detection using remote sensing and ground survey in the Blue Nile Area- Sudan, Master Thesis submitted to the Graduate studies and Scientific Research Journal-University of Khartoum, 77.
-  El-Abbas, M. M. and Csaplovics, E., 2012. Spatiotemporal object-based image analyses in the Blue Nile region using optical multispectral imagery. *SPIE Proceedings 8538 (85380X)*, doi:10.1117/12.974546.











-  El-Abbas, M. M.; Csaplovics, E. and Deafalla, T. H. H., 2013. Remote sensing and spatial analysis based study for detecting deforestation and the associated drivers. SPIE Proceedings 8893 (88930O), doi: 10.1117/12.2029252, 8.
-  Elmoula, A., 1985. On the problem of resource management in the Sudan. Environmental monograph series no. 4. Institute of Environmental Studies, University of Khartoum, Sudan, 131.
-  Elsiddig, E. A., 2004. Community based natural resource management in Sudan, In: Awimbo, J.; Barrow, E. and Karaba, M. 2004. Community Based Natural Resource Management in the IGAD region. IGAD; IUCN.
-  El Tayeb, A. M.; Abdelkareem, O. E. A. and Gadow, K., 2006. Quantitative methods in forest management. Universitätsverlag Gottingen, ISBN-10: 3-938616-59-8, pp. 251.
-  Estes, J. E. and Mooneyhan, D. W., 1994. Of maps and myths. Photogrammetric Engineering and Remote Sensing 60, 517– 524.
-  FAO, 1995. Forest resources assessment 1990. Tropical developing countries. Technical Report (FO: GPC/INT/474/FRA- FO: GCP/INT/475/NET). Rome. 152.
-  FAO and FNC, 1998. National forest inventory for the Sudan. GCP/SUD/047/NET.
-  Flanders, D.; Mryka, H. and Joan, P., 2003. Preliminary evaluation of eCognition object based software for cut block delineation and feature extraction. Canadian Journal of Remote Sensing 20, 441-452.
-  FNC, 2007. A brief account on the forests of the Sudan. Retrieved July 15, 2010, from http://www.fnc.gov.sd/Preif_account.htm
-  Foody, G. M., 2002. Status of land cover classification accuracy assessment. Remote Sensing of Environment 80, 185-201.
-  FRA, 2010. Global forest resources assessment, Country Report, Sudan. FAO, Rome.
-  Franklin, S. E.; Hall, R. J.; Moskal, L. M. et al., 2000. Incorporating texture into classification of forest species composition from airborne multispectral images. International Journal of Remote Sensing 21(1), 61-79.
-  Franklin, S. E., 2001. Remote sensing for sustainable forest management. CRC press LLC. 448.











-  Franklin, S. E., 2002, Image processing technology in support of satellite remote sensing, *Technology Letters*, 5(2), 33-44.
-  Fraser, R. H.; Abuelgasim, T. A. and Latifovic, R., 2005. A method for detecting large-scale forest cover change using coarse spatial resolution imagery. *Remote Sensing of Environment* 95, 414-427.
-  Gamanya, R.; Maeyer, P. D. and Dapper, M. D., 2007. An automated satellite image classification design using object-oriented segmentation algorithms: A move towards standardization, *Expert Systems with Applications* 32, 616-624.
-  Gao, Y.; Kerle, N.; Mas, J. F.; Navarrete, A. and Niemeyer, I., 2007. Optimised image segmentation and its effect on classification accuracy, *Spatial Data Quality 2007*, Enschede, 4.
-  GAPE, 2009. Report of cereal crops. Ministry of agriculture, General Administration of Planning and Economy, Sudan.
-  Gebreslasie, M. T.; Ahmed, F. B. and Aardt, J., 2008. Estimating plot-level forest structural attributes using high spectral resolution ASTER satellite data in even-aged Eucalyptus plantations in southern KwaZulu-Natal, South Africa. *Southern Forests* 70, 129-14.
-  Gemmell, F.; Varjo, J. and Standstorm, M., 2001. Estimating forest cover in a boreal forest test site using thematic mapper data from two dates. *Remote Sensing of Environment* 77, 197-211.
-  Geneletti, D. and Gorte, B. G. H., 2003. A method for object-oriented land cover classification combining Landsat TM data and aerial photographs. *International Journal of Remote Sensing* 24 (6), 1273-1286.
-  Genuer, R.; Poggi, J. and Tuleau-malot, C, 2010. Variable selection using random forests. *Pattern Recognition Letters*, 31, 2225–2236.
-  Gibbes, C.; Adhikari, S.; Rostant, L.; Southworth, J. and Qiu, Y., 2010. Application of object based classification and high resolution satellite imagery for savanna ecosystem analysis. *Remote Sens.* 2, doi:10.3390/rs2122748, 2748-2772.
-  Gillman, C., 1949. A vegetation-type map of Tanganyika Territory. *Geogr. Rev.* 39, 7-37.










-  Gong, P., 1996. Integrated analysis of spatial data from multiple sources: Using evidential reasoning and artificial neural network techniques for geological mapping, *Photogrammetric Engineering & Remote Sensing* 62(5), 513-523.
-  Gurney, C. M., 1981. The use of contextual information to improve land cover classification of digital remotely sensed data. *International Journal of Remote Sensing* 2 (4), 379-388.
-  Hall, O.; and Hay, G. J., 2003. A multiscale object-specific approach to digital change detection, *International Journal of Applied Earth Observation and Geoinformation* 4 (4), 311-327.
-  Hammond, T. O. and Verbyla, D. L., 1996. Optimistic bias in classification accuracy assessment. *International Journal of Remote Sensing* 17(6), 1261-1266.
-  Haralick, R. M.; Shanmugam, K. And Dinstein, I., 1973. Textural features for image classification. *IEEE Transactions on Systems, Man and Cybernetics* SMC-3 (6), 610-621.
-  Harrison, M. N and Jackson, J. K., 1958. Ecological classification of the vegetation of the Sudan, *Forestry Department Bulletin No. 2*, Ministry of Agriculture, Republic of the Sudan, Khartoum.
-  Hay, G. J. and Marceau, D.J., 1999. Remote sensing contributions to the scale issue. *Canadian Journal of Remote Sensing* 25 (4), 357-366.
-  Hay, G. J.; Blaschke, T.; Marceau, D. J.; Bouchard, A., 2003. A comparison of three image object methods for multi-scale analysis of landscape structure. *Journal of Photogrammetry and Remote Sensing* 57, 327-345.
-  Hay, G. J. and Castilla G., 2006. Object-based image analysis: Strengths, weaknesses, opportunities and threats (SWOT), 1st International Conference on Object-based Image Analysis (OBIA 2006), Salzburg University, Austria.
-  Hay, G. J. and Castilla, G., 2008. Geographic object-based image analysis (GEOBIA). In: Blaschke, T.; Lang, S.; Hay, G. J. (Eds.), *Object-Based Image Analysis – Spatial Concepts for Knowledge-Driven Remote Sensing Applications*. Springer-Verlag, Berlin, 77-92.












-  Herold, M.; Liu, X. and Clarke, K. C., 2003. Spatial metrics and image texture for mapping urban land use. *Photogrammetric Engineering and Remote Sensing* 69(9), 991-1001.
-  Henry, M.; Picard, N.; Trotta, C.; Manlay, R. J.; Valentini, R.; Bernoux, M. and Saint-André, L., 2011. Estimating tree biomass of sub-Saharan African forests: a review of available allometric equations. *Silva Fennica* 45(3B), 477-569.
-  Heymann, Y.; Steenmans, C.; Croisille, G.; Bossard, M.; Lenco, M.; Wyatt, B. K.; Weber, J.; O'Brian, C.; Sifaki, N., and Cornaer, M., 1993. CORINE land cover: technical guide. Luxembourg: Commission of the European Communities, Office for Official Publications of Mapping Urban Heat Islands.
-  Hofmann, P., 2001. Detecting urban features from ikonos data using an object-oriented approach, in *Proceedings of RSPS2001*, 79-91.
-  Holmstrom, H., 2002. Estimation of single-tree characteristics using the kNN method and plotwise aerial photograph interpretations. *Forest Ecol. Manage.* 167, 303-314.
-  Hudak, A. T.; Lefsky, M. A.; Cohen, W. B. and Berterretche, M., 2002. Integration of Lidar and Landsat ETM+ data for estimating and mapping forest and canopy height. *Remote Sensing of Environment* 82, 397-416.
-  Huth, J.; Kuenzer, C.; Wehrmann, T.; Gebhardt, S.; Tuan, V. and Dech, S., 2012. Land cover and land use classification with TWOPAC: towards automated processing for pixel- and object-based image classification. *Remote Sens.* 4, doi:10.3390/rs4092530, 2530-2553.
-  Hyypä, J.; Hyypä, H.; Inkinen, M. And Engdahl, M., 1998. Verification of the potential of various remote sensing devices for forest inventory. *Proceedings of IEEE geosciences and remote sensing society*, Pasadena, CA: California Institute of Electrical and Electronics Engineers, 1812-1814.
-  Im, J. and Jensen, J., 2005. A change detection model based on neighborhood correlation image analysis and decision tree classification. *Remote Sensing of Environment* 99(3), 326-340.
-  Ivits, E. and Koch, B., 2002. Object-oriented remote sensing tools for biodiversity assessment: A European approach. *Proceedings of the 22nd EARSeL symposium*,










Prague, Czech Republic, 4–6 June 2002. Rotterdam, Netherlands: Millpress Science Publishers.












-  Jakubauskas, M. E., Lulla, K. P. and Mausel, P. W., 1990. Assessment of vegetation change in a fire-altered forest landscape. *Photogramm. Eng. Rem. Sensing* 56, 371-377.
-  Jensen, J. R., 2000. *Remote sensing of the environment: an earth resource perspective*; Pearson Prentice Hall: Upper Saddle River, NJ, USA.
-  Jensen, J. R., 2005. *Introductory digital image processing, a remote sensing perspective*, 3rd. edition, Upper Saddle River: Pearson Prentice Hall, 526.
-  Jie S. and Ejaz H., 2010. Very High Resolution Remote Sensing Data: Processing Capabilities and Limitations in Urban Areas. *IEEE Geoscience and Remote Sensing Symposium*, Honolulu, Hawaii, USA, July 25-30.
-  Johansen, K.; Coops, N. C.; Gergel, S. E. and Stange, Y., 2007. Application of high spatial resolution satellite imagery for riparian and forest ecosystem classification, *Remote Sensing of Environment* 110, 29–44.
-  Johansen, K.; Phinn, S.; Witte, C.; Philip, S. and Newton, L., 2009. Mapping banana plantations from object-oriented classification of SPOT-5 imagery. *Photogrammetric Engineering and Remote Sensing* 75(9), 1069-1081.
-  Johnson, R. D. and Kasischke, E., 1998. Change vector analysis: a technique for multispectral monitoring of land cover and condition. *International Journal of Remote Sensing* 19, 411-426.
-  Kajisa, T.; Murakami, T.; Mizoue, N.; Top, N. and Yoshida, S., 2009. Object-based forest biomass estimation using Landsat ETM+ in Kampong Thom Province, Cambodia, the Japanese Forest Society and Springer 14, 203-211.
-  Kasischke, Eric S.; Melack, J. M. and Dobson, M. C., 1997. The use of imaging radars for applications a review ecological. *Remote Sensing of Environment* 59, 141-156.
-  Khorram, S.; Gregory S. Biging; Nicholas R.; Chrisman, R.; Colby, G.; Congalton, E.; Dobson, L.; Fer-guson, F.; Goodchild, R.; and Thomas H. M., 1994. Accuracy assessment of land cover change detection. *Computer Graphic Center Report No. 101*, Computer Graphic Cen-ter, North Carolina State University, Raleigh, North Carolina, 70.











-  Kim, M.; Madden, M. and Warner, T. A., 2009. Forest type mapping using object-specific texture measures from multispectral Ikonos imagery: segmentation quality and image classification issues. *Photogrammetric Engineering & Remote Sensing* 75 (7), 819-829.
-  Kim, S.; Lee, W.; Kwak, D.; Biging, G. S.; Gong, P.; Lee, J. and Cho, H., 2011. Forest cover classification by optimal segmentation of high resolution satellite imagery. *Sensors* 2011 (11), doi:10.3390/s110201943, 1943-1958.
-  Koukoulas, S. and Blackburn, G. A., 2001. Introducing new indices for accuracy evaluation of classified images representing semi-natural woodland environments. *Photogrammetric Engineering and Remote Sensing* 67, 499-510.
-  Kumar, N., 2007. *Multispectral image analysis using object oriented paradigm*. Taylor & Francis Group, New York.
-  Köhl, M.; Magnussen, S. M. and Marchetti, M., 2006. *Sampling methods, remote sensing and GIS multiresources forest inventory*. Springer-Verlag Berlin Heidelberg, Germany.
-  Laliberte, A. S.; Rango, A.; Havstad, K. M.; Paris, J. F.; Beck, R. F.; McNeely, R. and Gonzalez, A. L., 2004. Object-oriented image analysis for mapping shrub encroachment from 1937–2003 in southern New Mexico, *Remote Sensing of Environment* 93, 198-210.
-  Laliberte, A.S.; Rango, A.; Herrick, J. E.; Fredrickson, E.L. and Burkett, L., 2007 (a). An object-based image analysis approach for determining fractional cover of senescent and green vegetation with digital plot photography. *Journal of Arid Environments* 69, 1-14.
-  Laliberte, A. S.; Fredrickson, E. L. and Rango, A., 2007 (b). Combining decision trees with hierarchical object-oriented image analysis for mapping arid rangelands. *Photogrammetric Engineering and Remote Sensing* 73(2), 97-207.
-  Lambin, E. and Ehrlich, D., 1997. Land-cover changes in sub-Saharan Africa (1982-1991): application of a change index based on remotely sensed surface temperature and vegetation indices at a continental scale. *Remote Sensing of Environment* 61(2), 181-200.
-  Lambin, E. F.; Geist, H. and Lepers, E., 2003. Dynamics of land use and cover change in tropical regions. *Annual Review of Environment and Resources* 28, 205-241.











-  Lang, S., 2008. Object-based image analysis for remote sensing applications: modeling reality – dealing with complexity. In: Blaschke, T.; Hay, G. & Lang, S. (Eds.): Object-based image analysis - spatial concepts for knowledge-driven remote sensing applications. Lecture Notes in Geoinformation & Cartography (LNG&C), Springer, Berlin: ISBN: 978-3-540-77057-2, 3-28.
-  Leckie, D. G.; Gougeon, F.A.; Walsworth, N. and Paradine, D., 2003. Stand delineation and composition estimation using semi-automated individual tree crown analysis. *Remote Sensing of Environment* 85, 355-369
-  Lennartz, S. P. and Congalton, R. G., 2004. Classifying and mapping forest cover types using IKONOS imagery in the northeastern United States, *Proceedings of the ASPRS*, Denver, Colorado.
-  Lepers, E.; Lambin, E. F.; Janitos, A. C.; Defries, R.; Achard, F.; Ramankutty, N. and Scholes, R. J., 2005. A synthesis of information on rapid land-cover change for the period 1981-2000. *BioScience* 55 (2), 115-124.
-  Levick, S. R. and Rogers, K. H., 2008. Structural biodiversity monitoring in savanna ecosystems: integrating LiDAR and high resolution imagery through object-based image analysis. In: Blaschke, T.; Hay, G. & Lang, S. (Eds.): Object-Based Image Analysis - Spatial concepts for knowledge-driven remote sensing applications. Lecture Notes in Geoinformation & Cartography (LNG&C), Springer, Berlin: ISBN: 978-3-540-77057-2, 477-491.
-  Levin, N.; Shmida, A.; Levanoni, O.; Tamari, H. and Kark, S., 2007, Predicting mountain plant richness and rarity from space using satellite-derived vegetation indices, *Divers. Distrib.* 13, 692-703.
-  Lillesand, T. M., Kiefer, R. W. and Chipman, J. W., 2008. Remote sensing and image interpretation, 6th edition, John Wiley & Sons, Inc, New York.
-  Lu, D.; Mausel, P.; Brondizio, E. and Moran. E., 2004. Change detection techniques. *International Journal of Remote Sensing* 25(12), 2365-2407.
-  Lunetta, R. S.; and Elvidge, C., 1999. Remote sensing change detection. *Environmental monitoring methods and applications*. Taylor, Francis, London.











-  Macleod, D.; Congalton, G., 1998. A quantitative comparison of change-detection algorithms for monitoring eelgrass from remotely sensed data. *Photogrammetric Engineering and Remote Sensing* 64, 207-216.
-  Marpu, P. R., Niemeyer, I., Nussbaum, S., Gloaguen, R., 2008. A procedure for automatic object-based classification. In: Blaschke, T.; Hay, G. & Lang, S. (Eds.): *Object-Based Image Analysis - Spatial concepts for knowledge-driven remote sensing applications. Lecture Notes in Geoinformation & Cartography (LNG&C)*, Springer, Berlin: ISBN: 978-3-540-77057-2, 169-184.
-  Martin, D.; Fowlkes, C.; Tal, D. and Malik, J., 2001. A database of human segmented natural images and its application to evaluating segmentation algorithms and measuring ecological statistics. In *Proc. 8th Int'l Conf. Computer Vision* 2, 416-423.
-  Mas, J. F., 1999. Monitoring land-cover changes: A comparison of change detection techniques. *International Journal of Remote Sensing* 20 (1), 139-152.
-  Mather, P. M., 2006. *Computer processing of remotely sensed images*, St Edmundsbury Press Ltd., Bury St Edmunds, Suffolk, Wiley and Sons, 3rd ed., reprint. ISBN: 0-471-90648-4.
-  Mathieu, R.; Aryal, J. and Chong, A. K., 2007. Object based classification of IKONOS imagery for mapping large scale vegetation communities in urban areas, *Sensors* 7, 2860-2880.
-  Miller, M., 1999. Effect of deforestation on seed bank in a tropical deciduous forest of western Mexico. *Tropical Ecology*, 15 (2), 179-188.
-  Morgan, W.B. and Moss, P. A., 1985. Biomass energy and urbanisation: commercial factors in the production and use of biomass fuels in tropical Africa. *Biomass* 6, 285-299.
-  Moskal, L.M. and Franklin, S.E., 2002. Multistory forest stand discrimination with multiscale texture from high spatial detail airborne imagery, *Geocarto International* 17(4), 53-66.
-  Mueller, M.; Segl, K. and Kaufmann, H., 2004. Edge- and region-based segmentation technique for the extraction of large, man-made objects in high-resolution satellite imagery, *Pattern Recognition* 37, 1619-1628.
-  McCoy, R. M., 2005. *Field methods in remote sensing*. New York: Guilford Press.












-  Myers, N., 1994. Tropical deforestation: rates and patterns, in K. Brown and D. W. peace (Eds.). *The causes of tropical deforestation*, University College London Press, London, 27–40.
-  Myneni, R. B.; Hall, F. G.; Sellers, P. J. et al., 1995. The interpretation of spectral vegetation Indexes. *IEEE Transactions on Geoscience and Remote Sensing* 33(2), 481-486.
-  Navulur K., 2007. *Multispectral Image Analysis Using the Object-Oriented Paradigm*, CRC Press Taylor & Francis Group.
-  Niemeyer, I. and Canty, M. J., 2003. Pixel-based and object-oriented change detection analysis using high-resolution imagery. In *Proceedings of the 25th Symposium on Safeguards and Nuclear Material Management*, 13–15 May 2003, Stockholm, Sweden, 6.
-  Niemeyer, I., Marpu, P. R., and Nussbaum, S., 2008. Change detection using object features. In: Blaschke, T., Lang, S., Hay, G.J. (Eds.), *Object-Based Image Analysis – Spatial Concepts for Knowledge-Driven Remote Sensing Applications*. Springer-Verlag, Berlin, 185-201.
-  Nussbaum, S.; Niemeyer, I. and Canty, M. J., 2006. SEATH - A new tool for automated feature extraction in the context of object-based image analysis. *The International Archives of the Photogrammetry, Remote Sensing and Spatial Information Sciences*, Salzburg, Austria, XXXVI-4 (C42), 6.
-  Opitz, D. and Blundell, S., 2008. Object recognition and image segmentation: the Feature Analyst approach. In: Blaschke, T.; Hay, G. & Lang, S. (Eds.): *Object-Based Image Analysis - Spatial concepts for knowledge-driven remote sensing applications*. Lecture Notes in Geoinformation & Cartography (LNG&C), Springer, Berlin: ISBN: 978-3-540-77057-2, 153-167.
-  Ozdemir, I.; Norton, D. A.; Ozkan, U. Y.; Mert, A. and Senturk, O., 2008. Estimation of tree size diversity using object oriented texture analysis and Aster imagery. *Sensors*, 8, DOI: 10.3390/s8084709, 4709-4724.
-  Pascual, C.; Garcia-Abril, A.; Garca-Montero, L. G.; Martin-Fernandez, S. and Cohen, W. B., 2008. Object-based semi-automatic approach for forest structure characterization using lidar data in heterogeneous *Pinus sylvestris* stands. *Forest Ecology and Management* 255, 3677-3685.






-  Pavlidis, T. and Liow, Y., 1990. Integrating region growing and edge detection. *IEEE Trans. Pattern Anal. & Mach. Intell.* 12 (3), 225-233.
-  Perkins, W. A., 1980. Area segmentation of images using edge points. *IEEE Trans. Pattern Anal. & Mach. Intell. PAMI* (2), 8-15.
-  Pitt, D. G.; Wagner, R. G.; Hall, R.J.; King, D. J.; Leckie, D. G. and Runesson, U., 1997. Use of remote sensing for forest vegetation management: A problem analysis, *The Forestry Chronicle* 73(4), 459-477.
-  Platt, R. V. and Rapoza, L., 2008. An evaluation of an object-oriented paradigm for land use/land cover classification, *Professional Geographer* 60, 87-100.
-  Pontius J.; Huffaker, D.; and Denman, K., 2004. Useful techniques of validation for spatially explicit land-change models. *Ecological Modelling* 179(4), 445-461.
-  Pratt, N.D. et al., 1997. Estimating Areas of Land under Small-Scale Irrigation Using Satellite Imagery and Ground Data for a Study Area in N.E. Nigeria. *The Geographical Journal* 163(1), 65-77.
-  Pühr, C. B. and Donoghue, D. N. M., 2000. Remote sensing of upland conifer plantations using Landsat TM data: a case study from Galloway, south-west Scotland. *International Journal of Remote Sensing* 21, 633-646.
-  Rahman, M. M.; Csaplovics, E. and Koch, B., 2005. An efficient regression strategy for extracting forest biomass information from satellite sensor data. *International Journal of Remote Sensing* 26, 1511-1519.
-  Reineke, L. H., 1933. Perfecting a stand-density index for even-aged forests. *J. Agr. Res.* 46, 627-638.
-  Riedel, T.; Thiel, C. and Schmullius, C., 2008. Fusion of multispectral optical and SAR images towards operational land cover mapping in Central Europe. In: Blaschke, T.; Hay, G. & Lang, S. (Eds.): *Object-Based Image Analysis - Spatial concepts for knowledge-driven remote sensing applications. Lecture Notes in Geoinformation & Cartography (LNG&C)*, Springer, Berlin: ISBN 978-3-540-77057-2, 493-511.
-  Riggan, N. D. and Weih, R. C., 2009. A Comparison of pixel-based versus object-based land use/land cover classification methodologies. *Journal of the Arkansas Academy of Science* 63.

-  Rogan, J. and Chen, D. M., 2004. Remote sensing technology for mapping and monitoring land-cover and land-use change. *Progress in Planning* 61(4), 301-325.
-  Ruiz, L. A.; Recio, J. A. Fernandez-Sarria, A. and Hermosilla, T., 2010. A tool for object descriptive feature extraction: application to image classification and map updating. *The International Archives of the Photogrammetry, Remote Sensing and Spatial Information Sciences XXXVIII-4 (C7)*.
-  Salvador, R. and Pons, X., 1998. On reliability of Landsat TM for estimating forest variables by regression techniques: a methodological analysis. *IEEE Trans Geosci Remote Sens* 36, 1888-1897.
-  San miguel-ayanz, J. and Biging, G. S., 1996, An iterative classification approach for mapping natural resources from satellite imagery. *International Journal of Remote Sensing* 17 (5), 957-981.
-  Scarth, P.; Phinn, S. R. and McAlpine, C., 2001. Integrating high and moderate spatial resolution image data to estimate forest age structure. *Canadian Journal of Remote Sensing* 27, 129-142.
-  Schmidt, A., Karrasch, P. and Neubert, M., 2009. Vergleichende untersuhungen der atmosphärenkorrekturprogramme ATCOR und FLAASH auf der datengrundlage des satellitensystems IKONOS. Rhombos-verlag, Berlin.
-  Segl, K. ; Roessner, S. ; Heiden, U. and Kaufmann, H., 2003. Fusion of spectral and shape features for identification of urban surface cover types using reflective and thermal hyperspectral data *ISPRS Journal of Photogrammetry & Remote Sensing* 58, 99-112.
-  Short, Nicholas M., 2009. Remote sensing tutorial. Technical report. URL: <http://rst.gsfc.nasa.gov/>.
-  Singh, A., 1989. Digital change detection techniques using remotely-sensed data. *International Journal of Remote Sensing* 10, 989-1003.
-  Skirvin, S. M.; Kepner, W. G.; Marsh, S. E.; Drake, S. E.; Maingi, J. K.; Edmonds, C.M.; Watts, C.J. and Williams, D. R., 2004. Assessing the accuracy of satellite-derived land-cover classification using historical aerial photography, digital orthophoto quadrangles, and airborne video data. In: Ross S. Lunetta and John G. Lyon (Eds.), *Remote Sensing and GIS Accuracy Assessment* , CRC Press, Taylor & Francis Group, Boca Raton, Florida, 115-131.

-  Smith, J., 1949. Distribution of tree species in the Sudan in relation to rainfall and soil texture. Bulletin No. 4. Sudan Ministry of Agriculture, Khartoum.
-  Srinivasan, A. and Richards, J.A., 1990. Knowledge-based techniques for multisource classification, *International Journal of Remote Sensing* 11(3), 505-525.
-  Stenberg, P.; Möttus, M. and Rautiainen, M., 2008. Modeling the spectral signature of forests: application of remote sensing models to coniferous canopies. In: Liang, S. (Eds.). *Advances in land remote sensing: system, modeling, inversion and application*. Springer-Verlag, 147-171.
-  Stewart, J. S. and Lillesand T.M., 1994. Stratification of Landsat Thematic Mapper data, based on regional landscape patterns, to improve land-cover classification accuracy of large study areas.
-  Stojanova, D.; Panov, P.; Gjorgjioski, V.; Kobler, A. and Dzeroski, S., 2010. Estimating vegetation height and canopy cover from remotely sensed data with machine learning. *Ecological Informatics* 5 (4), 256-266.
-  Stow, D. A., 1999. Reducing mis-registration effects for pixel-level analysis of land-cover change. *International Journal of Remote Sensing* 20, 2477-2483.
-  Tarantino, E. and Figorito, B., 2012. Mapping rural areas with widespread plastic covered vineyards using true color aerial data. *Remote Sens.* 4 (1913-1928), doi:10.3390/rs4071913.
-  Thomas, N.; Hendrix, C. and Congalton, R.G., 2003. A comparison of urban mapping methods using high-resolution digital imagery, *Photogrammetric Engineering & Remote Sensing* 69(9), 963-972.
-  Tiede, D.; Lang, S. and Hoffmann, C., 2006. Supervised and forest type-specific multiscale segmentation for a one-level-representation of single trees. In: S. Lang, T. Blaschke and E. Schöpfer (eds.): *International Archives of Photogrammetry, Remote Sensing and Spatial Information Sciences XXXVI-4(C42)*.
-  Tiede, D.; Lang, S. and Hoffmann, C., 2008. Domain-specific class modelling for one-level representation of single trees. In: Blaschke, T.; Hay, G. & Lang, S. (Eds.): *Object-Based Image Analysis - Spatial concepts for knowledge-driven remote sensing applications*. *Lecture Notes in Geoinformation & Cartography (LNG&C)*, Springer, Berlin: ISBN 978-3-540-77057-2, 133-151.

-  Tokola, T.; PitkaEnen, J.; Partinen, S. and Muinonen, E., 1996. Point accuracy of a non-parametric method in estimation of forest characteristics with different satellite materials. *International Journal of Remote Sensing* 17, 2333-2351.
-  Townshend, J. R. G.; Justice, C. O.; Gurney, C. and McManus, J., 1992. The effect of image misregistration on the detection of vegetation change. *IEEE Transactions on Geoscience and Remote Sensing* 30, 1054-1060.
-  Tuceryan M. and Jain A.K., 1998. Texture analysis, *The Handbook of Pattern Recognition and Computer Vision* (2nd Edition), C. H. Chen, L. F. Pau, P. S. P. Wang (eds.), World Scientific Publishing Co. 207-248.
-  Tuominen, S., and Pekkarinen, A., 2004. Performance of different spectral and textural aerial photograph features in multi-source forest inventory. *Remote Sensing of Environment* 94, 256-268.
-  Tzotsos, A.; Iosifidis, C. and Argialas, D., 2008. A hybrid texture-based and region-based multiscale image segmentation algorithm. In: Blaschke, T.; Hay, G. & Lang, S. (Eds.): *Object-Based Image Analysis - Spatial concepts for knowledge-driven remote sensing applications. Lecture Notes in Geoinformation & Cartography (LNG&C)*, Springer, Berlin: ISBN 978-3-540-77057-2, 221-236.
-  UNCD, 1992. *Agenda 21, Annex III*. UN, New York.
-  Walker, J. S. and Blaschke, T., 2008. Object-based land cover classification for the Phoenix metropolitan area: optimization vs. transportability. *Int. J. Remote Sens.* 29, 2021-2040.
-  Warner, Timothy A., M. Duane Nellis, and Giles M. Foody (Eds.), 2009. *The sage handbook of remote sensing*. London: SAGE Publications Ltd. doi: <http://dx.doi.org/10.4135/9780857021052>.
-  Weishampel, J. F.; Blair, J. B.; Knox, R. G.; Dubayah, R. and Clark, D. B., 2000. Volumetric Lidar return patterns from an old-growth tropical rainforest canopy. *International Journal of Remote Sensing* 21(2), 409-415.
-  Weismiller, R., S. Kristof, et al., 1977. Evaluation of change detection techniques for monitoring coastal zone environments. *Proceedings of the Eleventh International Symposium on Remote Sensing of Environment ERIM*, Ann Arbor, MI.

-  Weska, J. S., 1978. A survey of threshold selection techniques. *Comput. Graph., Image Processing* 7, 259-265.
-  Wharton, S. W., 1982. A contextual classification method for recognizing land use patterns in high resolution remotely-sensed data, *Pattern Recognition* 15, 317-324.
-  Whiteside, T. G.; Boggs, G. S. and Maier, S. W., 2011. Comparing object-based and pixel-based classifications for mapping savannas. *International Journal of Applied Earth Observation and Geoinformation* 13, 884-893.
-  Willhauck, G., 2000. Comparison of object oriented classification techniques and standard image analysis for the use of change detection between SPOT multispectral satellite images and aerial photos. *ISPRS XXXIII*, Amsterdam.
-  Williams, M., 2006. *Deforesting the earth: from prehistory to global crisis, an abridgment*. Chicago: University of Chicago Press, 543.
-  Wolter, P. T.; Townsend, P. A. and Sturtevant, B. R. 2009. Estimation of forest structural parameters using 5 and 10 meter SPOT-5 satellite data. *Remote Sensing of Environment* 113, 2019-2036.
-  Woodcock, C. E. and Strahler, A. H., 1987. The factor of scale in remote sensing. *Remote Sensing of Environment* 21 (3), 311-332.
-  Wulder, M. A. and Seemann, D., 2003. Forest inventory height update through the integration of LIDAR data with segmented Landsat imagery. *Canadian Journal of Remote Sensing* 29 (5), 536-543.
-  Xu, C. and Yaping, Z., 2010. Land use change of China based on NDVI and landscape ecology, *Geoscience and Remote Sensing (IITA-GRS), 2010 Second IITA International Conference* 2, 540-543.
-  Yang, X. (Eds.), 2011. *Urban remote sensing: monitoring, synthesis and modeling in the urban environment*. Wiley-Blackwell, 408.
-  Yu, Q.; Gong, P.; Clinton, N.; Biging, G.; Kelly, M. and Schi-rokauer, D., 2006. Object-based detailed vegetation classification with airborne high spatial resolution remote sensing imagery. *Photogrammetric Engineering and Remote Sensing* 72(7), 799-811.

-  Zhan, Q.; Molenaar, M. and Tempfli, K., 2002. Finding spatial units for land use classification based on hierarchical image object. The international Achieves of photogrammetry and remote sensing 34 (4).
-  Zhang, C.; Franklin, S. E. and Wulder, M. A., 2004. Geostatistical and texture analysis of airborne-acquired images used in forest classification. International Journal of Remote Sensing 25(4), 859-865.
-  Zhang, G.; Wu, Z. and Yi, I., 2008. Organization and representation of objects in multi-source remote sensing image classification. The International Archives of the Photogrammetry, Remote Sensing and Spatial Information Sciences XXXVII (B7), Beijing.
-  Zhou, W.; Troy, A. and Grove, M., 2008. Object-based land cover classification and change analysis in the Baltimore metropolitan area using multitemporal high resolution remote sensing data, Sensors, 1613-1636.
-  Zucker, S., 1976. Region growing: Childhood and adolescence. Comput. Craph. Image Processing 5, 382-399.

APPENDIXES

Appendix 1: Field survey data sheet (LU/LC level)

Region..... Site/Photo
Reference.....Date.....
Sample NoCoordinate:
Lat.....Lon.....

Observer.....

LU/LC Type

TOPOGRAPHIC INFORMATION

Slope angle Slope

Aspect.....

SOILS INFORMATION

Texture: Sandy.....Silt..... Clay..... Loam.....

Color :

VEGETATION INFORMATION

Vegetative:

Grass% Shrub%

Trees% Mixed Trees%

Mixed Grass/Trees%

Regeneration:

Type:

Density:

Appendix 2: Field survey data sheet (forest structural attributes level)

Region..... Site/Photo
 Reference..... Date.....
 Sample No..... Coordinate:
 Lat..... Lon.....

Observer.....

STAND DESCRIPTION:

Species	DBH	Crown Width	Height	Phonological Status

SOIL:
 Texture Color

COMMENTS:

Appendix 3: Questionnaire of the local community perceptions for the change dynamics, its drivers and restoration solutions

I. General

- Questionnaire No.:

- Date:/...../ 2010

- Site of interview:

- Enumerator:

.....

II. Personal Information

1. Name:

2. Age: yrs

3. Education: a. Illiterate () b. *Khalwa* () c. Primary () d. Intermediate ()

e. Secondary () f. Graduate ()

4. Occupation:

III. Deforestation and land degradation

5. Do you get benefit (s) from forest?

a. Yes () b. No ()

6. If yes, what is (are) the benefit (s) achieved?

a. Woody products () b. Non-woody products () c. Associated with forest ()

d. Climate control () e. Recreation () f. Other ()

7. What is (are) the benefit(s) previously available but is (are) no longer exist?

a. Woody products () b. Non-woody products () c. Associated with forest ()

d. Climate control () e. Recreation () f. Other ()

8. Do you observed any changes in the species composition?

a. Yes () b. No ()

9. If yes, please specify? (Order from the mostly abundant)

- Currently: a. (.....) b. (.....) c. (.....) d. (.....) e. (.....) f. (.....)
- Previously: a. (.....) b. (.....) c. (.....) d. (.....) e. (.....) f. (.....)

10. What is (are) in your opinion the factor(s) caused deforestation on the specified areas shown in the attached map?

- a. Agricultural expansion () b. Harvesting of woody products () c. Manmade fire ()
 d. Natural phenomena () e. Other ()

IV. Restoration

11. What is (are) in your opinion the factor(s) caused reforestation on the specified areas shown in the attached map?

- a. Abandonment of agricultural fields () b. Reforestation programs () c. Awareness ()
 d. Other ()

12. If the cause of reforestation was the abandonment of agricultural fields; what is (are) in your opinion the factor(s) leads to abandonment?

- a. Decreased productivity () b. Insufficient rainfall () c. Financial shortage () d. Other ()

13. If the cause of abandonment was the decreased of productivity; what is (are) in your opinion the factor(s) leads to this decrease?

- a. Intensification and monocropping () b. Weeds infestation () c. Pests () d. Other ()

14. What is (are) in your opinion the mission(s) to be done to maintain and restore the forests?

- a. Afforestation and reforestation () b. Awareness programs () c. Job opportunities ()
 d. land management () e. Other ()

15. What is in your opinion the best land management system?

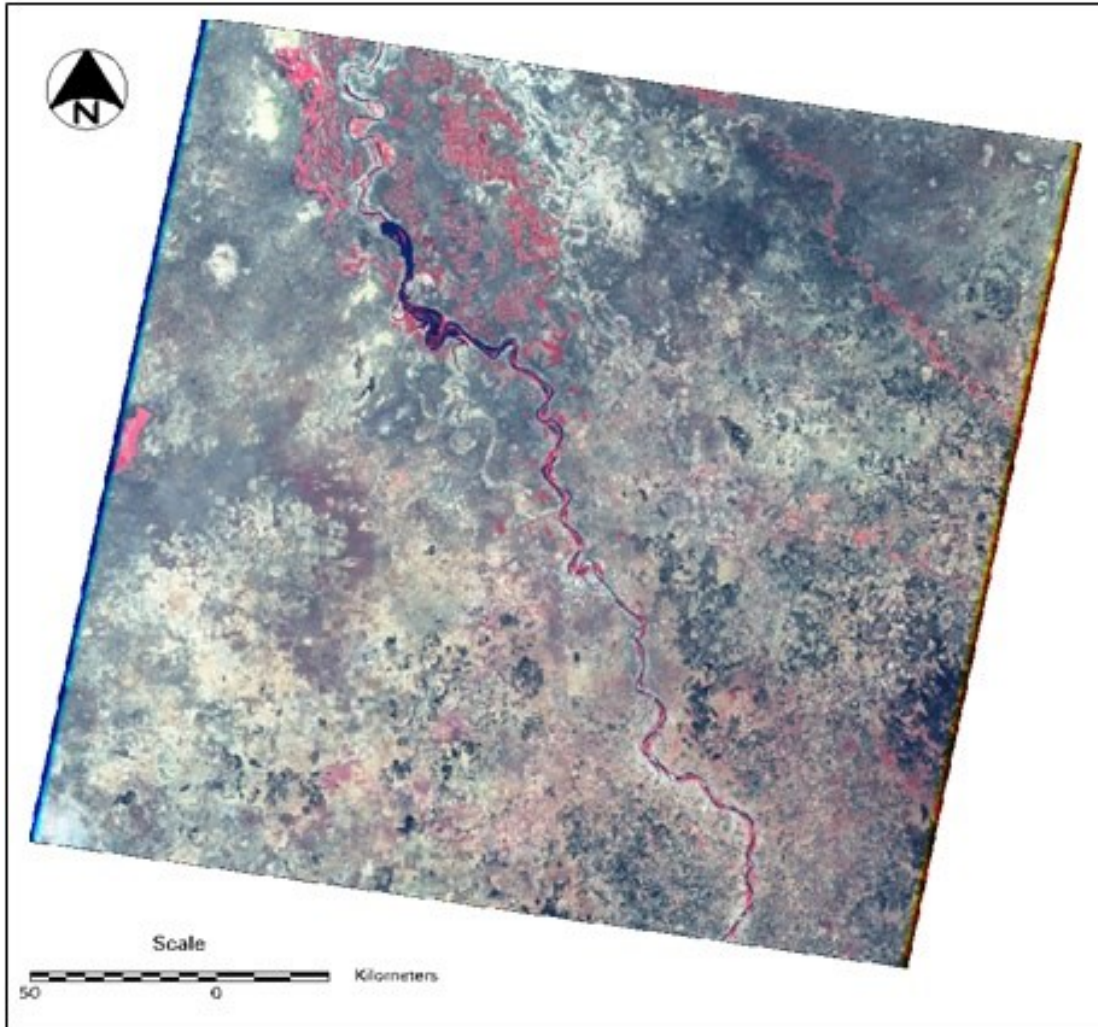
- a. Governmental () b. Community () c. participatory approach () d. private ()

16. What are in your opinion the advantages of you choice?

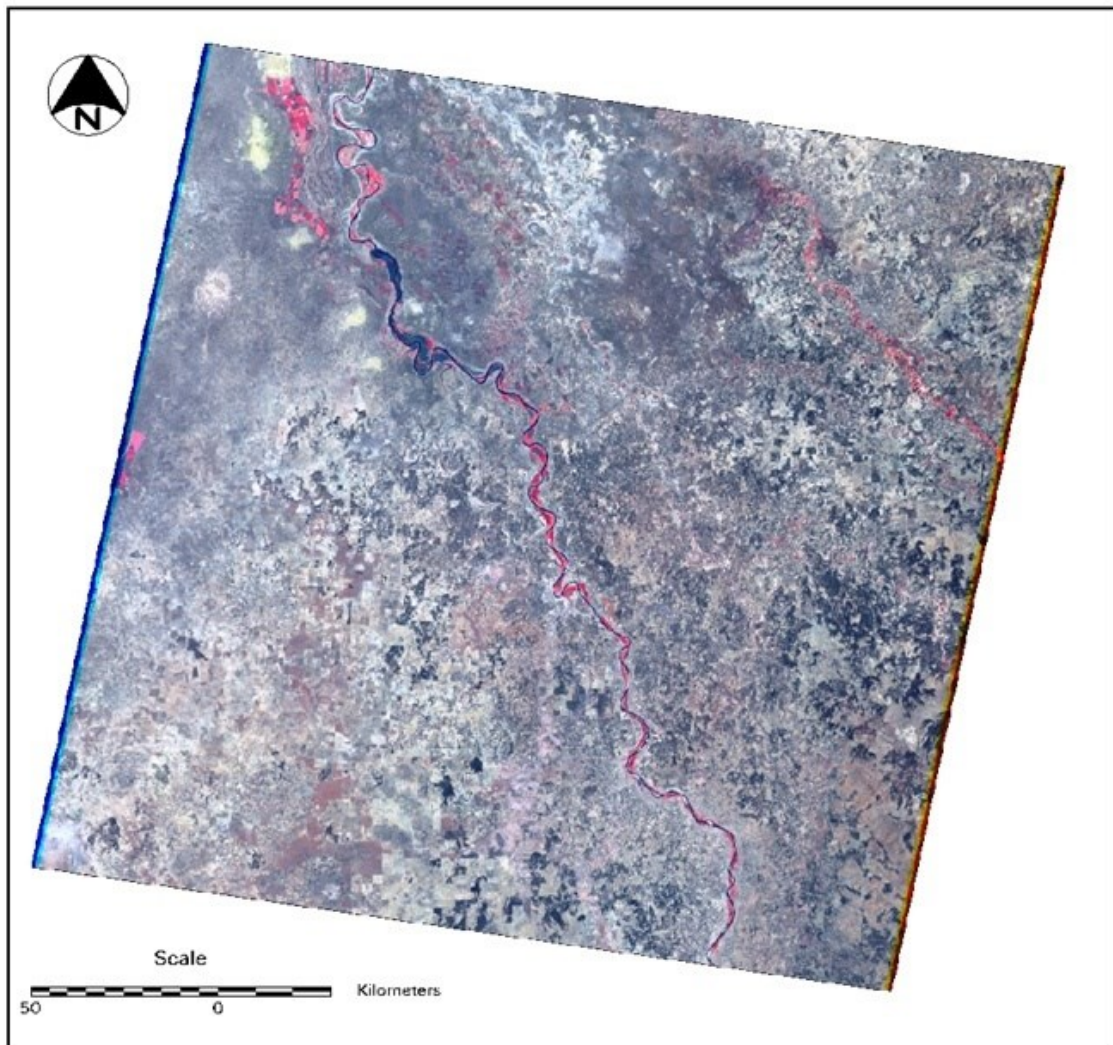
- a. (.....) b. (.....) c. (.....) d.
(.....)

Thanks

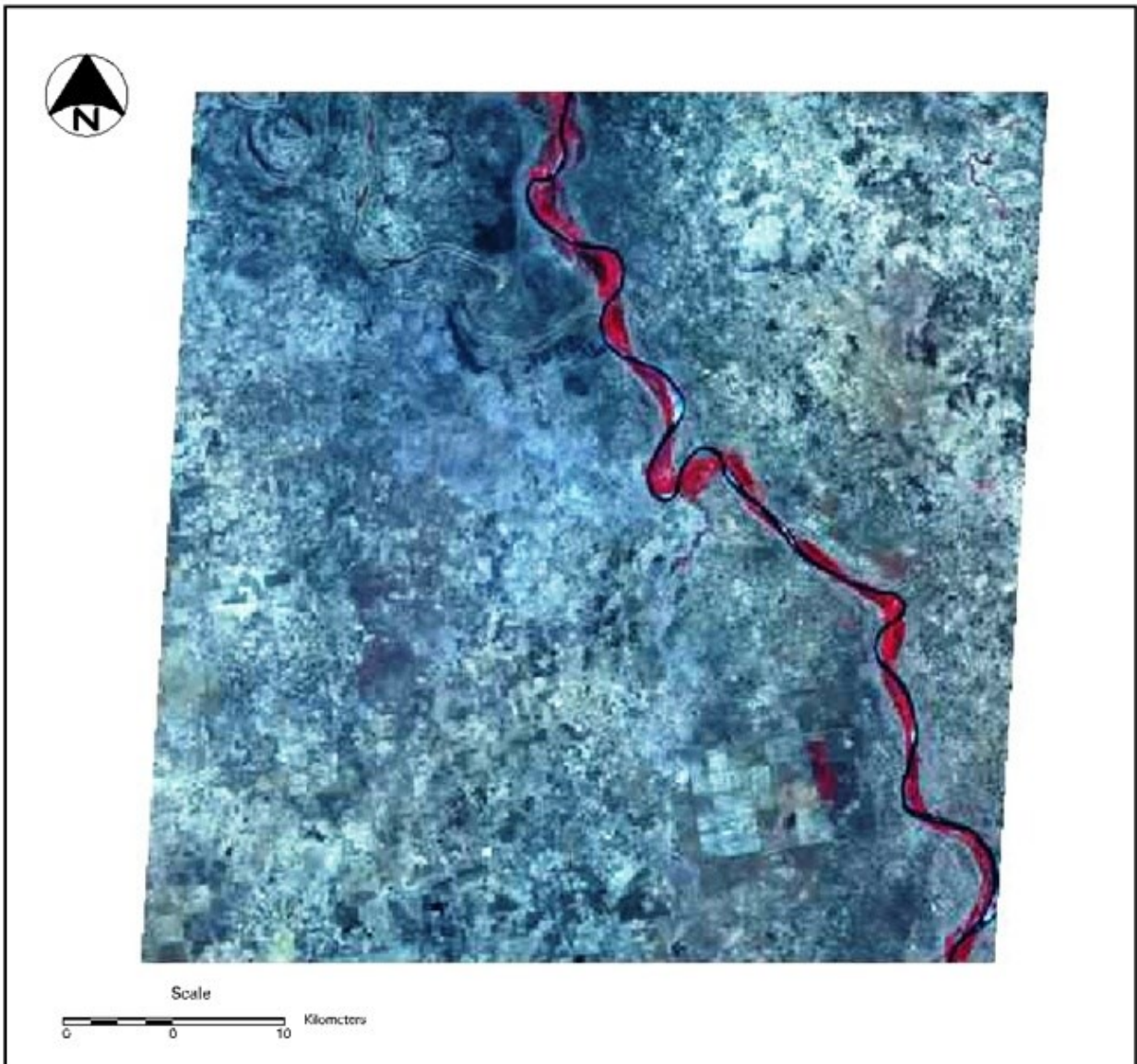
Appendix 4: Geometrically and atmospherically corrected scenes utilized for the study



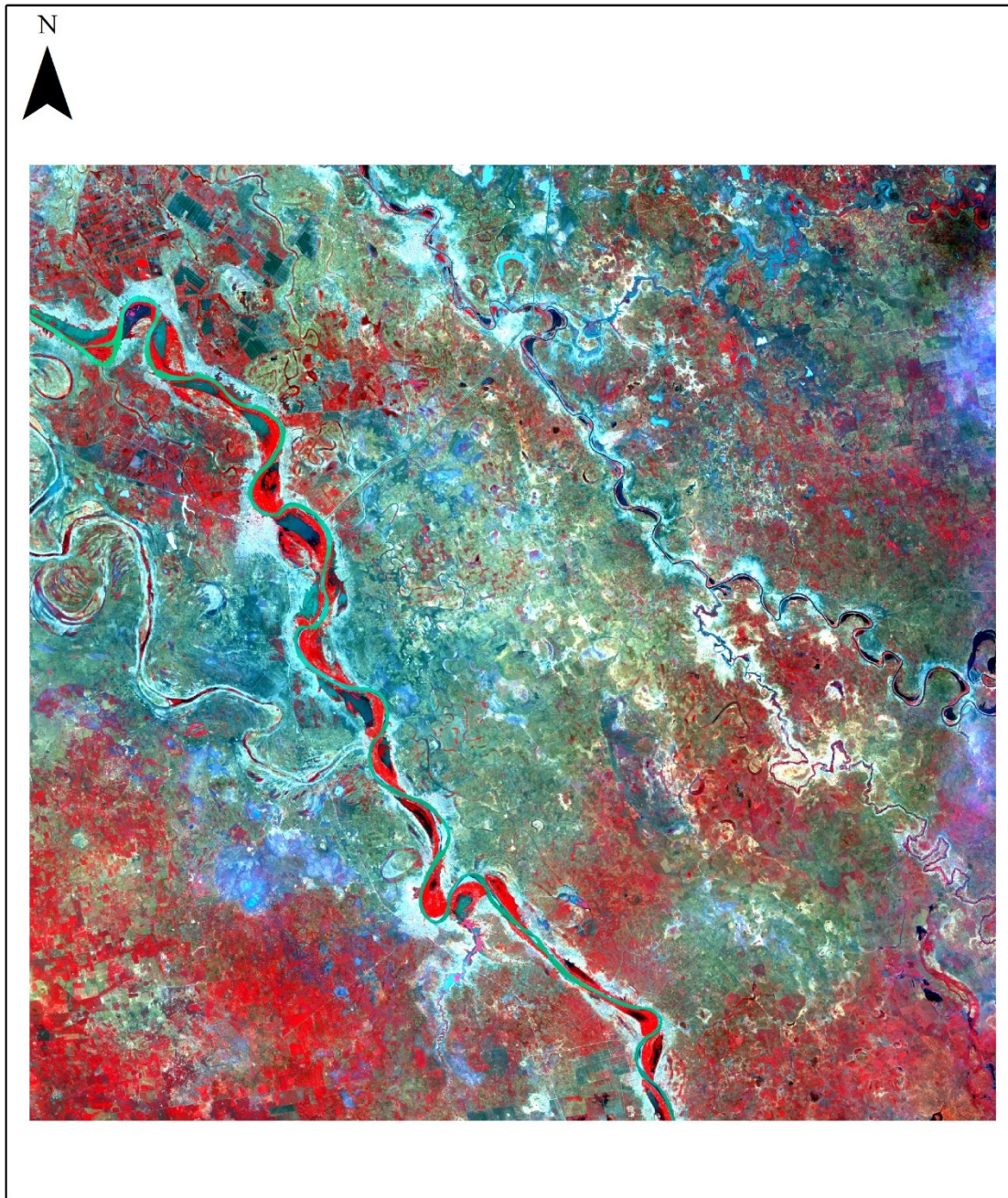
LANDSAT TM, acquisition in 4th January 1990



LANDSAT TM, acquisition in 26th March 1999



TERRA ASTER, acquisition in 13th March 2009

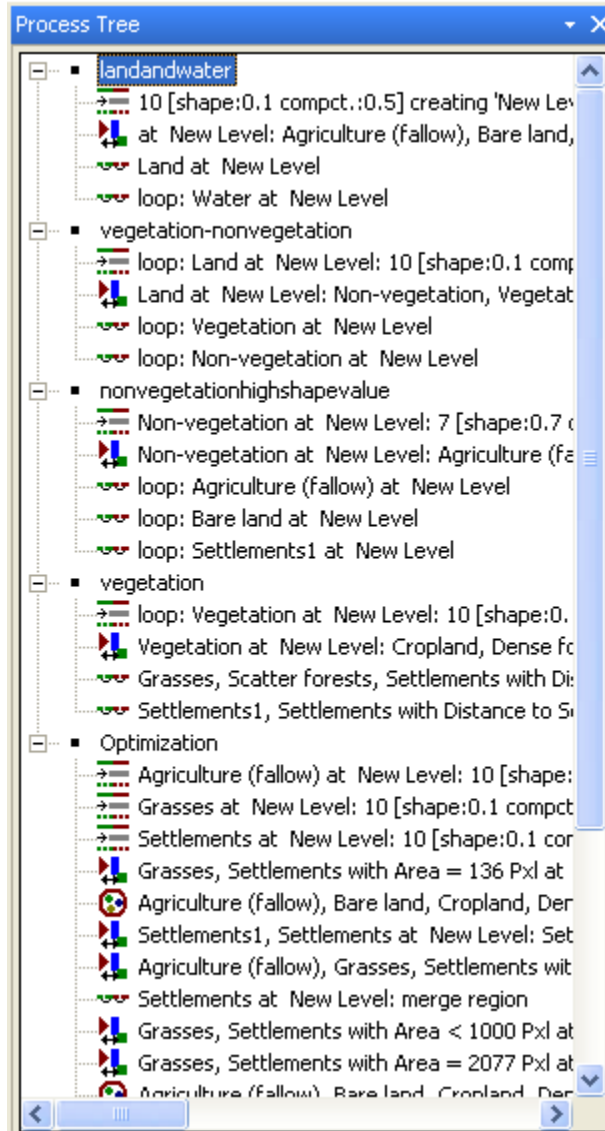


RapidEye, acquisition in 4th January 2010

Appendix 5: Polynomial rectification process report of LANDSAT TM 1999 image

NO	X Input	Y Input	X Ref.	Y Ref.	X Resid.	Y Resid.	Error
1	345.5156	3022.984	598740.2	1444512	0.15	0.42	0.44
2	55.01563	2947.109	594422.5	1443379	-0.01	-0.01	0.01
3	63.01563	2955.109	594541.2	1443497	-0.02	-0.04	0.04
4	93.14063	2960.109	594991.6	1443565	0.17	-0.48	0.51
5	188.0156	2637.984	596405.4	1438783	0.49	-0.33	0.59
6	204.8906	2634.109	596645.6	1438723	-0.22	-0.51	0.55
7	813.0156	1501.984	605678.9	1421921	-0.19	0.29	0.35
8	838.7656	1509.984	606064.9	1422039	0.04	0.22	0.22
9	1338.016	77.98438	613479.9	1400768	0.00	0.01	0.01
10	1343.766	89.98438	613564.7	1400952	-0.04	0.37	0.37
11	153.8906	2808.984	595890.8	1441333	-0.03	0.35	0.35
12	271.0156	3018.984	597634.4	1444451	0.21	0.27	0.34
13	1035.016	2602.984	608977.2	1438273	-0.19	0.31	0.37
14	1330.016	1705.984	613361	1424951	-0.06	0.30	0.30
15	1901.016	1057.984	621849.5	1415319	0.40	-0.20	0.45
16	1931.766	1034.234	622298.9	1414964	-0.10	-0.35	0.36
17	2490.891	463.9844	630601.8	1406499	-0.26	-0.11	0.28
18	2309.016	1525.109	627909	1422251	0.31	-0.56	0.64
19	2277.016	1538.984	627427.2	1422461	-0.13	-0.30	0.32
20	2300.891	1532.984	627785.3	1422372	0.10	-0.32	0.34
21	2249.016	1549.109	627005.6	1422616	-0.51	-0.04	0.52
22	2095.016	1836.234	624726.3	1426875	0.03	-0.37	0.37
23	2107.016	1837.734	624907	1426899	0.20	-0.22	0.30
24	708.2656	2435.984	604123.5	1435784	-0.18	-0.30	0.35
25	716.0156	2412.734	604240.8	1435448	-0.04	0.37	0.37
26	821.0156	2431.984	605800.4	1435722	-0.05	-0.46	0.47
27	969.7656	2898.484	608017.8	1442657	0.46	0.02	0.46
28	1028.766	2909.984	608887.2	1442833	-0.02	0.36	0.36
29	764.078	2423.984	604956.4	1435607	0.08	-0.21	0.22
30	775.9531	2423.984	605130.6	1435610	-0.07	0.04	0.08
Total Root Mean Square (RMS) Error							0.35

Appendix 6: Part of the hierarchical rules developed to extract categorical LU/LC classes



Appendix 7: Classification accuracies for the extracted LU/LC classes

Error matrix of rule-based classification for LANDSAT TM 1990

User Class...	Water	Bare...	Agric...	Gras...	Dens...	Scatte...	Crop-L...	Settle...	Hortic...	Sum
Confusion...										
Water	11	0	0	0	0	0	0	0	0	11
Bare-land	1	13	0	0	0	0	0	1	0	15
Agriculture	0	1	33	0	0	0	0	0	0	34
Grass-land	0	0	4	15	0	0	0	0	0	19
Dense-forests	0	0	0	0	19	0	0	0	1	20
Scatter forests	0	0	0	1	2	18	1	1	0	23
Crop-land	0	0	1	0	0	0	13	0	0	14
Settlements	0	0	0	0	0	0	0	9	0	9
Horticulture	0	0	0	0	0	0	0	0	18	18
unclassified	0	0	0	0	0	0	0	0	0	0
Sum	12	14	38	16	21	18	14	11	19	
Accuracy										
Producer	0.91666...	0.9285...	0.86842...	0.9375...	0.9047...	1	0.9285...	0.81818...	0.94736...	
User	1	0.8666...	0.97058...	0.7894...	0.95	0.7826087	0.9285...	1	1	
Hellden	0.95652...	0.8965...	0.91666...	0.8571...	0.9268...	0.878	0.9285...	0.9	0.973	
Short	0.91666...	0.8125...	0.84615...	0.75	0.8636...	0.7826087	0.8666...	0.81818...	0.94736...	
KIA Per Class	0.91063...	0.9213...	0.83374...	0.9292...	0.8914...	1	0.9218...	0.80755...	0.94083...	
Totals										
Overall A...	0.914...									
KIA	0.901...									

Error matrix of rule-based classification for LANDSAT TM 1999

User Class \ Sa...	Water	Bare...	Agri...	Gra...	Den...	Sc...	Cro...	Settl...	Horticul...	Sum
Confusion Matrix										
Water	11	0	0	0	0	0	0	0	0	11
Bare-land	1	13	0	0	0	0	0	0	0	14
Agriculture	0	1	33	0	0	0	0	0	0	34
Grass-land	0	0	4	16	0	0	0	0	0	20
Dense-forests	0	0	0	0	19	0	0	0	1	20
Scatter forests	0	0	0	0	2	18	1	1	0	22
Crop-land	0	0	1	0	0	0	13	0	0	14
Settlements	0	0	0	0	0	0	0	10	0	10
Horticulture	0	0	0	0	0	0	0	0	18	18
unclassified	0	0	0	0	0	0	0	0	0	0
Sum	12	14	38	16	21	18	14	11	19	
Accuracy										
Producer	0.9166...	0.9285...	0.868...	1	0.904...	1	0.928...	0.909	0.9473684	
User	1	0.9285...	0.970...	0.8	0.95	0.818...	0.928...	1	1	
Hellden	0.9565...	0.9285...	0.916...	0.888...	0.926...	0.9	0.928...	0.952...	0.973	
Short	0.9166...	0.8666...	0.846...	0.8	0.863...	0.818...	0.866...	0.909	0.9473684	
KIA Per Class	0.9106...	0.9218...	0.833...	1	0.891...	1	0.921...	0.903...	0.9408348	
Totals										
Overall Accuracy	0.926...									
KIA	0.915...									

**Appendix 8: Population Size and Growth Rates by State 1993-2008 (000),
source Ali *et al.* (2008).**

State	1993		2008		Growth Rate	
	Males	Females	Males	Females	Males	Females
Sudan	12962	12771	20074	19081	2.91	2.67
N. Sudan	10672	10590	15787	15107	2.61	2.37
Northern	244	267	354	345	2.47	1.71
Nahr Elnil	379	402	572	549	5.25	4.11
Red Sea	364	321	801	595	2.94	1.93
Kassala	637	598	991	799	0.79	1.35
Algadarif	595	554	670	679	3.39	2.77
Khartoum	1682	1631	2800	2474	1.74	1.92
Aljazeera	1328	1388	1724	1851	2.27	2.31
White Nile	604	623	849	881	1.64	1.99
Sinnar	489	489	626	659	3.07	3.38
Blue Nile	266	247	422	410	5.30	5.21
Northern Kordofan	635	692	1407	1514	2.35	2.14
Southern Kordofan	488	516	695	712	4.41	3.63
Northern Darfur	557	599	1080	1034	-0.04	-0.17
Western Darfur	644	686	640	668	4.64	3.90
Southern Darfur	1075	1078	2158	1936	4.17	14.13
S. Sudan	2291	476	4287	3973	22.52	6.92
Upper Nile	69	655	2031	1851	-0.83	-0.73
Bahr Algazel	1009	958	891	859	5.56	5.39
Equatoria	592	562	1365	1263	2.91	2.67

Appendix 9: Descriptive statistics of the change dynamics during the periods of study

Deforestation (90-99)

Change class	NO (polygon)	Area (pixels)			
		Minimum	Maximum	Mean	Std. Deviation
DF to Ag	216	1	139	18.59	23.774
DF to Br	112	1	78	11.84	15.550
DF to Gr	186	1	147	11.77	19.097
DF to O	242	1	217	22.83	36.357
DF to SF	408	1	240	16.72	29.416
DF to W	277	1	215	8.06	18.491
SF to Ag	5101	1	648	50.64	63.066
SF to Br	762	1	173	18.69	25.275
SF to Cr	69	1	178	38.70	43.265
SF to Gr	3431	1	574	30.20	45.893
SF to O	189	1	234	22.85	31.496
SF to St	56	1	187	13.66	29.617

Reforestation (90-99)

Change class	NO (polygon)	Area (pixels)			
		Minimum	Maximum	Mean	Std. Deviation
Ag to DF	49	1	87	7.69	13.671
Ag to SF	2749	1	282	23.03	29.532
Br to DF	2	6	18	12.00	8.485
Br to SF	23	1	147	17.83	30.904
Cr to SF	328	1	205	36.19	32.596
Gr to DF	53	1	118	15.28	25.096
Gr to SF	876	1	123	10.82	14.879
O to DF	89	1	184	25.21	36.953
O to SF	65	1	90	12.69	18.055
SF to DF	213	1	224	14.76	28.469
St to SF	35	1	55	14.57	14.683
W to DF	120	1	260	16.48	40.301
W to SF	270	1	198	10.57	20.483

Deforestation (99-09)

Change class	NO (polygon)	Area (pixels)			
		Minimum	Maximum	Mean	Std. Deviation
DF to Br	273	1	164	12.37	15.267
DF to Cr	71	1	64	9.41	14.398
DF to Gr	223	1	196	37.10	38.770
DF to O	431	1	282	39.33	52.387
DF to SF	867	1	573	38.50	54.097
SF to Ag	4862	1	719	24.60	39.004
SF to Br	907	1	156	12.86	16.634
SF to Cr	176	1	315	34.71	51.325
SF to Gr	3544	1	460	28.91	41.101
SF to O	340	1	216	23.95	36.032
SF to St	342	1	698	68.77	84.395

Reforestation (99-09)

Change class	NO (polygon)	Area (pixels)			
		Minimum	Maximum	Mean	Std. Deviation
Ag to SF	5642	1	740	71.67	69.539
Br to DF	189	1	151	14.21	22.372
Br to SF	669	1	318	18.75	31.399
Cr to SF	129	1	271	40.16	52.826
Gr to SF	2459	1	360	16.76	26.688
O to DF	640	1	241	24.68	31.710
O to SF	264	1	178	17.41	26.070
St to SF	186	1	158	19.26	29.117
W to SF	882	1	312	18.98	34.225

Appendix 10: Statistical summary of the TERRA ASTER metrics modeled and *Acacia nilotica* stand volume

The independent variable is Mean layer 1

Linear

Model Summary

R	R Square	Adjusted R Square	Std. Error of the Estimate
.770	.592	.586	51.197

ANOVA

	Sum of Squares	df	Mean Square	F	Sig.
Regression	259089.883	1	259089.883	98.847	.000
Residual	178236.880	68	2621.131		
Total	437326.763	69			

Logarithmic

Model Summary

R	R Square	Adjusted R Square	Std. Error of the Estimate
.777	.603	.598	50.504

ANOVA

	Sum of Squares	df	Mean Square	F	Sig.
Regression	263884.536	1	263884.536	103.459	.000
Residual	173442.227	68	2550.621		
Total	437326.763	69			

Inverse

Model Summary

R	R Square	Adjusted R Square	Std. Error of the Estimate
.783	.613	.607	49.893

ANOVA

	Sum of Squares	df	Mean Square	F	Sig.
Regression	268052.016	1	268052.016	107.680	.000
Residual	169274.747	68	2489.335		
Total	437326.763	69			

The independent variable is Mean layer 2.

Linear

Model Summary

R	R Square	Adjusted R Square	Std. Error of the Estimate
.786	.618	.612	49.562

ANOVA

	Sum of Squares	df	Mean Square	F	Sig.
Regression	270288.851	1	270288.851	110.033	.000
Residual	167037.912	68	2456.440		
Total	437326.763	69			

Logarithmic

Model Summary

R	R Square	Adjusted R Square	Std. Error of the Estimate
.797	.635	.630	48.445

ANOVA

	Sum of Squares	df	Mean Square	F	Sig.
Regression	277733.298	1	277733.298	118.337	.000
Residual	159593.465	68	2346.963		
Total	437326.763	69			

Inverse

Model Summary

R	R Square	Adjusted R Square	Std. Error of the Estimate
.805	.649	.644	47.534

ANOVA

	Sum of Squares	df	Mean Square	F	Sig.
Regression	283684.182	1	283684.182	125.555	.000
Residual	153642.581	68	2259.450		
Total	437326.763	69			

The independent variable is Mean layer 3.

Linear

Model Summary

R	R Square	Adjusted R Square	Std. Error of the Estimate
.819	.670	.665	46.060

ANOVA

	Sum of Squares	df	Mean Square	F	Sig.
Regression	293060.667	1	293060.667	138.135	.000
Residual	144266.096	68	2121.560		
Total	437326.763	69			

Logarithmic

Model Summary

R	R Square	Adjusted R Square	Std. Error of the Estimate
.800	.641	.635	48.072

ANOVA

	Sum of Squares	df	Mean Square	F	Sig.
Regression	280184.749	1	280184.749	121.244	.000
Residual	157142.014	68	2310.912		
Total	437326.763	69			

Inverse

Model Summary

R	R Square	Adjusted R Square	Std. Error of the Estimate
.776	.603	.597	50.544

ANOVA

	Sum of Squares	df	Mean Square	F	Sig.
Regression	263610.140	1	263610.140	103.188	.000
Residual	173716.623	68	2554.656		
Total	437326.763	69			

The independent variable is Homogeneity layer 1.

Linear

Model Summary

R	R Square	Adjusted R Square	Std. Error of the Estimate
.374	.140	.127	74.364

ANOVA

	Sum of Squares	df	Mean Square	F	Sig.
Regression	61287.066	1	61287.066	11.083	.001
Residual	376039.697	68	5529.996		
Total	437326.763	69			

Logarithmic

Model Summary

R	R Square	Adjusted R Square	Std. Error of the Estimate
.667	.444	.436	59.780

ANOVA

	Sum of Squares	df	Mean Square	F	Sig.
Regression	194322.113	1	194322.113	54.377	.000
Residual	243004.650	68	3573.598		
Total	437326.763	69			

Inverse

Model Summary

R	R Square	Adjusted R Square	Std. Error of the Estimate
.670	.448	.440	59.561

ANOVA

	Sum of Squares	df	Mean Square	F	Sig.
Regression	196098.933	1	196098.933	55.279	.000
Residual	241227.830	68	3547.468		
Total	437326.763	69			

The independent variable is Homogeneity layer 2.

Linear

Model Summary

R	R Square	Adjusted R Square	Std. Error of the Estimate
.568	.323	.313	66.001

ANOVA

	Sum of Squares	df	Mean Square	F	Sig.
Regression	141110.391	1	141110.391	32.394	.000
Residual	296216.372	68	4356.123		
Total	437326.763	69			

Logarithmic

Model Summary

R	R Square	Adjusted R Square	Std. Error of the Estimate
.693	.480	.472	57.836

ANOVA

	Sum of Squares	df	Mean Square	F	Sig.
Regression	209866.623	1	209866.623	62.740	.000
Residual	227460.140	68	3345.002		
Total	437326.763	69			

Inverse

Model Summary

R	R Square	Adjusted R Square	Std. Error of the Estimate
.629	.395	.386	62.368

ANOVA

	Sum of Squares	df	Mean Square	F	Sig.
Regression	172821.494	1	172821.494	44.430	.000
Residual	264505.268	68	3889.783		
Total	437326.763	69			

The independent variable is Homogeneity layer 3.

Linear

Model Summary

R	R Square	Adjusted R Square	Std. Error of the Estimate
.453	.205	.193	71.509

ANOVA

	Sum of Squares	df	Mean Square	F	Sig.
Regression	89607.650	1	89607.650	17.524	.000
Residual	347719.113	68	5113.516		
Total	437326.763	69			

Logarithmic

Model Summary

R	R Square	Adjusted R Square	Std. Error of the Estimate
.488	.238	.227	70.014

ANOVA

	Sum of Squares	df	Mean Square	F	Sig.
Regression	103989.712	1	103989.712	21.214	.000
Residual	333337.051	68	4902.015		
Total	437326.763	69			

Inverse

Model Summary

R	R Square	Adjusted R Square	Std. Error of the Estimate
.184	.034	.020	78.819

ANOVA

	Sum of Squares	df	Mean Square	F	Sig.
Regression	14877.907	1	14877.907	2.395	.126
Residual	422448.856	68	6212.483		
Total	437326.763	69			

The independent variable is Dissimilarity layer 1.

Linear

Model Summary

R	R Square	Adjusted R Square	Std. Error of the Estimate
.501	.251	.240	69.421

ANOVA

	Sum of Squares	df	Mean Square	F	Sig.
Regression	109614.350	1	109614.350	22.745	.000
Residual	327712.413	68	4819.300		
Total	437326.763	69			

The independent variable is Dissimilarity layer 2.

Linear

Model Summary			
R	R Square	Adjusted R Square	Std. Error of the Estimate
.561	.314	.304	66.409

ANOVA					
	Sum of Squares	df	Mean Square	F	Sig.
Regression	137438.410	1	137438.410	31.164	.000
Residual	299888.352	68	4410.123		
Total	437326.763	69			

The independent variable is Dissimilarity layer 3.

Linear

Model Summary			
R	R Square	Adjusted R Square	Std. Error of the Estimate
.465	.217	.205	70.979

ANOVA					
	Sum of Squares	df	Mean Square	F	Sig.
Regression	94739.108	1	94739.108	18.805	.000
Residual	342587.655	68	5038.054		
Total	437326.763	69			

Logarithmic

Model Summary			
R	R Square	Adjusted R Square	Std. Error of the Estimate
.448	.201	.189	71.681

ANOVA					
	Sum of Squares	df	Mean Square	F	Sig.
Regression	87931.115	1	87931.115	17.113	.000
Residual	349395.648	68	5138.171		
Total	437326.763	69			

Inverse

Model Summary			
R	R Square	Adjusted R Square	Std. Error of the Estimate
.416	.173	.161	72.911

ANOVA					
	Sum of Squares	df	Mean Square	F	Sig.
Regression	75838.548	1	75838.548	14.266	.000
Residual	361488.214	68	5316.003		
Total	437326.763	69			

The independent variable is Correlation layer 1.

Linear

Model Summary

R	R Square	Adjusted R Square	Std. Error of the Estimate
.715	.511	.503	56.103

ANOVA

	Sum of Squares	df	Mean Square	F	Sig.
Regression	223294.605	1	223294.605	70.943	.000
Residual	214032.158	68	3147.532		
Total	437326.763	69			

Logarithmic

Model Summary

R	R Square	Adjusted R Square	Std. Error of the Estimate
.713	.509	.502	56.209

ANOVA

	Sum of Squares	df	Mean Square	F	Sig.
Regression	222486.368	1	222486.368	70.420	.000
Residual	214840.395	68	3159.418		
Total	437326.763	69			

Inverse

Model Summary

R	R Square	Adjusted R Square	Std. Error of the Estimate
.671	.450	.442	59.460

ANOVA

	Sum of Squares	df	Mean Square	F	Sig.
Regression	196910.283	1	196910.283	55.695	.000
Residual	240416.480	68	3535.536		
Total	437326.763	69			

The independent variable is Correlation layer 2.

Linear

Model Summary

R	R Square	Adjusted R Square	Std. Error of the Estimate
.684	.468	.460	58.492

ANOVA

	Sum of Squares	df	Mean Square	F	Sig.
Regression	204674.514	1	204674.514	59.823	.000
Residual	232652.249	68	3421.357		
Total	437326.763	69			

Logarithmic

Model Summary

R	R Square	Adjusted R Square	Std. Error of the Estimate
.662	.438	.429	60.138

ANOVA

	Sum of Squares	df	Mean Square	F	Sig.
Regression	191401.753	1	191401.753	52.924	.000
Residual	245925.010	68	3616.544		
Total	437326.763	69			

Inverse

Model Summary

R	R Square	Adjusted R Square	Std. Error of the Estimate
.512	.262	.251	68.898

ANOVA

	Sum of Squares	df	Mean Square	F	Sig.
Regression	114538.836	1	114538.836	24.129	.000
Residual	322787.927	68	4746.881		
Total	437326.763	69			

The independent variable is Correlation layer 3.

Linear

Model Summary

R	R Square	Adjusted R Square	Std. Error of the Estimate
.563	.317	.307	66.262

ANOVA

	Sum of Squares	df	Mean Square	F	Sig.
Regression	138761.144	1	138761.144	31.604	.000
Residual	298565.619	68	4390.671		
Total	437326.763	69			

Logarithmic

Model Summary

R	R Square	Adjusted R Square	Std. Error of the Estimate
.583	.340	.330	65.173

ANOVA

	Sum of Squares	df	Mean Square	F	Sig.
Regression	148494.335	1	148494.335	34.960	.000
Residual	288832.428	68	4247.536		
Total	437326.763	69			

Inverse

Model Summary

R	R Square	Adjusted R Square	Std. Error of the Estimate
.572	.327	.317	65.780

ANOVA

	Sum of Squares	df	Mean Square	F	Sig.
Regression	143090.662	1	143090.662	33.069	.000
Residual	294236.101	68	4327.001		
Total	437326.763	69			

The independent variable is DN layer 1.

Linear

Model Summary

R	R Square	Adjusted R Square	Std. Error of the Estimate
.497	.247	.236	69.577

ANOVA

	Sum of Squares	df	Mean Square	F	Sig.
Regression	108140.799	1	108140.799	22.339	.000
Residual	329185.963	68	4840.970		
Total	437326.763	69			

Logarithmic

Model Summary

R	R Square	Adjusted R Square	Std. Error of the Estimate
.509	.259	.249	69.011

ANOVA

	Sum of Squares	df	Mean Square	F	Sig.
Regression	113477.375	1	113477.375	23.827	.000
Residual	323849.387	68	4762.491		
Total	437326.763	69			

Inverse

Model Summary

R	R Square	Adjusted R Square	Std. Error of the Estimate
.520	.270	.260	68.497

ANOVA

	Sum of Squares	df	Mean Square	F	Sig.
Regression	118278.021	1	118278.021	25.209	.000
Residual	319048.742	68	4691.893		
Total	437326.763	69			

The independent variable is DN layer 2.

Linear

Model Summary

R	R Square	Adjusted R Square	Std. Error of the Estimate
.666	.444	.435	59.824

ANOVA

	Sum of Squares	df	Mean Square	F	Sig.
Regression	193962.808	1	193962.808	54.196	.000
Residual	243363.955	68	3578.882		
Total	437326.763	69			

Logarithmic

Model Summary

R	R Square	Adjusted R Square	Std. Error of the Estimate
.671	.450	.442	59.489

ANOVA

	Sum of Squares	df	Mean Square	F	Sig.
Regression	196678.470	1	196678.470	55.575	.000
Residual	240648.293	68	3538.945		
Total	437326.763	69			

Inverse

Model Summary

R	R Square	Adjusted R Square	Std. Error of the Estimate
.673	.453	.444	59.337

ANOVA

	Sum of Squares	df	Mean Square	F	Sig.
Regression	197909.537	1	197909.537	56.211	.000
Residual	239417.226	68	3520.842		
Total	437326.763	69			

The independent variable is DN layer 3.

Linear

Model Summary

R	R Square	Adjusted R Square	Std. Error of the Estimate
.554	.307	.297	66.751

ANOVA

	Sum of Squares	df	Mean Square	F	Sig.
Regression	134337.776	1	134337.776	30.150	.000
Residual	302988.987	68	4455.720		
Total	437326.763	69			

Logarithmic

Model Summary

R	R Square	Adjusted R Square	Std. Error of the Estimate
.550	.303	.293	66.961

ANOVA

	Sum of Squares	df	Mean Square	F	Sig.
Regression	132432.822	1	132432.822	29.536	.000
Residual	304893.941	68	4483.734		
Total	437326.763	69			

Inverse

Model Summary

R	R Square	Adjusted R Square	Std. Error of the Estimate
.538	.290	.279	67.581

ANOVA

	Sum of Squares	df	Mean Square	F	Sig.
Regression	126757.661	1	126757.661	27.754	.000
Residual	310569.101	68	4567.193		
Total	437326.763	69			

Appendix 11: Statistical summary of the RapidEye metrics modeled and *Acacia nilotica* stand volume

The independent variable is Mean layer 1

Linear

Model Summary

R	R Square	Adjusted R Square	Std. Error of the Estimate
.794	.631	.626	46.790

ANOVA

	Sum of Squares	df	Mean Square	F	Sig.
Regression	254778.516	1	254778.516	116.375	.000
Residual	148871.188	68	2189.282		
Total	403649.704	69			

Logarithmic

Model Summary

R	R Square	Adjusted R Square	Std. Error of the Estimate
.810	.655	.650	45.223

ANOVA

	Sum of Squares	df	Mean Square	F	Sig.
Regression	264581.016	1	264581.016	129.371	.000
Residual	139068.688	68	2045.128		
Total	403649.704	69			

Inverse

Model Summary

R	R Square	Adjusted R Square	Std. Error of the Estimate
.824	.679	.674	43.653

ANOVA

	Sum of Squares	df	Mean Square	F	Sig.
Regression	274070.377	1	274070.377	143.825	.000
Residual	129579.327	68	1905.578		
Total	403649.704	69			

The independent variable is Mean layer 2.

Linear

Model Summary

R	R Square	Adjusted R Square	Std. Error of the Estimate
.794	.631	.625	46.831

ANOVA

	Sum of Squares	df	Mean Square	F	Sig.
Regression	254516.600	1	254516.600	116.052	.000
Residual	149133.105	68	2193.134		
Total	403649.704	69			

Logarithmic

Model Summary

R	R Square	Adjusted R Square	Std. Error of the Estimate
.822	.676	.672	43.830

ANOVA

	Sum of Squares	df	Mean Square	F	Sig.
Regression	273014.408	1	273014.408	142.113	.000
Residual	130635.297	68	1921.107		
Total	403649.704	69			

Inverse

Model Summary

R	R Square	Adjusted R Square	Std. Error of the Estimate
.849	.720	.716	40.765

ANOVA

	Sum of Squares	df	Mean Square	F	Sig.
Regression	290650.083	1	290650.083	174.905	.000
Residual	112999.621	68	1661.759		
Total	403649.704	69			

The independent variable is Mean layer 3.

Linear

Model Summary

R	R Square	Adjusted R Square	Std. Error of the Estimate
.783	.613	.607	47.919

ANOVA

	Sum of Squares	df	Mean Square	F	Sig.
Regression	247506.223	1	247506.223	107.788	.000
Residual	156143.481	68	2296.228		
Total	403649.704	69			

Logarithmic

Model Summary

R	R Square	Adjusted R Square	Std. Error of the Estimate
.829	.687	.682	43.112

ANOVA

	Sum of Squares	df	Mean Square	F	Sig.
Regression	277261.962	1	277261.962	149.174	.000
Residual	126387.742	68	1858.643		
Total	403649.704	69			

Inverse

Model Summary

R	R Square	Adjusted R Square	Std. Error of the Estimate
.865	.748	.744	38.697

ANOVA

	Sum of Squares	df	Mean Square	F	Sig.
Regression	301821.197	1	301821.197	201.553	.000
Residual	101828.507	68	1497.478		
Total	403649.704	69			

The independent variable is Homogeneity layer 1.

Linear

Model Summary

R	R Square	Adjusted R Square	Std. Error of the Estimate
.007	.000	-.015	77.044

ANOVA

	Sum of Squares	df	Mean Square	F	Sig.
Regression	18.243	1	18.243	.003	.956
Residual	403631.462	68	5935.757		
Total	403649.704	69			

Logarithmic

Model Summary

R	R Square	Adjusted R Square	Std. Error of the Estimate
.046	.002	-.013	76.965

ANOVA

	Sum of Squares	df	Mean Square	F	Sig.
Regression	849.230	1	849.230	.143	.706
Residual	402800.475	68	5923.536		
Total	403649.704	69			

Inverse

Model Summary

R	R Square	Adjusted R Square	Std. Error of the Estimate
.088	.008	-.007	76.749

ANOVA

	Sum of Squares	df	Mean Square	F	Sig.
Regression	3104.229	1	3104.229	.527	.470
Residual	400545.475	68	5890.375		
Total	403649.704	69			

The independent variable is Homogeneity layer 2.

Linear

Model Summary

R	R Square	Adjusted R Square	Std. Error of the Estimate
.229	.052	.038	74.999

ANOVA

	Sum of Squares	df	Mean Square	F	Sig.
Regression	21158.251	1	21158.251	3.762	.057
Residual	382491.453	68	5624.874		
Total	403649.704	69			

Logarithmic

Model Summary

R	R Square	Adjusted R Square	Std. Error of the Estimate
.158	.025	.011	76.078

ANOVA

	Sum of Squares	df	Mean Square	F	Sig.
Regression	10074.079	1	10074.079	1.741	.191
Residual	393575.625	68	5787.877		
Total	403649.704	69			

Inverse

Model Summary

R	R Square	Adjusted R Square	Std. Error of the Estimate
.056	.003	-.012	76.925

ANOVA

	Sum of Squares	df	Mean Square	F	Sig.
Regression	1259.548	1	1259.548	.213	.646
Residual	402390.156	68	5917.502		
Total	403649.704	69			

The independent variable is Homogeneity layer 3.

Linear

Model Summary

R	R Square	Adjusted R Square	Std. Error of the Estimate
.337	.114	.101	72.528

ANOVA

	Sum of Squares	df	Mean Square	F	Sig.
Regression	45948.789	1	45948.789	8.735	.004
Residual	357700.915	68	5260.308		
Total	403649.704	69			

Logarithmic

Model Summary

R	R Square	Adjusted R Square	Std. Error of the Estimate
.433	.188	.176	69.442

ANOVA

	Sum of Squares	df	Mean Square	F	Sig.
Regression	75737.288	1	75737.288	15.706	.000
Residual	327912.416	68	4822.241		
Total	403649.704	69			

Inverse

Model Summary

R	R Square	Adjusted R Square	Std. Error of the Estimate
.325	.106	.093	72.856

ANOVA

	Sum of Squares	df	Mean Square	F	Sig.
Regression	42707.316	1	42707.316	8.046	.006
Residual	360942.388	68	5307.976		
Total	403649.704	69			

The independent variable is Dissimilarity layer 1.

Linear

Model Summary

R	R Square	Adjusted R Square	Std. Error of the Estimate
.520	.270	.260	65.814

ANOVA

	Sum of Squares	df	Mean Square	F	Sig.
Regression	109112.145	1	109112.145	25.191	.000
Residual	294537.559	68	4331.435		
Total	403649.704	69			

Logarithmic

Model Summary

R	R Square	Adjusted R Square	Std. Error of the Estimate
.546	.298	.288	64.538

ANOVA

	Sum of Squares	df	Mean Square	F	Sig.
Regression	120421.191	1	120421.191	28.912	.000
Residual	283228.513	68	4165.125		
Total	403649.704	69			

Inverse

Model Summary

R	R Square	Adjusted R Square	Std. Error of the Estimate
.557	.310	.300	63.992

ANOVA

	Sum of Squares	df	Mean Square	F	Sig.
Regression	125193.283	1	125193.283	30.573	.000
Residual	278456.421	68	4094.947		
Total	403649.704	69			

The independent variable is Dissimilarity layer 2.

Linear

Model Summary

R	R Square	Adjusted R Square	Std. Error of the Estimate
.266	.071	.057	74.274

ANOVA

	Sum of Squares	df	Mean Square	F	Sig.
Regression	28515.774	1	28515.774	5.169	.026
Residual	375133.930	68	5516.675		
Total	403649.704	69			

Logarithmic

Model Summary

R	R Square	Adjusted R Square	Std. Error of the Estimate
.280	.078	.065	73.962

ANOVA

	Sum of Squares	df	Mean Square	F	Sig.
Regression	31667.088	1	31667.088	5.789	.019
Residual	371982.616	68	5470.333		
Total	403649.704	69			

Inverse

Model Summary

R	R Square	Adjusted R Square	Std. Error of the Estimate
.288	.083	.070	73.771

ANOVA

	Sum of Squares	df	Mean Square	F	Sig.
Regression	33585.142	1	33585.142	6.171	.015
Residual	370064.562	68	5442.126		
Total	403649.704	69			

The independent variable is Dissimilarity layer 3.

Linear

Model Summary

R	R Square	Adjusted R Square	Std. Error of the Estimate
.531	.282	.272	65.263

ANOVA

	Sum of Squares	df	Mean Square	F	Sig.
Regression	114022.523	1	114022.523	26.771	.000
Residual	289627.181	68	4259.223		
Total	403649.704	69			

Logarithmic

Model Summary

R	R Square	Adjusted R Square	Std. Error of the Estimate
.523	.273	.263	65.678

ANOVA

	Sum of Squares	df	Mean Square	F	Sig.
Regression	110325.437	1	110325.437	25.576	.000
Residual	293324.268	68	4313.592		
Total	403649.704	69			

Inverse

Model Summary

R	R Square	Adjusted R Square	Std. Error of the Estimate
.503	.253	.242	66.576

ANOVA

	Sum of Squares	df	Mean Square	F	Sig.
Regression	102248.074	1	102248.074	23.068	.000
Residual	301401.631	68	4432.377		
Total	403649.704	69			

The independent variable is Correlation layer 1.

Linear

Model Summary

R	R Square	Adjusted R Square	Std. Error of the Estimate
.040	.002	-.013	76.984

ANOVA

	Sum of Squares	df	Mean Square	F	Sig.
Regression	647.874	1	647.874	.109	.742
Residual	403001.831	68	5926.498		
Total	403649.704	69			

Logarithmic

Model Summary

R	R Square	Adjusted R Square	Std. Error of the Estimate
.029	.001	-.014	77.013

ANOVA

	Sum of Squares	df	Mean Square	F	Sig.
Regression	346.475	1	346.475	.058	.810
Residual	403303.229	68	5930.930		
Total	403649.704	69			

Inverse

Model Summary

R	R Square	Adjusted R Square	Std. Error of the Estimate
.006	.000	-.015	77.044

ANOVA

	Sum of Squares	df	Mean Square	F	Sig.
Regression	12.426	1	12.426	.002	.964
Residual	403637.278	68	5935.842		
Total	403649.704	69			

The independent variable is Correlation layer 2.

Linear

Model Summary

R	R Square	Adjusted R Square	Std. Error of the Estimate
.173	.030	.016	75.878

ANOVA

	Sum of Squares	df	Mean Square	F	Sig.
Regression	12141.864	1	12141.864	2.109	.151
Residual	391507.840	68	5757.468		
Total	403649.704	69			

Logarithmic

Model Summary

R	R Square	Adjusted R Square	Std. Error of the Estimate
.101	.010	-.004	76.651

ANOVA

	Sum of Squares	df	Mean Square	F	Sig.
Regression	4128.420	1	4128.420	.703	.405
Residual	399521.284	68	5875.313		
Total	403649.704	69			

Inverse

Model Summary

R	R Square	Adjusted R Square	Std. Error of the Estimate
.019	.000	-.014	77.032

ANOVA

	Sum of Squares	df	Mean Square	F	Sig.
Regression	146.269	1	146.269	.025	.876
Residual	403503.436	68	5933.874		
Total	403649.704	69			

The independent variable is Correlation layer 3.

Linear

Model Summary

R	R Square	Adjusted R Square	Std. Error of the Estimate
.060	.004	-.011	76.908

ANOVA

	Sum of Squares	df	Mean Square	F	Sig.
Regression	1439.425	1	1439.425	.243	.623
Residual	402210.279	68	5914.857		
Total	403649.704	69			

Logarithmic

Model Summary

R	R Square	Adjusted R Square	Std. Error of the Estimate
.019	.000	-.014	77.031

ANOVA

	Sum of Squares	df	Mean Square	F	Sig.
Regression	149.005	1	149.005	.025	.875
Residual	403500.699	68	5933.834		
Total	403649.704	69			

Inverse

Model Summary

R	R Square	Adjusted R Square	Std. Error of the Estimate
.080	.006	-.008	76.800

ANOVA

	Sum of Squares	df	Mean Square	F	Sig.
Regression	2574.423	1	2574.423	.436	.511
Residual	401075.281	68	5898.166		
Total	403649.704	69			

The independent variable is DN layer 1.

Linear

Model Summary

R	R Square	Adjusted R Square	Std. Error of the Estimate
.635	.404	.395	59.504

ANOVA

	Sum of Squares	df	Mean Square	F	Sig.
Regression	162882.722	1	162882.722	46.003	.000
Residual	240766.982	68	3540.691		
Total	403649.704	69			

Logarithmic

Model Summary

R	R Square	Adjusted R Square	Std. Error of the Estimate
.648	.420	.411	58.684

ANOVA

	Sum of Squares	df	Mean Square	F	Sig.
Regression	169469.677	1	169469.677	49.210	.000
Residual	234180.028	68	3443.824		
Total	403649.704	69			

Inverse

Model Summary

R	R Square	Adjusted R Square	Std. Error of the Estimate
.650	.422	.414	58.567

ANOVA

	Sum of Squares	df	Mean Square	F	Sig.
Regression	170406.445	1	170406.445	49.680	.000
Residual	233243.260	68	3430.048		
Total	403649.704	69			

The independent variable is DN layer 2.

Linear

Model Summary

R	R Square	Adjusted R Square	Std. Error of the Estimate
.682	.465	.457	56.358

ANOVA

	Sum of Squares	df	Mean Square	F	Sig.
Regression	187663.541	1	187663.541	59.083	.000
Residual	215986.163	68	3176.267		
Total	403649.704	69			

Logarithmic

Model Summary

R	R Square	Adjusted R Square	Std. Error of the Estimate
.678	.460	.452	56.602

ANOVA

	Sum of Squares	df	Mean Square	F	Sig.
Regression	185795.590	1	185795.590	57.993	.000
Residual	217854.115	68	3203.737		
Total	403649.704	69			

Inverse

Model Summary

R	R Square	Adjusted R Square	Std. Error of the Estimate
.664	.441	.433	57.586

ANOVA

	Sum of Squares	df	Mean Square	F	Sig.
Regression	178147.796	1	178147.796	53.720	.000
Residual	225501.908	68	3316.205		
Total	403649.704	69			

The independent variable is DN layer 3.

Linear

Model Summary

R	R Square	Adjusted R Square	Std. Error of the Estimate
.658	.433	.424	58.034

ANOVA

	Sum of Squares	df	Mean Square	F	Sig.
Regression	174630.034	1	174630.034	51.851	.000
Residual	229019.671	68	3367.936		
Total	403649.704	69			

Logarithmic

Model Summary

R	R Square	Adjusted R Square	Std. Error of the Estimate
.659	.435	.427	57.918

ANOVA

	Sum of Squares	df	Mean Square	F	Sig.
Regression	175543.867	1	175543.867	52.331	.000
Residual	228105.838	68	3354.498		
Total	403649.704	69			

Inverse

Model Summary

R	R Square	Adjusted R Square	Std. Error of the Estimate
.651	.423	.415	58.513

ANOVA

	Sum of Squares	df	Mean Square	F	Sig.
Regression	170831.090	1	170831.090	49.895	.000
Residual	232818.614	68	3423.803		
Total	403649.704	69			